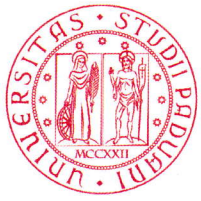

UNIVERSITÀ
DEGLI STUDI
DI PADOVA

Sede Amministrativa: Università degli Studi di Padova

Dipartimento di Biologia

SCUOLA DI DOTTORATO DI RICERCA IN : Bioscienze e Biotecnologie

INDIRIZZO: Genetica e Biologia Molecolare dello Sviluppo

CICLO XXVIII

Global analysis of the genetic and epigenetic contributions to phenotypic plasticity in a wild yeast strain

Direttore della Scuola: Ch.mo Prof. Paolo Bernardi

Coordinatore d'indirizzo: Ch.mo Prof. Rodolfo Costa

Supervisore: Ch.mo Prof. Chiara Romualdi

Co-supervisore: Dott. Attila Csikasz-Nagy

Dottorando: Valentina Cappelletti

Contents

Abstract (Italian)

M28 è un ceppo naturale di *Saccharomyces cerevisiae*, isolato da vitigni di Montalcino (Toscana), che mostra una affascinante segregazione 2:2 di due tratti non collegati tra loro: la resistenza recessiva ad un analogo tossico della leucina (5'5'5 trifloroleucina, TFL) ed il morfotipo di colonia. Due dei quattro prodotti meiotici (spore) di M28, infatti, crescono generando colonie lisce mentre gli altri due generano complesse strutture filamentose. Analisi preliminari a questo lavoro di tesi hanno dimostrato l'unicità di questo sistema data dall'osservazione che i quattro prodotti meiotici di M28 mostrano una elevata variabilità fenotipica riguardo l'abilità di differenziare in strutture pseudo-ifali nonché la capacità di invadere substrati solidi. Abbiamo successivamente dimostrato che ogni spora è capace di passare da un fenotipo di colonia liscio ad un rugoso, e viceversa, in un processo spontaneo e reversibile che avviene ad alte frequenze. Sedotti da questo intrigante sistema dove le teorie Lamarckiane e Darwiniane sembrano riconciliarsi abbiamo iniziato una investigazione globale volta ad investigare il genoma, il proteoma e la struttura cromatinica di tutti e quattro i prodotti meiotici di una tetrade di M28. Abbiamo così utilizzato tecnologie all'avanguardia sia nel campo della spettrometria di massa che del sequenziamento di ultima generazione, ottenendo i seguenti risultati:

i) abbiamo confermato il determinante genetico della resistenza alla TFL mostrando inoltre come una mutazione associata alla perdita di funzione di un gene possa interferire sul metabolismo cellulare, degli amino acidi in questo caso, alterando l'accessibilità della cromatina attraverso modifiche istoniche quali la bi- e tri-metilazione della lisina 4 dell'istone H3 o l'acetilazione dell'istone H4;

ii) abbiamo dimostrato che non vi sono polimorfismi che segregano con il tratto "morfologia di colonia" ma piuttosto abbiamo identificato alcuni epi-alleli che segregrano

2:2 con il morfotipo e che potrebbero essere quindi responsabili della segregazione osservata;

iii) abbiamo mostrato per la prima volta l'elevata variabilità a livello dell'epigenoma di quattro prodotti meiotici di un ceppo naturale di *S. cerevisiae*;

iv) abbiamo identificato riarrangiamenti proteici strutturali, a carico di alcune proteine associabili ai prioni, durante la transizione da morfotipo di colonia filamentoso a liscio (e viceversa) mostrando che la proteina Hrp1 genera aggregati proteici a localizzazione nucleare il cui numero cambia statisticamente durante la transizione dimorfica.

In conclusione i risultati di questo lavoro evidenziano come meccanismi di tipo genetico ed epigenetico possano regolare la plasticità fenotipica in M28 portandoci ad ipotizzare un aggiornamento della teoria del "rinnovamento del genoma" che introduca le variazioni della struttura cromatinica come un meccanismo di adattamento evolutivo che permette l'insorgere di nuovi tratti, potenzialmente vantaggiosi, nella progenie di ceppi di lievito diplodi.

Abstract (English)

The natural M28 *Saccharomyces cerevisiae* strain, isolated from damaged grapes in Montalcino area (Tuscany), showed a fascinating 2:2 segregation of two unlinked loci: the recessive resistance to a toxic analogue of leucine (5'5'5 trifloroleucine, TFL) and the morphotype. Two of the four M28 meiotic products (spores) in fact grow as smooth colonies while the other two exhibit complex structured filigreed colonies. In this work, preliminary phenotypic investigations demonstrated the uniqueness of the M28 system since the four meiotic products displayed a remarkable phenotypic variability concerning the ability to generate pseudohyphal structures or to invade solid substrates. Additionally, we showed that each spore is able to spontaneously and reversibly switch between the two described morphotypes at high frequencies. Seduced by this puzzling system where Mendelian and Lamarckian theories seems to be reconciled we started a global investigation of the genetic, proteomic and chromatin profiles across the four spores. Using cutting-edge mass spectrometry and sequencing technologies we obtained the following results:

i) we confirmed the genetic determinant of the TFL-phenotype additionally illustrating how this loss of function can massively reshape the amino acid metabolism through the alteration of chromatin accessibility via histone modifications (trimethylation of lysine 4 of histone H3 and acetylation of histone H4);

ii) we demonstrated there are no genetic polymorphisms segregating with the morphotype but rather we identified few epialleles segregating 2:2 with the morphotype;

iii) for the first time we showed the extensive epigenome variability among four meiotic products of a natural *S. cerevisiae* strain;

iv) we found structural protein rearrangements in several prion-like proteins during

the dimorphic transition from filigreed to smooth and vice-versa and showed that for Hrp1 protein this switch is accompanied by a significant change in the number of cells per population bearing the Hrp1p-aggregate.

These results evidenced that both genetic and epigenetic contributions are affecting the phenotypic plasticity in the M28 system proposing an update of the "genome renewal" theory that introduces chromatin reshaping as a rapid adaptive mechanism allowing the appearance of new stable and potentially advantageous traits in the progeny of diploid strains.

Chapter 1

Material and Methods

1.1 Yeast strains and media

The M28 *Saccharomyces cerevisiae* strain was isolated from a damaged grape berry in a Montalcino vineyard (Tuscany, Italy) and described by Cavalieri et al. [33, 34]. Briefly, by inducing M28 to sporulate the authors isolated several tetrads that were dissected into individual meiotic segregants. As the 69% of all the vineyard strains [143] M28 strain is homothallic thus the individuals of the progeny generated from sporulation are homozygous diploid [143]. By inducing M28 to sporulate the authors isolated four tetrads (marked with a sequential number from 1 to 4) that were dissected into individual meiotic segregants (each identified with a letter from A to D). All the dissected tetrads showed a mendelian segregation of two unlinked traits: the recessive resistance to a toxic analogue of leucine (5',5',5',trifluoroleucine, TFL) and colony morphology. Cavalieri and colleagues characterized the TFL resistance phenotype to be associated with a single nucleotide insertion (T9) in the coding region of the SSY1 gene, encoding for a key component of a plasma-membrane amino acid sensor system [26]. The colony morphology in each tetrad was peculiar being characterized by two meiotic segregants with smooth phenotype and two exhibiting a filamentous growth. In this work were used the strains M281A, M281B, M281C and M281D corresponding to the individual meiotic segregants of the M28 tetrad 1. In addition, the diploid strain BY4743 was used as a reference for the comparison

in our analyses. All *S.cerevisiae* strains are listed in Table 1.1. In order to perform the genetic crossing between all the four M28 tetrad 1 spores (M281A-D strains), necessary to confirm the previously observed mendelian segregation of filamentous trait, we decided to delete the HO gene in the homozygous diploid spores. Since the HO gene encodes an endonuclease necessary for the initiation of the interconversion of the mating-type locus that promotes diploidization of haploid strains [82], its deletion allowed the generation of stable haploid strains, unable to switch their mating type. Thus, we deleted the HO gene in all the homozygous diploid spores of M28 tetrad 1 as described below. M281A-D strains were transformed using the lithium acetate protocol [67]. The HO gene was replaced with either the KanMX6 or HphMX6 cassettes by using a PCR-based gene deletion strategy previously described [67]. After transformation, cells were re-suspended in 1 ml YPAD (Yeast extract 1%, peptone 2%, D-glucose 2% supplemented with 75mg/L adenine), and, after 2 hours of adaptation, plated onto YPD supplemented with either 300µg/ml Hygromycin B or 150µg/ml Geneticin. The KanMX6 cassette, flanked by the upstream and downstream regions of HO, was PCR amplified from genomic DNA of the strain BY4742 HO::KanMX6 (Euroscarf collection, University of Frankfurt, Germany) extracted by phenol-chloroform-isoamyl alcohol method. The amplification was carried out with the primers A and D (sequences located upstream and downstream the 3' and 5' nucleotide of the HO gene, respectively). The geneticin-resistant cells were checked for a proper integration by qualitative PCR. The integration was considered proper when all the fragments PCR-amplified showed the expected length as indicated in Table 1.3. The PCR mixture consisted of 1.25 µL buffer (10x), 1µL MgCl2 (2 mM final concentration) 2.5 µL dNTP (0,1 mM final concentration each), 0.4 µL forward primers (10 mM), 0.4 µL reverse primer (10 mM) (final concentration 0,32 mM) 0.02 U AmpliTaqGold DNA Polymerase (Life Technologies, cat. No. 4311816), 25 ng DNA template, water to a final volume of 25 µl. The PCR program consisted of an initial step at 94°C for 3 minutes, followed by 35 cycles of 94°C for 15 seconds, 57°C for 15 seconds and 72°C for 1 minute, before a final elongation step at 72°C for 3 minutes. The KanMX6 cassette was replaced with the HphMX6 cassette in the BY4742 HO::KanMX6 strain through transformation with 15 µg of SacI-SalI-digested plasmid pAG32 [70]. Cells in which the replacement was successful (BY4742 HO::HphMX6) were selected on solid YPD supplemented with Hygromycin B and

validated through qualitative PCR. The HphMX6 cassette, flanked by the upstream and downstream regions of HO, was then PCR amplified from the obtained strain BY4742 HO::HphMX6 as done for the KanMX6 cassette. The following steps of the transformation protocol and validation of the proper insertion of the HphMX6 cassette were identical to the protocol adopted for the transformation with the KanMX6 cassette. In general if not explicitly reported, strains were grown in standard media YPD 2% at 30°C and shaking 180 rpm. For the modified YP media the standard YP composition was maintained except for the concentration of the glucose being 2% glucose for YPD 2% and 10% glucose for YPD 10%. Differently, glucose was replaced as carbon source in the media YPG with galactose, in YPS with sucrose, in YPE with ethanol, in YPGly glycerole and in YPM with mannose at the reported concentrations.

1.2 Colony morphology detection and invasiveness assays

To analyze the morphological phenotype each meiotic segregant of the M28 tetrad 1-4 was initially grown overnight in YPD liquid medium. The following day cells were sequentially diluted in sterile water to a final concentrations of $2x10^6$ cell/ml. 20 µl of each suspension were spotted on solid medium with the appropriate carbon source and left air dry at room temperature under sterile conditions. The culture were then incubated at 30°C. Colony morphology was after 5 days of growth if not specified. To test the capability of natural *Saccharomyces cerevisiae* strains to invade solid substrates we followed the protocol described by Vopalenska et al. [216]. Briefly, 20 µl suspensions of $2x10^6$ cells/ml were separately spotted on plates containing YP glucose 2%, YP ethanol 2% or YP glucose 10%. After four days of incubation colonies were photographed with a digital camera and then washed out from the agar plate using a spatula and water. The media on the plate was stained for 1 h with Coomassie Blue solution (1,25 mg Coomassie Blue, 20 ml 100% Methanol and 5ml Acetic Acid in 50 ml final volume) under gentle shaking. The media was then washed several times for 15 min with water. After this a decoloration step

Strain	TFL- phenotype	Morphotype in YPDE 2%	Genotype	Background	Reference
M281A	Sensitive	Filigreed	Wt (homozygous diploid, MATa/MATα)	*S. cerevisiae* natural strain	Cavalieri (1,2)
M281B	Resistant	Filigreed	Wt (homozygous diploid, MATa/MATα)	*S. cerevisiae* natural strain	Cavalieri (1,2)
M281C	Sensitive	Filigreed	Wt (homozygous diploid, MATa/MATα)	*S. cerevisiae* natural strain	Cavalieri (1,2)
M281D	Resistant	Smooth	Wt (homozygous diploid, MATa/MATα)	*S. cerevisiae* natural strain	Cavalieri (1,2)
M281B_sw	Resistant	Smooth	Wt (homozygous diploid, MATa/MATα)	*S. cerevisiae* natural strain	This work
M281D_sw	Resistant	Filigreed	Wt (homozygous diploid, MATa/MATα)	*S. cerevisiae* natural strain	This work
M282A	Sensitive	Filigreed	Wt (homozygous diploid, MATa/MATα)	*S. cerevisiae* natural strain	Cavalieri (1,2)
M282B	Resistant	Smooth	Wt (homozygous diploid, MATa/MATα)	*S. cerevisiae* natural strain	Cavalieri (1,2)
M282C	Sensitive	Smooth	Wt (homozygous diploid, MATa/MATα)	*S. cerevisiae* natural strain	Cavalieri (1,2)
M282D	Resistant	Filigreed	Wt (homozygous diploid, MATa/MATα)	*S. cerevisiae* natural strain	Cavalieri (1,2)
M283A	Resistant	Smooth	Wt (homozygous diploid, MATa/MATα)	*S. cerevisiae* natural strain	Cavalieri (1,2)
M283B	Resistant	Smooth	Wt (homozygous diploid, MATa/MATα)	*S. cerevisiae* natural strain	Cavalieri (1,2)
M283C	Sensitive	Filigreed	Wt (homozygous diploid, MATa/MATα)	*S. cerevisiae* natural strain	Cavalieri (1,2)
M283D	Sensitive	Filigreed	Wt (homozygous diploid, MATa/MATα)	*S. cerevisiae* natural strain	Cavalieri (1,2)
M284A	Sensitive	Smooth	Wt (homozygous diploid, MATa/MATα)	*S. cerevisiae* natural strain	Cavalieri (1,2)
M284B	Sensitive	Smooth	Wt (homozygous diploid, MATa/MATα)	*S. cerevisiae* natural strain	Cavalieri (1,2)
M284C	Resistant	Filigreed	Wt (homozygous diploid, MATa/MATα)	*S. cerevisiae* natural strain	Cavalieri (1,2)
M284D	Resistant	Filigreed	Wt (homozygous diploid, MATa/MATα)	*S. cerevisiae* natural strain	Cavalieri (1,2)
M281A haploid	Sensitive	Filigreed	hoD::KanMX6, MATa	*S. cerevisiae* natural strain	This work
M281A haploid	Sensitive	Filigreed	hoD::KanMX6, MATα	*S. cerevisiae* natural strain	This work
M281A haploid	Sensitive	Filigreed	hoD::HphMX6, MATa	*S. cerevisiae* natural strain	This work
M281B haploid	Resistant	Filigreed	hoD::KanMX6, MATα	*S. cerevisiae* natural strain	This work
M281B haploid	Resistant	Filigreed	hoD::KanMX6, MATa	*S. cerevisiae* natural strain	This work
M281C haploid	Sensitive	Filigreed	hoD::KanMX6, MATa	*S. cerevisiae* natural strain	This work
M281C haploid	Sensitive	Filigreed	hoD::HphMX6, MATα	*S. cerevisiae* natural strain	This work
M281D haploid	Resistant	Smooth	hoD::HphMX6, MATa	*S. cerevisiae* natural strain	This work
M281D haploid	Resistant	Smooth	hoD::HphMX6, MATα	*S. cerevisiae* natural strain	This work
M281D haploid	Resistant	Smooth	hoD::KanMX6, MATa	*S. cerevisiae* natural strain	This work
M281D HRP1-GFP	Resistant	Smooth	HRP1-GFP:HphMX6	*S. cerevisiae* natural strain	This work
M281D_sw HRP1-GFP	Resistant	Filigreed	HRP1-GFP:HphMX6	*S. cerevisiae* natural strain	This work
BY4743	Sensitive	Smooth	MATa/alpha; his3D1/his3D1; leu2D0/leu2D0; met15D0/MET15; LYS2/lys2D0; ura3D0/ura3D0	*S. cerevisiae* S288C isogenic yeast strain	[23]

Table 1.1: *Saccharomyces cerevisiae* strains used in this work

Primer name	Orientation	Sequence
A	FW	5'-TATTAGGTGTGAAACCACGAAAAGT-3'
B	RV	5'-ACTGTCATTGGGAATGTCTTATGAT-3'
C	FW	5'- GAGTGGTAAAAATCGAGTATGTGCT-3'
D	RV	5'-CATGTCTTCTCGTTAAGACTGCAT-3'
KANFW	FW	5'-TGATTTTGATGACGAGCGTAAT-3'
KANRV	RV	5'-CTGCAGCGAGGAGCCGTAAT-3'

Table 1.2: List of primers used for the HO gene replacement with the KanMX6 and HphMX6 cassettes

Primer FW	Primer RV	Expected length wild-type (bp)	Expected length *HO::KanMX6* (*HO::HphMX6*) (bp)
Primer A	Primer D	2407	2230
Primer A	Primer B	679	NA
Primer A	Primer KANRV	NA	565
Primer C	Primer D	638	NA
Primer KANFW	Primer D	NA	1007

Table 1.3: Expected band lenght of all all the PCR-amplified fragments of HO deletion

was carried out with destaining solution (2,5 ml Methanol and 3,75 ml acetic acid in a total volume of 50 ml). Cell invasion patterns were then photographed with a digital camera combined with the Leica MZ16 F stereomicroscope.

The analysis of phenotypic switch frequencies was performed as follow. Strains were initially grown overnight in YPD liquid medium at 30°C and under continuous shaking (180 rpm). The following day cells were sequentially diluted in sterile water to a final concentrations of $2x10^3$ cell/ml and then spotted on YPE 2%. To have statistically robust switch frequency we screening in average 5000 colonies per sample per condition. Switch frequency was then calculated as the ratio between switched and not-switched colonies analyzing the morphotype after 5 days incubation at 30°.

1.3 Growth curves and doubling times calculation

S. cerevisiae strains M281A-D and BY4743 growth was monitored using the Synergy 2 (BioTek) multi-mode microplate reader. Optical density was measured every hour for 24 hours at a wavelength of 600 nm (OD600), keeping the plate under continuous shaking. Since in YP supplemented with both 2% glucose and 2% ethanol the high aggregation rate led to low reproducible OD measurements for those conditions we repeated the experiment using the ClarioStar microplate reader (Molecular Devices) that allowed a more suitable samples shaking. We used the following settings: wavelength 600nm, double orbital shaking, 145 cycles with a 600 seconds cycle time. In order to measure the cell doubling time a linear regression was carried out on the resultant growth curves by correlating log2 (OD600) with time. The exponential phase growth was identified as the interval of time in which the fitted curves showed the following characteristics: the best fitting (namely, when the growth curve is linear), slopes differing from zero. The doubling time was thus calculated in this interval as the ratio log2(2)/slope of the fitted curve.

1.4 Guanidine GdHCL curing

For each tested strain two identical liquid cultures were developed and incubated overnight at 30° with shaking at 180 rpm on an orbital shaker. Medium used for the pre-inoculum was the same used for the curing (YPE 2% if not reported). The xext day, 10^5 cells/ml were inoculated in fresh medium containing the appropriate carbon source. After 4h growth allowing cells to reach the early exponential phase, one of the two culture was treated with 5mM GdHCl. During the course of the experiment, culture aliquots were removed after 8 hours (approximately 4 generations) and 16 hours (approximately 8 generations) and the cells were harvested. After each sampling, half of the medium was replaced with fresh medium scontaining 5mM GdHCl. Sampled cells were washed with sterile water and diluted, and aliquots were spread onto solid medium supplemented with the reported carbon source to determine the ratio of filigreed and smooth colonies (after 4-days growth at 30°C). To have statistically robust switch frequency we screening in average 5000 colonies per sample per condition.

1.5 Microarray sample preparation

Strains were inoculated in both YPE 2% and YPD 2% liquid medium and were grown overnight at 28°C with shaking. The next day, when cells reached a 0.6 OD (corresponding to growth in exponential phase) were harvested through flash freezing in liquid nitrogen. Next, RNA was extracted from flash-frozen pellets using the hot-acid–phenol method. RNAs were quantified spectrophotometrically using NanoDrop (Thermo scientific) and measuring absorbance at 230, 260, 280 nm and 260/230 and 260/280 ratios, considering good data around 1.8-2.2. Integrity of RNA was checked both by electrophoresis in agarose gel 1% stained with ethidium bromide and through the Agilent 2100 Bioanalyzer system (Agilent Technologies, Palo Alto, USA). Gene expression analysis was carried out using Agilent Yeast Oligo Microarray 4x44 (V1) (Agilent Technologies), using Spike-Ins as internal controls (Two-Color RNA Spike-In Kit, Agilent Technologies). Total RNA (300ng) was reverse transcribed into cDNA by incorporating a T7 oligo-dT promoter primer prior

to the generation of fluorescent cRNA using Agilent Quick Amp Labelling Kit (Agilent Technologies, Palo Alto, USA). The labelled cRNA was purified using a Quiagen RNeasy Mini Kit (Qiagen) and quantified using a NanoDrop instrument. Cy3- (reference) and Cy5-labelled (sample) cRNAs were hybridised to the array using a Gene Expression Hybridisation Kit (Agilent Technologies, Palo Alto, USA). The hybridisation chamber was incubated in Agilent SureHyb chambers for 16 hours at 65°C and rotating at 15 rpm. The microarray slides were washed according to the manufacturer's instructions and then scanned on a Agilent DNA Microarray Scanner (G2505C, Agilent Technologies, Palo Alto, USA)

1.6 Microarray data analysis

The scanned TIFF images were analyzed numerically using the Agilent Feature Extraction Software (v 10.7.3.1) to quantify microarray fluorescence. The "GE2_107_Sep09" default protocol, recommended for the 2-color microarray-based gene expression analysis (Quick Amp Labeling), was used. Feature Extraction produces a QC report for each array aimed to help evaluate the quality as well as the reproducibility and reliability of each microarray. Differential expression analysis was performed using Bioconductor limma package [171]. Data have been corrected for the background with the "subtract" method which subtracted the average background intensities from the foreground intensities for each spot. To remove any systematic trends from the expression measures due to the microarray technology rather than to real biological differences between RNAs, data were also normalized within-array (loess normalization) so that the log-ratios average to zero within each array. We selected significantly differentially expressed genes applying a 4-fold change cutoff and a multiple test corrected (Benjamini and Hochberg's method) p-value cutoff of 0.05.

1.7 Yeast sampling and processing for MS

Yeast cells (strain M281A-D as previously described and diploid *S. cerevisiae* strain BY4743) were grown in either liquid YPD (2% glucose) or YPE (2% ethanol) to

an OD600 between 0.6 and 0.8. The respective YP-medium was removed by centrifugation and the cells were washed twice with synthetic complete (SC) medium before being resuspended in the respective SC medium. Subsequently, cells were quenched by the addition of pure trichloroacetic acid (TCA, Sigma Aldrich) to a final concentration of 10% (v/v) followed by a centrifugation step (4000 rcf, 5 min at 4°C) to yield the cell pellet. The pellet was washed twice with cold acetone before being either snap-frozen or subjected to the cell lysis procedure. To lyse the cells, the pellet was first mixed with acid-washed glass beads (Sigma) and lysis buffer containing 8M urea, 0.1M ammonium bicarbonate (ABC) and 5mM EDTA. The mixture was then transferred to a FastPrep-24TM 5G Instrument (MP Biomedicals) where the cells were disrupted by 6 rounds of beads-beating à 30 seconds with 120 seconds pause between the runs, all at 4°C. The beads and cell debris were removed by centrifugation at 16'000 rcf for 10 minutes at 4°C and the remaining supernatant was collected followed by the determination of its protein concentration with the bichinonic acid (BCA) assay (Thermo Fisher Scientific). Based on the protein concentration determined by the BCA assay, equal amounts of extracts were employed to subsequent sample preparation steps for MS analysis. In the first step, Tris(2-carboxyethyl)phosphine-HCl (TCEP-HCl, Thermo Fisher Scientific) was added to a final concentration of 5mM (30 min, 37°C) to reduce the disulfide bridges which is followed by the alkylation of free cysteine residues with iodoacetamide (IAA, Sigma) at 10mM final concentration (30 min, RT). LysC digestion was performed in undiluted extracts (8M urea), at an enzyme to substrate (E/S) ratio of 1/100 for at least 2 hours at 37°C. Prior to the addition of trypsin, the reaction mixtures were diluted with 0.1M ABC to reach a urea concentration lower than 1.5M. Trypsin digestion was carried out at an E/S ratio of 1/100, overnight at 37°C. Protease digestions were quenched by lowering the reaction pH to < 3 with the addition of formic acid. Peptides were desalted using Sep-Pak C18 cartridges according to manufacturer's instructions. After elution from the cartridges, peptides were dried using a vacuum centrifuge and resuspended in 0.1% formic acid for MS measurement.

1.8 LC-MS/MS and data analysis

Peptide separation was achieved on an online EASY-nLC 1000 HPLC system (Thermo Fisher Scientific) operated with a 40 cm long reversed-phase analytical column (packed in house, with Reprosil Pur C18 Aq, Dr. Maisch, 1.9 µm) prior to the injection via electrospray ionization (ESI) into a Q-Exactive Plus (QE+) mass spectrometer. Peptides were eluted from the column within a 3 hour-gradient from 5% to 25% acetonitrile, at a constant flowrate of 300 nl/min. Resolution for the precursor ion scans was set to 70'000 at 200 m/z, followed by a Top20 MS/MS spectra acquisition in the Orbitrap after higher-energy induced dissociation (HCD) at 17'500 at 200 m/z with a dynamic exclusion of 30 seconds. Using SEQUEST embedded in the Proteome Discoverer software v1.4 (both Thermo Fisher Scientific), raw data were searched against the in-house assembled M28 database (previously described) or the *S. cerevisiae* S288C SGD reference database respectively, with trypsin as the digestion enzyme, allowing two missed cleavages and no cleavages at lysine-proline (KP) and arginine-proline (RP) sites. Mass tolerance was set at 10 ppm for precursor ions and 0.02 Da for fragment ions. Cysteine carbamidomethylation (+ 57.021 Da) was set as static modification and methionine oxidation (+15.995 Da) as dynamic modification. To filter the search results, false discovery rate (FDR) estimated by the Percolator (in Proteome Discoverer) was set to 1% on the peptide level. Label-free quantitation was carried out with the Progenesis-QI Software (Nonlinear Dynamics, Waters) followed by subsequent statistical analysis with the SafeQuant package as previously described [68]. Pair-wise comparisons were performed among all four spores (A, B, C and D) of M28 grown on YPE. An additional comparison was drawn between the pool of TFL-sensitive spores (A and C) and the pool of TFL-resistant spores (B and D), grown on YPE.

1.9 Limited proteolysis

For limited proteolysis experiments, yeast cells were collected by centrifugation and washed twice with PBS buffer. The pellet was mixed with acid-washed glass beads (Sigma) and non-denaturing LiP-buffer containing 20 mM HEPES, 150mM KCl and

10 mM MgCl2. Cells were disrupted gently at 4°C on a FastPrep-24TM 5G Instrument (MP Biomedicals) by 3 rounds of beads-beating for 30 seconds with 5 minutes pause between the runs. The mixture was cleared by centrifugation at 800 rcf for 5minutes at 4°C and the protein concentration of the remaining supernatant was determined by with the bicinchoninic acid (BCA) assay (Thermo Fisher Scientific). Limited proteolysis was carried out using proteinase K (PK, Sigma Aldrich). Yeast extracts were treated with PK at an E/S ratio of 1/100, at 25°C with constant agitation in a Thermomixer and the reaction was quenched immediately after 5 minutes by boiling the tubes at 100°C. After cooling down, a sodium deoxycholate (DOC) solution (10% w/v) was added to a final concentration of 5% (w/v) and the samples were subjected to downstream MS sample preparation as described above with the following modifications: 1) LysC and trypsin digestion were both performed at 1% DOC concentration; 2) After the addition of formic acid to inactivate the proteases, the reaction mixture was cleared by centrifugation at 16'000 rcf, for 10 minutes to remove DOC precipitates.

1.10 Whole genome sequencing and analysis (Appendix data)

For PacBio and Illumina whole genome sequencing, genomic DNA was prepared using a Qiagen Genomic-tip kit (50-100 kb). DNA quality was assessed by mean of agarose gel electrophoresis and quantification was performed through the Qubit® Fluorometric Quantitation system (Thermo Fisher Scientific). PacBio standard library preparation, SMRT cell sequencing and titration SMRT (Single Molecule Real Time) cells were performed at the Lausanne Genomic Technologies Facility, Center for Integrative Genomics of the University of Lausanne. The Illumina libraries were prepared at the National Genome Analysis Center (CNAG) using the TruSeq DNA Library Prep Kit (Illumina). DNA sequencing was performed with the Genome Analyzer II (GA II) system using the 2x150 bp paired-end sequencing protocol (Illumina). Base-calling was performed with Illumina RTA (Real-Time Analysis) Version 1.8.70.0. Reads quality was visually inspected by means FastQC software

(http://www.bioinformatics.babraham.ac.uk/projects/fastqc/) and required trimming and filtering were performed with trimmomatic software [22] using a mean Phred score cutoff of 30 on sliding windows of 20 bp and a step size of 5 bp. Reads were aligned against the assembled genome using Bowtie2 in strict mode [110] while Genome Analysis Toolkit (GATK) from Broad Institute was used to call genetic variants across all the 4 meiotic segregants (M281-A,B,C,D). All variant steps (calling, merging and filtering) were performed according to GATK Best Practices recommendations [47, 135]

1.11 Genome Assembly (Appendix data)

M28 genome was obtained from roughly 100X coverage of PacBio reads assembled using Hierarchical Genome Assembly Process (HGAP) (PMID: 23644548). This strategy consists of 3 main steps: pre-assembly, assembly and consensus polishing. During the first step (pre-assembly) reads were mapped one to each other to produce long and highly accurate sequences used in the second step. De novo assembly phase exploits an Overlap - Layout - Consensus (OLC) (PMID: 20211242) approach to produce consensus sequences (contigs) that were compared against the initial set of stata to measure inconsistencies, mainly insertion-deletion and base substitution, on contigs (consensus polishing step). Currently various implementation of this approach are available (PMID: 23644548) and, to assembly m28, the software directly developed by PacBio company was used.

1.12 Chromatin Immunoprecipitation Sequencing (ChIP - Seq) procedure

Chromatin extraction was performed essentially as described by Aparicio et al., [7] with the following modifications. Yeast cells were grown in YPE liquid medium at 27°C with shaking at 200 rpm for 4/5 h on an orbital shaker. This step allowed cells to pre-adapt to fermentative growth, reducing the long lag period before log phase growth. Next, 10^5 cells/ml were inoculated in 60 ml liquid YPE and incubate at

27°C with shaking at 200 rpm on an orbital shaker. When cells were in exponential phase, 37% formaldehyde was added to a final concentration of 1%. Cross-link was performed for 30 minutes at room temperature by shaking slowly (70 rpm) on an orbital shaker. Cell lysis was carried out using the Qiagen TissueLyser for 30 seconds at oscillation frequencies of 30 Hz, followed by 1 minute ice incubation. This cycle was repeated 4 times. Chromatin was sheared by sonicating samples with a Bioruptor (Diagenode) 6 times with the following cycle: 30 sec ON, 30 sec OFF, low power mode. Chromatin Immunoprecipitation was carried out with Dynabeads ® (Life Technology) Protein A/G with a chromatin to antibody 5:1 ratio. All the antibodies used in this work are listed in Table 1.4. Washing and elution steps were performed as suggested by the manufacturer instructions (Dynabeads ®, Life Technology). Reverse cross linking was carried out adding 10 µl of 5M Nacl to the samples. After an overnight incubation at 65°C, 1 µl of DNAse-free RNase A (100 mg/ml) was added. After a 15 min incubation at 37° C DNA was purified using a Qiagen PCR-purification spin column as per manufacturer's instructions. Finally, DNA was eluted in 43 µl of 40°C pre-warmed nuclease-free water (or buffer TE). Indexed paired-end libraries of DNA obtained from chromatin immunoprecipitation were prepared as described in the Illumina TruSeq Nano DNA Sample Preparation Guide, for subsequent DNA sequencing through Illumina MiSeq sequencer. We followed the 350 bp insert size workflow starting with 100ng of DNA for each library. The quality control, to verify fragments size, was performed with the Bioanalyzer System through the Agilent DNA 12000 Kit. Libraries quantification was performed through the Qubit® Fluorometric Quantitation (Thermo Fisher Scientific) in order to optimize cluster densities across every lane of a flow cell. The target DNA (pool) was prepared as reported in the Appendix B of the Illumina Sequencing Library qPCR Quantification Guide. The quantification of a set of random libraries was controlled through the Real-Time PCR system (BIO RAD preferred) using the KAPA Library Quantification Kit – Illumina Sequencing platforms.

Antibody	Description	Supplier	Catalog #
Anti-Histone H3 antibody - Nuclear Loading Control and ChIP Grade	Rabbit polyclonal to Histone H3	AbCam	ab1791
Anti-Histone H3 (tri methyl K4) antibody - ChIP Grade	Rabbit polyclonal to Histone H3 (tri methyl K4)	AbCam	ab8580
Anti-Histone H3 (di methyl K4) antibody - ChIP Grade	Rabbit polyclonal to Histone H3 (di methyl K4)	AbCam	ab7766
Anti-Histone H4 (ChIP Grade)	Rabbit polyclonal to Histone H4	AbCam	ab10158
Anti-Acetyl-Histone H4	Rabbit Polyclonal Antibody	Upstate(Millipore)	08-866

Table 1.4: List of antibodies used for the chromatin immunoprecipitation of histones H3 and H4 and relative modifications

1.13 Bioinformatic pipeline for ChIP sequencing data analysis

52 ChIP libraries were sequenced on an Illumina MiSeq sequencing system using a 15 Gb flowcell. The MiSeq Reagent v3 chemistry was used to produce paired-end reads with an average length of 300 bp. A QC check was performed in each library, stored as a FASTQ file using the FastQC program (http://www.bioinformatics.babraham.ac.uk/projects/fastqc/). We evaluated quality of libraries analyzing read length, per base quality score, per sequence quality scores, GC content, nucleotide content, sequence duplication and overrepresented sequences. Raw reads were preprocessed by trimming the 3'end using a cut-off Phred score of 30 through FASTX-Toolkit (http://hannonlab.cshl.edu/fastx_toolkit/). High quality reads were then aligned to the M281B newly assembled genome with Bowtie 2 (http://bowtie-bio.sourceforge.net/ bowtie2/index.shtml) using paired-end alignment with default parameters but allowing 1 mismatch in the aligning seed region. The Sequence Alignment/Map (SAM) format generated by Bowtie2 (version 2.2.4; bowtie-bio.sourceforge.net/ bowtie2/index.shtml) was then first converted to BAM (the binary form of SAM) and then indexed using SAMtools (version 1.2; http://samtools.sourceforge.net/). Percentage of aligned reads was evaluated with SAMtools and corresponds to the fraction of paired end reads that map with the maximum quality value 255. Coverage

was calculated counting the number of reads per genomic position using the "genomecov" tool of Bedtools 2.25.0 (http://bedtools.readthedocs.io/en/ latest/content/tools /genomecov.html). ChIP-enriched regions were identified with SICER (version 1.1)[228]. The window size for the peak calling was set as 200 bp with a gap value for the allowed distance between two consecutive peaks set to 0. The fragment size was set to 350, the false discovery rate (FDR) for the peak call to 0.01 and the E-value for the background threshold to 0.01. SICER-df.sh was applied to compare libraries in a pairwise mode and call differentially enriched region with a FDR = 0.01. The algorithm first performs a pre-screening identifying a set of candidate enriched regions (islands) using a random background model with a lenient E-value threshold using SICER.sh in each of the two pairs. Next, ChIP per nucleotide densities (chromatin-associated DNA immunoprecipitated with Anti-Histone H3 (tri methyl K4) antibody, Anti-Histone (bi methyl K4) antibody, Acetyl anti-Histone H4 antibody, 3 replicates per sample) were compared with input DNA per nucleotide densities (chromatin-associated DNA immunoprecipitated with Anti-Histone H3/H4 antibodies, 2 replicates per sample) to determine the significance of enrichment at the called islands. This step computes p-value and q-value of each candidate island. Next, the two sets of significant islands are merged and used for the comparison. On each merged island, level in sample 1 (i.e M281A H3 2MetK4) is compared with that in sample 2 (i.e M281B H3 2MetK4) to determine the significance of changes. This step computes fold-change differences and p-value for each merged island. The FDR is next calculated using p-value adjusted for multiple testing, following the approach developed by Benjamini and Hochberg [16]. A q-value cutoff of 0.01 was applied to filter out not significant candidate islands. In order to compare different samples for the same histone modification, overlapping or "book-ended" ChIP-enriched regions were combined together with the "mergeBed" tool of Bedtools 2.25.0. M281A genomic sequences corresponding to the region defined by each selected merged island were retrieved and a BLASTN alignment was carried out against the reference *S. cerevisiae* genome (S288C, version R64-2-1). Further, functional annotation was retrieved for each ChIP enriched island by comparison with. the "SGD_features.tab" file downloaded from the SGD website (S288c Genome Version R64-2-1) reporting the information on chromosomal features. Additionally, promoter regions were defined as those DNA sequences located at the 5' of the corresponding ORF and

stretching for 455 bp [100]. Differently, intergenic regions were defined as those DNA sequences lacking a chromosomal feature. We performed all possible pairwise set of measurements between all the different samples at each island. Given an island i, we measured the relative abundance of island i in sample A compared to sample B which we call ab_{i}. With four samples, we thus obtained 6 relative measurements (ab_{i} ac_{i} ad_{i} bc_{i} bd_{i} cd_{i}) which we define as $\mathrm{ER_i}$ (the Experimentally measured Ratios of abundances in island i). To be able to compare multiple samples at the same time, we sought to recover relative amounts these ratio measurements. We define the vector I as: [a_{i}, b_{i}, c_{i}, d_i] - corresponding to the original amounts of samples that gave rise to the observed ratios.

Our problem can then be posed as:

$argmin(I) = (jk_i - j_ik_i)2$

Where jk_i are the experimentally measured ratios of abundances, and j_i/k_i are the ratios of abundances we calculated from elements of i, and the summation is over all combinations of j and k present in I. More simply, we are looking to find abundance values that can reproduce the ratios we observe in experiments. This problem is obviously not convex: as we are aiming to reproduce ratios, if I is a solution, then 2*I will be a solution as well. To solve this problem, we normalize each row i by the maximum value to define a unique solution - with 1 as the maximum value. These relative values do not allow comparisons between islands, but they do allow us to quickly compare elements within a single island, and they allow us to identify experiments with potentially problematic values, where we cannot recover any abundance value I that reproduce all of the experimentally measured ratios.

1.14 Enrichment Analysis

We used the Gene Ontology (GO) downloaded from the "Curated Data" session of the SGD website (http://www.yeastgenome.org/). The GO ontology is structured as a directed acyclic graph (DAG), where terms (nodes) are linked together according to their parent-child relationship. Parent nodes correspond to broad terms while children terms describe more specific annotations. Taking advantage of the ontology

	M281 strain	Total number of raw reads	Number of reads mapped	Number of reads mapped and paired	Number of reads mapped but not paired (%)	Numbero fo unmapped reads (%)	Total covered nucleotides	Mean insert size in bp (calculated from the mean distance between paired reads aligned positions)
Met3	M281A	693232	677299	674053	3246 (0.48)	15933 (2.3)	2E+08	436.5
		994004	971624	966539	5085 (0.52)	22380 (2.25)	2.9E+08	427.8
		987653	964680	960462	4218 (0.44)	22973 (2.33)	2.9E+08	439.2
	M281B	881564	858189	853319	4870 (0.57)	23375 (2.65)	2.6E+08	432.4
		962638	937625	932807	4818 (0.51)	25013 (2.6)	2.8E+08	427.2
		912808	891639	888229	3410 (0.38)	21169 (2.32)	2.6E+08	427.3
	M281C	832609	816668	812442	4226 (0.52)	15941 (1.91)	2.4E+08	434.1
		828570	812586	808940	3646 (0.45)	15984 (1.93)	2.4E+08	429.5
		1042992	1022182	1016581	5601 (0.55)	20810 (2)	3E+08	430.1
	M281D	1047771	1024663	1020147	4516 (0.44)	23108 (2.21)	3E+08	420.8
		1020539	997547	991999	5548 (0.56)	22992 (2.25)	3E+08	426.5
		980295	960074	955831	4143 (0.43)	20221 (2.06)	2.8E+08	426.3
Met2	M281A	757647	738167	734723	3444 (0.47)	19480 (2.57)	2.2E+08	429.6
		1085950	1056359	1050173	6186 (0.59)	29591 (2.72)	3.1E+08	431.6
		1161672	1131856	1126615	5241 (0.46)	29816 (2.57)	3.4E+08	432.9
	M281B	980300	951550	946399	5151 (0.54)	28750 (2.93)	2.8E+08	438.1
		918810	890526	886138	4388 (0.49)	28284 (3.08)	2.6E+08	437
		965239	939100	934768	4332 (0.46)	26139 (2.71)	2.8E+08	436.1
	M281C	976627	955870	950221	5649 (0.59)	20757 (2.13)	2.8E+08	442.3
		1111451	1087186	1081436	5750 (0.53)	24265 (2.18)	3.2E+08	432
		1118491	1094535	1087385	7150 (0.65)	23956 (2.14)	3.3E+08	442.5
	M281D	1105575	1078853	1073858	4995 (0.46)	26722 (2.42)	3.2E+08	429.6
		1226363	1194380	1187013	7367 (0.62)	31983 (2.61)	3.5E+08	438.5
		1026231	1001343	996218	5125 (0.51)	24888 (2.43)	3E+08	431.6
Ac	M281A	927038	888518	883333	5185 (0.58)	38520 (4.16)	2.5E+08	392.6
		619600	593775	590267	3508 (0.59)	25825 (4.17)	1.7E+08	396.8
		1010437	969140	962986	6154 (0.63)	41297 (4.09)	2.7E+08	391.8
	M281B	1125884	1074967	1068940	6027 (0.56)	50917 (4.52)	3E+08	396.2
		573013	544232	541065	3167 (0.58)	28781 (5.02)	1.6E+08	452.4
		608861	582925	579665	3260 (0.56)	25936 (4.26)	1.7E+08	433.3
	M281C	1178369	1143585	1135254	8331 (0.73)	34784 (2.95)	3.4E+08	422.9
		1110472	1077006	1069412	7594 (0.71)	33466 (3.01)	3.2E+08	434
		1237586	1201816	1194014	7802 (0.65)	35770 (2.89)	3.5E+08	420.3
	M281D	868745	835719	831159	4560 (0.55)	33026 (3.8)	2.5E+08	424.9
		1368185	1316431	1311066	5365 (0.41)	51754 (3.78)	3.8E+08	380
		1029783	984801	979697	5104 (0.52)	38982 (3.81)	2.9E+08	419.7
H3 INPUT	M281A	1139112	1119161	1112330	6831 (0.61)	19951 (1.75)	3.3E+08	432
		1059050	1040845	1033861	6984 (0.67)	18205 (1.72)	3.1E+08	429.1
	M281B	1044273	1022054	1016184	5870 (0.57)	22219 (2.13)	3E+08	430
		1055642	1032249	1026751	5498 (0.53)	23393 (2.22)	3.1E+08	430.7
	M281C	1119973	1103983	1094841	9142 (0.83)	15990 (1.43)	3.3E+08	434.8
		1018185	1003006	995505	7501 (0.75)	15179 (1.49)	3E+08	437.3
	M281D	1076180	1055601	1049574	6027 (0.57)	20579 (1.91)	3.1E+08	429.3
		844875	829873	813184	16689 (0.61)	15002 (1.78)	2.5E+08	429.5
H4 INPUT	M281A	1243852	1222341	1213952	8389 (0.69)	21511 (1.73)	3.6E+08	424.3
		1140826	1120521	1112566	7955 (0.71)	20305 (1.78)	3.3E+08	435.4
	M281B	919172	899761	893644	6117 (0.68)	19411 (2.11)	2.7E+08	430.9
		672758	657913	653460	4453 (0.68)	14845 (2.21)	2E+08	433.6
	M281C	1051099	1037060	1029773	7287 (0.7)	14039 (1.34)	3.1E+08	421.5
		767710	756641	750771	5870 (0.78)	11069 (1.44)	2.2E+08	434.5
	M281D	1090087	1070825	1064491	6334 (0.59)	19262 (1.77)	3.2E+08	419.1
		787473	773973	769492	4481 (0.58)	13500 (1.71)	2.3E+08	421.5

Table 1.5: Chromatin immunoprecipitation sequencing (ChIP-seq) libraries statistics. For each sample the total number of raw, mapped and not mapped reads as well as the total number of covered nucleotides and the mean insert size were reported. M3Met K4 H3 (Met3), 2Met K4 H3 (Met2), H4 Ac (Ac) were performed in triplicate while the relative inputs (H3 INPUT, H4 INPUT) in duplicate.

structure, all genes annotated to a child term were also annotated to the corresponding parent term. Particularly for each 'parent' term all the genes belonging to the corresponding 'child' terms were tracked and added to the 'parent' term. When the 'parent' term did not contain the same qualifier than the 'child' term, the qualifier was added to the parent thus allowing the transfer of the information. Once all genes were annotated to both children and parent terms throughout the ontologies the enrichment analysis was performed. The hypergeometric statistical test was used to identify significant enriched GO categories within a class of significantly differentially expressed proteins. The multiple testing correction was performed with the Bonferroni procedure. The final enriched categories were ranked according to the adjusted P-value. Starting from the more significant enriched category all the related categories ('parent' or 'child') were removed in order to reduce the complexity and the redundancy of the result but preserving the biological outcome

1.15 Network Analysis

A high quality interaction network (Interactome) was constructed as proposed by Stuart and collaborators [195] using curated interaction data available in both SGD (Saccharomyces Genome Database) and YEASTRACT (www.yeastract.com, http://www.yeastract.com/download.php) websites. From SGD the "interaction_data.tab" file, containing the interaction data incorporated from BioGRID was downloaded

(http://downloads.yeastgenome.org/curation/literature/interaction_data.tab).

The list of documented regulations between all transcription factors and genes interactions (tf interactions) was downloaded from the yeast transcription factors YEASTRACT database ("RegulationTwoColumnTable_Documented_2013927.tsv.gz "). The interactome was imported in Cytoscape 3.2.0 to perform network analysis. If not otherwise reported the force-directed Fruchterman-Reingold layout was used to display the network.

1.16 Fluorescence microscopy

M281D strain was transformed by using the lithium acetate protocol [67]. The endogenous HRP1 gene was tagged integrating GFP-HphMX6 cassette at endogenous locus following the protocol of Janke et Al. [89]. S1 and S2 primers were designed as follow: S1-primer 50 bases upstream of the ATG (including ATG = start codon) of the HRP1 gene, followed by 5´-CGTACGCTGCAGGTCGAC-3´; S2-primer, the reverse complement of 50 bases downstream of the STOP-codon including STOP) of the HRP1 gene, followed by 5´-ATCGATGAATTCGAGCTCG-3. All images were acquired on a DeltaVision microscope (Applied Precision) equipped with a sCMOS camera (Roper) and solid-state light-emitting diodes (Insight SSI) controlled by Softworx. Fluorescein isothiocyanate (FITC) filter was used for imaging GFP. Images were deconvolved with Softworx software (Applied Precision). All image analyses were performed with Image J software (http://imagej.nih.gov/ij/). The aggregation foci were scored by eye from maximum intensity projected images (spanning the entire volume of the cell) and were defined as region that display high-intensity over the surrounding background signal.

Chapter 2

Introduction

2.1 An introduction to *Saccharomyces cerevisiae*

Thousand years ago, the human mankind made its first encounter with one of those organisms that became a trusted fellow in our cultural and nutritional evolution: the yeast. Among the various yeast species one in particular played a relevant role, the budding yeast *Saccharomyces cerevisiae.* The first evidence of the awareness about the feature of this microorganism are dated back to 7000 B.C [127] witnessed by the dawn of conscious production of fermented foods and drinks. From that period on, humans exploited the capability of yeast to modify and conserve food allowing the beginning of a new nutritional era in human history. Nowadays, we still profit from the activity of this useful microorganism involved in the production of bread, wine, beer and last, but of great relevance, from the capability of yeast to stimulate and interact with our immune system: possibly the beginning of a renewed era for this organism. Yeasts are small eukaryotes being unicellular fungi classified for the most part in the group of Ascomycetes. The yeast cells can exhibit different shapes (spherical, oval or cylindrical) and are surrounded by a cell wall composed of glucans, mannoproteins, often modified by the addition of glycosyl-phosphatidyl-inositol. *S. cerevisiae* (commonly known as baker's yeast) is the first eukaryote whose genome has been completely sequenced in 1996 [33]. Its genome consists of 17 chromosomes with a size ranging from 85 Mb to 1.5Kb (12 Kb in total), and a plasmid known as

2 μm for its mean size. Most of the genome contains encoding DNA (6275 ORFs, verified for 75.25%) while intronic sequences are present only in the 3.8% of the open reading frame (ORF), in contrast to higher eukaryotic organisms which show a wider content of non-coding regions. Since many yeast proteins are similar in sequence and function to those found in other organisms, *S. cerevisiae* has been for many years the most commonly used eukaryotic model for studies on the cell cycle [190], apoptosis [154], mitochondrial functions [112] and many other biological processes. Recently there was a renewed impulse for the research using yeast for studies on aging [193], neurodegenerative disorders [222], and interactions with our immune system [172]. *S. cerevisiae* mainly reproduces through mitosis by a division process known as "budding", which means that the original, "mother" cell gives rise to an ellipsoidal daughter cell; the daughter cell gradually increases in size and finally separates leaving a cellular bud scar [83]. *S. cerevisiae* can exist stably as either a diploid or a haploid and both forms reproduce by mitosis, with daughter cells budding off of mother cells. The haploid individuals exist in two different sex types, defined mating type, "a" or "α", due to the single gene locus "MAT". The haploid cells can mate with other haploid cells of the opposite mating type, producing a diploid cell. Under certain stresses, such as nutrient deficiency, the diploid cells can undergo the process of meiosis producing four haploid spores contained within a defined structure called "ascus". Rather than dividing the chromosomes through mitosis and the mother and daughter cells by cytokinesis at the bud neck, in sporulation the chromosomes are segregated by meiosis, resulting in the production of four haploid nuclei contained in autonomous structured cells called spores. If the environmental conditions are optimal spores can germinate, meaning they re-enter the mitotic cell cycle and resume vegetative growth or they can mate with a cell having an opposite mating type thus generating a diploid cell. This feature makes *S. cerevisiae* a powerful genetic tool since recessive mutations can be conveniently isolated and manifested in haploid strains, and complementation tests can be carried out in diploid strains. MATa and MATα cells secrete a and α pheromones, respectively, that are recognized by sex-specific receptors on the surface cell of the opposite mating type. Pheromones bind to particular cell surface receptors defined G-protein coupled with trimeric G protein (GPCR) leading to the activation of a signal transduction cascade involving the mitogen-activated protein kinase pathway,

MAPK (Fig.2.1). This process ends with the accumulation in the nucleus of Fus3p kinase phosphorylated, which activates Ste12p transcription factor involved in the transcriptional regulation of genes participating in mating, as well as in the invasive and pseudohyphal pathways [92]. Based on their sexual behavior, natural strains of *S. cerevisiae* can be classified as "homothallic", able to change the sexual type, or "heterothallic", unable to change their sexual nature. Both heterothallic and homothallic yeasts can undergo sporulation, the main condition being their ploidy (they should be at least diploid). In order to make yeasts more suitable for genetic analysis, laboratory strains are usually deleted for the HO gene, responsible for the mating type switch as encoding for a site-specific endonuclease that introduces a double-stranded nick at the mating-type locus of homothallic strains initiating the interconversion of sexual types [210]. Existing in both haploid and diploid stably states makes *S. cerevisiae* a powerful tool for genetic investigations allowing the isolation of recessive mutants and mapping of genes responsible for a particular phenotype. This aspect, together with all the curated data available for this organism (well annotated genome, transcriptome and proteome, extensive phenotypic and functional characterizations), the facility to culturing yeast (short doubling time of about. 90 min in rich media, well adapted to both aerobic and anaerobic large-scale cultures) and the presence of several features common to higher eukaryotes makes *S. cerevisiae* a robust model organism for basic biological research.

2.2 Environmental adaptation and the "genome renewal" theory

Since the identification of *S. cerevisiae* as the causing agent of fermentation [158] and the isolation of multiple strains of *S. cerevisiae* from wine grapes [162], thousands of natural strains have been isolated from different sources [145, 155, 65, 111, 189, 149, 80, 140, 146, 45, 134]. Wine *S. cerevisiae* populations are highly diverse, with genetic/genomic differences ranging from single-nucleotide substitutions to chromosome-length polymorphisms and whole-genome duplication (reviewed in [187]). This variability allowed the *S. cerevisiae* population fermenting grapes to ad-

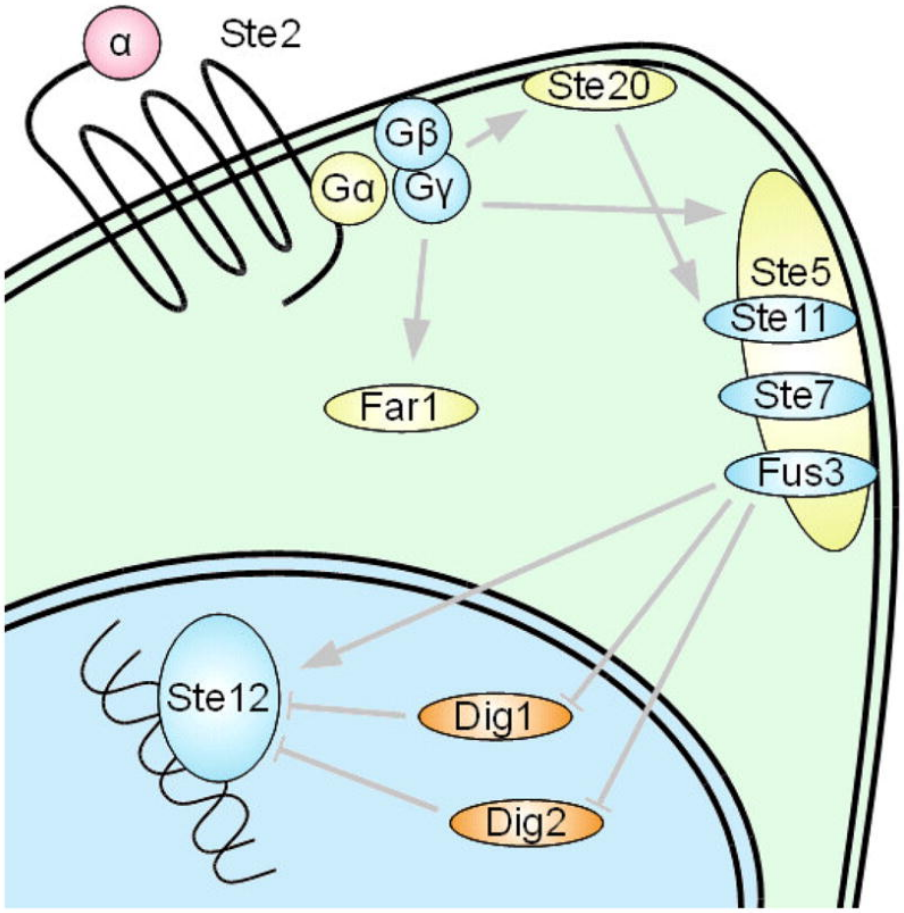

Figure 2.1: The mating MAPK signaling cascade: after the activation of the pheromone receptor the associated G-protein α subunit exchanges GDP with GTP, and releases the βγ complex that successively interacts with both Ste5 and Ste20 activating Ste11, Ste7 and Fus3 kinases. Entering the nucleus, Fus3 regulates the Ste12 transcription factor Ste12 which controls two distinct developmental programs of mating and filamentation (Figure from [92])

apt to fast and continuous changes in the fermentation environment. Also diploidy plays a central role in this adaptation. Beside wine strains are predominantly diploid [143], aneuploidy [8][74], triploidy [200], polyploidy [225] and rarely haploidy [120] are also observed in the natural yeast population fermenting wine. Aneuploidy has been proposed to confer selective advantages by increasing the number of beneficial genes copies or by protecting the yeast against lethal or deleterious mutations [74]. Similarly, diploidy can be advantageous as masking a harmful recessive mutation thanks to the presence of a homologous chromosome carrying the beneficial allele. As a consequence, natural strains are often highly heterozygous [103]. Additionally to heterozygosity, the wine population is mainly characterized by homothallic strains [200] [40][142]. If an homothallic diploid strain is starved for nitrogen or carbon, a complex differentiation program (sporulation) takes place leading to the production of cellular structures called "asci" bearing sexual spores (reviewed in [104]). Each ascus contains four meiotic segregants generated from the parental strain through two rounds of meiosis followed by spore morphogenesis. Although sporulation usually takes place in low-nutrient conditions, Mortimer observed the sporulation of certain wine strains also in sugar-rich media [142]. If the spores produced by an homothallic strain germinate they can produce completely homozygous diploids through the mating type switch followed by auto-diploidization. The generation of new homozygous diploids, termed "genome renewal", was proposed to represent a rapid means for evolution wiping out deleterious heterozygous mutations of the heterozygous parental strain [142]. This hypothesis was criticized by Puig and collaborators [164], based on the observations that i) yeast population are sexually isolated; ii) wine yeasts are highly heterozygous and exhibit low sporulation rates. They rather proposed a gradual adaption to vinification conditions involving mainly aneuploidies and chromosomal rearrangements. Besides this discrepancy, sporulation represents a direct way to genetic adaptation allowing the loss or acquisition of traits thus representing a key process of evolution.

2.3 How the environment shapes yeast physiology and morphology

Several microorganisms evolved with the ability to answer to nutrient variations in the growth environment being immotile and impossibilitate to rapidly reach habitats more suitable for their growth. The transition from nutrient-rich to nutrient-poor environments activates intracellular mechanisms which in turn activates the so-called "adaptive programs". Such programs are connected to phenotypes as invasive growth, hyphae formation and flocculation. The complete absence of nutrients cause haploid cells to stop at the G0 phase of the cellular cycle and to establish a quiescent status. Instead, in diploid cells these environmental conditions trigger the meiosis and sporulation, and finally the generation of haploid spores able to survive in disadvantageous environmental conditions. The filamentous colony growth like that observed in some meiotic segregants analyzed in this work could represent a metabolic strategy for the survival in unfavourable growth conditions. Actually, the formation of colonies with a filamentous aspect has been proposed to be a strategy adopted by the cells to survive in presence of limited nutrients, i.e. because the surface of the colony in direct contact with the environment (thus the number of cells able to import nutrients) is wider in filamentous colonies than in smooth colonies [211].

2.4 Nutritional sensing and signaling and their relationship with filamentous growth

2.4.1 Glucose sensing

Among the nutrients shown to be relevant in defining the colony morphology, sugars play a major role. Glucose is the most abundant monosaccharide in nature and represents the preferential carbon source for *S. cerevisiae*. The sensing for the glucose in the growth environment and the cellular responses activated by the presence of this molecule were widely analyzed in the last years. In particular, *S. cerevisiae*

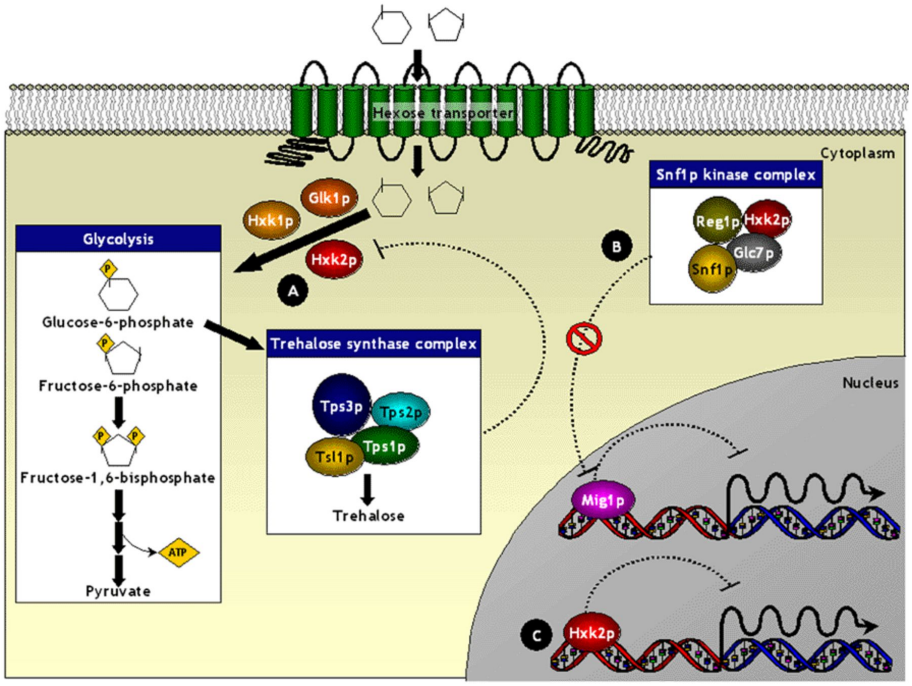

Figure 2.2: Proposed model for the sensing and transmission of glucose signals. In A) the products of hexose kinase catalytic activity exert a regulatory function via Tps1p; in B) Hxk2p indirectly exerts a regulatory role via the Snf1p; in C) Hxk2p directly regulates the SUC2 gene (Figure from [62])

preferentially ferments glucose, therefore it adapted to grow in presence of various concentrations of this sugar activating different cellular responses based on the availability of the molecule in the habitat. Gpr1 and two other glucose transporters, Rgt2 (high glucose concentration sensor) and Snf3 (low glucose concentration sensor), have been proposed as responsible for the the activation of specific intracellular responses based on the perceived glucose concentration, by means of the RAS/PKA pathway (Fig. 2.2). In addition, some enzymes for the glucose phosphorylation, for instance the glucokinase Glk1 and the hexokinases Hxk1 and Hxk2, play a fundamental role in the glucose sensing process and in the regulation of specific genes involved in glucose metabolism [62]. Furthermore, Gpr1 is associated with Gpa2, the alpha subunit of the heterotrimeric G protein. Heitman and collaborators proposed that Gpa2 could regulate the filamentous growth by means of the RAS/PKA pathway, showing how homozygous yeasts defective for the GPA genes are defective also for this phenotype [125]. Gpr1 transmits the signal deriving by the cellular sensing through the pathway RAS/PKA to genes like FLO11 (Fig. 2.3, [39]). Flo11p is a cell-surface flocculin encoding gene shown to be required for filament formation, pseudohyphal formation and invasion in the Σ1278b *S. cerevisiae* strain [219]. FLO11 is co-expressed with STA2 and PGU1 genes, the first encoding for a glucoamylase which allows amid degradation, the latter encoding for an endopolygalacturonase necessary for the depolymerization of the cell wall [129, 62].

2.4.2 Sensing of alternative carbon sources

Although glucose is the preferred carbon source for *S. cerevisiae*, this yeast is able to utilize other sugar types for its own metabolism. Fructose, like glucose, is rapidly phosphorylated and enters the glycolytic cycle. Instead, galactose and mannose are initially converted in glucose-6-phosphate and fructose-6-phosphate respectively, and only after they can be metabolized through the glycolytic cycle. Disaccharides, trisaccharides and oligosaccharides can be utilized as carbon source but they must be first hydrolyzed to free the relative monosaccharides and only subsequently can be metabolized. As an example, sucrose is hydrolysed in glucose and fructose from an enzyme called invertase. Maltose instead is converted in glucose by the action of the maltase. Trisaccharides and polysaccharides are converted in the relative

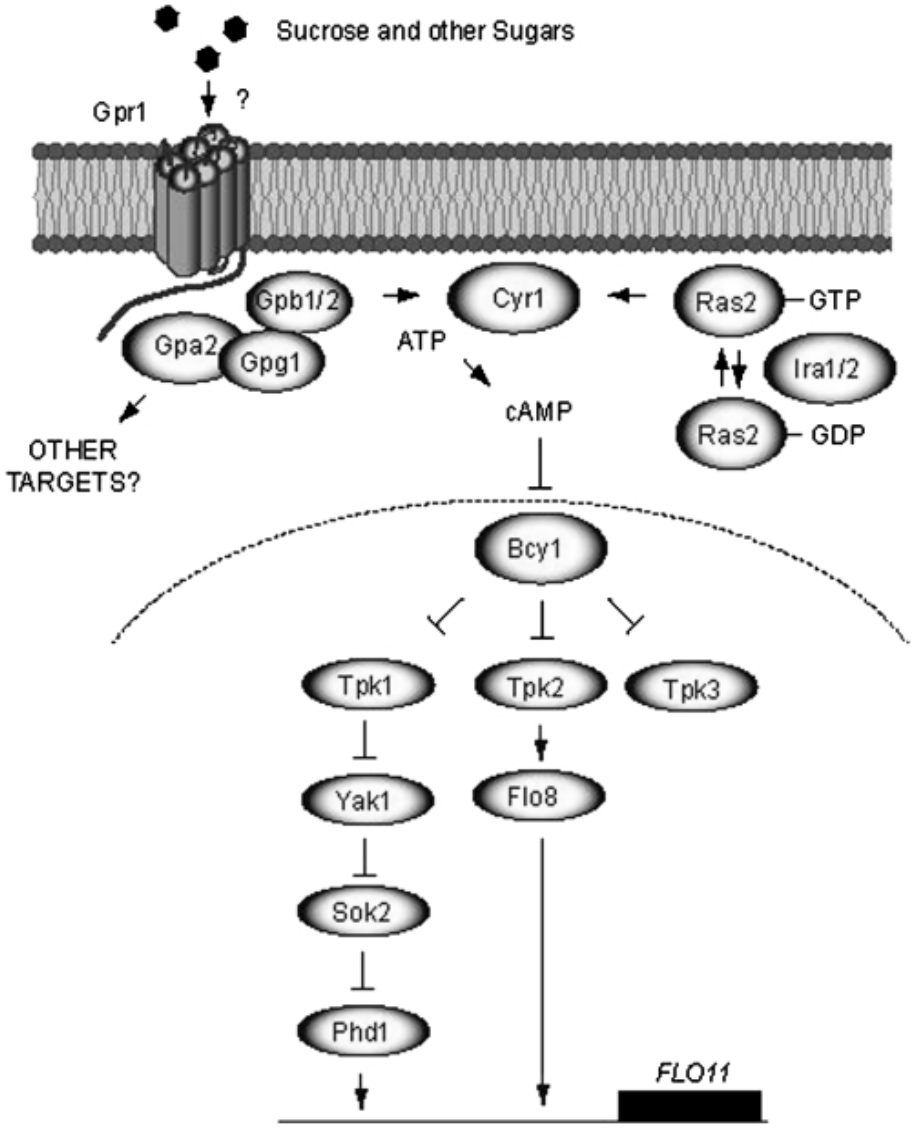

Figure 2.3: The RAS/PKA pathway and its connection to filamentous growth: the Gpr1 receptor transmits an external signal to Flo11 through Flo8 which is activated by Tpk1, Tpk2, Tpk3, all released by Bcy1 after the cAMP binding (Figure from [39]).

monosaccharides by a combination of enzymes. In the vast majority of cases, sugars are not directly perceived by yeast but they rather interact with specific membrane receptors only after their conversion into glucose and fructose in the extracellular environment thanks to the activity of enzymes secreted by the microorganism. In Fig. is reported a scheme representing the proposed mechanism for the sugar sensing in *S cerevisiae* [62]. Additionally, beyond sugars, even other molecules like alcohols can be used as carbon source by the budding yeast. Ethanol and glycerol, are oxidized by *S. cerevisiae* through aerobic metabolism and in particular through the Krebs cycle.

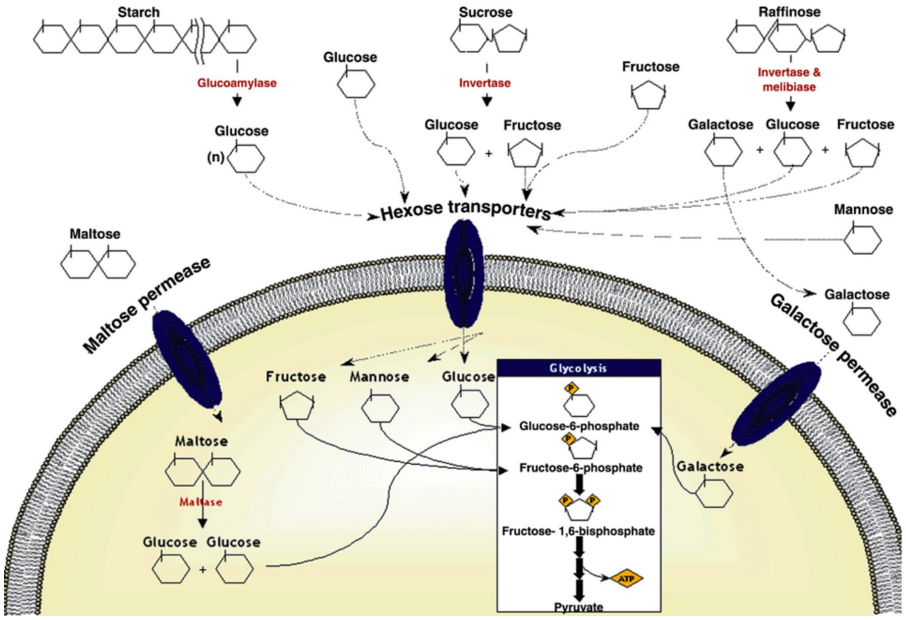

Figure 2.4: A schematic illustration of the different steps involved in the carbon source uptake and utilisation in *S. cerevisiae* (Figure from [62])

2.5 From one cell to many: multicellular yeast communities

The generation of multicellular structures represents a widespread process among fungi. The morphological characteristics of filamentous structures vary among the

different fungal genera and species. The species commonly called "filamentous fungi", form mycelia or hyphae, characterized by elongated and multi-nucleated cells. Other fungal species and strains, among which some *S. cerevisiae* strains, change the shape of their cells and generate pseudo-hyphal structures, similar to hyphae, but composed by multiple cells in spite of a single multi-nucleated cell. Only recently, for some species (i.e. *Schizosaccharomyces pombe*) it has been shown that filamentation is a constitutive part of the cell cycle [5]. So far, the dissection of filamentation has been carried out mainly in pathogenic fungi (i.e. *Candida albicans and Aspergillus fumigatus*), in which this trait is associated to the strain virulence. As a further example, the plant pathogen *Ustilago maydis* cells unable to form filaments are avirulent [13, 79]. In other pathogenic fungi, such as the human fungal pathogen Histoplasma capsulatum, a dimorphic transition from filamentous to yeast growth occurs during infection and is thought to be required for virulence [136]. In general, pathogenic species rely in filamentation to interact with the host, invade its tissues and express virulence traits. As a consequence, human pathogenic fungi are particularly harmful for individuals having a compromised immune system, a consequence of HIV or chemotherapeutic agents [15]. In C. albicans, the single-cell to filaments transition and pathogenicity are strictly connected [118] and the transition is triggered by several extracellular factors among which temperature and the nutrient availability in the environment [18]. This holds the truth even for other pathogenic fungi. In many fungi, nitrogen starvation stimulates filamentous differentiation. The human pathogen *Cryptococcus neoformansmates* forms filaments in response to nitrogen limitation and basidia during its sexual cycle [106, 4] while the emerging opportunistic yeast pathogen *Candida lusitaniae* form filaments if starved for nitrogen on SLAD medium [69]. Finally, the most common fungal pathogen to infect humans, C. albicans, forms both pseudohyphae and true hyphae when grown on nitrogen-poor spider medium [116]. As the recent isolation of *S. cerevisiae* from different sources gave fundamental contributions to the dissection of the genetic variability of this yeast, it also allowed the observation of phenotypes previously not observed in laboratory strains. Some natural *S. cerevisiae* strains indeed were shown to be able to form filamentous structures in which cells are interconnected by an extracellular matrix that can be observed via electron microscopy [105]. When growing in filamentous structures, cells do not completely divide after nuclear duplic-

ation, remaining instead connected [129]. What happens afterwards determines the morphology of the filament. The filamentous growth begins with an asymmetric cell division in which a round-shaped cell generates two elongated cells, either divided or not by the cell wall [129]. Some yeast strains are able to reverse their filamentous morphology to the single-cell one [156]. Filamentous cells are considered more prone to deal with unfavourable environmental conditions compared to single-rounded cells [157]. Indeed, in natural environments the ability to perceive the nutrient availability and to rapidly react to environmental changes are two traits pivotal to survival. The environment is perceived by cells through a process that can be divided in several phases: i) sensing of nutrients, when cells perceive the environmental nutrients ii) signalling, when the perceived information is transferred to the nucleus and iii) transcription, with the expression of genes specifically required to react to the perceived external condition. Such responses range from sporulation (in absence of nutrients) to formation of filamentous structures [62]. As already mentioned, the interaction of the microbial cell with the environment may result in flocculation, invasiveness and colony morphology are different processes and result from complex metabolic pathways somehow interconnected among each-other. The curation of these pathways is crucial to establish the ecological role and evolutive relevance of these phenotypes. The in depth knowledge of these processes is fundamental for the understanding the genetic lying at the basis of pathogenic fungi pathogenicity. In this optic, some step forward have been moved by elucidating some pathways (or part of them) involved in the filamentation process or in its regulation. The cAMP-PKA pathway regulates filamentation via cAMP levels (Fig. 2.5) through the modulation of FLO11 (MUC1) transcription mediated by Gpa2p and the ammonium permease Mep2p [125, 123, 124, 122]. High intracellular levels of cAMP in fact correlate with the increase of FLO11 expression levels (26). Further, a second pathway involved in filamentation regulation is the pheromone-responsive MAPK cascade (30, Fig. 2.5) that is stimulated by the binding of the mating pheromone and culminates with the reorientation of cell polarity. Ste7p, Ste11p, Ste20p, Ste12p and Kss1p [117] together with Cdc42p and Cdc24p are involved in the establishment of filamentous growth [186, 231]. As shown in Fig. 2.5. Ste12p and Tec1p activate the transcription of FLO11 gene. The MAPK and cAMP-regulated pathways have been shown to converge in the unusually large (2.5 Kb) promoter of FLO11, thus being es-

sential for the unicellular-to-multicellular *S. cerevisiae* differentiation [176]. Finally, the conserved TOR (target of rapamycin) pathway regulates filamentation differentiation in response to nutritional status through Tap42–Sit4 phosphatase complex (Fig. 2.5 , [41]). Additionally, also glucose repression could regulate filamentation through the involvement of several transcription factors (like Tup1p, Cyc8 and hexokinase Hxk2p), shown to regulate FLO11 transcription levels [166]. As proposed by Verstrepen and Klis [211] flocculation can represent a stress-defense mechanism for the yeast community, allowing cells inside the flocs to be protected from the environment. Moreover, cell-cell adhesion represents a pathogenic mechanism that allows fungi to adhere and thrive human tissues [211]. Interestingly, fungal adhesion is also controlled epigenetically. The transcriptional state of FLO11 gene can be inherited from mother to daughter cells for several generations and appears to be completely reversible, with cells able to switch between states [77]. The epigenetic state of FLO11 was reported to be regulated by the histone deacetylase (HDAC) Hda1p [77]. The Snf1p kinase is the key element of glucose repression [62]. At high concentration of glucose this kinase is inactive and the transcriptional repression of glucose-repressed genes is achieved through the DNA-binding transcription factor Mig1p acting together with Tup1p and Cyc8 [209, 203, 152]. Intriguingly, the filamentation-related transcription factor Tup1p directly binds the deacetylated, but not acetylated, histone tails of H3 and H4 [58].

2.6 Chromatin structure and its role in yeast filamentation

In eukaryotic cells, the genome is highly organized within the nucleus in a complex compact structure known as chromatin. The basic unit of chromatin is the nucleosome, which consists of 146 bp of DNA wrapped around the four histone proteins arranged as an octamer composed by two histone H2A-H2B dimers and a histone H3-H4 tetramer ([85][98] Fig. 2.6). Each histone protein contain the so called "histone fold" structural motif, flanked by unstructured N- and C-terminal tails, ranging from 15 (H2A) to 35 (H3) amino acids, that protrude from the nucleosomal core

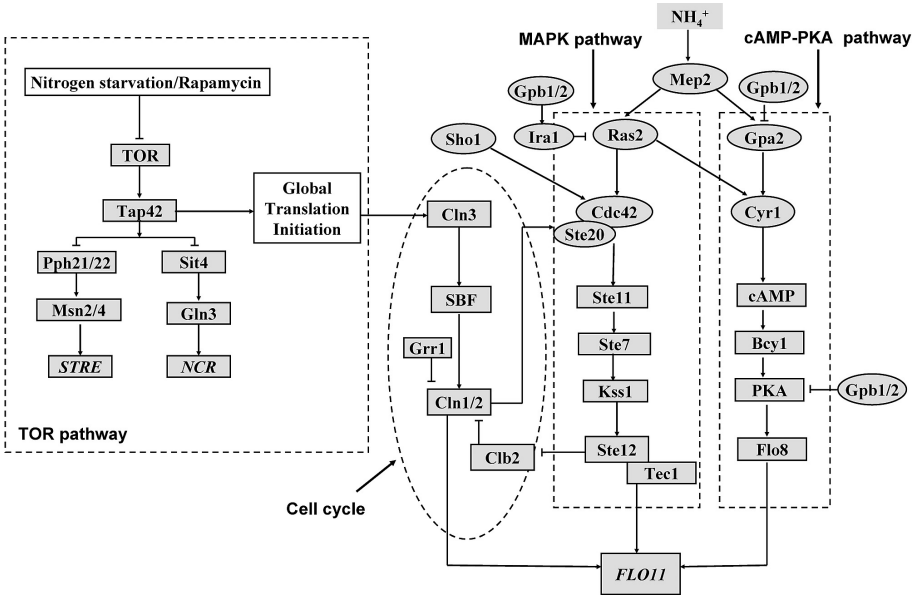

Figure 2.5: Convergence of three different pathways (TOR, MAPK, cAMP-PKA pathways) at the FLO11 gene.The ammonium sensor Mep2, functions upstream of cAMP and MAPK pathways while the nitrogen starvation or rapamycin treatment is shown to inactivate TOR pathway (Figure from [214]).

([151][126]). The positively charged basic amino acids lysine and arginine within these flexible tails are frequently posttranslationally modified through acetylation (K residues), methylation (K and R residues), ubiquitination (K residues), phosphorylation (S and T residues), sumoylation (K residues) and poly ADP-ribosylation (E residues) [17]. The fascinating "histone code" hypothesis suggests the possibility that multiple histone modifications act in a combinatorial fashion to generate alternative chromatin states [194, 221]. Acetylation and methylation of specific lysine or arginine residues in histones H3 and H4 are reversible and have been associated to gene transcription regulation [160]. Additionally, the organization of DNA around histones itself can regulate transcription by hindering accessibility to DNA binding factors [151]. Acetylation occurs on the ε-amino groups of specific lysine residues at the N-terminus of all the four histone proteins reducing the net positive charge and can be dynamically removed by the activity of histone deacetylases (HDACs) [2]. The neutralization of lysine positive charge can weaken interactions between histone and DNA by disrupting the stabilizing effect of electrostatic interactions (reviewed

in [9]). This can facilitate the access of transcription machinery to DNA. Moreover, histone acetylation can directly influence gene transcription. Acetyl-lysines in fact create binding sites to recruit other effectors containing the bromodomain, a protein domain showed to be responsible for lysine acetylation signal transduction [230]. Acetylation is carried out by a set of enzyme complexes called acetyl-transferases (HACs). Two classes of HACs have been described: 1) type-A HATs, transcription related, acetylating nuclear histones (in both histone N-terminal tail and in the globular histone core, for example in H3K56 [201]), often associated in multiprotein complexes [226]; 2) type-B HATs, highly conserved, predominantly cytoplasmic, only acetylating free histones. The positive charge of lysine is dynamically restored thanks to the activity of HDAC enzymes. In *Saccharomyces cerevisiae* more than 10 HDACs have been described and grouped into three classes: I, II, and III. Rpd3 is the most studied class I histone deacetylase [212, 93, 165]. Filamentation is one of the morphological characters known to be regulated by histone deacetylases (REF). In *S.cerevisiae* the two histone deacetylases Rpd3 and Hos2 contribute to regulate the expression of cell-surface protein Flo11p, involved in cell–cell and cell-surface adhesion as well as filamentation [11]. Rpd3 and Hos2 have been shown to redundantly regulate the basal FLO11 expression level though, differently to Hos2, Rpd3 control FLO11 expression repressing the transcription of the ncRNA ICR1 thus counteracting Sfl1 expression activation [28, 29]. Moreover, Rpd3 and Hda1 homologs together regulates the high frequency white-to-opaque phenotypic switching in *Candida albicans* [191]. Remarkably, this morphotype switch has been classified as a higher-order virulence factor [188]. Contrary to acetylation, methylation does not alter the overall charge of the histone tails. Nevertheless, methyl addition (mono, di or tri) does increase lysine basicity and hydrophobicity as well as the the affinity to DNA. Similarly to acetylation, methylation can thus alter nucleosomal structure and function [170]. The effect of histone methylation on transcription does not seem to be merely due to the opening of chromatin structure but rather a dynamic process in which the extent of lysine methylation can be selectively read by effector proteins. Histone methylation is catalyzed by protein arginine and lysine methyltransferases (HMTs), which use S-adenosylmethionine (SAM) as methyl-donor substrate in a similar way HATs utilize acetyl-coenzyme A as a cofactor. In contrast to acetylation, several studies suggest that histone methylation is relatively irreversible

[199, 24, 25]. Lysine methyltransferases (HKMTs) that methylate N-terminal lysine contain the so-called SET (Su(var)3-9, Enhancer of Zeste, Trithorax) domain. In *S. cerevisiae*, the HKMT Set1 is responsible for the K4 H3 methylation [179] while the HKMT Set2p for K36 H3 methylation [218]. The association of Set1p and Set2p with RNA polymerase II (RNA pol II) through the PAF transcription elongation complex, demonstrates their involvement in transcriptional initiation or elongation [78]. Arginine methyltransferases (PRMTs) transfer a methyl group from SAM to the ω-guanidino group of arginine within a variety of substrates. In Human, PRMTs form a 11 members family that can mediate mono- or di- methylation of arginine residues while in yeast only four PRMTs have been described: Rmt1/Hmt1, Rmt2, Rmt3, Hsl7/Skb1. Even though histone methylation was considered irreversible for many years, from 2002 a number of different pathways were proposed as potentially involved in demethylation of both lysine and arginine [12]. H3K4, H3K36, and H3K79 methylations are generally linked to active gene expression, whereas H3K9, H3K27, and H4K20 di- and tri-methylations have been associated with gene silencing. H3K4me2 and H3K4me3 have been both found predominantly on active loci, although H3K4me3 is associated with active genes, H3K4me2 can be present also in inactive genes [180, 20]. It has been proposed that H3K4me2 determines a 'permissive' chromatin state, in which genes are either active or potentially active [179]. This hypothesis is consistent with the localization of di-methylated K4 in promoter and coding regions of genes in yeast but with a bias towards the coding region [19]. In addition to histone modification, chromatin structure can be altered by ATP-dependent chromatin-remodeling complexes that contain an ATPase subunit belonging to the SNF2 superfamily of proteins [213]. ATP-dependent chromatin-remodeling complexes work in concert with histone modifying enzymes since the they specifically recognize histone marks (acetylation, methylation, phosphorylation, ribosylation and ubiquitination) left by the latter [198]. Next, thanks to the energy generated by the hydrolysis of ATP, they unwrap, move, eject or restructure nucleosomes recruiting the transcriptional apparatus and thus regulating gene expression [153, 113, 38]. All the ATP-dependent chromatin-remodeling complexes have been classified in 3 groups: 1) SWI2/SNF2 group 2) SWI (ISWI) group 3) Snf2-like ATPase with deacetylase activity [213]. The yeast SWI/SNF complex, the first to be described as involved in the intensely studied sucrose fermentation and mating-type

switching pathways [224, 196], is found in both prokaryotes and eukaryotes. It contains the ATPase Swi2/Snf2p, Arp7p and Arp9, two actin-related proteins, and other subunits involved in DNA and protein-protein interactions [198]. The SWI2/SNF2 group also contains the closely related RSC (Remodeling the Structure of Chromatin) complex, firstly identified in *S. cerevisiae* by Cairns and collaborators [30]. It is composed by 15 subunits, several of which are essential for viability. Sth1 is the homolog of the Swi2/Snf2 ATPase while Sfh1, Rsc8/Swh3 and Rsc6 are homologs of the Snf5, Swi3, and Swp73 Swi2/Snf2 members. Interestingly, conserved Swi/Snf complex in C. albicans is required for hyphal development and pathogenicity [131]. Moreover, the Swi/Snf chromatin-remodeling complex together with the deacetylase Rpd3L was shown to regulate FLO11 in *S. cerevisiae* [11]. The Swi/Snf complex, recruited at the STA1 promoter by Ste12 and Tec1, is also described to regulate the expression of STA1 through the DNA-binding activators Flo8 and Mss11 [95]. Interestingly, STA1 and FLO11 promoters show high homology (94.6%) [63]. Based on this homology, Barrales and co-authors proposed a mechanism in which the Swi/Snf complex could model the chromatin structure in the FLO11 promoter preventing the Sfl1 binding but enhancing Flo8 binding, thus activating FLO11 expression [11].

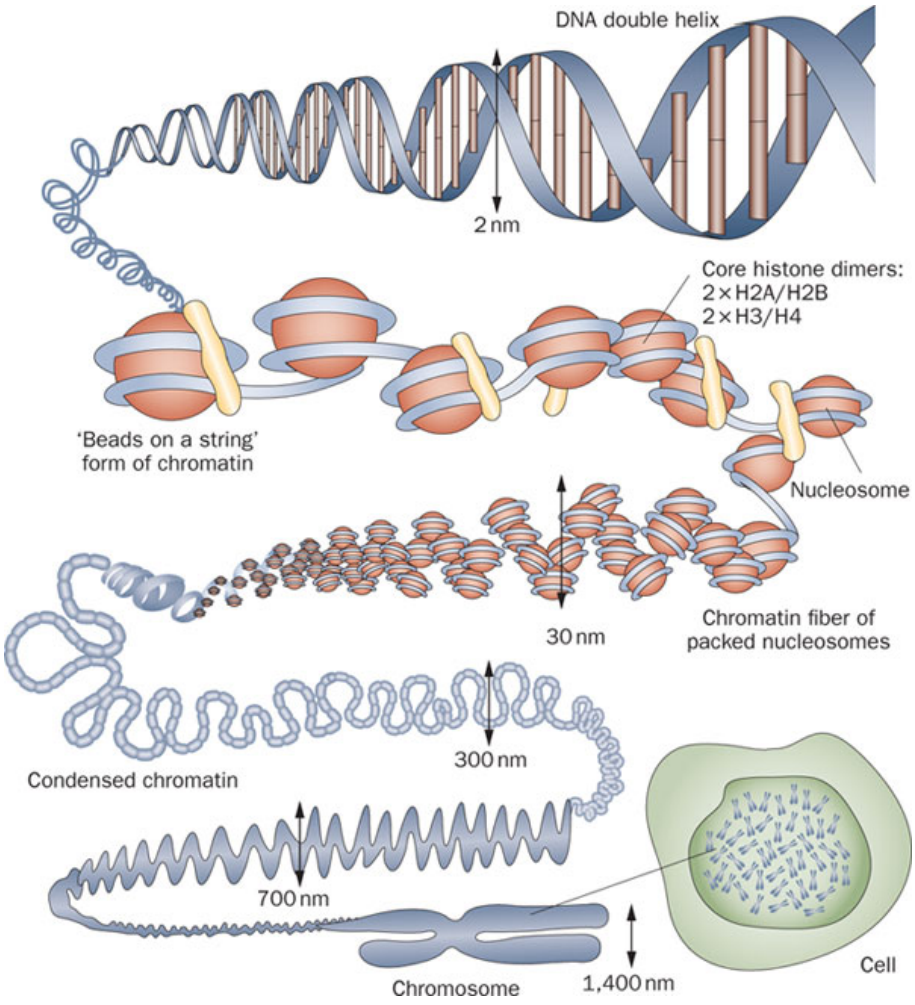

Figure 2.6: Schematic representation of chromatin structure: DNA is complexed to histone and nonhistone nuclear proteins to form chromosomes with a width of approximately 1400 nm. The completely condensed chromatin has a diameter of up to 700 nm and is composed of a 300 nm chromatin diameter thick fiber complexed with nucleosomes (30 nm in diameter). Nucleosomes are the basic unit of chromatin, composed by 146 bp of genomic DNA wrapped around a histone octamer that consists of two molecules of the major types of histones (H2A, H2B, H3 and H4) (Figure from [202]).

Chapter 3

Results

3.1 The natural *Saccharomyces cerevisiae* strain M28 is characterized by a carbon source dependent intra-tetrad phenotypic variability

In 1998 Cavalieri and collaborators isolated the *Saccharomyces cerevisiae* M28 strain [33] from a damaged grape berry in a Montalcino vineyard (Tuscany, Italy); by inducing M28 to sporulate the authors isolated several tetrads (marked with a sequential number from 1 to 4) that were dissected into individual meiotic segregants. As the 69% of all the vineyard strains [143] M28 strain is homothallic thus the individuals of the progeny generated from sporulation are homozygous diploid [143]. Interestingly, all the dissected tetrads showed a Mendelian segregation of the recessive resistance to a toxic analogue of leucine (5',5',5',trifluoroleucine, TFL). Cavalieri and colleagues characterized the TFL resistance phenotype to be associated with a single nucleotide insertion (T9) in the coding region of the SSY1 gene [26], encoding for a key component of a plasma-membrane amino acid sensor system together with PTR3 and SSY5 (20, 21). Ssy1p is the largest member of the amino acid permease protein family and the only one that does not have a transporter function. The insertion of a thymine (T9) into a mononucleotide repeat disrupts the reading frame of SSY1, creating a truncated protein without any residual function [26]. This trig-

gers the down-regulation of several amino acid permeases and transporters and the consequent up-regulation of the amino acid catabolism. Even though the signalling cascade downstream of the amino acid sensor system still remains unclear, Grr1p, Dal81p (Uga35p), Abf1p and Stp1/1p were shown to be required for the transcription of Ssy1p-regulated genes [42, 43]. At the interface between cellular metabolism and environment Ssyp serves as a key protein in cellular communication.

Additionally, Cavalieri et al. showed that the M28 natural *S. cerevisiae* strain possesses the peculiar characteristic of generating tetrads with two distinct morphotypes (smooth and fluffy/filigreed). As shown in Fig. 3.1, this trait mostly segregates 2:2 in YPD 2% with the tetrad 3 being an exception since the M283A spore displayed a mildly filigreed phenotype, with filamentous structures only externally surrounding the colony (Fig. 3.1). Notably, the TFL resistance and morphotype traits were independently inherited in the different tetrads indicating that the two traits were not in linkage disequilibrium (Fg. 3.1).

At the beginning of this project, the sequence of the M28 genome was already available since one spore of the M28 tetrad 1, M281B, was completely sequenced using the recent PacBio sequencing technique (data not published, details reported in Appendix E). The M281B assembly was used to compare the genomes of this filamentous TFL-resistant spore with the reference S288c strain estimating their genetic divergence by means of whole genome alignment. Our results showed a 3% genetic divergence among the two strains with a total of 43,257 mismatches. As shown by the collinearity plots (Appendix E) we did not identified wide chromosome rearrangements but rather single nucleotide polymorphisms or small insertions/deletions. As expected the SSY T9 insertion was found in M281B but not in the reference S288c strain (TFL-sensitive). In addition to the PacBio sequencing, all the four spores of Tetrad 1 (M281A, M281B, M281C and M281D), Tetrad 2 (M282A, M282B, M282C, M282D) and Tetrad 4 (M284A, M284B, M284C and M284D) were completely sequenced through the Illumina sequencing platform (Illumina paired-end 2X150 pb). These libraries were used to compare the four spores using the M281B PacBio assembly as reference genome. This analysis showed a 99.9% similarity between the four M28-meiotic derivatives. As expected, the SSY1 insertions responsible for the TFL-trait was found in all the TFL-resistant strains

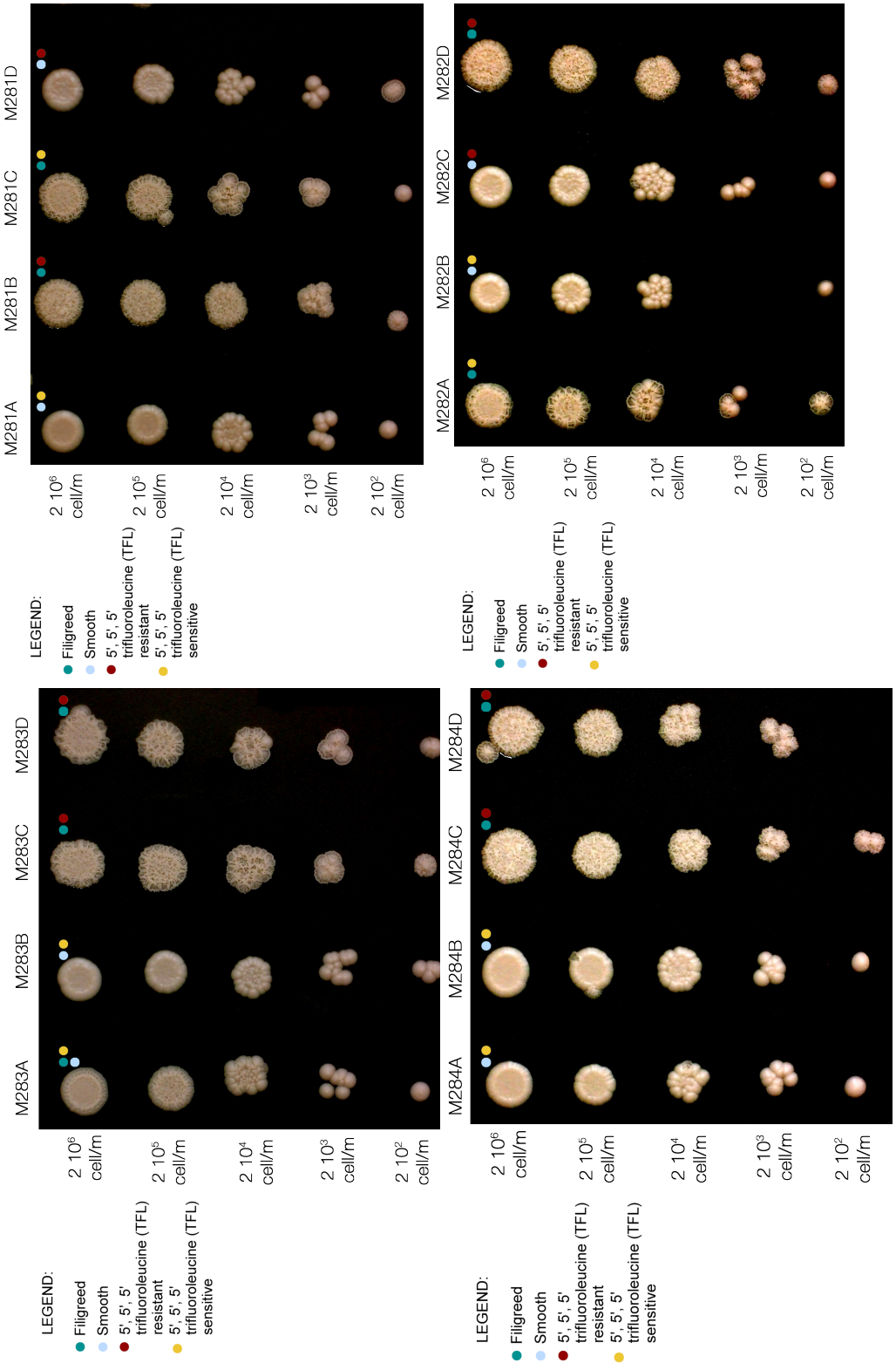

Figure 3.1: Analysis of TFL-resistance and filamentous traits in four M28 tetrads. Each tetrad is marked with a sequential number from 1 to 4 while each spore inside the tetrad is marked with a sequential letter from A to D. Each colony was generated by spotting 5 µl of the reported cellular concentration in solid YPD 2%. Morphotype was detected after 5-days growth at 30°C. Both the traits are reported using the color code indicated in legend.

(M281B, M281D, M282A, M282B, M284C, M284D) but not in the TFL-sensitive ones (M281A, M281C, M282C, M282D, M284A, M284B). Surprisingly, despite the previously observed mendelian segregation of the morphotype [33], no genetic variations were found to segregate with morphotype.

Altogether this was the initial and available knowledge on M28 when this thesis work started. To further investigate the morphotype and the peculiar segregation it was decided to focus on the M28 tetrad 1. We selected the four segregants M281A-D since in this tetrad we observed all the possible combinations between the TFL and filamentous traits. First of all, we carried out a series of experiments to deepen into the Mendelian segregation of the morphotype in M281A-D. Thus, we crossed the smooth strains (M281A and M281D) with the filigreed strains (M281B and M281C) to investigate the phenotype of the second generation in the Mendelian perspective. Since M28 is homothallic, we converted the four spores to heterothallic through HO gene disruption (*Material and methods, 2.1*). Next, we crossed all the haploid spores, generating all the possible phenotypic combinations: M281AxM281B, M281AxM281C, M281AxM281D, M281BxM281C, M281BxM281D, M281CxM281D. All the diploid clones showed a smooth phenotype in YPD 2% (Table 3.1), similarly to the M28 parental strain [33], suggesting that smooth phenotype is dominant. These diploid strains were further investigated and induced to sporulate and tetrad analysis was performed as described by Mortimer and Hawthorne [141]. Single spores were next grown in both optimal yeast medium (YPD 2%) and YP supplemented with 2% ethanol (YPE 2%), since this carbon source was shown to induce filamentation [121].

As shown in Table 3.1, when single spores deriving from the diploid strains were grown in YP supplemented with 2% ethanol the filamentous morphotype followed a 2:2 segregation from the smooth x filigreed cross, while the smooth x smooth and filigreed x filigreed crosses produced four spores with the parental phenotypes, smooth and filigreed, respectively. The phenotype observed in YPD 2% did not follow the same patterns. Particularly, the M281BxM281C (filigreed x filigreed) cross unexpectedly produced a 2:2 Mendelian segregation while the M281CxM281D (filigreed x smooth) did not. Conversely, the M281BxM281D (filigreed x smooth) cross produced a 2:2 Mendelian segregation in YPD 2%. These results reflected

strain 1	resistence1	mating type strain 1	Strain 1 phenotype (YPD 2%)	Strain 1 Phenotype (YPE 2%)	strain 2	resistence2	mating type strain 2	Strain 2 phenotype (YPD 2%)	Strain 2 phenotype (YPE 2%)	Diploid phenotype (YPD 2%)	spore#	Morphotype YPD 2% (F=Filigreed, S=Smooth)	Morphotype YPE 2% (F=Filigreed, S=Smooth)
												tetrad1	tetrad1
1A	Hph	a	S	S	1B	KAN	alpha	F	F	S	1	S	S
											2	S	S
											3	F	F
											4	F	F
1A	KAN	a	S	S	1C	Hph	alpha	F(S)	F	S	1	S	S
											2	F	F
											3	S	S
											4	F	F
1A	KAN	alpha	S	S	1D	Hph	a	S	S	S	1	S	S
											2	S	S
											3	S	S
											4	S	S
1B	KAN	a	F	F	1C	Hph	alpha	F(S)	F	S	1	S	F
											2	F	F
											3	F	F
											4	S	F
1B	KAN	a	F	F	1D	Hph	alpha	S	S	S	1	F	F
											2	S	S
											3	S	S
											4	F	F
1C	Hph	alpha	F(S)	F	1D	KAN	a	S	S	S	1	F (S)	F
											2	F (S)	F
											3	S	S
											4	S	S

Table 3.1: M28-haploid spores crossing and phenotypic characterization of the parental M28 strains (M281A haploid = 1A, M281B haploid= 1B, M281C haploid = 1C, M281D haploid = 1D), the F0 (diploid strains obtained by crossing haploid strains) and spores obtained inducing the F0 to sporulate and dissecting tetrads (the reported phenotype was observed in 10 different tetrads for each crossing). Morphotype was detected in the reported solid media after 5-days growth at 30°C.

our preliminary observations of a different degree of filamentation for the M281C and M281B filigreed strains in several media (Fig. 3.2), with the first one showing an attenuated morphotype compared to the TFL-resistant M281B spore. This phenotypic gradient was not observed in YPE 2%.

To further characterize the behaviour of the meiotic segregants in response to different nutritional stimuli, we tested colony phenotype in different growth conditions to investigate whether the morphotype is maintained when different nutritional sources are provided. Filamentous growth in fact is regulated by nutritional signals, as reviewed by Gagiano et al. [62]. The colony morphology of M28 meiotic segregants (M281A, M281B, M281C and M281D) was investigated in media containing both rapidly metabolisable fermentable sugars (glucose, galactose, sucrose, mannose) and non-fermentable carbon sources (ethanol, glycerol). In YPD 2% solid medium, M281B and M281C strains showed a morphotype characterized by two distinct sections separated by a high cell density ring: the central section was characterized by a conic structure while the radial section showed grooves in which cells

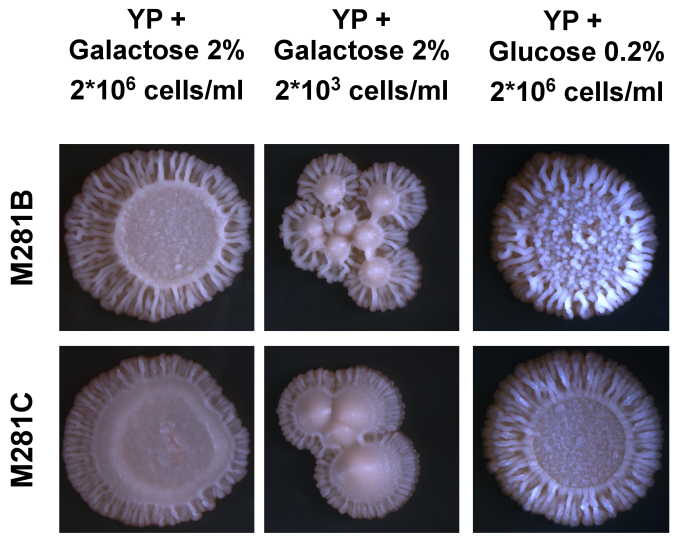

Figure 3.2: Morphotype differences between M281B and M281C in solid YP supplemented with the reported carbon source at the reported concentration. Each colony was generated by spotting 5 µl of the reported cellular concentration. Morphotype was detected after 5-days growth at 30°C. The two spores exhibit different colony architectures and the presence of filamentous structures is clearly detectable in both.

spread forming filaments (Fig 3.3, panel a). The "filigreed" term used in this thesis refers to this filamentous growth generating complex structured colonies. The TFL-resistant strain M281B presented a more evident filigreed phenotype with a high cell density central section. On the contrary, the TFL-sensitive strain M281C showed a less pronounced filigreed morphotype that became more pronounced when the strain was grown in YP supplemented with 2% ethanol. At the cellular level filigreed colonies in liquid were characterized by an atypical cell phenotype with elongated cells, tightly associated with each other. During filamentous growth, cells remain physically attached to form chains named pseudohyphae, distinct from hyphae in which cells form continuous smooth tubes without constrictions [129]. Pseudohyphal growth was more evident in the M281B strain, suggesting a possible link between the SSY T9 mutation, responsible for the TFL phenotype [34] and cellular morphology. Actually, a possible role has been proposed for the Ptr3p-Ssypp-Sy5p complex in filamentation regulation via the cAMP pathway [62]. Conversely, M281A and M281D strains formed smooth colonies without filaments. This phenotype resembles the cell morphology characterized by oval shaped cells separated from each other observed in the BY4743 *S. cerevisiae* laboratory strains (Fig. 3.3, panel c). Despite the smooth phenotype, the TFL-resistant strain M281D presented a marked tendency to pseudohyphal growth (Fig. 3.3, panel b). Noteworthy, filamentous structures were not observed in growth media with high glucose concentration (YPD 10%), even in those segregants showing a filigreed morphotype on YPD (Fig. 3.3, panel a); this data suggests that an increase in glucose concentration inhibits filigreed colony morphology. These observations are coherent with the view of filamentation as a stress phenotype in response to nutrient limitation and starvation [62].

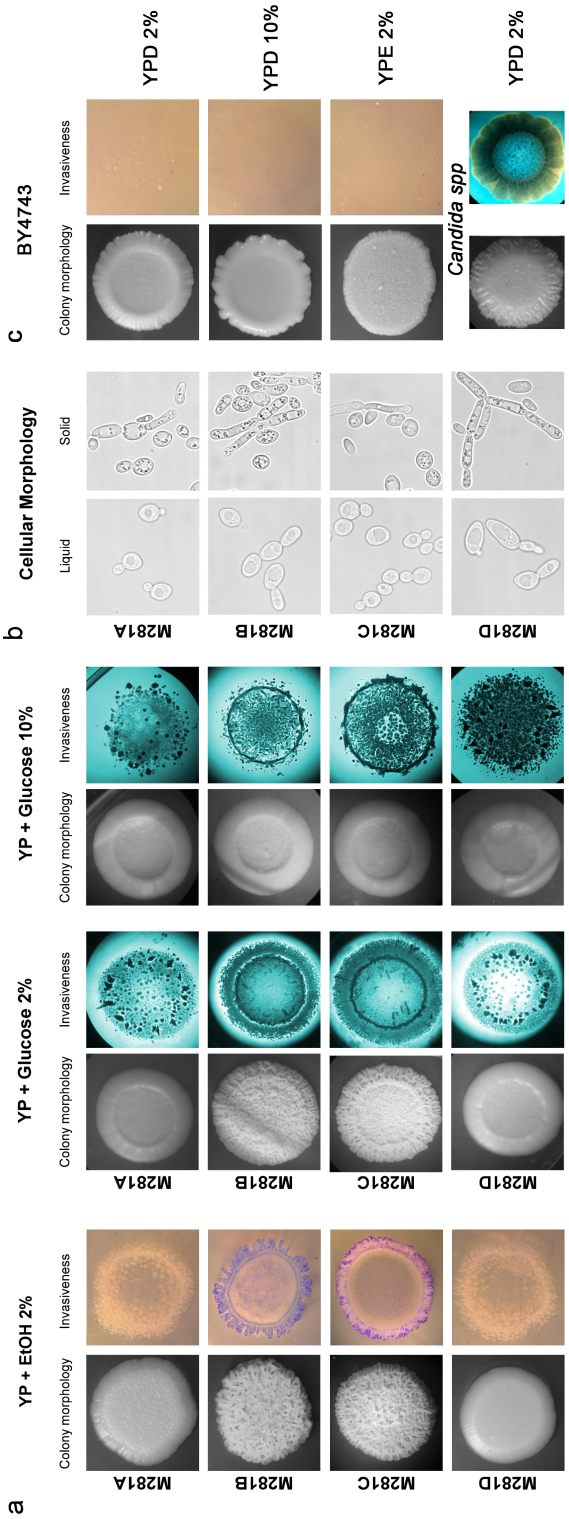

Figure 3.3: M28 meiotic derivatives phenotypic variability (description below)

[Global picture of the phenotypic variability among the four M28 spores. Colony morphology was observed after 5-days growth at 30°C. Invasiveness was analysed as reported in *Material and methods 1.2* a) the colony morphology and invasiveness analysis in both solid YPE 2% and YPD% shows the presence of filamentous structures in both M281B and M281C and not in M281A and M281D. These strains invade solid substrates with more efficiency as demonstrated by the more intense invasive pattern on agar. In YPD 10% all the spores displayed a smooth morphotype and a decreased invasiveness except M281D whose invasive pattern is more pronounced in YPD10% compared to YPE 2% and YPD 2%. b) cellular morphology in both liquid and solid YPD 2%. In liquid media the two TFL-resistant strains (M281B and M281D) displayed a slight tendency to pseudohyphal growth that is more accentuated in solid YPD 2% where all the spores generated pseudohyphal structures although with different efficiency. c) Colony morphology and invasiveness of the reference diploid strain BY4743. In all the tested media (YPE 2%, YPD 2% and YPD 10%) we did not identify filamentous structures or ability to invade agar. Invasiveness is also reported for *Candida spp*]

A Mendelian segregation of the filamentous trait was also observed providing galactose 2%, sucrose 2% and mannose 2% as sole carbon source (Fig. 3.4). On YP containing 2% glycerol or ethanol, M281B and M281C colonies showed a colony morphology different from those observed on other media: the distinction between radial and central regions was not detectable and colonies presented filamentous structures equally distributed on the surface creating circular foldings (Fig. 3.3 and 3.5). Ethanol was shown to induce hyper filamentation of diploid strains when grown on low-nitrogen medium without affecting colony and cellular morphology of haploid cells [121]. Differently, diploid M28-derivatives showed hyper filamentation on rich YP medium supplemented with ethanol at different concentrations (1%, 2%, 5%, Fig. 3.5). whereas filamentation was repressed during growth in minimal medium containing ammonium for both haploid and diploid M28 derived strains (Fig. 3.6). Surprisingly, the same result was observed in low-nitrogen medium with both haploid and diploid spores growing as smooth colonies (data not shown).

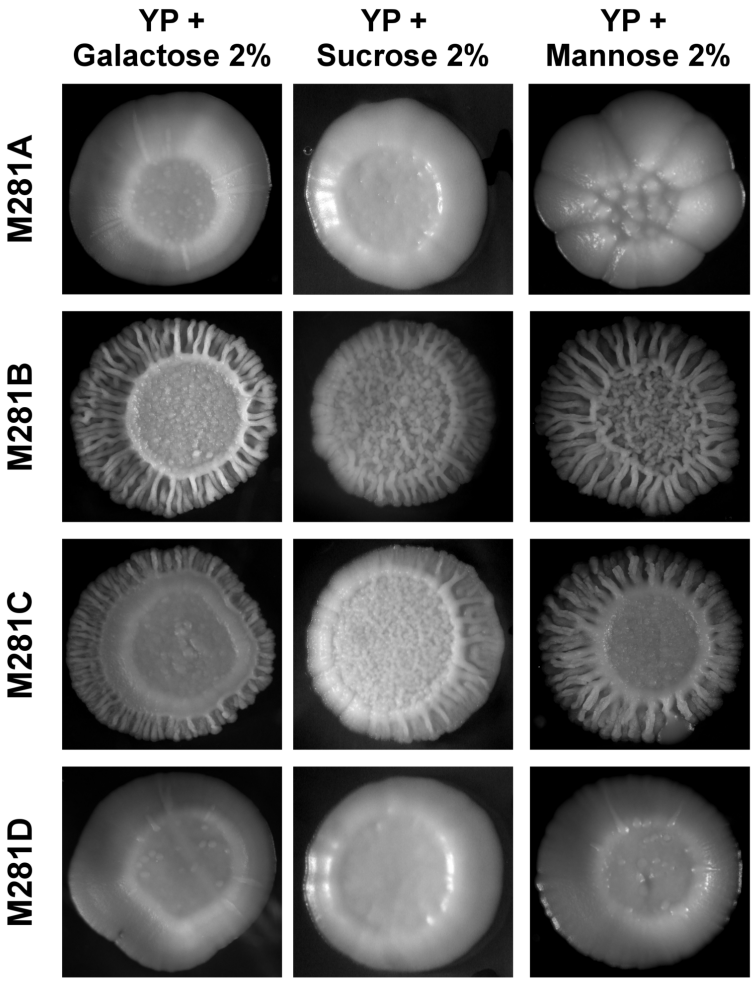

Figure 3.4: Colony morphology of M28 meiotic derivatives in solid media supplemented with 2% of the reported carbon source. Morphotype was analyzed after 5-days growth at 30°C. The two spores M281B and M281D generated filamentous structures but showed slightly different colony architectures

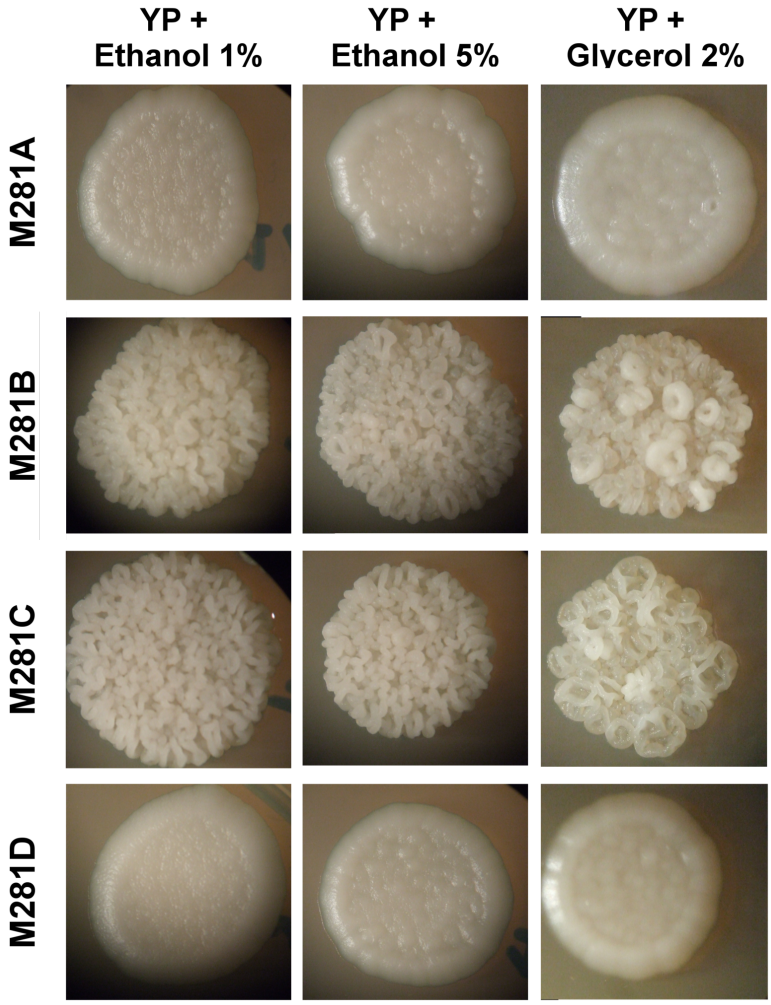

Figure 3.5: Colony morphology of M28 meiotic derivatives in solid media supplemented with different concentration of ethanol (1% and 5%) and 2% glycerol. Morphotype was analyzed after 5-days growth at 30°C. The two spores M281B and M281D generated filamentous structures organized in similar colony architectures

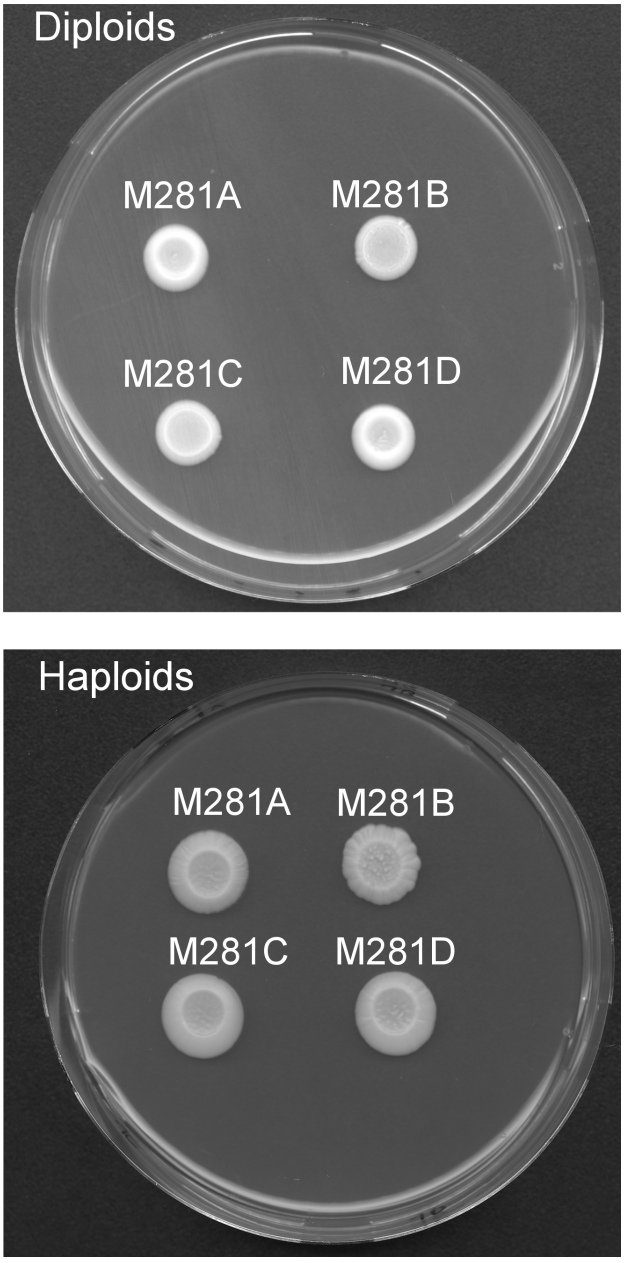

Figure 3.6: Colony morphology of M28 meiotic derivatives (both haploid and diploid) in YNB minimal media. Morphotype was analyzed after 5-days growth at 30°C. None of the spores generated clear filamentous structures and morphotype of diploids was comparable with those of haploids.

3.2 In 2% ethanol- and 2% glucose- supplemented media M28-spores grow significantly faster than the reference strain

S.cerevisiae is able to use a wide range of chemical compounds as carbon source, but not all of them are used with equal efficiency [62]. We asked if the intra-tetrad variability observed at the phenotypic level is associated with a different metabolic efficiency. To this aim, we measured the doubling time of each M28 meiotic segregant in several media. Moreover, we compared these growth rates with the doubling time of the *Saccharomyces cerevisiae* commonly used diploid laboratory strain BY4743. Growth was monitored in complete media with two different glucose concentrations (2%, 10%; YPD) as well as in YP supplemented with either 2% sucrose (YPS 2%) or 2% galactose (YPG 2%) or 2% mannose (YPM 2%) or 2% ethanol (YPE 2%). All the doubling times of M28 tetrad 1 and BY4743 are reported in Fig. 3.7 while the growth curves used this calculation are shown in Appendix F.

In YPM 2% and YPG 2% we did not observe variations neither among all the M28 spores nor between the four spores and the reference diploid strain (Pvalue $>$ 0.05, Welch Two Sample t-test with Bonferroni correction for multiple testing). In YPS 2% all the spores, except M281B displayed a doubling time of roughly 2h as the reference strain. The prolonged doubling time of M281B in YPS 2% could be due to an elevated rate of cellular aggregation strongly affecting OD measurement. Surprisingly, in YP supplemented with 10% glucose, where all the spores grown as smooth colonies, we identified small but significant growth rate variations between M281D and M281A (2.3h vs 2h, Bonferroni-adjusted p-value = 0.001), M281D and M281B (2.3h vs 2.4h, Bonferroni-adjusted p-value = 0.02) and M281D and BY4743 (2.3h vs 2.5h, Bonferroni-adjusted p-value = 0.009). Moreover, M281A grew faster than BY4743 (2.5h doubling time) and M281B (2.4h doubling time), displaying a generation time of 2 hours. Variations between M28 meiotic segregants and the reference strain were enhanced in YPD 2%. In the optimal medium in fact the doubling time of the diploid reference strain (2.2 h) was significantly faster when compared to all the M28-spores (Pvalue $<$ 0.05, Welch Two Sample t-test with

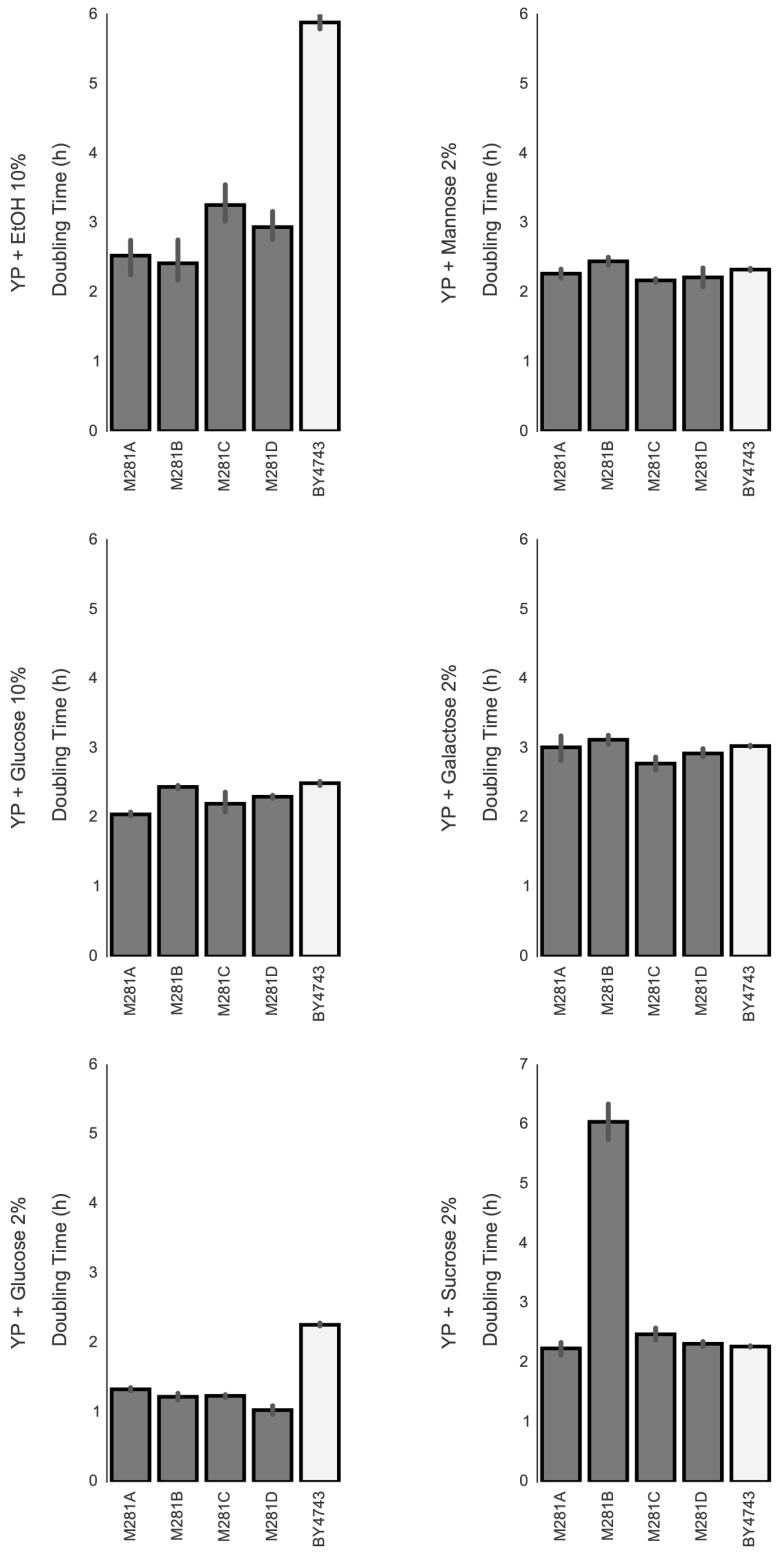

Figure 3.7: Doubling time of M281A-D and diploid reference strain BY4743 in the reported liquid media. Growth curves used to calculate doubling times are reported in Appendix F

Bonferroni correction for multiple testing). Moreover, with a doubling time of 1.3 h M281A is the slowest growing spore of M28 tetrad 1. Notably, the difference between growth rate of M28-derivatives and the reference strain was accentuated in YP supplemented with 2% ethanol, the same media in which morphotype variability increased. Indeed, the doubling time was reduced from roughly 6 hours, for BY4743 to 2.5/3 hours (M281A 2,5; M281B 2,4; M281C 3,2; M281D 2,9), for the M28 strains. Such a reduction in the doubling time would reflect an adaptation to the wine environment where the M28 parental strain was isolated.

3.3 Pseudohyphal growth and ability to invade agar are not inhibited by glucose and are strongly pronounced in filigreed colonies

Invasiveness is the ability of cells to penetrate and grow inside a solid substrate. In *Candida albicans*, the major human fungal pathogen, this trait contributes to its virulence, since its filamentous structures enables the microorganism to invade and thrive in human tissues. Beside being considered safe organisms for human, some natural *S.cerevisiae* strains characterized by structured filigreed colonies have been shown to efficiently invade solid substrates [105]. We analyzed the capability of M28 meiotic segregants to invade solid media. Invasiveness was tested on the solid media in which we observed a different degree of filamentation: YPD 2%, YPD 10% and YPE 2%. As shown in Fig 3.3 Panel A, beside all the four meiotic derivatives were able to penetrate the solid medium in all the tested conditions, the smooth spores M281A and M281D weakly invaded agar. The invasion pattern revealed a possible differentiation inside the colony, with external cells exhibiting higher invasiveness. Morphological differentiation was detected also at cellular level, with both filigreed and smooth colonies exhibiting both cellular type: yeast-shaped cells and pseudohyphae. Such differentiation appeared less pronounced in liquid media, where pseudohyphal growth was barely detected (Fig. 3.3, panel b). Although cells do not extremely change morphology in liquid media, they rather display cell-cell adhesion (Fig. 3.3 panel B). M281B and M281C in fact strongly flocculated during

growth in liquid YP supplemented with ethanol (data not shown). In YPD 10% all the strains showed a reduced invasiveness with the exception of the M281D spores, shown to exhibit the most pronounced pseudohyphal growth. Additionally, we did not observe the same complex structured pattern observed in YPD 2% and cells growing more distantly from the colony core totally lost the ability to invade agar.

The ability to invade agar was also analyzed in the haploidized M281A-D (Fig. 3.8). In YPD 2% and YPE 2% we obtained results similar to those for the diploid spores, with all the strains invading agar in both media with an increased effciency for M281B and M281C. Differently, in YPD supplemented with 10% glucose we detected a weak invasiveness for all the spores while the diploid strains were still able to invade agar, even though with a reduced efficiency.

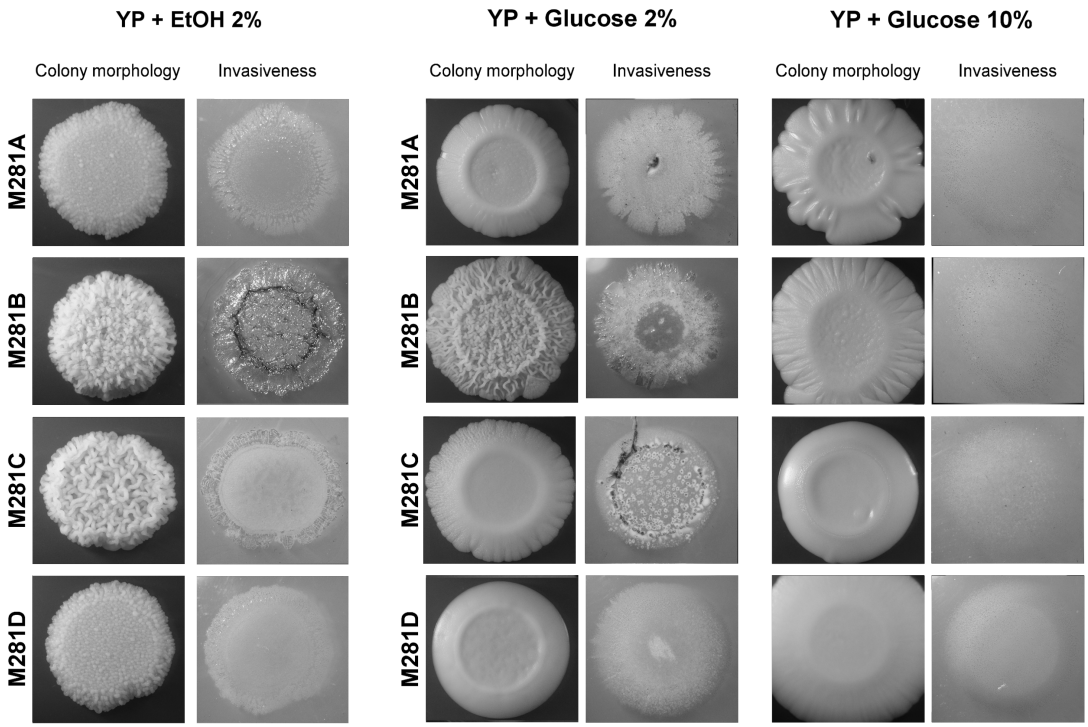

Figure 3.8: Phenotypic variability among the four haploid M28 spores. Colony morphology was observed after 5-days growth at 30°C in YPD 2%, YPD 10% and YPE 2%. Invasiveness was analysed in the same media as reported in *Material and methods, 1.1*

3.4 Whole proteome analysis shows extensive variations at the protein level among the M28-spores

The surprisingly high phenotypic variability in the M28 system prompted us to further investigate the source of spore-dependent variations. Firstly, we measured differential protein abundance profiles across the M28 tetrad by label-free shotgun proteomics (*Materials and methods, 1.7, 1.8*). Shotgun proteomics represents a powerful tool to identify and quantify protein abundances in complex biological systems as well as to comprehensively investigate protein abundance differences between samples or conditions. Protein abundance changes were measured in YPE 2%, the medium found to accentuate morphotype differences between spores. Moreover, the same experiment was carried out in the diploid reference strain BY4743 to simultaneously evaluate protein variability between genetically distant *S. cerevisiae* strains. Two third of the annotated publicly available yeast translated proteome were identified and quantified in both the M28 (3913 proteins identified) and the laboratory strain (3647 proteins identified).

Hierarchical clustering (HC) quantifies the similarity of samples by calculating the pairwise distance between them. Subsequently, the relationships between samples are subjected to a tree-like graph called dendrogram representing the distances in terms of similarity among samples. The HC analysis applied to the protein abundances dataset indicated a higher clusteredness of M28 spores whose abundance profiles formed a separated cluster compared to reference strain BY4743 (Fig. 3.9).

Further analyses of the protein abundance profiles were carried out to understand whether there are common patterns that could be linked to either the TFL or the morphological phenotypes. To overcome possible undersampling biases of the technique, the protein abundance datasets were pooled for TFL-R (M281B and M281D) and TFL-S (M281A and M281C) strains, respectively, and compared to identify R- and S-specific expression patterns. We applied the same approach to morphotype, by pooling M281B (filigreed) with M281C (filigreed) and M281A (smooth) with M281D (smooth) protein abundance datasets. As expected, in the TFL-R vs TFL-S comparison, the amino acid (Leu, Ser, Thr, Cys, Met and Asn) membrane transporter Gnp1p, previously shown to block amino acid sensing in the environ-

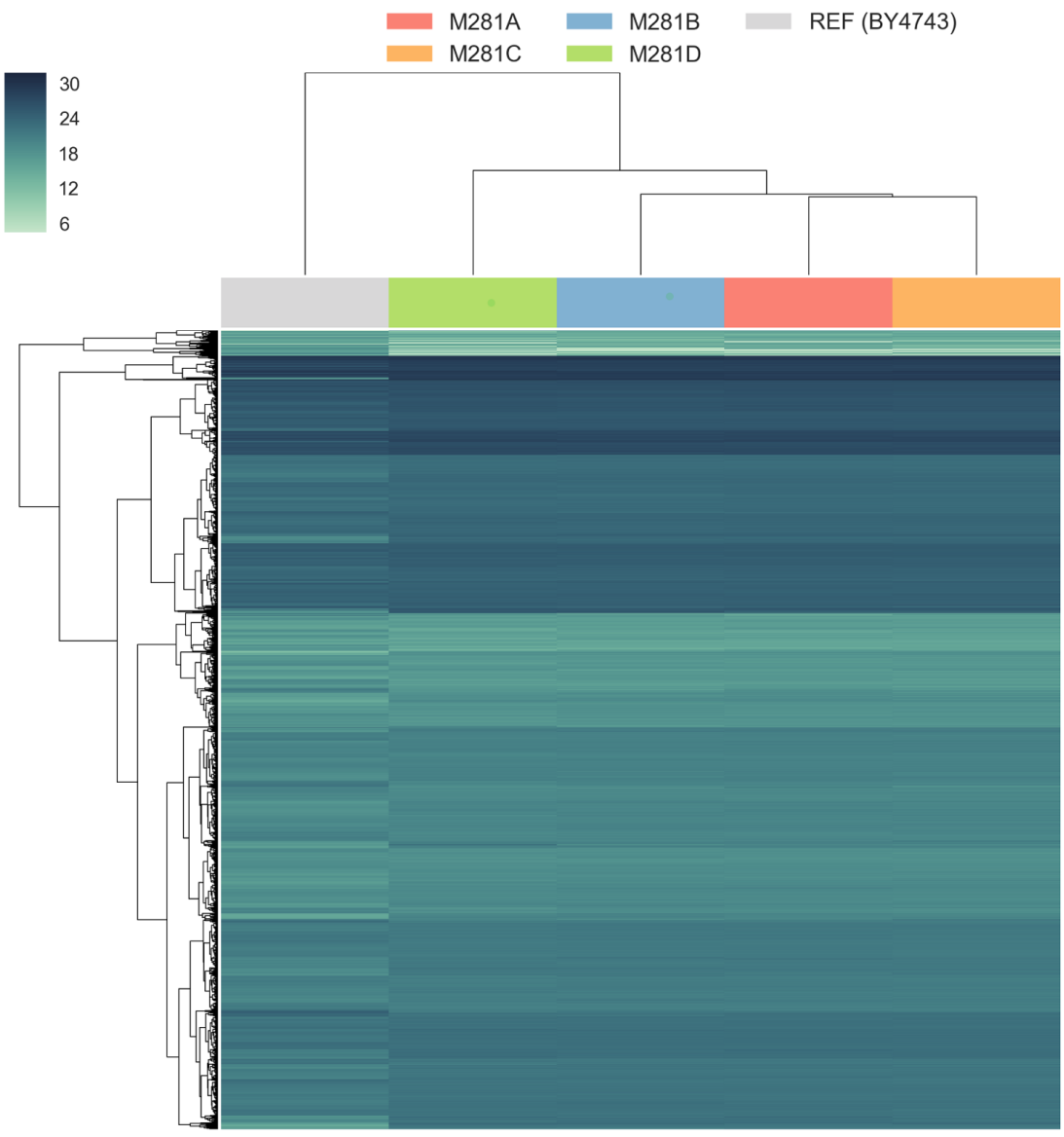

Figure 3.9: Plot of the hierarchically clustered heatmap of protein abundances (metric='euclidean, abundances reported in base-2 logarithm) of M28 meiotic derivatives and BY4743 grown in liquid YPE 2%. The four M28 spores form a disjoint subcluster revealing the high variability between natural and reference strains

ment, was down-regulated 10-fold in the two spores carrying the SSY1 T9 mutation thus strongly affecting cellular metabolism [34]. Notably, the expression of several peptide transporter genes, including Gnp1p, was reported to be induced by Ssyp (15). Additionally, Dip5p and Bap2p permeases were significantly under expressed in the M281B and M281D TFL-R spores (8-fold and 23-fold respectively). On the other hand, as a cellular compensatory response, several proteins related to the amino acid metabolism were up-regulated in the TFL-resistant background (Fig. 3.10) varying from 2-fold to 6-fold with respect to the TFL-susceptible strains: Met3p, Met14p, Met16p, Met5p (sulfur metabolism), Leu1p, Leu2p (branched chain amino acids metabolism), Dur1,2p and Dal3p (allantoin metabolism), His4p (histidine metabolism), Ser33p, Ser3p, Met6p, (glycine, serine, methionine and cysteine metabolism).

Curiously, Aro9p, Aro10p, Bat2p and Gdh2p, proteins involved in several amino acid metabolisms, were down-regulated in the TFL-R spores, together with Cha1p, a catabolic L-serine/L-threonine deaminase.

When performing a network analysis (*Material and methods, 1.15*) the protein-protein-interactions (ppi) network of TFL-related proteins showed a high connectivity between nodes highlighting the presence of a regulated metabolic rearrangement due to the mutated SSY1 gene (Fig. 3.10). When comparing pooled smooth strains with filigreed strains we only identified 14 proteins significantly changing abundance. The degree of differential expression between morphotypes varied from 2-fold to 8-fold. Only one protein, Htz1p, corresponding to the histones H2A variant H2AZ and up-regulated 2 fold in the filigreed spores, has been described as associated to the filamentous phenotype (SGD database). However, no connection was found between these proteins when performing the network analysis as reported in *Material and methods, 1.15* (Fig. 3.11).

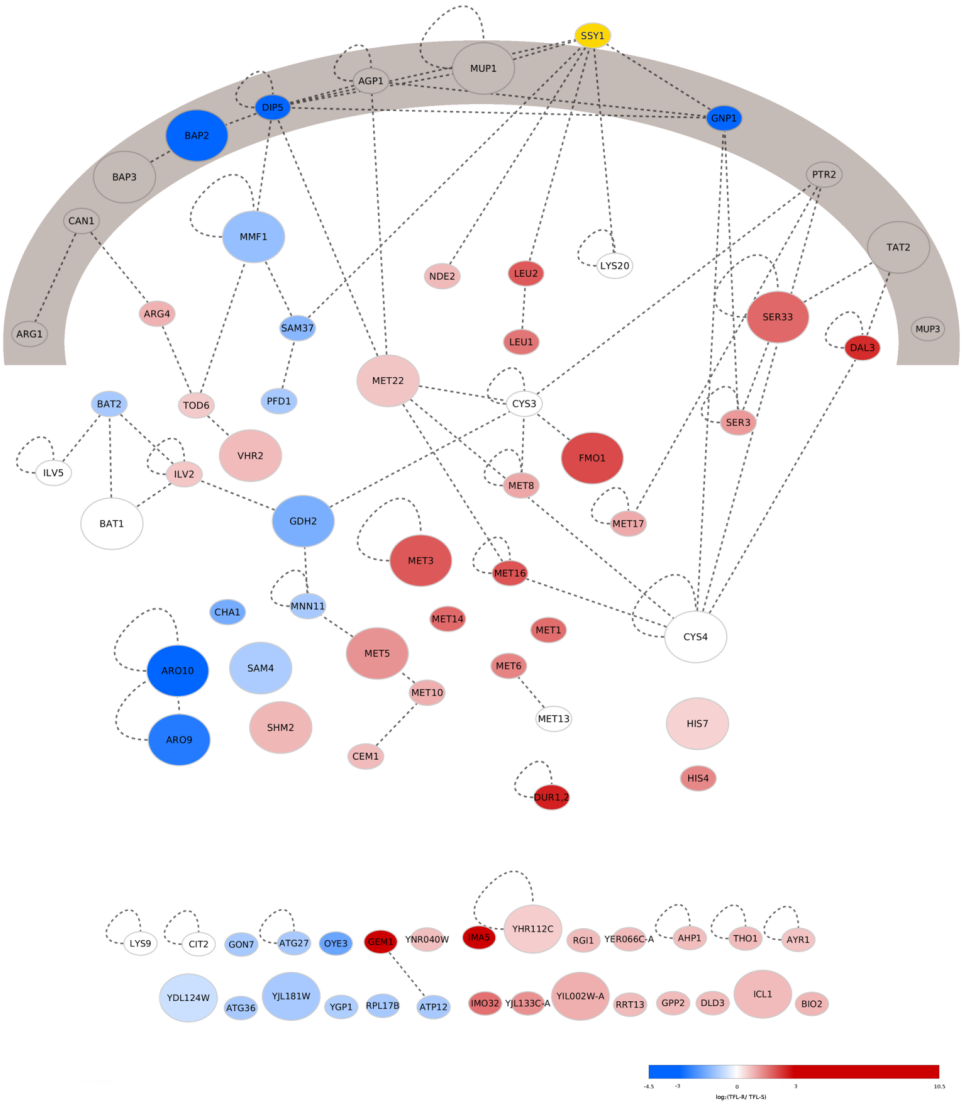

Figure 3.10: ppi-interaction network of differentially abundant proteins in the TFL-resistance vs TFL-sensitive comparison. Node color reflect protein abundance as reported in colorbar. The yellow node represents the SSY1 gene found mutated in the TFL-resistant spores (M281B and M281D). In grey a schematic representation of cell membrane showing the localization of reported proteins (nodes). White nodes have been added using the list of [60]. These proteins have been functionally associated to the Ssy1 protein and they have been used in this analysis to connect detected proteins. This strategy allowed to overcome possible biases due to the undersampling associated to the mass spectrometry technique. Big nodes correspond to proteins encoded by a gene showing a ChIP significative enrichment.

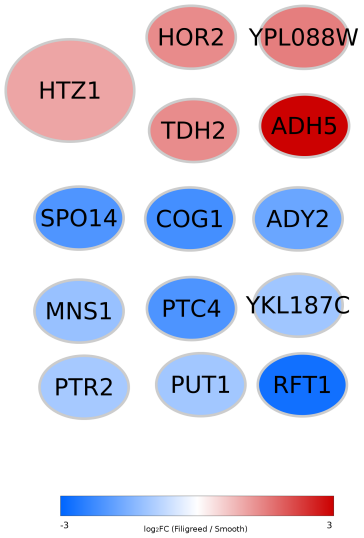

Figure 3.11: ppi-interaction network of differentially abundant proteins in the filigreed vs smooth comparison. Node color reflect protein abundance as reported in colorbar. Nodes are not connected by ppi or TF interactions.

Protein abundance leveles were next compared among the four meiotic segregants through pairwise comparisons. A total of 370 proteins were found differentially expressed among the M28 spores, by applying the following cutoffs: $|FC| > 2$, q-value < 0.05. The two meiotic segregants showing the highest number of differentially expressed proteins were the TFL-R spores characterized by an opposite morphotype, M281B (filigreed, TFL-R) and M281D (smooth, TFL-R). The total number of proteins found in this pairwise analysis was 169 ($|FC| > 2$, q-value $<$ 0.05) (Table 3.2 and Fig. 3.12). 94 proteins were down-regulated and 75 were up-regulated in M281D. Among the up-regulated, 10 were characterized by over 15-fold over expression in M281D whereas among the down-regulated the lowest level was found for PRY2, a sterol binding protein, showing a >1000-fold decrease in expression. Among the proteins showing the highest expression level in M281D, the transcription repressor Xbp1p (>1000-fold) and SSN3 (>200-fold) are known to be involved in pseudohyphal growth. Another interesting protein, Bud4p (up-regulated 3-fold) is also known to be required for the axial budding pattern. In addition,

the serine/threonine protein kinase Ksp1p, up-regulated more than 60-fold in the filamentous spore M281B, is also known to be involvement in filamentation [21]. Finally, SSK1, DFG10, ISW2 and RVS167 genes all have an ortholog in *Candida albicans* annotated in the "filamentous growth" GO category. 101 proteins were found differentially abundant between M281A (smooth, TFL-S) and M281B (filigreed, TFL-R), with 49 proteins up-regulated in the filigreed strain (M281B) and 52 down-regulated. 16 proteins showed an up-regulation more than 3-fold and among these 8 belong to amino acid metabolic pathways, strongly affected by the SSY1 mutation. Coherently, a subset of the pool of proteins down-regulated more than 3-fold involved several plasmamembrane transporters. When comparing M281A (smooth, TFL-S) with M281C (filigreed, TFL-S), 70 proteins significantly changed their expression. Being the TFL phenotype the same for these two strains, in this pairwise comparison we did not probe variations at the level of amino acid transporters. Instead, we identified 2 plasmamembrane carbohydrate transporters, HXT6 and HXT7, changing abundance between different morphological phenotypes. The comparison between M281C and M281B, both spores carrying the same morphotype but different TFL-phenotype, identified 132 proteins as differentially abundant. 79 proteins were up-regulated in the TFL-resistant spore, with 14 proteins involved in amino acid metabolism as result of the inactivation of amino acid sensing at the membrane level due to the SSY1 inactivation. Conversely, 11 proteins belonging to the central carbon metabolism as well as to the lipid metabolism were down-regulated in the TFL-resistant spore, together with GNP1 and DIP5, two amino acid plasmamembrane transporters. Remarkably, FLO11, the major read-out of filamentation was found over 4.5 fold more abundant in M281B, the spore that exhibits the strongest filigreed morphotype. This data strengthened the hypothesis of a different regulatory mechanism for the two filigreed spores based on previously shown phenotypic results. When comparing the two smooth spores (M281A and M281D) 133 proteins were found differentially abundant of which 25 were down-regulated more than 10-fold in M281D whereas 11 up-regulated more than 10-fold in M281D. Besides the colony morphology similarity, the two spores exhibit a marked variability at the cellular level. If M281A in fact mainly growths generating the classical oval shaped cells observed in *Saccharomyces cerevisiae*, M281D has a pronounced tendency to pseudohyphal growth, generating multicellular chains with elongated

cells (Fig. 3.3 Panel B). The TORC1-associated serine/threonine protein kinase Ksp1p, already shown to be associated with pseudohyphal growth (SGD database), was 40 times more abundant in M281A when compared with M281D. As for the previously described M281D vs M281B comparison, KSP1 was strongly down-regulated in M281D even though the SGD database reports a decrease in both filamentation and pseudohyphal growth for null mutant. This result was similarly detected in the pairwise M281C vs M281D comparison where Ksp1p was 50-fold down-regulated in M281D. Finally, the M281D vs M281C comparison highlighted 73 proteins as differentially abundant between the two spores, of which 35 up-regulated and 38 down-regulated in M281D. Besides the filamentous phenotype observed in M281C, Flo11p was more abundant in M281D (7-fold up-regulation). Interestingly, when comparing one spore versus all the other ones and focusing on those proteins changing expression in the same direction (always up-regulated or always down-regulated) it was possible to identify 1 protein for M281A, 27 for M281B, 13 for M281C and 9 for M281D which putatively represent signature peculiar to each strain. Together with Ksp1p, other 8 proteins were always found differentially abundant when comparing M281D with all the spores. PHO3, SBE22, PHO12, SIP5 and DBP1 were all less abundant in M281D when compared with M281A-C (4/500 fold down-regulation). Among the M281D-most abundant proteins, NTG1 was always up-regulated more than 8000-fold, together with NGL1 (4-fold up regulation) and SNF2 (more than 5-fold up-regulation).

	UP-regulated	DOWN-regulated
M281B vs M281A	52	49
M281C vs M281A	21	49
M281D vs M281A	49	84
M281C vs M281B	53	79
M281D vs M281B	75	94
M281D vs M281C	35	38

Table 3.2: Pairwise comparison of protein abundance changes between M281A-D spores. The direction of comparison is indicated by the order of writing.

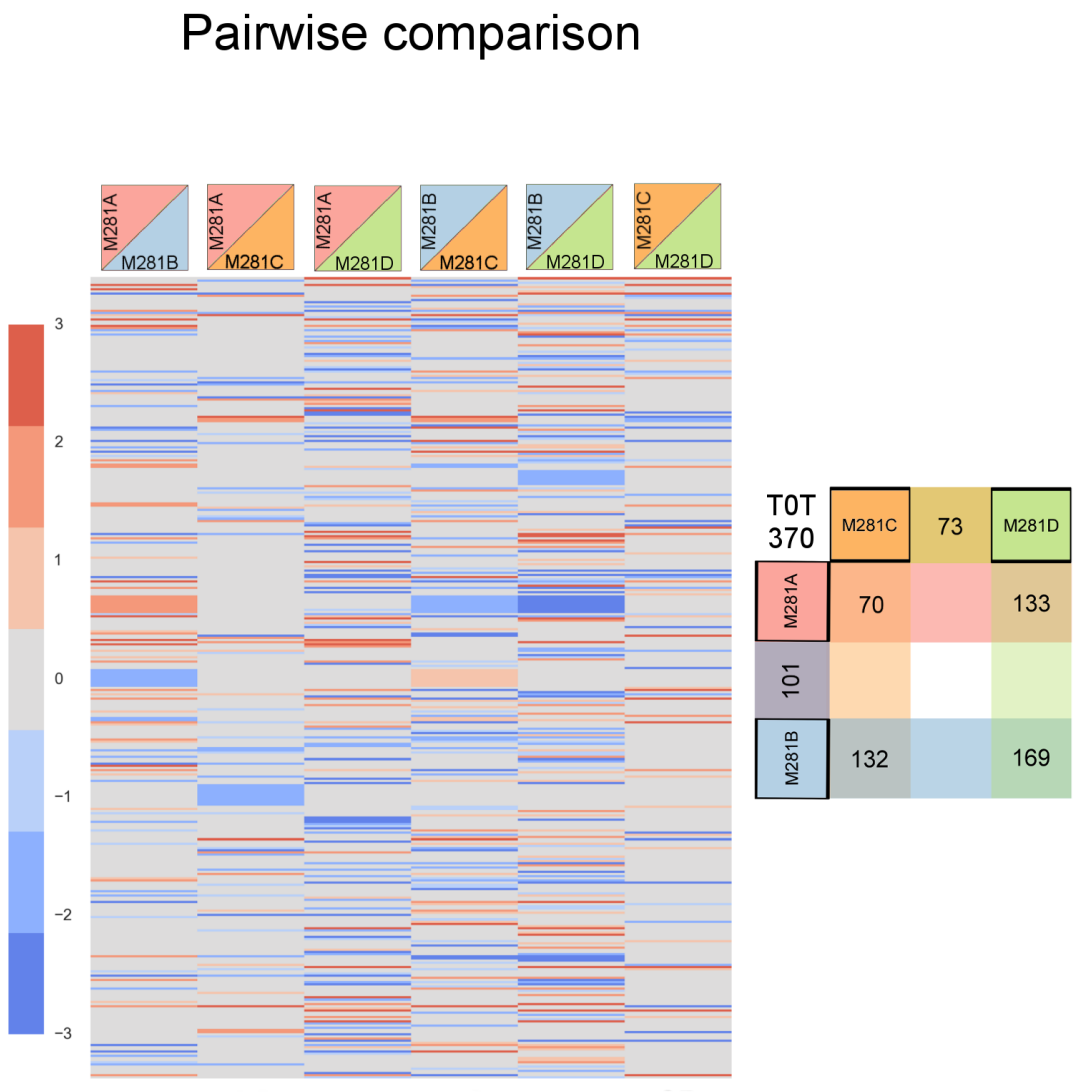

Figure 3.12: Heatmap profiles of differentially abundant proteins ($|FC| > 2$, q-value < 0.05) in the pairwise comparison reported in the upper box. The total number of significantly changing proteins in each comparison is reported in the right matrix.A total number of 370 proteins was found to significantly change in the M28 system with the M281B (filigreed, TFL-R)/M281D (smooth, TFL-S) comparison showing the highest variability.

3.5 Analysis of the trimethylated and dimethylated state of Lys 4 of histone H3 and global acetylation state of histone H4 shows spore-specific patterns

The metabolic rearrangement uncovered with the proteomic investigation was found associated with the Ssy1 T9 insertion (TFL-R vs TFL-S). Nevertheless, the source of morphological variability still remained elusive with any genetic variation segregating with the phenotype. However, proteomics revealed different protein expression patterns accompanying filamentous differentiation in M281B and M281C. If in YP supplemented with 2% ethanol the two phenotypes were bona fide identical, in YPG 2% and YPD 2% the two spores developed a different colony shape characterized by a different degree of filamentation (Fig. 3.2). In eukaryotic cells, the genome is highly organized within the nucleus in a complex compact structure known as chromatin, whose basic unit are nucleosomes, consisting of 146 bp of DNA wrapped around the four histone proteins [85, 98]. Nucleosome repositioning as well as topological changes due to histone modifications, changing the accessibility to regulatory proteins, are two mechanisms shown to affect allelic phenotypes [178]. Particularly, epialleles represent heritable states of sequence-identical genes showing a different chromatin pattern thus being potentially associated with distinct gene expression profiles. Once established, epialleles can be stably inherited over many generations but still showing higher reversion rates compared to genetic alleles. Our findings, with few genetic variations explaining only a part of the expected heritable variability prompted us to explore the chromatin organization across the M28 tetrad 1 with the aim to unveil the hidden source of M28 physiological variability. Actually, increasing evidences show the key role of chromatin remodeling in multiple cellular processes like transcription, replication, DNA repair, recombination and so forth (reviewed in 88). We therefore decided to investigate the chromatin state of the whole tetrad 1 concerning the methylation at level of the Lysin 4 for the histone H3 and the global acetylation of the histone H4. Histones H3 and H4 methylation and acetylation play in fact a leading role in gene expression regulation. Particularly,

the experiment was setup to capture the H3-K4 tri and bi-methylation and the H4 acetylation during the exponential phase of the strains growth. For each modification to be tested three independent biological replicates were inoculated for each strain in YP complete medium containing 2% ethanol. As previously described, ethanol enhances filamentous phenotype thus being the optimal medium to study spore variability in the M28 system. Once cells reached the early exponential phase (OD = 0.6) the culture was blocked and the chromatin fixed with formaldehyde followed by ChIP procedure (*Material and methods 1.12*). We extracted chromatin from M281A, M281B, M281C and M281D and immunoprecipitated DNA with Anti-Histone H3 (tri methyl K4) antibody, Anti-Histone H3 (bi methyl K4) antibody, and acetyl anti-Histone H4 antibody. For each strain (M281A-D), an aliquot of the same isolated chromatin of two biological replicates was used to immunoprecipitate DNA with Anti-Histone H3 and H4 antibodies, separately. These two immunoprecipitated sets, done in duplicates, represented the input controls for the H3 tri/bi methyl K4 and the acetyl datasets, respectively. The DNA associated with the immunoprecipitated chromatin was then purified and sequenced with Illumina technology, producing paired-end reads of 300 bp length. We obtained 52 libraries (see Table 1.5 in *Materials and methods 1.13*) with a total output of about 12 Gb. Reads were next mapped to the M281B newly assembled genome. We obtained an overall coverage of about 20X (average number of reads per nucleotide that align to M281B reference genome), uniformly distributed across the genome. The application of the Sicer pipeline [228] allowed us to identify ChIP-enriched signals for each sample by a spatial clustering approach, thus producing histone modification profiles. We chose a window size of 200 pb, with an extension of 350 bp as region where the peak can be called by Sicer, thus probing chromatin conformational changes involving from few histones to larger regions with several nucleosomes (200 bp is approximately the length of a single nucleosome plus the linker [53]). This choice reflects our aim of analyzing histone modifications domains rather than single nucleosome modifications. Identification of enriched ChIP regions was performed comparing pairs of samples for each histone modification. Initially, control libraries (input) were used to delineate significant islands enriched during the histone mark-specific immunoprecipitation. Then, a pairwise comparison was carried out to identify differential ChIP profiles between the four strains. To do that, the enriched islands were sub-

sequently used to calculate the differences in terms of enrichment patterns (presence or absence of significant islands) as well as of degree of enrichment (peaks more or less enriched in term of fold-difference but present in both the compared samples) between samples. Significant islands were selected applying a q-value cut-off of 0.01 and and $|FC| > 2$. Table 3.3 shows the number of peaks identified as enriched for each spore.

	H3 2Met K4	H2 3Met K4	H4 Ac
M281A	3301	4941	2784
M281B	3007	4759	2475
M281C	3542	5251	3075
M281D	2535	4980	2705

Table 3.3: Total number of ChIP enriched islands identified in each spore for each histone H3 and H4 modification

In all the spores with the anti-Histone H3 (tri methyl K4) antibody we identified the highest number of regions, corresponding to roughly 80 % (81 % for M281A, 79 % for M281B, 87 % for M281C and 82 % for M281D) of all genes identified in M281B. In Fig. 3.14 the information on chromosomal features relative to these loci is reported: 59% of H3 tri-methyl K4 regions fall into genes, 35% into promoters while the 5% into intergenic regions. The global profile of histone H3 tri-methylation for the 6051 ORFs of M28 indicates the prevalence of this modification at the 5' start of genes (Fig. 3.13).

These data are coherent with the general view of histone methyl status as an active mark for transcription [179]. Notably, the distribution of enriched regions of H3 bi- methylation and H4 acetylation are slightly different. Coherently with previous works showing the prevalence of H3 2Met K4 in gene body, in Fig. 3.14 we found the 72,1% of enriched regions fall in genes while only 18,9% in promoters.

As further confirmation of this finding, the distribution in Fig. 3.13 showed a much lower presence of 2Met K4 H3 on the 5' region upstream to the coding region start and a more even distribution toward the gene body compared to 3Met K4 H3.

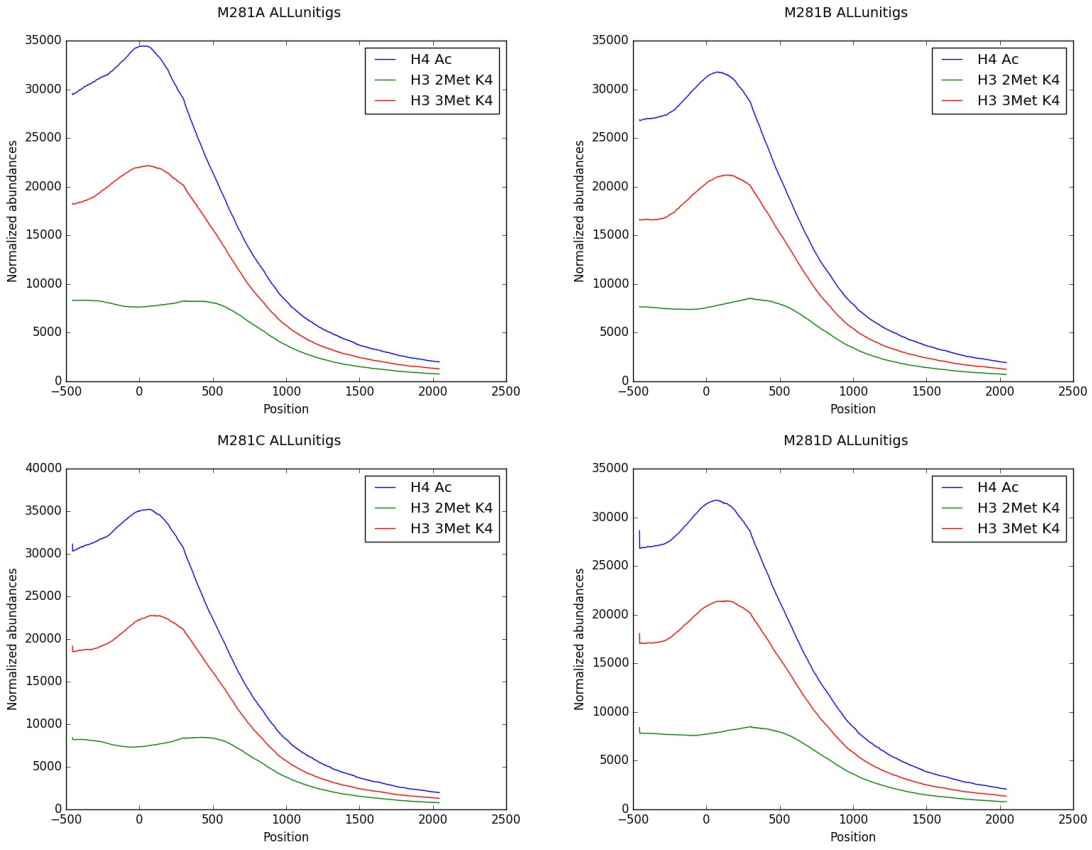

Figure 3.13: Reads distribution of H3 3Met K4, H3 2Met K4 and H4 Ac across the promoter and the 5' region of the entire M281A-D gene set (Appendix B reports gene distribution patterns for single chromosome)

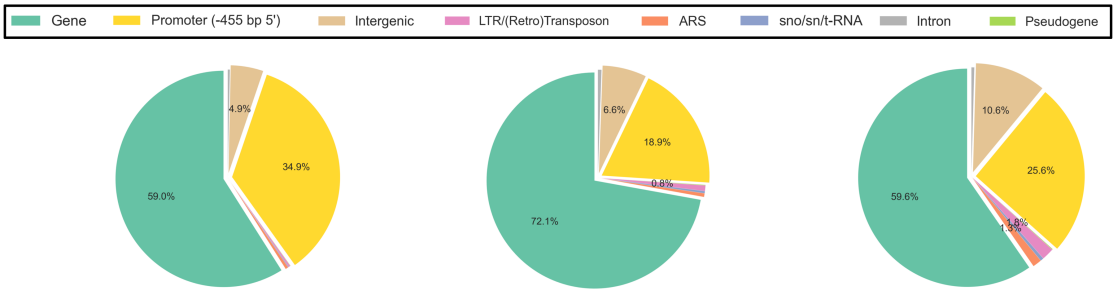

Figure 3.14: Pie chart showing the distribution of genomic features associated with ChIP enriched islands (from left to right: 3Met K4 H3, 2Met K4 H3, Ac H4) globally identified in the M281A-D system.

The H4 acetylation followed the same distribution than 3Met K4 H3, with the highest fraction of peaks falling in promoters or genes. Interestingly, the fraction of transposons was found to be higher compared to the other 2 modifications, reaching roughly 2% of the total number of significant peaks. To more accurately define the relationships between this histone H3 3Met K4 modification and transcription we analyzed the fraction of active proteome associated with this modification. Both the shotgun MS analysis and the ChIP investigation were realized under the same experimental conditions: growth in YP complete medium supplemented with 2% ethanol and harvesting at OD = 0.6 when cells are in exponential phase. This allowed a direct comparison of the two datasets. Interestingly, about 70% of the proteins identified with MS (70 % for M281A, 69 % for M281B, 74 % for M281C and 71 % for M281D) were associated to an enriched profile for the tri-methylation at the Lys 4 of histone H3 at the 5' region (promoter plus gene start) at the relative gene. The investigation of bi-methyl K4 status of histone H3 identified a low number of regions carrying this modification. The 2 TFL-sensitive spores showed the highest number of H3 2Met K4 regions with 3301 peaks for M281A (smooth) and 3542 for M281C (filigreed), while 3007 and 2535 regions were found enriched in M281B and M281D, respectively (Table 3.3). The ChIP/MS cross-referenced datasets revealed that in average only 44.5% of identified proteins (48 % for M281A, 43 % for M281B, 50 % for M281C and 37 % for M281D) were associated with the by-methylation of histone H3. The acetylation of histone H4 has been identified to be associated to a lower number of regions when compared to H3 2Met K4 and H3 3Met K4: 2784 for M281A, 2475 for M281B, 3075 for M281C and 2705 for M281D (Table 3.3). By combining ChiP data with the MS dataset we found 43% of identified proteins to be encoded by genes characterized by an enrichment in acetylation of histone H4 in M281A, 38% in M281B, 47% in M281C and 41% in M281D. Since histone acetylation and methylation have been reported to be combinatorial players in the regulation of gene expression [2] we asked which percentage of genes enriched in histone acetylation signal also carry the Lys4 tri- methylation. Considering only unique annotations (more than one peak can fall within the same gene), in M281A 1969/2494 (79%) enriched H4 Ac regions also showed the H3 3Met K4, 1749/2247 (78%) in M281B, 2229/2735 (81 %) in M281C and 1949/2441 (80%) in M281D. When looking at the protein levels, considering only the subset of proteins associated

with an enrichment for the H4 acetylation mark, those presenting also the histone H3 tri-methylation mark were comparable in all the four spores: 82% for M281A, 82% for M281B, 85% for M281C and 84% for M281D. This data showed that the major part of the proteins having the acetylation mark also presented an associated H3 tri-methylation enrichment. 1349/1733 (78%) identified proteins are associated to both tri- and bi- methylation of histone H3 in M281A, 1240/1569 (79%) in M281B, 1464/1817 (80%) in M281C and 1078/1358 (79%). In summary, the investigation of chromatin status for each single spore showed a similar pattern for all the 4 spores, with the histone H3 tri-methylation resulting in the highest number of islands in the genome and spanning over the promoter and the 5' region of gene, like the histone H4 global acetylation. Conversely, the histone H3 bi-methylation was found enriched over the gene body. Next, we asked if the 4 spores showed different chromatin status at specific loci. To answer this question we performed all the possible pairwise sets of measurements between all the different samples at each island. We identified a total of 2557 enriched loci when comparing tri-methylation of lys 4 in histone H3 between the 4 spores, subdivided as shown in Table 3.4. Despite the highest number of significant islands was identified in the H3 3Met K4 compared to the other two modifications, the major variability between spores was observed when analysing H3 2Met K4 and H4 Ac histone marks. It is intriguing to notice that in the H3 3Met K4 experiment the comparisons showing the highest number of differentially enriched peaks were those involving the M281D spore (M281A vs M281D, M281D vs M281B, M281C vs M281D). This finding is consistent with the clustering analysis of the proteomic dataset showing the formation of a disjoint subgroup with the M281A-C spores clearly separated from the smooth/TFL-sensitive M281D spore.

To investigate the role of histone modifications in shaping phenotypic variability of tetrad 1 we analyzed the TFL-response as well as the filamentous phenotype at the level of chromatin structure. For the first, we selected all the ChIP islands showing an up (or down) regulation in the TFL-sensitive spores and a down (or up) regulation in the TFL-resistant spores but not changing when comparing spores carrying the same SSY1 allele (M281A/M281C and M281B/M281D). The analysis was repeated

H3 3Met K4	Depleted	Enriched
M281A_vs_M281B	319	417
M281A_vs_M281C	358	178
M281A_vs_M281D	281	900
M281B_vs_M281C	608	314
M281D_vs_M281B	827	313
M281C_vs_M281D	194	970
H3 2Met K4	Depleted	Enriched
M281A_vs_M281B	553	644
M281A_vs_M281C	310	523
M281A_vs_M281D	455	1370
M281B_vs_M281C	638	802
M281D_vs_M281B	1137	349
M281C_vs_M281D	427	1042
H4 Ac	Depleted	Enriched
M281A_vs_M281B	620	697
M281A_vs_M281C	550	289
M281A_vs_M281D	505	991
M281B_vs_M281C	917	587
M281D_vs_M281B	817	407
M281C_vs_M281D	460	1195

Table 3.4: Table of differentially enriched regions for all the three measured histone modifications in the reported pairwise comparison. The direction of the change (depleted or enriched) is referred to the first name to the left.

for all the 3 histone marks. We identified an higher number of enriched regions in the TFL-sensitive spores compared to TFL-resistants (Table 3.5, Fig3.15) and the genes associated with these regions were retrieved.

TFL-associated ChIP islands	Depleted in TFL-S	Enriched in TFL-S
H3 3Met K4	24	76
H3 2Met K4	39	80
H4 Ac	79	152

Table 3.5: Table of ChIP islands showing an enrichment (or a depletion) in the TFL sensitive spores (M281A and M281C) and a depletion (or an enrichment) in the TFL resistant spores (M281B and M281D)

Remarkably, several genes encoding proteins involved in amino acid uptake were enriched in M281A and M281C for the H3 3Met K4 mark: BAP3 (uptake of cysteine, leucine, isoleucine and valine), GNP1 (Gln, Leu, Ser, Thr, Cys, Met and Asn transporter) , GAP1 (General amino acid permease), BAP2 (leucine, isoleucine and valine uptake), TAT1 (amino acid transporter for valine, leucine, isoleucine, and tyrosine), TAT2 (High affinity tryptophan and tyrosine permease), and MUP1 (cysteine uptake). This result is in agreement with proteomic data showing several amino acids transporters protein levels to be more abundant in the TFL-sensitive spores. Notably, all the reported genes only showed an enrichment for the H3 3Met K4 and not for the H4 acetylation, thus identifying in the histone H3 trimethylation the histone mark responsible of the SSY1-associated response. Proteomic investigation also highlighted the activation of several amino acid metabolic pathways in the TFL-R spores due to inability of Ssy1, carrying the T9 insertion, to sense amino acid in the environment thus modulating the rate of uptake of such nutrients (Fig. 3.10). Conversely, only three metabolic genes, MET3,GDH2 and SER33 showed a chromatin enrichment in the TFL-R spores at the H3 3Met K4 mark. While MET3 is involved in methionine metabolism, SER33 is part of the glycine, serine and threonine metabolism; GDH2 is a NAD(+)-dependent glutamate dehydrogenase involved in alanine, aspartate and glutamate metabolism as well as arginine biosynthesis. A higher number of metabolic genes was observed to be enriched for the H4 acetylation. STR2 (Cysteine, methionine and sulfur metabolism), BAT1 (valine, leucine and isoleucine biosynthesis), THR1 (glycine, serine and threonine metabolism), LYS1/4

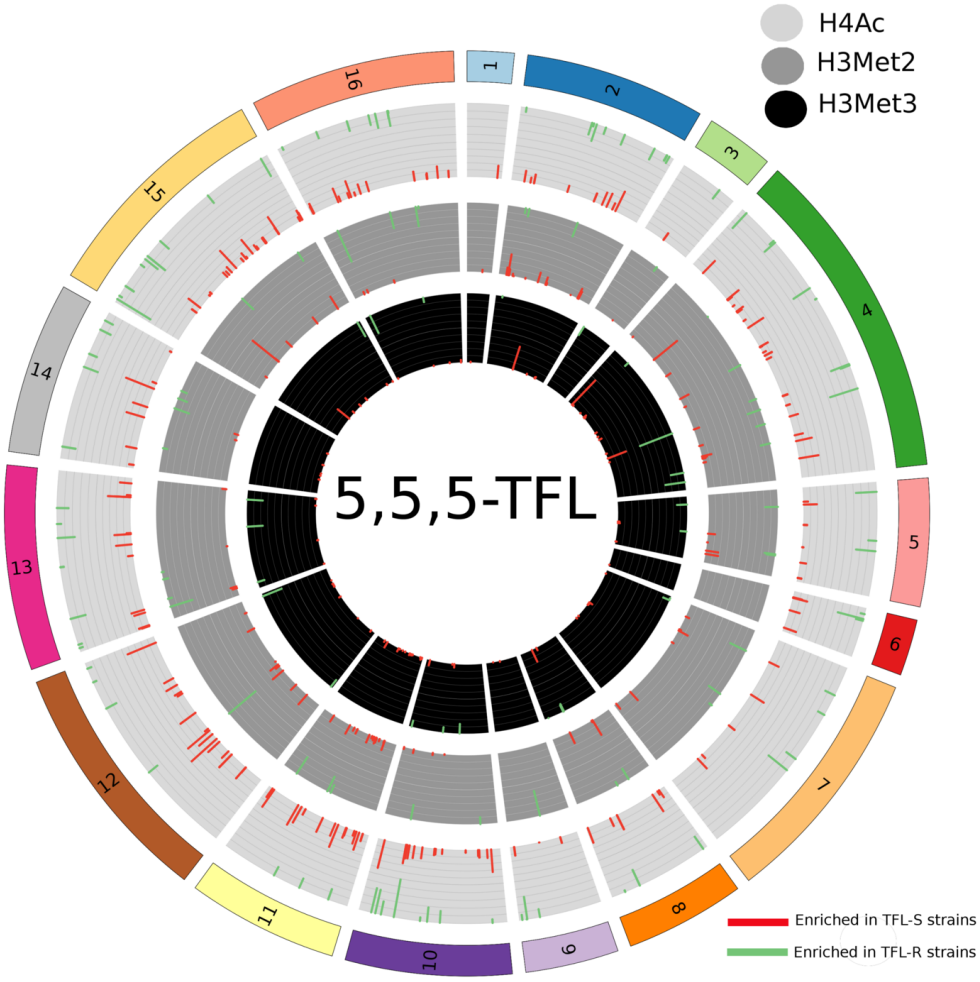

Figure 3.15: Distribution of TFL-associated ChIP enriched islands (for all the three measured modifications: 3Met K4 H3, 2Met K4 H3, Ac H4) over the 16 Saccharomyces cerevisiae chromosomes (indicated with a sequential number from 1 to 16).

(lysine metabolism), GAD1 (alanine, aspartate and glutamate metabolism), DAL2 (D-alanine metabolism), ARO4 (phenylalanine, tyrosine and tryptophan biosynthesis) and HIS3/7 (histidine metabolism) were all enriched in the TFL resistant spores. The amino acid transporters found to be differentially methylated in the TFL-R spores did not show significant variations for the H4 acetylation. Although the number of islands showing a significant variation for the H3 2Met K4 mark was higher than the number of H3 3Met K4 enriched domains, only one amino acid permease, TAT2, showed both the modifications. To assess the enrichment distribution related to morphotype, we selected all the ChIP islands showing an up (or down) regulation in the smooth spores and a down (or up) regulation in the filigreed spores but not changing when comparing spores with the same phenotype (smooth vs smooth or filigreed vs filigreed) (Fig. 3.16).

As reported in Table 3.6, a few loci showed a differential enrichment based on the phenotypic comparison. For the H3 3Met K4 we identified 18 regions depleted in the filamentous spores and only 1 enriched (UBP14). 4/18 regions associated with genes having an effect on filamentous growth. RGI2 and RPL14B were shown to decrease the filamentation growth in null mutants (SGD database) and coherently they were found among the genes showing an enriched profile in the filigreed background; conversely, SWD2 and RPL21B, previously found associated to decreased filamentation growth when over-expressed (SGD database), were characterized by an enrichment in the H3 3Met profile/s in the filamentous spores. A total of 45 regions associated with H4 acetylation were found as morphotype-related. Among these, 30 were enriched islands and 15 were depleted islands. However, only three of the differentially acetylated regions were reported associated with genes involved in filamentation (SGD database). Notably, KSP1 resulted enriched in both M281B and M281C when compared to the two smooth spores. This finding could explain the 60-fold variation at the protein level of Ks1p in the M281B vs M281D comparison. The two filigreed spores showed an enrichment for the bi-methylation of histone H3 in 6 loci and a depletion in 5. Among those, only two genes have been associated with filamentation: NOP53, shown to increased filamentous growth in null mutants (SGD database) was in fact depleted in M281B and M281C (filamentous spores) while VPS53, characterized by enriched island in the filigreed spores, showed to

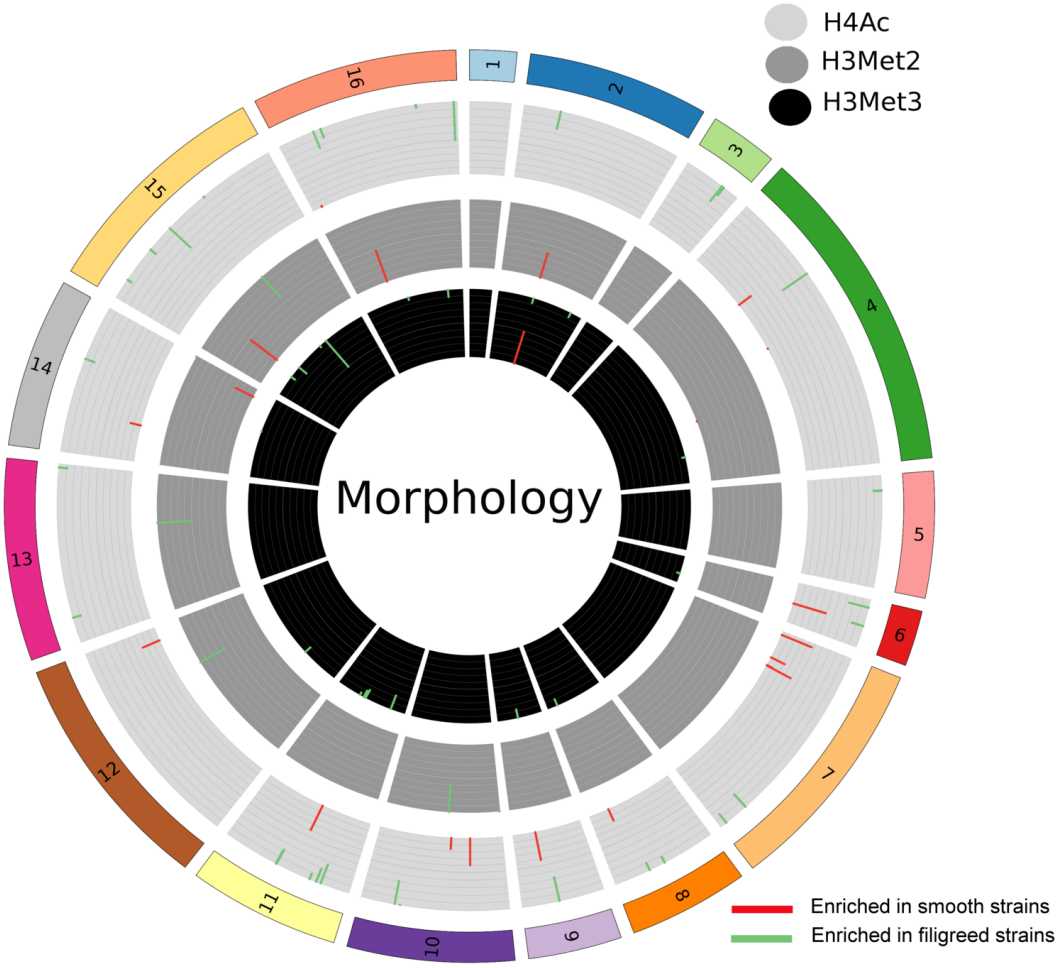

Figure 3.16: Distribution of morphology-associated ChIP enriched islands (for all the three measured modifications: 3Met K4 H3, 2Met K4 H3, Ac H4) over the 16 Saccharomyces cerevisiae chromosomes (indicated with a sequential number from 1 to 16).

decrease filamentous growth when over-expressed.

Morphotype-associated ChIP islands	DOWN in Smooth	UP in Smooth
H3 3Met K4	18	1
H3 2Met K4	6	5
H4 Ac	30	15

Table 3.6: Table of ChIP islands showing an enrichment (or a depletion) in the filigreed spores (M281B and M281C) and a depletion (or an enrichment) in the smooth spores (M281A and M281D)

To be able to compare histone modification patterns of all the 4 spores at the same time we decided to combine overlapping or "book-ended" ChIP-enriched regions identified in each pairwise comparison. Moreover, given an island i, we measured the relative abundance of island i in sample A compared to sample B which we call abi. With four samples, we thus obtained 6 relative measurements (ab_i ac_i ad_i bc_i bd_i cd_i) which we defined as ERi (the Experimentally Measured ratios of abundances in island i). Significant changes were selected applying a q-value cut-off of 0.01 and $|FC| > 2$. To be able to compare multiple samples at the same time, we sought to recover relative amounts from ratio measurements. Following the approach described in the *Materials and methods 1.13* we obtained relative values that allowed us to quickly compare elements within a single island. This approach additionally allowed us to to identify experiments with potentially problematic values, where we could not estimate any values that recover the experimentally measured ratios. We used relative abundances to investigate the presence of subgroups in our ChIP dataset. The hierarchical clustering in Fig. 3.17 showed the formation of a disjoint subcluster with the spores M281A, M281B and M281C coherently with the previously reported protein cluster.

Interestingly, when clustering acetylated data two subclusters appeared: the TFL-sensitive cluster (M281A and M281C) and the TFL-resistant cluster (M281B and M281D). Besides several amino acid transporters and permeases associated with depleted regions when analysing the H3 3Met K4 mark, as consequence of the SSY1

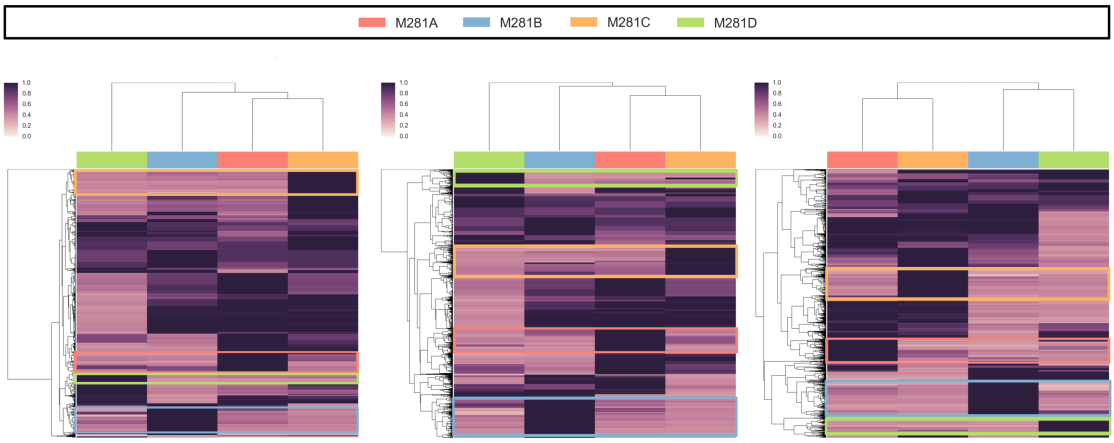

Figure 3.17: Plot of the hierarchically clustered heatmap (metric='euclidean) of relative abundances of significant enriched ChIP islands identified for all the three histone modifications: 3Met K4 H3, 2Met K4 H3, Ac H4. Highlighted regions show strain-specific chromatin domains.

T9 mutation, severals metabolic pathways were enriched for the H4 Ac mark. When comparing relative abundances of the 4 spores we unexpectedly found an high number of regions showing a chromatin status significantly enriched in one spore when compared with all the other ones. We defined "strain-specific chromatin domains" those regions having a relative abundance of 1 in a specific spore and less than 0.5 in all the other three. In Fig. 3.17 strain-specific chromatin domains are highlighted with coloured boxes. The highest number of spore specific domains was observed for the histone H4 acetylation, with up to 221 regions enriched in M281B (Table 3.7). Notably, between the unique histone acetylation patterns of M281B we identified three members of the FLO gene family, including cell-wall glycoproteins involved in the regulation of cell-cell and cell-surface adhesion: FLO1, FLO9 and FLO11 (Fig. 3.18). While FLO1 and FLO9 are located in subtelomeric regions, FLO11 is neither adjacent to a centromere nor to a telomere. From the MS dataset, we only measured protein level for Flo11p while the protein products of the two telomere-proximal FLO1 and FLO9 genes, shown to be silent in the Σ1278b genetic background (100), have not been detected neither in M281B nor in the other three spores. The expression of FLO11 has been shown to be epigenetically regulated by Hda1p and Sfl1p [77]. HDA1 encodes a putative catalytic subunit of a class II histone deacetylase

complex with a role in heat shock response [173].

M281B also showed a high number of specific chromatin domains relative to the bi-methylation of histone H3. Genes displaying enrichment in both acetylation and bi-methylation in M281B were 65, including FLO8 but not FLO11 nor FLO1. The number of strain-specific chromatin domains tri-methylated at the level of histone H3 was generally smaller with 32 domains for M281A, 76 for M281B, 118 for M281C and 70 for M281D. The 98 % of those chromatin domains falls in different genes, with almost no overlap between the 4 spores. We observed the same picture for the histone H3 K4 bi-methylation and histone H4 acetylation where a very few domains fell in the same genomic region when comparing the 4 spores.

H3 3Met K4	strain-specific chromatin domains (SSCDs)
M281A	32
M281B	76
M281C	118
M281D	70
H3 2Met K4	strain-specific chromatin domains (SSCDs)
M281A	92
M281B	243
M281C	131
M281D	99
H4 Ac	strain-specific chromatin domains (SSCDs)
M281A	75
M281B	221
M281C	192
M281D	113

Table 3.7: Total number of strain-specific chromatin domains (SSCDs) per strain per histone modification

Figure 3.18: Spore specific H4 acetylation domains at the chromosome IX. Highlighted the acetylation at the FLO11 gene in the M281B filigreed TFL-resistant spores (in Appendix A1, A2, A3 spore-specific chromatin domains are reported for all the 16 chromosomes and all the 3 analyzed histone modifications).

3.6 The M28-spores phenotypically switch from smooth to filigreed morphotype and viceversa at high frequency

In our investigations we found the ability of M281B and M281C strains to generate atypical fluffy-structured (filigreed) colonies characterized by elongated cells tightly associated with each other. Conversely, the M281A and M281D strains exhibit smooth colony morphology on solid medium, indistinguishable from that observed in the S288c *S. cerevisiae* laboratory strain. By analysing the morphotype stability in different growth conditions we found the ability of each strain to spontaneously and reversibly switch from a filamentous to a smooth phenotype and vice-versa with a surprisingly elevated reversion rate (from 2.5 × 10−3 to 0.04 in YPE 2%), several orders of magnitude higher than the yeast natural mutation rate. The recently estimated single-nucleotide mutation rate of 1.67 ± 0.04 × 10−10 per base per generation and the indel mutation rate of 5.03 ± 0.99 × 10−12 per base per generation [227] can not explain the morphological switch as a consequence of mutational events. As further confirmation, each switched spore was also able to switch back to the original phenotype. Since the filamentous morphotype was enhanced in YP supplemented with 2% ethanol, with a clear recognizability of smooth and filigreed phenotypes, we used this condition as the standard medium to investigate phenotypic switch. To have a robust evaluation of switch frequencies, we analysed between 5000 and 10.000 single-cell colonies for each spore in YPE 2% and detected colony morphology after 5 days. The TFL-resistant M281D spore exhibited the highest phenotypic switch frequency (2.7%) when compared to the other smooth TFL-sensitive spore M281A (0.8%). Among the two filigreed spores, the TFL-sensitive M281C showed the highest smooth-to-filigreed switch frequency (3%) compared to M281B (0.25%). Once each spore had switched the new phenotype was stably inherited from generation to generation. Since M28-meiotic derivatives are homothallic, we took advantage of the spontaneous generation of diploid homozygous strains inducing them to sporulate, dissecting the tetrads and analyzing the phenotypic switch frequency of the isolated spores. All the dissected spores showed the same phenotype observed in the diploid strains but with a general reduction of

the morphotype conversion frequency. As shown in Fig. 3.19, the spores dissected from each diploid strain displayed a relevant reduction of the switch frequency for all the M28 strains. For M281A we observed a 11-fold switch frequency reduction from the initial 0.77% to less than 0.07%; M281B dissected spores slightly reduced the switch frequency comparing to the diploid strain passing from 0.25% to roughly 0.1%. In both M281C and M281D this reduction was considerable, from 3% to less than 0.1% in M281C and from 2.7% to 0.2/0.4% in M281D.

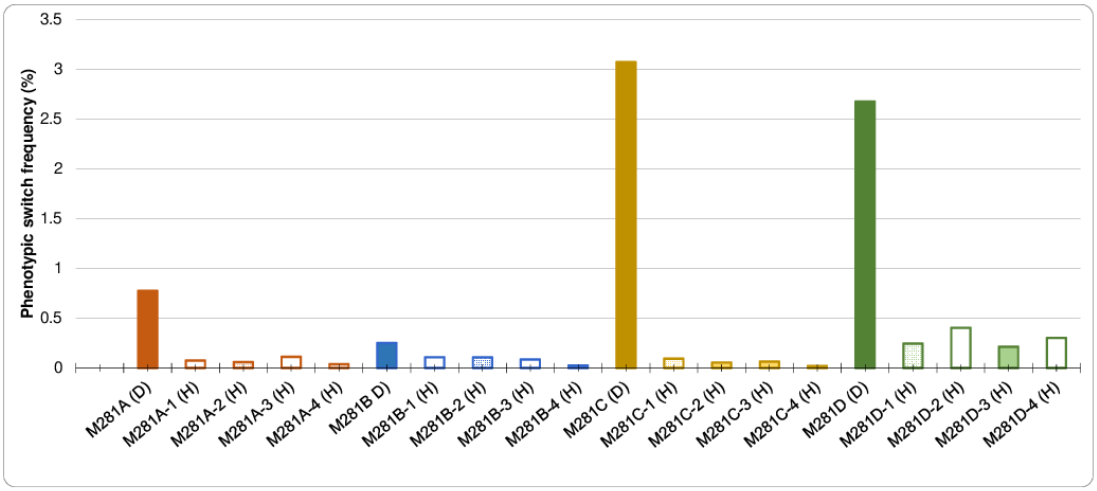

Figure 3.19: Phenotypic switch frequencies of the progeny of diploid (D) M281A (smooth), M281B (filigreed), M281C (filigreed) and M281D (smooth) obtained by inducing the diploid spores to sporulate, dissecting the tetrads and isolating the spores. Morphotype was detected in solid YPE 2% after 5-days growth at 30°C. The average number of screened colonies is 5000. Phenotypic switch frequency is calculated as the ratio between switched and not-switched colonies.

Recently, the acquisition of facultative multicellularity in budding yeast has been reported to be regulated by protein conformational changes [86]. Holmes and collaborators demonstrated that a prion formed by the transcription factor Mot3 drives the multicellular-development programs in wild yeasts probably enabling the expression of different FLO11 alleles. Prions are conformationally promiscuous proteins characterized by the ability to switch from an unstructured state to a highly ordered structure through a homotypic or heterotypic structural conversion. The conformationally changed protein acts as a seed able to structurally corrupt other proteins,

causing them to aggregate thus triggering a self-sustaining feedback loop. Prions are extremely stable and can be cytoplasmically inherited. We asked if prion-like non-Mendelian epigenetic elements could be associated to the high frequency reversible phenotypic switch of M28-strains. To investigate this possibility, we treated the spores with millimolar concentrations of guanidine hydrochloride (GdHCl, 5mM), a strong chaotropic agent known to reversibly inhibit prion propagation in yeast [55]. Since cell division was shown to be a prerequisite for GdHCl curing [52], we decided to measure the guanidine effect on phenotypic switch after both 4 and 8 generations. As shown in Fig. 3.20 our results indicated that the GdHCl treatment significantly affected the multicellular-to-unicellular and viceversa transitions in all the four spores with a comparable effect after 4 and 8 generations.

In M281A, M281B and M281C the GdHCl treatment reduced the phenotypic switch frequency. M281A displayed a 100-fold significant reduction (Bonferroni-adjusted p-value < 0.05, Welch's t test) of switch frequency passing from 0.7% to 0.07% after 4 generations and 0.02% after 8 generations. The switch frequency of M281C was instead significantly reduced from $\simeq 3\%$ to 0.05% and 0.2% for the 4th and 8th generation respectively (Bonferroni-adjusted p-value < 0.05, Welch's t test). A lower, but still significant, reduction was detected for M281B, passing from 0.26% to 0.22% (4th generation) and 0.19% (8th generation). For all the 3 described spores no significant differences between the 4- and the 8-generations GdHCl treatments were detected (Bonferroni-adjusted p-value > 0.05, Welch's t test). Interestingly, GdHCl exerted the opposite effect on M281D, the spore found to differ from the other 3 at the proteomic and chromatin structure levels (see previous results). After the GdHCl treatment in fact M281D increased its ability to switch from the smooth phenotype to the filigreed one, passing from 2.7% to 6.4% of the 4th and 8th generations. Once again the difference between the 4th and 8th generation was not statistically significant (Bonferroni-adjusted p-value > 0.05, Welch's t test). To further investigate this additional discrepancy among M281D and M281A-C and to deepen into the possible involvement of protein conformational changes in morphotype switch we decided to focus on the phenotypic transitions observed in M281D (SmR) as well as on M281B (FR). The choice of M281D and M281B spore reflects several aspects: a) the opposite direction of phenotypic switch: from filigreed to

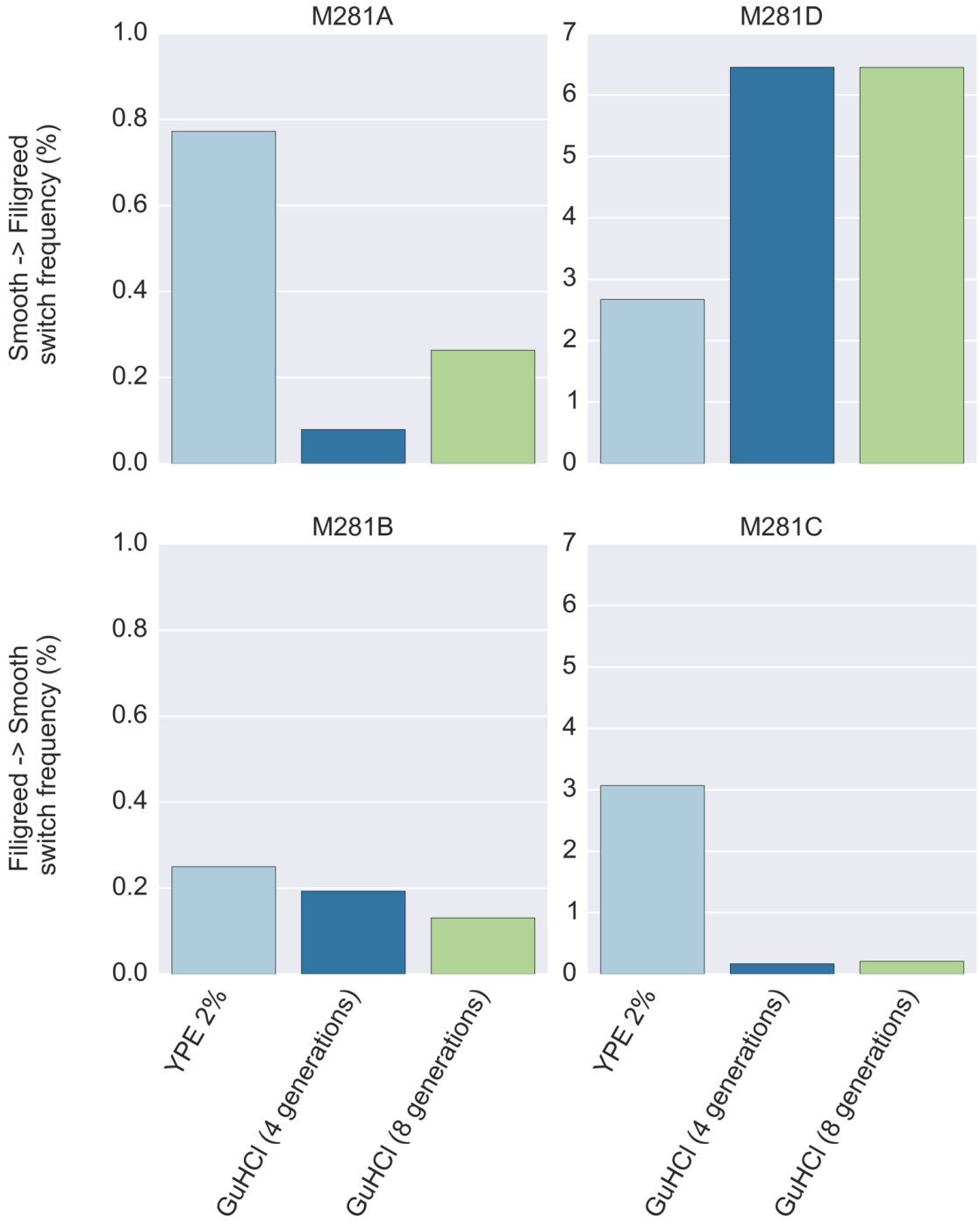

Figure 3.20: Guanidine hydrochloride (5mM) treatment of M281B and M281D spores after four or eight generations. Morphotype was detected in solid YPE 2% after 5-days growth at 30°C. The average number of screened colonies is 5000. Phenotypic switch frequency is calculated as the ratio between switched and not-switched colonies.

smooth for M281B and from smooth to filigreed for M281D; b) between the two smooth spores, M281D showed the highest phenotypic switch frequency, thus facilitating phenotypic screening; c) although M281B displayed a lower switch frequency when compared with the other filigreed spore M281C, its phenotypic transitions produce more extreme phenotypes thus simplifying the phenotypic classification; d) being M281D and M281B both TFL-resistant, we can exclude a possible role of the Ssy1p T9 mutation in driving morphotype variability between the two spores. We started our investigation analysing the global gene expression profiles, before and after the phenotypic switch, of both M281D and M281B strains. We performed a microarray gene expression experiment, directly comparing M281D (smooth) with M281D switched (filigreed), both growing in triplicate YPE 2% as well as M281B (filigreed) with M281B switched (smooth), growing in triplicate on YPE 2%. The comparison M281B/M281B switched produced 562 differentially expressed genes (BH-adjusted p-value < 0.05, $|\log2FC| > 2$), of which 153 up-regulated and 409 down-regulated in M281B relatively to the switched form. As expected the FLO11 gene, encoding for a cell-wall mucin-like glycoprotein essential for pseudohyphal formation, invasive growth and flocculation, was highly expressed in the filigreed colonies, confirming the central role of this gene in filaments formation [215]. Notably, the 70% of yeast heat shock proteins (Hsps) was differentially expressed as reported in Table 3.8. Conversely, only 1 on 8 co-chaperones, the Hsp70/90 family co-chaperone CNS1, significantly changed between M281B and M281B-switched (2.5 FC difference) (Table 3.9).

The major part of the differentially expressed Hsps appeared to be over-expressed in the filigreed background, with the environmental stress responsive HSP12 gene reaching 200-fold up-regulation. The SSA1 gene, involved in the assistance of protein folding and aggregation/misfolding prevention, was up-regulated more than 5-fold together with its target HSP104, also involved in protein aggregation and prion propagation [183]. Together with SSA1, other two members of the Hsp70 family were up-regulated more than 6-times in the filigreed background. Conversely, SSA2, SSB1 and SSB2, three members of the Hsp70 family were down-regulated in M281B. In the Hsp90 family only 1 member, HSP82, was 5-fold down-regulated in M281B. HSP104 was more than 5-fold up-regulated in M281B compared to the switched

Systematic Name	Gene Name	log2FC	Description
YAL005C	SSA1	-2.6871245	Hsp70 family (ATPase)
YLL024C	SSA2	4.41446459	Hsp70 family (chaperone)
YBL075C	SSA3	-2.7700204	Hsp70 family (ATPase)
YER103W	SSA4	-1.739651	Hsp70 family (chaperone)
YDL229W	SSB1	2.95724655	Hsp70 family (ATPase)
YNL209W	SSB2	1.85659807	Hsp70 family (ATPase)
YLR369W	SSQ1		Hsp70 family (ATPase)
YEL030W	ECM10		Hsp70 family (ATPase)
YJL034W	KAR2	2.11335451	Hsp70 family (ATPase)
YKL073W	LHS1	1.3497607	Hsp70 family (chaperone)
YJR045C	SSC1		Hsp70 family (ATPase)
YMR186W	HSC82		Hsp90 family (chaperone)
YPL240C	HSP82	-2.5179433	Hsp90 family (chaperone)
YLL026W	HSP104	-2.4943759	chaperone ATPase
YDR258C	HSP78	-2.9707344	Mitochondrial chaperone ATPase
YLR259C	HSP60		Mitochondrial chaperone ATPase
YMR322C	SNO4	-5.0346432	Possible chaperone
YOR391C	HSP33	-4.7483887	Possible chaperone
YPL280W	HSP32	-5.1781173	Possible chaperone
YBR072W	HSP26	-5.2649057	Small heat shock protein (sHSP)
YDR171W	HSP42	-3.5760395	Small heat shock protein (sHSP)
YFL014W	HSP12	-7.7514485	Heat Shock Protein
YDR533C	HSP31	-1.2844328	Heat Shock Protein
YCR021C	HSP30	-3.8913379	Heat Shock Protein
YJL159W	HSP150		Heat Shock Protein

Table 3.8: Yeast heat shock proteins (HSPs) both differentially expressed in the M281B/M281B switched comparison and not changing in this comparison

Sheet1

Systematic Name	Gene Name	log2FC	Description
YMR161W	HLJ1		Hsp40 cochaperone
YNL064C	YDJ1		HSP40 co-chaperone
YNL007C	SIS1		HSP40 co-chaperone
YOR027W	STI1		Hsp90 cochaperone
YIL104C	SHQ1		Hsp90 cochaperone
YKL117W	SBA1		Hsp90 cochaperone
YBR155W	CNS1	1.3497607	Hsp70/90 family co-chaperone
YOR020C	HSP10		Mitochondrial co-chaperonin

Table 3.9: Yeast co-chaperone both differentially expressed in the M281B/M281B switched comparison and not changing in this comparison

spore. Remarkably, Hsp104 chaperones have been shown to assume a critical and universal role [204, 36] in controlling prion propagation in yeast. If a remarkable number of Hsps was up-regulated in the fluffy morphotype, several genes involved in the osmotic stress response appeared to be strongly down-expressed. The transcripts of two hexose transporters encoded by HXT3 and HXT4 genes and reported to be heavily repressed during hyperosmotic stress [205], were down-regulated 20-fold and more than 50-fold,respectively. In addition, the hexokinase encoding HXK2 gene was down-regulated more than 18-fold in M281B. Coherently, the glucokinase encoding gene GLK1 was 15-fold up-regulated. Glk1p is rapidly de-repressed if cells are shifted to a non-fermentable carbon source, after the repression of HXK2 [119, 174]. Several genes implicated in the protection from oxidative damage and whose expression is significantly up-regulated under hyperosmotic stress showed a significant increase of expression. Among these genes CTT1 (64-fold up-regulated), encoding a cytosolic catalase, TSA2 (4.5-fold up-regulated), encoding for a stress inducible thioredoxin peroxidase and SOD2 (5.5-fold up-regulated), encoding for a mitochondrial manganese superoxide dismutase, has been shown to affect prion formation [49]. As shown in Table 3.10 41 genes out of 561 have been associated with filamentous growth (SGD database). 8 genes showed to increased filamentation when over-expressed (SGD database) were effectively over-expressed in the filigreed M281B (ADH2, CRC1, NCE103, YPK2, FMP45, RNY1, SPI1, and ARF2). Addi-

tionally, TKL1, IZH2 and RPS9A, associated to a decrease in filamentation when over-expressed (SGD database), were over-expressed in the smooth switched M281B. Conversely, for 4 genes (MLS1, MHO1, LAP3, PKR1) we observed expression levels that in our system did not fit with the effect on the phenotype described in the SGD database.

The gene ontology enrichment analysis (Table 3.11) revealed the protein refolding and unfolding processes to be among the most significantly affected ones (adjusted p-value$<$0.01) together with the oxidative stress response, known to be linked to protein oxidation, protein misfolding and aggregate formation [81].

The massive gene expression variation accompanying the M281B morphological transition during ethanol growth, with ~ 9 % of the protein-encoding transcriptome changing in expression by at least a factor 4, was not identified in the other M28 meiotic segregant. Gene expression investigation in M281D in fact did not highlight any transcript significantly changing among the wt spore and the switched spore. This considerable discrepancy between the two spores induced us to repeat the gene expression investigation in M281D. The experiment was then repeated in the same conditions with 3 independent biological replicates for each sample (M281D and M281D-switched) growing in liquid YPE 2% and starved in exponential phase (*Material and methods 1.5*). Once again, the microarray data analysis did not show any significant gene expression variation between the two conditions applying a 4-fold difference and a multiple test-adjusted p-value cutoff of 0.05. We attributed this result to the heterogeneity of the M281D community which could represent (differently to the proteomic and ChIPseq analyses) a bottleneck for the analysis of the gene expression due to the higher noise in transcript level detection As shown in Fig. 3.3 panel B, the liquid culture of M281D appeared highly heterogeneous with differentiated cell-types. Moreover, as extensively described by the works of Palkovà, *S. cerevisiae* is able to grow in organized multicellular structures characterized by sub-populations with unique metabolic properties differentiate to accomplish specific tasks [156].

Gene Name	log2FC	Phenotype	Mutant Information
RGI2	-7.272404322	filamentous growth_ decreased	null
MLS1	-6.5501423334	filamentous growth_ decreased	overexpression
ADH2	-6.4966355892	filamentous growth_ increased	overexpression
HEF3	-6.3346143352	filamentous growth_ increased	null
CRC1	-6.035622017	filamentous growth_ increased	overexpression
YRO2	-5.5638561472	filamentous growth_ decreased	null
NCE103	-5.153020963	filamentous growth_ increased	overexpression
SNO4	-5.0346431714	filamentous growth_ decreased	null
MHO1	-4.2749164394	filamentous growth_ decreased	overexpression
MUC1	-3.8582855371	filamentous growth_ decreased	null
YDR018C	-3.4830021383	filamentous growth_ increased	null
YPK2	-3.1979150441	filamentous growth_ increased	overexpression
FMP45	-3.1389688831	filamentous growth_ increased	overexpression
CLD1	-3.0108075323	filamentous growth_ decreased	null
ROM1	-2.7931663945	filamentous growth_ decreased	null
RNY1	-2.7588049359	filamentous growth_ increased	overexpression
BCY1	-2.6688950222	filamentous growth_ normal	null
OPI3	-2.6570577224	filamentous growth_ decreased	null
YHR033W	-2.5491080304	filamentous growth_ decreased	null
SPI1	-2.5416228661	filamentous growth_ increased	overexpression
APJ1	-2.4470254439	filamentous growth_ decreased	null
ATG32	-2.3358763579	filamentous growth_ decreased	null
LAP3	-2.2576135069	filamentous growth_ decreased	overexpression
YOR228C	-2.2142257397	filamentous growth_ decreased	null
FIS1	-2.1135659274	filamentous growth_ decreased	null
HOS4	-2.0820091434	filamentous growth_ decreased	null
ARF2	-2.0772916169	filamentous growth_ increased	overexpression
TPK2	-2.0341264538	filamentous growth_ decreased	null
TPK2	-2.0341264538	filamentous growth_ decreased	null
YOR343C	-2.0084329369	filamentous growth_ decreased	null
GIM3	2.0667165517	filamentous growth_ increased	null
PKR1	2.08161928	filamentous growth_ increased	overexpression
RPL14B	2.1372122614	filamentous growth_ decreased	null
FUR1	2.1944578094	filamentous growth_ decreased	null
TKL1	2.2154124002	filamentous growth_ decreased	overexpression
IZH2	2.3274391015	filamentous growth_ decreased	overexpression
RPS27A	2.3569662616	filamentous growth_ decreased	null
DUR1,2	2.427641285	filamentous growth_ increased	null
EEB1	2.6819323054	filamentous growth_ decreased	null
RPL21A	3.4302173482	filamentous growth_ absent	null
HXT4	4.3418029472	filamentous growth_ decreased	null
RPS9A	5.4148981652	filamentous growth_ decreased	overexpression

Table 3.10: Differentially expressed genes in the M281B/M281B switched comparison known to affect filamentous growth after deletion or overexpression (source: SGD database)

GO category	Multiple test-corrected P-value	GO description
GO:0055114	9.01807E-034	oxidation-reduction process
GO:0006091	2.37406E-026	generation of precursor metabolites and energy
GO:0019752	2.76886E-024	carboxylic acid metabolic process
GO:0044712	1.06960E-016	single-organism catabolic process
GO:0044262	2.18515E-016	cellular carbohydrate metabolic process
GO:0002181	2.24524E-010	cytoplasmic translation
GO:0009117	6.46893E-009	nucleotide metabolic process
GO:0034308	6.63883E-007	primary alcohol metabolic process
GO:0006790	0.000065639	sulfur compound metabolic process
GO:0042743	0.0001921678	hydrogen peroxide metabolic process
GO:0055085	0.0002450868	transmembrane transport
GO:0006979	0.0003640802	response to oxidative stress
GO:0070941	0.0005386984	eisosome assembly
GO:0008643	0.0006413075	carbohydrate transport
GO:0042221	0.0006413075	response to chemical
GO:0015718	0.0010739314	monocarboxylic acid transport
GO:0009991	0.0012785917	response to extracellular stimulus
GO:0006833	0.0012785917	water transport
GO:0006577	0.0012785917	amino-acid betaine metabolic process
GO:0010906	0.0019705161	regulation of glucose metabolic process
GO:0042026	0.0029417115	protein refolding
GO:0010466	0.003661326	negative regulation of peptidase activity
GO:0052548	0.003661326	regulation of endopeptidase activity
GO:0019740	0.0198927159	nitrogen utilization
GO:0043335	0.0236237568	protein unfolding
GO:0006613	0.031618127	cotranslational protein targeting to membrane
GO:0007039	0.0338490213	protein catabolic process in the vacuole
GO:0015976	0.0358754185	carbon utilization
GO:0000461	0.0358754185	endonucleolytic cleavage to generate mature 3'-end of SSU-rRNA from (SSU-rRNA, 5.8S rRNA, LSU-rRNA)
GO:0000028	0.0358754185	ribosomal small subunit assembly
GO:0045454	0.0400376715	cell redox homeostasis

Table 3.11: GO significantly enriched categories (Bonferroni-adjusted P-value $<$ 0.05) in the smooth/filigreed gene expression comparison

3.7 Large scale mass spectrometry-based analysis of protein structural changes during the unicellular-to-multicellular epigenetic transition

The results of gene expression investigation showed an extensive variation in the heat shock response, with the 70% of Hsps changing expression in M281B. Surprisingly, the smooth-to-filigreed transition of M281D did not produce significant variations, most likely due to the heterogeneity of the M281D population. As expected, FLO11 was up-regulated in the filigreed spore compared to its smooth counterpart. The mechanism through which FLO11 is involved in the epigenetic regulation of phenotypic switch and how the protein folding machinery is involved in this regulation still remain elusive. Nevertheless, these results encouraged us to follow the hypothesis of an involvement of protein aggregation in the epigenetic regulation of multicellularity in the M28 strains. We therefore decided to investigate the protein rearrangements occurring during the M281B-D phenotypic transitions using the LiP-coupled SRM (LiP-SRM) technique [54]; A novel method that combines limited proteolysis with MS analysis. The LiP-MS method identifies proteins that drastically increase their resistance to proteolysis (a known feature of prion-like aggregates) upon a given environmental perturbation, therefore it could potentially discover novel prion-like proteins directly in a complex biological sample. We performed the LiP-SRM investigation before and after the phenotypic switch, in M281B and M281D growing in both YPD 2% and YPE 2%. The choice of two different growth conditions reflects our interest in evaluating the effect of growth medium in the regulation of this phenotypic transition. The LiP-SRM workflow consists in a first step in which the proteomes of M281B filigreed, M281B smooth (switched), M281D smooth and M281D filigreed (switched) were extracted under native conditions. Strains were grown in triplicate in either glucose- or ethanol-supplemented liquid media. Next, a limited proteolysis of the samples was conducted with the broad-specific proteinase K, for a short reaction time (5 min) and at a low enzyme to substrate ratio (1:100). This step allowed the cleavage to be dictated by structural properties of the substrate [59]. After quenching of the protease activity achieved by shifting the proteome to denaturing conditions, a complete trypsin digestion was carried out. As a control,

a fraction of the untreated samples was subjected to the trypsinization step only. Finally a liquid chromatography-tandem mass spectrometry (LC-MS/MS) analysis was performed. The shotgun analysis identified 15194 peptides mapping to 1885 proteins (protein false discovery rate (FDR) ~1%) for M281D grown in YPD 2% and 17355 peptides mapping to 2196 proteins for the same spore but grown in YPE 2%. The number of peptides identified in M281B grown in YPD 2% was 15295 (mapping to 1974 proteins) and 18979 (mapping to 2258 proteins) for M281B grown in YPE 2%. The peptide abundances distribution reported in Appendix G (Fig. G.1) significantly changed among different sample and conditions (Bonferroni-adjusted Pvalue < 0.05, Mann-Whitney two-sided test) with the exception of the following comparisons: M281D compared with its filigreed counterpart and M281B with its smooth counterpart, both growing in YPD 2% (Bonferroni-adjusted Pvalue $= 0.832$, Mann-Whitney two-sided test).

Additionally, the correlation matrix reported in Table 3.12and Fig. 3.21 highlighted a positive correlation (Spearmanr = 0.388) between protein modifications following the phenotypic switch during glucose-growth for both M281B and M281D. In YP supplemented with 2% ethanol the M281D/M281B phenotypic transitions weakly correlated (Spearmanr = 0.096). When comparing protein rearrangements probed in the same genetic background but different media, we identified a weak anti-correlation in M281D (Spearmanr = -0.084) and a modest correlation in M281B (Spearmanr = 0.145).

	M281Dswitched vs M281D (YPD)	M281Dswitched vs M281D (YPE)	M281Bswitched vs M281B (YPD)	M281Bswitched vs M281B (YPE)
M281Dswitched vs M281D (YPD)	1	-0.0841942931	0.3885136692	0.0027110248
M281Dswitched vs M281D (YPE)	-0.0841942931	1	-0.0145256427	0.0960688339
M281Bswitched vs M281B (YPD)	0.3885136692	-0.0145256427	1	0.145412503
M281Bswitched vs M281B (YPE)	0.0027110248	0.0960688339	0.145412503	1

Table 3.12: Spearman correlation matrix of peptide abundances between M281B switched and not switched strains and M281D switched and not switched strains

At the protein level, abundances distribution varied among different samples and

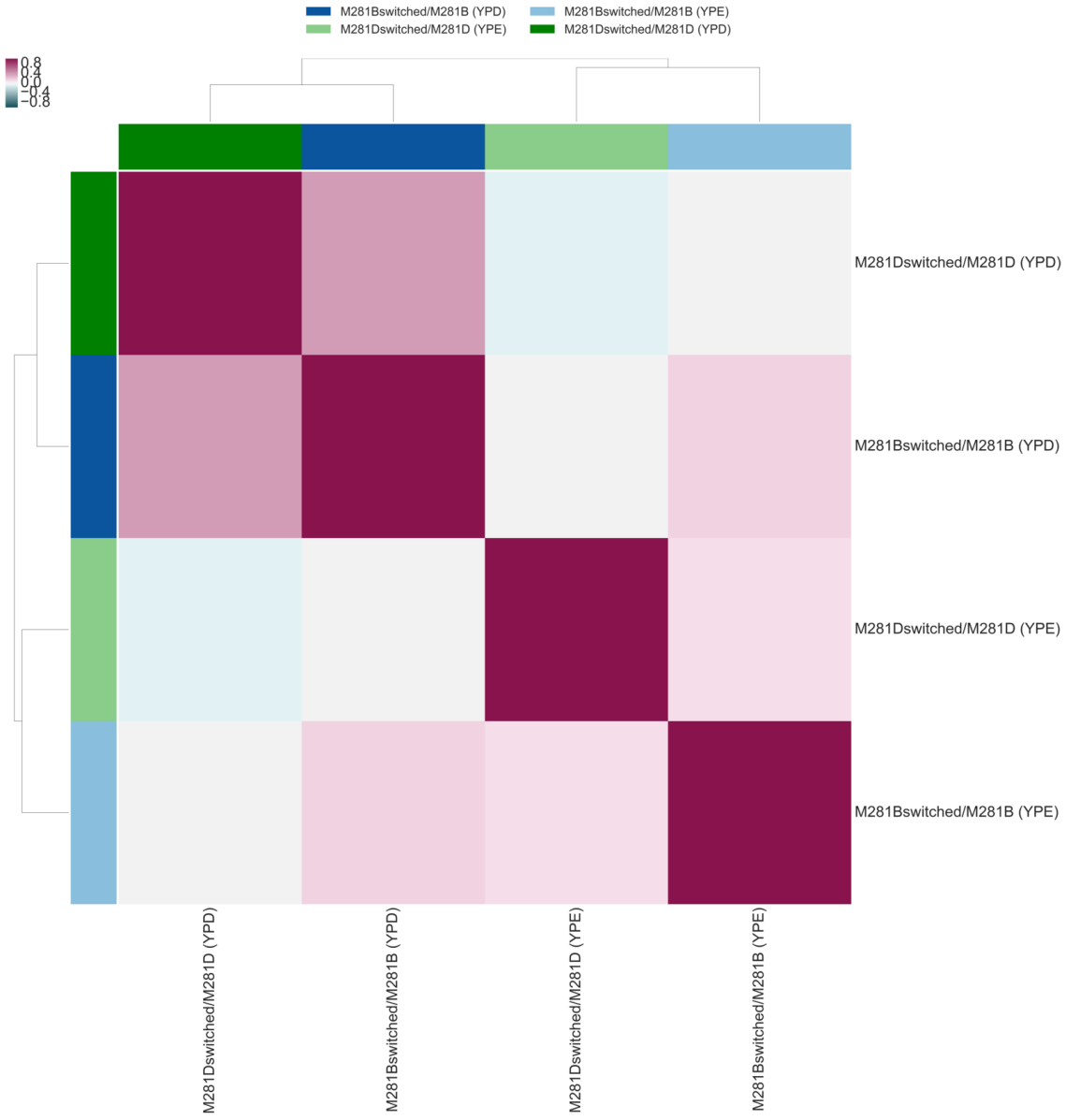

Figure 3.21: Hierarchical clustering of spearman correlation values relative to pairwise peptide abundances comparisons between M281B switched and not switched strains and M281D switched and not switched strains

different conditions (Bonferroni-adjusted Pvalue < 0.05, Mann-Whitney two-sided test) (Fig G.2). As for the peptides level, the correlation analysis showed a moderate positive correlation for M281B grown in YPD 2% compared with M281D grown in the same condition (Spearmanr = 0.243) and M281B grown in YPE 2% (Spearmanr = 0.194). (Table 3.13 and Fig. 3.22).

	M281Dswitched vs M281D (YPD)	M281Dswitched vs M281D (YPE)	M281Bswitched vs M281B (YPD)	M281Bswitched vs M281B (YPE)
M281Dswitched vs M281D (YPD)	1	-0.1005122803	0.2431707068	0.1826879067
M281Dswitched vs M281D (YPE)	-0.1005122803	1	0.0533569289	-0.0240853857
M281Bswitched vs M281B (YPD)	0.2431707068	0.0533569289	1	0.1939115843
M281Bswitched vs M281B (YPE)	0.1826879067	-0.0240853857	0.1939115843	1

Table 3.13: Spearman correlation matrix of protein abundances between M281B switched and not switched strains and M281D switched and not switched strains

To select peptides significantly changing their conformation among different phenotypic states ("conformotypic peptides") we applied an FDR-adjust p-value cutoff of 0.05 and an absolute fold change cutoff of 5 to the measured abundances (Appendix G Fig. G.3, G.4, G.5, G6).

Our results showed a significant impact of the carbon source in shaping proteome rearrangements. When phenotypically switching in rpesence of glucose as sole carbon source, the spore M281B showed a conformational change involving 511 proteins compare to 750 proteins changing conformation in M281D. Interestingly, only 329 were commonly changing in both segregants. This data confirmed our previous finding of a spore-specific regulation of the epigenetic switch. The phenotypic switch of M281B growing in YP supplemented with 2% ethanol was associated with a structural rearrangement involving 694 proteins, 258 of which were also changing in glucose. During the morphological transition of M281D 626 proteins showed a change in conformation (307/626 were also changing in YP + glucose).Results of the LiP analysis are summarized in the Venn diagrams reported in Functional enrichment analysis of proteins changing conformation in M281B before and after the phenotypic switch in YPE 2% revealed the "protein folding" (Bonferroni-adjusted p-value, 1.02 × 10-6), "cytoplasmic translation" (Bonferroni-adjusted p-value, 6.49 ×

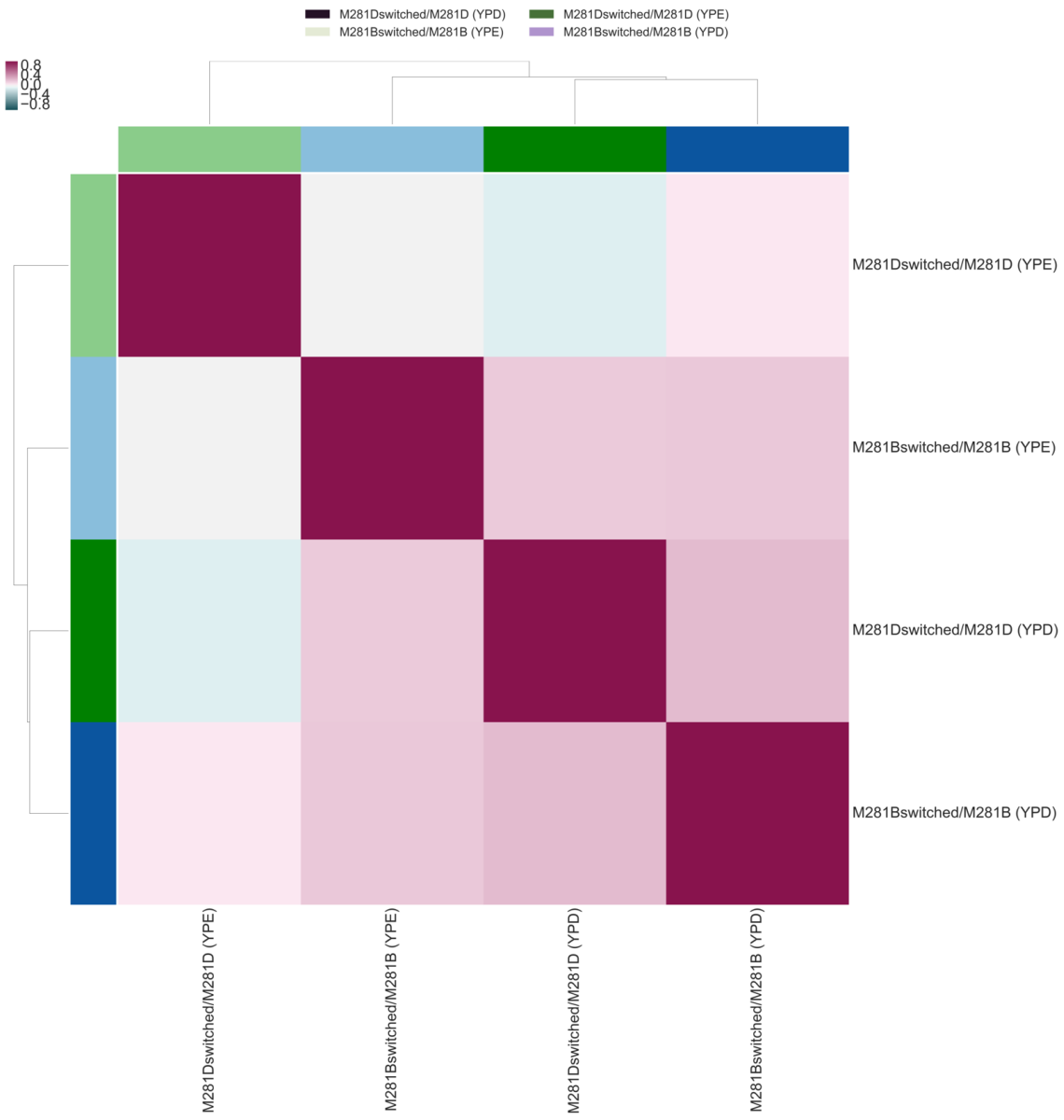

Figure 3.22: Hierarchical clustering of spearman correlation values relative to pairwise protein abundances comparisons between M281B switched and not switched strains and M281D switched and not switched strains

10-11) and "response to oxidative stress" (Bonferroni-adjusted p-value, 3.67 × 10-6) among the top-scoring GO categories together, as reported for the gene expression analysis performed in the same experimental conditions (Table 3.14).

A very similar result was observed in M281D grown in the same medium, as reported in Table 3.11. The results of functional enrichment analysis of the M281B filigreed spore when compared with its smooth counterpart in YPD 2% and M281D spore (smooth) compared to M281D switched (filigreed) are reported in Tables 3.15, 3.16, 3.17.

3.8 Prion-like proteins undergo a structural rearrangement during the M281B-D dimorphic transition

The LiP-MS approach allowed the unbiased identification of a large number of proteins drastically increasing their resistance to proteolysis during the phenotypic switch in both ethanol and glucose-supplemented media. The ability to exist in different structural conformations is a unique property of prion-like proteins together with the propagation of this alteration to unaltered form of the same (homotypic conversion) or different (heterotypic conversion) proteins. We asked if the structural transition observed in prion-like proteins could be a mechanism employed by the M28-spores to epigenetically regulate the phenotypic switch observed during ethanol-growth. Prion-like sequences are highly enriched in proteins that are functionally associated with gene expression pathways, such as RNA-binding proteins and transcription factors [3, 130]. Actually, for M281B we demonstrated a massive rearrangement at the gene expression level following the epigenetic transition. Interestingly, the Mot3 transcription factor, recently shown to regulate the acquisition of facultative multicellularity in natural yeasts (Holmes et al., 2013), did not show a conformational rearrangement in the M281B and M281D strains, suggesting an alternative scenario in which multiple players contribute to the unicellular-to-multicellular transition. Notably, an RNA binding proteins (RBPs) repertoire including 170 proteins identified in the most recent screenings [139, 206, 84], we identified a total of 82 RBPs undergoing a structural transition in one of the tested

GO category	Multiple test-corrected P-value	GO description
GO:0019752	4.012E-39	carboxylic acid metabolic process
GO:0055114	2.82857E-26	oxidation-reduction process
GO:0006091	1.15764E-17	generation of precursor metabolites and energy
GO:0006753	3.52479E-12	nucleoside phosphate metabolic process
GO:0006006	3.25834E-11	glucose metabolic process
GO:0002181	6.49418E-11	cytoplasmic translation
GO:0044724	1.16436E-10	single-organism carbohydrate catabolic process
GO:0019693	4.72142E-09	ribose phosphate metabolic process
GO:0006790	1.96113E-08	sulfur compound metabolic process
GO:0006457	1.01843E-06	protein folding
GO:0006979	3.66702E-06	response to oxidative stress
GO:0043603	0.000152578	cellular amide metabolic process
GO:0006066	0.000445569	alcohol metabolic process
GO:0015991	0.000601783	ATP hydrolysis coupled proton transport
GO:0043248	0.000880202	proteasome assembly
GO:0006417	0.001010703	regulation of translation
GO:0071941	0.001845088	nitrogen cycle metabolic process
GO:0042254	0.002630367	ribosome biogenesis
GO:0032984	0.003808082	macromolecular complex disassembly
GO:0048311	0.004371247	mitochondrion distribution
GO:0051029	0.005796585	rRNA transport
GO:0052803	0.006379172	imidazole-containing compound metabolic process
GO:0007568	0.008526472	aging
GO:0060304	0.00902513	regulation of phosphatidylinositol dephosphorylation
GO:0042743	0.010154724	hydrogen peroxide metabolic process
GO:0060260	0.016767215	regulation of transcription initiation from RNA polymerase II promote
GO:0042593	0.019730233	glucose homeostasis
GO:0000414	0.019755853	regulation of histone H3-K36 methylation
GO:0030817	0.019755853	regulation of cAMP biosynthetic process
GO:0036010	0.019755853	protein localization to endosome
GO:0015909	0.020761604	long-chain fatty acid transport
GO:0031126	0.022221677	snoRNA 3'-end processing
GO:0030036	0.023978203	actin cytoskeleton organization
GO:0007039	0.029213133	protein catabolic process in the vacuole
GO:0051453	0.030770426	regulation of intracellular pH
GO:0060303	0.030986307	regulation of nucleosome density
GO:0060548	0.030986307	negative regulation of cell death
GO:0090158	0.030986307	endoplasmic reticulum membrane organization
GO:0045851	0.033263409	pH reduction
GO:0033750	0.034603363	ribosome localization
GO:0045454	0.034911697	cell redox homeostasis
GO:0006515	0.038809337	misfolded or incompletely synthesized protein catabolic process
GO:0006890	0.03979593	retrograde vesicle-mediated transport, Golgi to ER
GO:0061163	0.04018891	endoplasmic reticulum polarization
GO:0051349	0.04018891	positive regulation of lyase activity
GO:0036257	0.04018891	multivesicular body organization
GO:0042992	0.04018891	negative regulation of transcription factor import into nucleus
GO:0008216	0.04018891	spermidine metabolic process
GO:1990116	0.041088229	ribosome-associated ubiquitin-dependent protein catabolic process
GO:1902591	0.042520217	single-organism membrane budding
GO:0001172	0.044313435	transcription, RNA-templated

Table 3.14: GO significantly enriched categories (Bonferroni-adjusted P-value $<$ 0.05) relative to the LiP dataset generated comparing M281B before and after the phenotypic switch in YPE 2%

GO category	Multiple test-corrected P-value	GO description
GO:0019752	1.34869E-44	carboxylic acid metabolic process
GO:0055114	5.23289E-27	oxidation-reduction process
GO:0006091	1.80748E-18	generation of precursor metabolites and energy
GO:0009117	3.61898E-14	nucleotide metabolic process
GO:0002181	3.779E-13	cytoplasmic translation
GO:0019693	1.7263E-11	ribose phosphate metabolic process
GO:0006006	3.56809E-11	glucose metabolic process
GO:0006732	7.41691E-10	coenzyme metabolic process
GO:0006790	1.4217E-08	sulfur compound metabolic process
GO:0006575	6.80048E-07	cellular modified amino acid metabolic process
GO:0072593	3.31272E-06	reactive oxygen species metabolic process
GO:0043603	3.34502E-06	cellular amide metabolic process
GO:0044282	4.86183E-06	small molecule catabolic process
GO:0006417	3.86049E-05	regulation of translation
GO:1902600	5.68239E-05	hydrogen ion transmembrane transport
GO:0046148	5.96643E-05	pigment biosynthetic process
GO:0000028	7.58822E-05	ribosomal small subunit assembly
GO:0006730	7.67626E-05	one-carbon metabolic process
GO:1901565	0.000101371	organonitrogen compound catabolic process
GO:0042542	0.000303121	response to hydrogen peroxide
GO:0006067	0.000435009	ethanol metabolic process
GO:0006458	0.001780593	'de novo' protein folding
GO:0042026	0.002606902	protein refolding
GO:0043248	0.004193181	proteasome assembly
GO:0051196	0.007520359	regulation of coenzyme metabolic process
GO:0045454	0.008422701	cell redox homeostasis
GO:0006913	0.01008822	nucleocytoplasmic transport
GO:0045047	0.01224924	protein targeting to ER
GO:0051029	0.013069074	rRNA transport
GO:0070941	0.015016505	eisosome assembly
GO:0031440	0.015016505	regulation of mRNA 3'-end processing
GO:0045041	0.015016505	protein import into mitochondrial intermembrane space
GO:0007568	0.01517036	aging
GO:0043624	0.018886517	cellular protein complex disassembly
GO:0052803	0.021032005	imidazole-containing compound metabolic process
GO:0010499	0.021577125	proteasomal ubiquitin-independent protein catabolic process
GO:0032956	0.023573492	regulation of actin cytoskeleton organization
GO:0009308	0.024256446	amine metabolic process
GO:0060988	0.033778975	lipid tube assembly
GO:0007089	0.033778975	traversing start control point of mitotic cell cycle
GO:0043455	0.033778975	regulation of secondary metabolic process
GO:0006577	0.033778975	amino-acid betaine metabolic process
GO:0042593	0.04385632	glucose homeostasis

Table 3.15: GO significantly enriched categories (Bonferroni-adjusted P-value $<$ 0.05) relative to the LiP dataset generated comparing M281D before and after the phenotypic switch in YPE 2%

GO category	Multiple test-corrected P-value	GO description
GO:0043436	4.84038E-29	oxoacid metabolic process
GO:0044283	2.78489E-19	small molecule biosynthetic process
GO:1901566	8.81146E-18	organonitrogen compound biosynthetic process
GO:0006412	1.55373E-12	translation
GO:0055114	2.77964E-10	oxidation-reduction process
GO:0006790	9.94041E-09	sulfur compound metabolic process
GO:0006094	4.22773E-08	gluconeogenesis
GO:0006448	1.30694E-07	regulation of translational elongation
GO:0019693	6.25326E-07	ribose phosphate metabolic process
GO:0006753	6.25326E-07	nucleoside phosphate metabolic process
GO:0042254	1.08482E-05	ribosome biogenesis
GO:0006458	1.09412E-05	'de novo' protein folding
GO:0015991	0.000121371	ATP hydrolysis coupled proton transport
GO:0008299	0.000121371	isoprenoid biosynthetic process
GO:0006913	0.000225447	nucleocytoplasmic transport
GO:0072593	0.000428795	reactive oxygen species metabolic process
GO:0006575	0.000547476	cellular modified amino acid metabolic process
GO:0010501	0.000805883	RNA secondary structure unwinding
GO:0043603	0.001375517	cellular amide metabolic process
GO:0051453	0.00251293	regulation of intracellular pH
GO:0010499	0.002657149	proteasomal ubiquitin-independent protein catabolic process
GO:0045851	0.002884795	pH reduction
GO:0006730	0.003359597	one-carbon metabolic process
GO:0043248	0.004316678	proteasome assembly
GO:0033753	0.005603555	establishment of ribosome localization
GO:0044036	0.009470123	cell wall macromolecule metabolic process
GO:0007119	0.009825675	budding cell isotropic bud growth
GO:0030150	0.012638242	protein import into mitochondrial matrix
GO:1902626	0.012944438	assembly of large subunit precursor of preribosome
GO:0070972	0.013827498	protein localization to endoplasmic reticulum
GO:0051051	0.022465298	negative regulation of transport
GO:0070843	0.026674007	misfolded protein transport
GO:0035950	0.026674007	regulation of oligopeptide transport by regulation of transcription from RNA polymerase II promoter
GO:0072353	0.026674007	cellular age-dependent response to reactive oxygen species
GO:0090036	0.026674007	regulation of protein kinase C signaling
GO:0032889	0.034218698	regulation of vacuole fusion, non-autophagic
GO:0006888	0.03979751	ER to Golgi vesicle-mediated transport
GO:0051262	0.043017708	protein tetramerization
GO:0000916	0.043017708	actomyosin contractile ring contraction
GO:2000531	0.043017708	regulation of fatty acid biosynthetic process by regulation of transcription from RNA polymerase II promoter

Table 3.16: GO significantly enriched categories (Bonferroni-adjusted P-value $<$ 0.05) relative to the LiP dataset generated comparing M281B before and after the phenotypic switch in YPD 2%

GO category	Multiple test-corrected P-value	GO description
GO:0060261	0.012274176	positive regulation of transcription initiation from RNA polymerase II promoter
GO:0071166	0.002996612	ribonucleoprotein complex localization
GO:0006457	6.80228E-06	protein folding
GO:0034059	0.046370697	response to anoxia
GO:0043954	0.036476141	cellular component maintenance
GO:0006730	0.005948319	one-carbon metabolic process
GO:0034724	0.02524943	DNA replication-independent nucleosome organization
GO:0050657	1.61477E-05	nucleic acid transport
GO:0045039	0.003034911	protein import into mitochondrial inner membrane
GO:2000877	0.046370697	negative regulation of oligopeptide transport
GO:0043248	0.000476556	proteasome assembly
GO:0051453	0.018559029	regulation of intracellular pH
GO:0008219	0.018559029	cell death
GO:0071826	2.56525E-06	ribonucleoprotein complex subunit organization
GO:0042304	0.036476141	regulation of fatty acid biosynthetic process
GO:0015991	1.87701E-05	ATP hydrolysis coupled proton transport
GO:0035950	0.046370697	regulation of oligopeptide transport by regulation of transcription from RNA polymerase II promoter
GO:0043161	0.001275443	proteasome-mediated ubiquitin-dependent protein catabolic process
GO:0042254	9.63124E-13	ribosome biogenesis
GO:1900151	0.035815697	regulation of nuclear-transcribed mRNA catabolic process, deadenylation-dependent decay
GO:0002181	2.31966E-28	cytoplasmic translation
GO:0010501	0.000507042	RNA secondary structure unwinding
GO:0034517	0.011832257	ribophagy
GO:0045851	0.018559029	pH reduction
GO:0090158	0.036476141	endoplasmic reticulum membrane organization
GO:0006913	4.28311E-06	nucleocytoplasmic transport
GO:0072593	0.003134185	reactive oxygen species metabolic process
GO:0009117	6.77062E-15	nucleotide metabolic process
GO:0045047	0.017172607	protein targeting to ER
GO:0043436	4.9451E-30	oxoacid metabolic process
GO:0045454	0.003138034	cell redox homeostasis
GO:0033753	0.005244495	establishment of ribosome localization
GO:0006979	0.025284836	response to oxidative stress
GO:0055114	1.9207E-09	oxidation-reduction process
GO:0035306	0.022374699	positive regulation of dephosphorylation
GO:0043094	0.035815697	cellular metabolic compound salvage
GO:0090114	0.010958897	COPII-coated vesicle budding
GO:0006403	9.6991E-07	RNA localization
GO:0001302	0.017172607	replicative cell aging
GO:0031440	0.02524943	regulation of mRNA 3'-end processing
GO:0060988	0.046370697	lipid tube assembly
GO:0006334	0.022374699	nucleosome assembly
GO:0010499	8.88006E-07	proteasomal ubiquitin-independent protein catabolic process
GO:0019693	9.63124E-13	ribose phosphate metabolic process
GO:0006067	0.000159414	ethanol metabolic process
GO:0052803	0.001378781	imidazole-containing compound metabolic process
GO:0045945	0.046370697	positive regulation of transcription from RNA polymerase III promoter
GO:0006417	1.97274E-11	regulation of translation
GO:0006006	7.1586E-06	glucose metabolic process
GO:0051788	0.046370697	response to misfolded protein
GO:1903310	0.014763363	positive regulation of chromatin modification
GO:0008216	0.046370697	spermidine metabolic process

Table 3.17: GO significantly enriched categories (Bonferroni-adjusted P-value $<$ 0.05) relative to the LiP dataset generated comparing M281D before and after the phenotypic switch in YPD 2%

conditions (see Table 3.18).

Taken together these data led us to hypothesize the involvement of multiple prion-like transcription factors in the epigenetic regulation of multicellularity in our yeast model. To deepen into this possibility, we integrated proteomic data with genomic and expression data. Using a list of putative prion-like proteins recently published [3] we aimed to find aggregation-prone transcription factors whose conformational change is associated with the extensive transcriptional changes accompanying the phenotypic switch. Briefly, we cross-referenced the LiP datasets with the following 3 databases: the "variant DB" containing M28-tetrad 1 genetic variations (SNPs/indels), the "DEGs DB", containing gene differentially expressed in the filigreed strain when compared with its smooth version and finally the "Prion DB", containing the putative prion proteins predicted by Alberti et al [3]. Additionally, we used the yeast interactome containing both ppi and gi interactions (*Materials and methods 1.15*) to identify the first interactors of the LiP targets. Final selected targets were prion-like proteins displaying a conformational change during the phenotypic transition and being directly connected (first neighbour in the yeast interactome) to a gene changing expression during the transition. To not exclude indirect effects of the structural transitions in gene expression, we also selected prion-like proteins not directly associated to expression variations. This analysis produced 25 proteins (see Table 3.19) whose structural rearrangements could epigenetically regulate the unicellular-to-multicellular transition by modulating the expression of genes involved in morphogenesis.

All the targets we identified were highly connected by protein-protein interactions, as shown in Fig. 3.23, 3.24. Interestingly, 11/25 targets were RNA-binding proteins. In order to validate this result we decided to exploit the protein-protein interaction capability as well as the RNA binding feature to investigate the cellular localization patterns produced by each candidate selected in our analysis.

The result of an orthogonal validation performed by the Lindquist laboratory (dr. Erinc Hallacli's personal communication, data not shown), confirming the aggregation of Hrp1p in M281D and showing a different percentage of aggregation in the strain before and after the phenotypic switch, prompted us to focus on this candidate. Therefore, we fused the GFP protein to N-terminus of HRP1 (*Material and*

Gene_Name	Gene_Name	Sample	Condition
YAR007C	RFA1	M281D	YPE
YBL004W	UTP20	M281B/M281D	YPE/YPD
YBL032W	HEK2	M281D	YPD
YBR079C	RPG1	M281B/M281D	YPE/YPD
YCL037C	SRO9	M281B/M281D	YPD
YCL059C	KRR1	M281B	YPE
YCR057C	PWP2	M281D	YPD
YCR077C	PAT1	M281B/M281D	YPD
YDL051W	LHP1	M281B/M281D	YPD
YDL088C	ASM4	M281D	YPD
YDL160C	DHH1	M281D	YPD
YDL185W	VMA1	M281B/M281D	YPE/YPD
YDL213C	NOP6	M281B	YPE/YPD
YDR037W	KRS1	M281B/M281D	YPE/YPD
YDR060W	MAK21	M281B/M281D	YPD
YDR172W	SUP35	M281B/M281D	YPD
YDR293C	SSD1	M281B/M281D	YPE/YPD
YDR429C	TIF35	M281B/M281D	YPE/YPD
YDR432W	NPL3	M281B	YPE/YPD
YDR496C	PUF6	M281D	YPD
YDR505C	PSP1	M281D	YPE
YER165W	PAB1	M281D	YPD
YGL014W	PUF4	M281D	YPD
YGL049C	TIF4632	M281B/M281D	YPD
YGL120C	PRP43	M281D	YPD
YGL122C	NAB2	M281B/M281D	YPD
YGL173C	XRN1	M281B/M281D	YPE/YPD
YGL245W	GUS1	M281B/M281D	YPE/YPD
YGR054W	YGR054W	M281D	YPD
YGR103W	NOP7	M281B/M281D	YPE/YPD
YGR155W	CYS4	M281B/M281D	YPD
YGR159C	NSR1	M281B/M281D	YPD
YGR162W	TIF4631	M281B/M281D	YPD
YGR178C	PBP1	M281B/M281D	YPE
YGR185C	TYS1	M281B/M281D	YPE/YPD
YGR279C	SCW4	M281D	YPD
YHL015W	RPS20	M281B/M281D	YPE/YPD
YHL034C	SBP1	M281D	YPD
YHR216W	IMD2	M281D	YPD
YJL050W	MTR4	M281B/M281D	YPE/YPD
YJL080C	SCP160	M281B/M281D	YPD
YKL204W	EAP1	M281B	YPE
YLR175W	CBF5	M281B/M281D	YPE/YPD
YLR197W	NOP56	M281B/M281D	YPE/YPD
YLR276C	DBP9	M281D	YPD
YLR401C	DUS3	M281D	YPD
YLR419W	YLR419W	M281B/M281D	YPE/YPD
YLR432W	IMD3	M281B/M281D	YPE/YPD
YML056C	IMD4	M281D	YPD
YMR012W	CLU1	M281B/M281D	YPE/YPD
YMR125W	STO1	M281D	YPD
YMR229C	RRP5	M281B/M281D	YPE/YPD
YMR302C	YME2	M281B/M281D	YPE/YPD
YMR309C	NIP1	M281B/M281D	YPD
YNL002C	RLP7	M281D	YPD
YNL016W	PUB1	M281D	YPD
YNL110C	NOP15	M281B	YPD
YNL175C	NOP13	M281B/M281D	YPD
YNL178W	RPS3	M281B/M281D	YPE/YPD
YNL210W	MER1	M281D	YPD
YNL255C	GIS2	M281B/M281D	YPE/YPD
YNR051C	BRE5	M281D	YPD
YOL041C	NOP12	M281B	YPE
YOL123W	HRP1	M281B	YPD
YOR056C	NOB1	M281D	YPD
YOR151C	RPB2	M281B/M281D	YPE/YPD
YOR168W	GLN4	M281D	YPD
YOR198C	BFR1	M281B/M281D	YPD
YOR204W	DED1	M281B/M281D	YPE/YPD
YOR206W	NOC2	M281D	YPD
YOR310C	NOP58	M281D	YPD
YOR361C	PRT1	M281B/M281D	YPE/YPD
YPL009C	RQC2	M281B	YPE/YPD
YPL012W	RRP12	M281B/M281D	YPD
YPL043W	NOP4	M281B/M281D	YPE/YPD
YPL126W	NAN1	M281B/M281D	YPE/YPD
YPL169C	MEX67	M281D	YPD
YPL212C	PUS1	M281B/M281D	YPD
YPL217C	BMS1	M281D	YPD
YPL226W	NEW1	M281B/M281D	YPE/YPD
YPR033C	HTS1	M281B/M281D	YPE/YPD
YPR163C	TIF3	M281B/M281D	YPE/YPD

Table 3.18: RNA binding proteins displaying a protein structural rearrangements during the epigenetic phenotypic trasnsition

	peptides	start AA	end AA	is in PrD domain?	Gene name	qvalue	log2FC
M281BvsM281B switched / Glucose	SGTPFEK	186	194	false	IF4F2	0.031557717	-3.7676713
	NIYCLFR	465	473	false	NAB2	0.000754466	-10.27362
	SNPPQVPSGWK	5	17	false	WWM1	0.007836788	-3.0616405
	LNQPQQDSNATQGSPAPSDSDNN	420	446	true	HRP1	5.31E-05	-10.688527
	EEKPVQTEEK	195	206	false	ERF3	0.039819183	4.49014742
	EVSNQSPAVVESNTNNTSQEEKPV	761	788	false	CYC8	5.31E-05	11.0922826
	GQIKEESTPK	286	297	false	IF4F1	0.037990493	6.76729541
	NNNETSKPAFSF	350	363	false	NSP1	0.032908992	-2.5400932
	DSDSSKPAFSF	484	496	false	NSP1	6.19E-05	10.0482712
	EFPSEEILVEALER	243	258	false	NOP3	0.007836788	-3.6372256
	LNNIEFR	257	265	false	NOP3	0.003454572	3.52673241
	LQEQQLQEQQLQQQQQQQQLF	456	479	true	KC11	5.31E-05	11.0000547
M281DvsM281D switched / Glucose	SSQWEPPR	34	43	false	WWM1	0.00730811	-3.6611916
	NIYCLFR	465	473	false	NAB2	0.001091748	-9.8607513
	LSEIVAPLLVGPIR	858	873	false	PUF4	0.008184031	9.14369712
	YTILDAPGHK	339	350	false	ERF3	0.003744495	-3.4783832
	AIGYNIK	432	440	false	ERF3	0.006316396	2.82068648
	LVSSSGIK	145	154	false	ERF3	0.034673678	5.52496394
	KGEYETGFER	372	383	false	ERF3	0.000517496	7.28139233
	EEKPVQTEEKTEEK	195	210	false	ERF3	0.020398403	10.3937465
	EVSNQSPAVVESNTNNTSQEEKPV	761	788	false	CYC8	0.001206841	12.3190314
	FVGDLNVNVDDETLR	164	180	false	PUB1	8.14E-06	-9.2234891
	GITYLNEVLEK	518	530	false	NUP57	0.036875399	3.39620644
	NEIESFIPLLLPGIQK	421	438	false	NEW1	0.026827708	-9.2205739
	ELTPISQFLSK	136	148	false	NEW1	0.014944751	-4.4158362
	SSSQEQLR	397	406	false	NEW1	0.001594101	-3.6866198
	ADILLLDEPTNHLDVSNVK	705	725	false	NEW1	2.92E-05	11.9598743
	QPQPQQQQQHLQFNGSSDASSLF	37	61	true	NUP59	0.029566172	-7.2279509
	HDVPQDSNDNNNEELEAQ	171	190	false	DEF1	1.25E-05	-12.740538
	SEASEEKVNEQETSAQ	281	298	false	DEF1	1.76E-05	-11.224728
	EQEEQQQQEGHNNKEEHK	200	219	true	DEF1	0.02161085	-6.7522262
	EQVKEEEQTAEEL	329	343	false	DEF1	0.041452347	7.46091722
M281BvsM281B switched / Ethanol	NFYTGR	639	646	true	AKL1	0.035924934	8.90705645
	QQHPQPQSQQPQSQQSPQSQK	478	500	true	DEF1	0.029944955	-11.379066
	KLEDYCR	382	390	false	NUP49	0.021376569	5.08902362
	LNNIEFR	257	265	false	NOP3	0.013024659	3.52276362
	VEFEEAESAAK	162	174	false	NOP3	0.018881132	4.31464501
	VITVERDDNPPPIR	266	281	false	NOP3	0.008457582	11.6107866
	IVDVLSK	387	395	false	NEW1	0.008904377	5.09008178
	SVNHSSSTLQTDDISVDK	752	771	false	PAN1	0.019840689	-4.7112226
	TEDYLNR	630	638	false	CCR4	0.012247033	4.10206163
	APEFVSVNPNAR	152	165	false	URE2	0.039863695	3.72328689
	NGSQNNDNENNIK	65	79	true	URE2	0.000301836	10.2175397
	NNNETSKPAFSF	350	363	false	NSP1	0.012247033	-3.3943427
	DSDSSKPAFSF	484	496	false	NSP1	0.031592454	4.43840305
	VDLNILDR	868	877	false	SSD1	0.029294221	3.10601831
	LVAGILR	358	366	false	SSD1	0.049599829	6.56148504
	SSTINNDSDSLSSPTK	479	496	false	SSD1	0.000527369	10.9699306
M281DvsM281D switched / Ethanol	DNVALFLK	641	650	false	CCR4	0.013061516	-2.4353046
	EQVKEEEQTAEEL	329	343	false	DEF1	0.026501809	4.12609732
	EFGGQGR	183	191	true	YNU8	0.003335219	4.01660361
	YQFDPQQDGDLGLKPGDK	62	81	false	PIN3	0.032118231	3.47060431
	SELPKVEDLK	209	220	false	ERF3	0.011422001	-4.5230588
	KMKDLGTIVEGK	496	509	false	ERF3	0.020396496	2.54964303
	AEFDGTNR	1102	1111	false	SSD1	0.005065661	-4.1263401
	NIELDKEAESEPLISDPLSK	1152	1173	false	SSD1	0.000590649	11.0742286
	LNEIYIR	65	73	false	LSM4	0.015697234	-7.6665452
	NIYCLFR	465	473	false	NAB2	7.23E-05	-10.552972
	LFPHCPLGR	263	273	false	NAB2	0.001148583	-9.4358693

Table 3.19: Target proteins showing a structural rearrangements being potentially responsable for the epigenetic unicellular-to-multicellular M281B/D transition

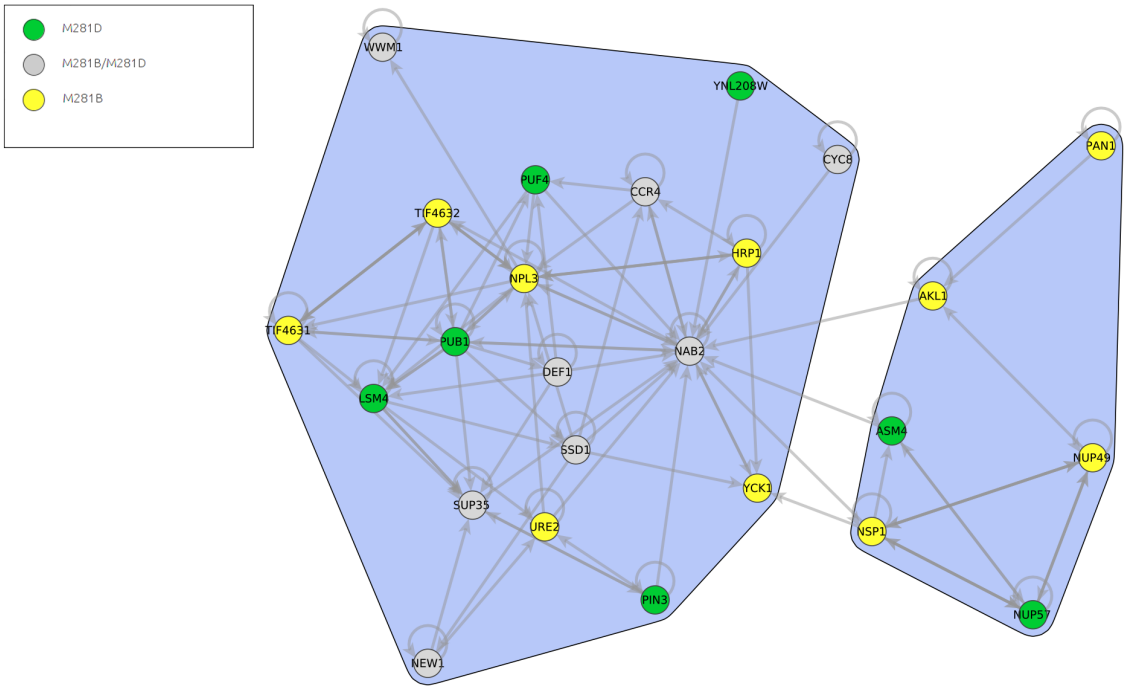

Figure 3.23: Protein-protein interaction + TF interaction network connecting 25 candidate as regulators of the morphotype transition in both M281B and M281D spores. Node color reflects the strain in which the conformational changes were identified (yellow = M281B, green = M281D, grey = M281B/M281D).

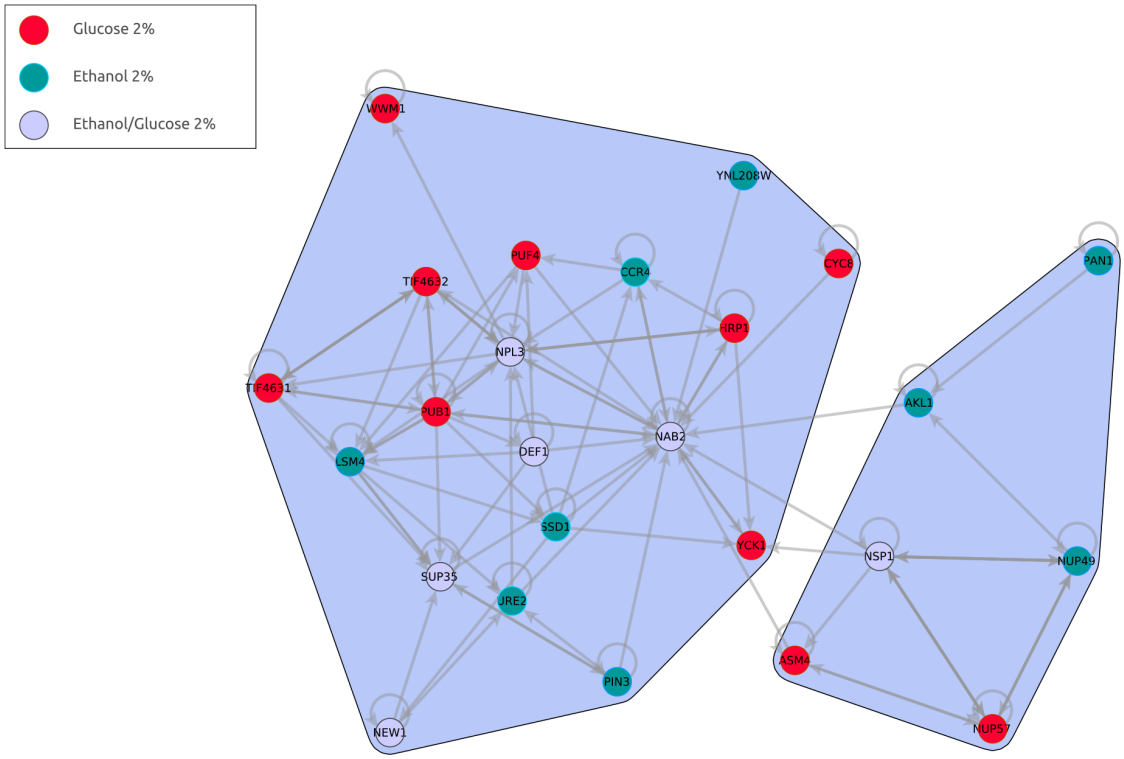

Figure 3.24: Protein-protein interaction + TF interaction network connecting 25 candidate as regulators of the morphotype transition in both M281B and M281D spores. Node color reflects the medium in which the conformational changes were identified (red = YPD 2%, blue = YPE 2%, grey = both).

methods 1.16) and followed its localization in both M281D smooth and M281D filigreed (switched). Since in the filigreed colonies, flat (smooth) regions coexist with filamentous structures, we decided to detect the presence of Hrp1 aggregation foci in both these regions. To note, the Hrp1 RNA-binding protein clearly showed foci formation with a nuclear localization when GFP-tagged, indicating that aggregation is taking place in this compartment (Fig. 3.25). The number of M281D cells showing Hrp1 foci were the 8.5 % compared to the 34% detected in the M281D switched population. Notably, this percentage is referred to cells isolated from the filamentous region of the filigreed colony. Remarkably, when counting the number of hrp1 foci in the flat region of the colony, only the 3.7% showed foci formation. The different percentage between not-switched and switched M281D is significant for both the flat (Bonferroni-adjusted p-value = 2.59e-03, two-tailed t-test) and the filamentous regions (Bonferroni-adjusted p-value = 8.66e-10, two-tailed t-test).

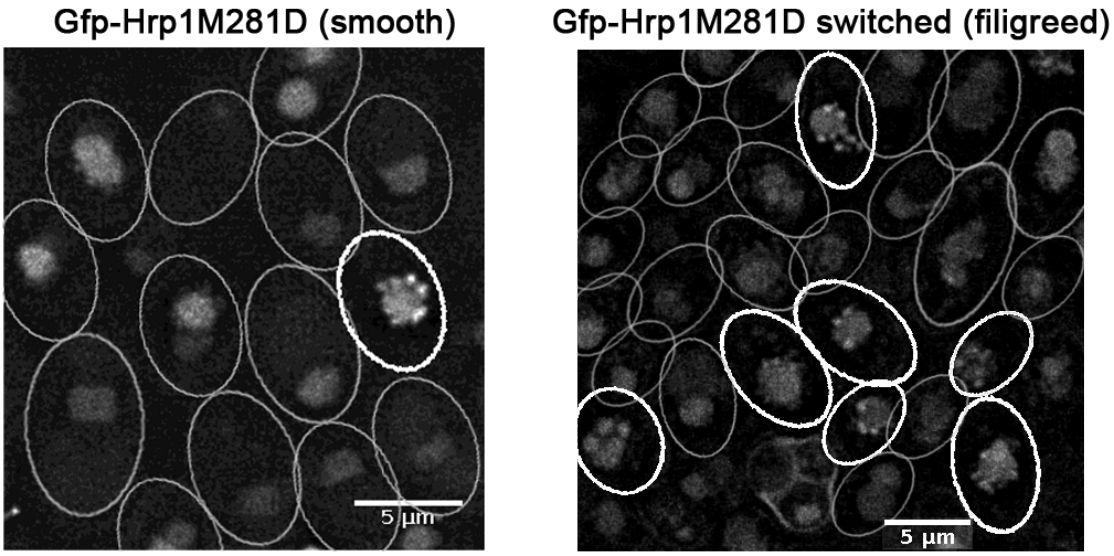

Figure 3.25: Gfp-Hrp1 loci formation at the nucleus of M281D before (left) and after (right) the phenotypic switch (maximum projection of 21 focal planes). White oval shapes highlight cells with the presence of protein aggregates.

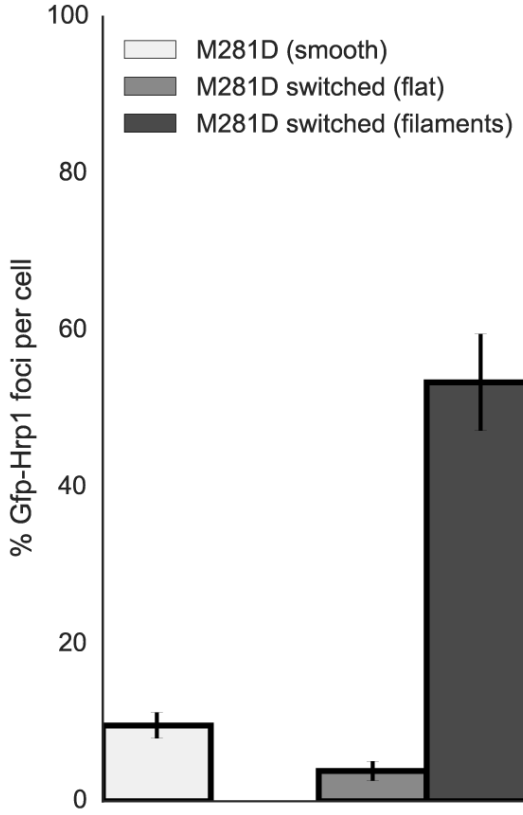

Figure 3.26: Percentage of Gfp-Hrp1 foci per cell in both M281D (smooth) and M281D (filigreed). In the second one we both analyzed cells isolated from the "flat" (not showing filaments) and "filaments" region of the filigreed colony. Each analysis was carried out in three independent Gfp-Hrp1 clones for all the three categories

Chapter 4

Discussion

4.1 M28: a fascinating wild yeast producing phenotypically heterogeneous tetrads

In 2000 Cavalieri and collaborators found and described a single nucleotide mutation in the natural M28 *Saccharomyces cerevisiae* strain isolated from damaged grapes in Montalcino area (Tuscany, Italy) [34] causing a massive rearrangement of the global expression profile of a large number of metabolic genes. Responsible of this metabolic readjustment is a single thymine insertion (T9) in the coding region of the SSY1 gene products [26], encoding for a key component of a plasma-membrane amino acid sensor composed by the SSY1, PTR3 and SSY5 genes [96, 61]. The T9 SSY mutation, found in heterozygosity in the diploid M28 strain, segregates 2:2 in the progeny of M28 produced through sporulation. Haploid spores subsequently undergo auto-diploidization being M28 a natural homothallic strain. The presence of the mutation confers recessive resistance to a toxic analogue of leucine (5',5',5' - trifluoroleucine, TFL) thus, after dissection of the M28 ascii, 2/4 spores containing the T9 insertion display the resistance to TFL (TFL-R spores) while 2/4 are sensitive to TFL (TFL-S spores). The TFL resistance/sensitivity characterizing M28 is a stable and inheritable trait since Cavalieri and collaborators found that all the segregating spores showed the same physiological behavior in a 2:2 ratio in all the tested tetrads. Intriguingly, they described another trait characterizing the

meiotic products of M28 that is the ability to grow in structured fluffy colonies. As shown in Fig. 3.1 this trait segregates 2:2 in each dissected tetrad where two spores showed a smooth colony morphology in YPD 2%, as detected in the M28 parental strain [34] and identical to the one observed in the *S. cerevisiae* reference strain; the other two grew generating filamentous colonies characterized by complex structures. We termed this phenotype "filigreed". The phenotypic characterization of the four tetrads showed that the TFL and filamentous traits are genetically unlinked since all the possible combinations between smooth, filigreed, TFL-R and TFL-S were observed. Curiously, careful observations of the two filigreed spores of tetrad 1 (M281B and M281D) revealed that there is a slightly different filamentous morphotype among them as shown in Fig. 3.2. Additionally, the M283D spore displayed a mildly filigreed phenotype, with filamentous structures only externally surrounding the colony (Fig. 3.1), thus probably revealing a deviation from a mendelian inheritance of the filamentous trait in YPD 2%. These observations, together with the lack of a clear genetic determinant of this fascinating phenotype, prompted us to start an investigation aimed to dissect the filamentation trait of this wine strain and to spot the source of this phenotypic variability. We decided to focus our research on the M28 tetrad 1 since it displays all the possible combinations between the two described traits (TFL-R/smooth, TFL-R/filigreed, TFL-S/smooth and TFL-S/filigreed). First of all, to confirm the proposed mendelian segregation of the filamentous trait [34] we evaluated whether the F0 obtained mating couples of spores of the selected tetrad showed the same segregation as the parental strains. Aiming at this, we produced haploid M28 tetrad 1 spores through the HO gene deletion. This step is necessary since M28 is homothallic and therefore able to switch its mating type from "a" to "alpha" and viceversa thus producing completely homozygous diploid spores. The M281A-D haploid spores were subsequently mated in order to follow the morphotype over the F0 generation. Colony morphology was detected in solid YP supplemented with either 2% glucose or 2% ethanol. This choice reflects two considerations: the YPD 2% medium allowed us to be consistent with previously reported data for the M28 strain obtained in this condition; YPE 2% was chosen since in this media we observed the enhancement of filamentation, a behaviour also observed previously in other studies [71]. For the smooth per smooth and filigreed per smooth crossings the resulting diploid strains (F0) were smooth (Table 3.1) in

YPD 2%, indicating that this trait is dominant when in heterozygous background. To our surprise, the filigreed x filigreed comparison did not produce a filigreed diploid strain in YPD 2% but rather displayed a smooth phenotype. Furthermore, the analysis of the morphotypes of the spores produced inducing the F0 to sporulate and then dissecting the tetrads, showed some deviations from the expected Mendelian segregation. Actually, when the spores dissected from the diploid obtained in the M281B (filigreed) per M281C (filigreed) crossing were grown in YP supplemented with glucose 2% in fact we unexpectedly observed a 2:2 segregation of the morphotype, with two spores displaying a smooth colony morphology (not observed in the original strains) and two growing as expected as filigreed colonies. Conversely, when grown in YPE 2% the spores dissected from the diploid obtained by crossing M281B with M281C showed a 4:0 segregation of the filamentous phenotype, as expected by crossing two filigreed spores. Analyzing the M281C (filigreed) per M281D (smooth) crossing we did not not observe a clear Mendelian segregation of morphotype in YPD 2% since some of the dissected tetrads showed a 4:0 segregation with all the spores displaying a smooth phenotype. Again, the expected Mendelian segregation was detectable in YP supplemented with 2% ethanol, with all the dissected spores producing half of the progeny carrying the smooth phenotype and half showing clear filamentation structures. Finally, the M281A (smooth) x M281D (smooth) produced a 4:0 segregation of the morphotype in both YPD 2% and YPE 2%, with four spores displaying a smooth phenotype. Altogether these results highlighted the importance of the media for the strains in manifesting a Mendelian segregation of the morphological trait. Moreover, the data for the YPD media indicated that two filigreed strains present differences in the capability to exhibit the filamentous phenotype with the TFL-resistant M281B spore having the most pronounced filigreed morphology. In order to complete the phenotypic characterization of M28 tetrad 1, we investigated the ability of M281B (filigreed) and M281C (filigreed) to differentiate into filamentous colonies in several media. As reported in (Fig. 3.3Fig. 3.4Fig. 3.5) we observed a 2:2 morphotype segregation in all the tested solid media (YPD 2%, YPE 2%, YPS 2%, YPM 2%, YPG 2%). Interestingly, when drastically increasing glucose concentration in growth media up to 10% we did not observed the filamentous differentiation in any of the four spores. Coherently, in YPD 10% the growth rate of the four spores was close to the one measured in the reference

strain. The same similarity was observed in YP supplemented with 2% mannose or galactose. Conversely, in both YPD % and YPE 2% M281A-D showed a significant decrease of doubling time, more accentuated in ethanol-growth where the reference strain exhibits a $\simeq$ 6h doubling time compared to a doubling time smaller than 4h for the four spores. Further characterizations of M28 tetrad 1 revealed additional phenotypic features. All the four spores of tetrad 1 (M281A, M281B, M281C and M281D) were in fact able to invade solid substrates with an efficiency comparable to *Candida albicans* (see Fig. 3.3), a well known human pathogen able to switch from a commensal colonization to a pathogenic invasive state activating the host immune response (reviewed in [51]). Notably, the two filigreed colonies M281B and M281C were associated with a more pronounced invasive pattern compared to that of the two smooth spores M281A and M281D. Still, among the filigreed spores the invasive motives differed revealing two distinct differentiation programs within the M281B and M281C colonies. This meiotic segregants also diverge at the cellular level where the M281B spore displayed a more pronounced tendency to pseudohyphal growth, a condition characterised by elongated cell, physically attached to each other but still separated by the cell wall (Fig. 3.3). Pseudohyphal growth was more pronounced in the TFL-resistant smooth less invasive M281D spore, thus being independent from invasive efficiency. Interestingly filamentous growth was observed in both optimal (YPD 2%) and ethanol-supplemented (YPE 2%). Coherently with Granek et al. [71], our data showed colony morphology development to be carbon-source dependent with the strongest effect associated with non-fermentable carbon sources. Discordantly, we did not observe an effect of ploidy in colony morphology. Both haploid and diploid cells, presented in fact the same behavior in terms of colony morphology in all the tested media (Fig. 3.3, 3.8). Conversely, the ability of haploid spores to invade solid media was drastically reduced in YPD 10% compared to the diploid spores while was comparable in both YPD 2% and YPE 2%. Notably, we confirmed the effect of SSY1 mutations (in this case a frameshift mutation) in inducing cell elongation [96] but not filamentous growth since the TFL-resistant M281D spore displayed a smooth morphotype. In addition, a slight tendency to pseudohyphal growth was also observed in the TFL-sensitive spores (Fig. 3.3) demonstrating that defects in the amino acid import are not the only stimulus triggering pseudohyphal growth. Being M28 a wine strain it could have evolved evolutionary strategy

aimed to cope with frequent fluctuations of the surrounding environment. Actually, filamentous growth is generally considered an adaptive response allowing wild yeast communities to dynamically react to fluctuation of environmental conditions as for example nutrient availability or temperature or pH changes [157]. Similarly, pseudohyphal growth could provide a selective advantage upon nutrient deprivation facilitating the search for food [64]. This view could explain the loss of pseudohyphal growth in the domesticated laboratory strain [101]. Remarkably, all the four spores showed the presence of pseudohyphae when grown in solid media. Additionally, pseudohyphal growth was found accentuated in in the TFL-resistant smooth M281D spore. Thus, the formation of pseudohyphae does not directly influences the development of three-dimensional fluffy colonies, as already reported [192] but appeared to be an alternative differentiation programs adopted also by the spores lacking the filamentation trait. Besides the similarity at the level of colony morphology, the two smooth spores significantly differ from the laboratory strain, showing a modest ability to invade agar as well as the already mentioned ability to differentiate in pseudohyphae. These observations showed the profound effect exerted by fluctuating environments, as the fermenting wine is, on shaping the phenotype at different levels. However, understanding the mechanisms through which external conditions can forge phenotypic plasticity still represents a big challenge.

4.2 The whole genome sequencing of the M28 tetrad 1 excluded a monogenic determinant of the filamentous trait

As soon as we expanded the phenotypic characterization of M28 tetrad 1 we realized the complexity of this natural system in which multiple levels of differentiation coexists and interchange generating a plethora of phenotypes. Following the phenotype over the generations we found the F0 of the haploid M281A-D spores always being characterized by a smooth phenotype in YPD 2%, also when crossing two filigreed spores. Additionally, the meiotic product of F0 generation did not show a mendelian segregation in YPD 2% but a 2:2 Mendelian segregation in YPE 2%.

Since M28-meiotic derivatives were not sequenced we decided to take advantage of the single-molecule real-time (SMRT) sequencing, developed by Pacific BioSciences (PacBio), to fully assembly the M281B (filigreed, TFL-resistant) spore to be used as scaffold to understand the genetic settings of the complete tetrad. Generating read lengths over 10 kb, with an N50 of more than 20 kb [168] this third-generation sequencing technique is a powerful tool to assemble and characterize new genomes as well as to identify variants between samples or conditions. Genetic divergence between M281B PacBio assembly and S288c was estimated by means whole genome alignment. Such diversity is about 3% with a total of 43,257 mismatches over 11,822,554 nucleotides of the complete genome. As shown by the collinearity plots (Appendix) none big chromosome rearrangements were detected but rather single nucleotide polymorphisms or small insertions/deletions. Being the yeast filamentation a diffusely studied process, especially in the human pathogen *Candida albicans*, whose filamentous structures have been associated with pathogenicity [185], the M281B (filigreed/TFL-resistant) new assembly will represent a valuable high quality resource for the yeast community. An additional NGS dataset of Illumina 2x150 bp paired-end reads was produced to entirely sequenced 3 M28 tetrads (tetrad 1, tetrad 3, tetrad 4) to assess the genetic variability between the M28 spores. Reads were aligned to the newly assembled M281B genome. As confirmation of the good quality of the M281B genome as well as of the Illumina libraries, in each tetrads we identified the SSY1 single thymine insertion responsible of the TFL resistance in the spores showing this phenotype (M281B, M281D, M282C, M282D, M284C, M284D). Coherently with previously described results, when looking for a genetic variations segregating with the phenotype we did not find a single SNP or insertion/deletion, segregating with the filamentous phenotype in all the three sequenced tetrads. In light of what observed with these results, together with the analyses of the phenotypic data, we supported the hypothesis of an epigenetic regulation of filamentation rather than simple genetic polymorphisms determinants for the observed morphological differences.

4.3 Exploring spore-variability at the protein level

In 2002 Cavalieri et al. focused on the description of the M28 natural strain [34], reporting a massive gene expression rearrangement involving 6% of the genome, when comparing the TFL-sensitive spores (M281A and M281C) with the TFL-resistant one (M281B and M281D). Our genomic investigation confirmed the involvement of the SSY1 T9 insertion in the TFL phenotype but did not identify a single variation segregating with the morphotype in the four fully sequenced tetrads. To further characterized the M28 system we decided to move a step forward and analyze spore variability at the protein level. We took advantage of shotgun proteomics, a powerful technology allowing the systematic identification as well as quantification of proteins from complex biological matrices. We analyzed and compare protein abundances of the four spores of tetrad 1. To our knowledge this represents the first global proteomic investigation of an entire *S. cerevisiae* tetrad thus representing a valuable dataset as well as a useful source of information for the yeast community. Tetrads are in fact a widely used well-defined genetic system allowing to both genetically determine the order and distances between genes (meiotic mapping) and to assess or confirm the association between a mutation and a phenotype of interest. Additionally, tetrad analysis can be used to study the inheritance of non-Mendelian elements such as the cytoplasmically inherited prions [35]. Since we showed that ethanol-growth is associated to a 2:2 manifestation of enhanced filamentous phenotype, we performed the MS shotgun analysis in M281A-D grown in YP supplemented with 2% ethanol. We also extracted and analysed the proteome of the diploid *S. cerevisiae* BY4743 strain in the same conditions to evaluate if the two smooth strains showed a common expression pattern when compared to the reference strain. We identified and quantified almost the half of the publicly available annotated yeast translated proteome (6713 in total) in both the M28 (3913 proteins identified) and the laboratory strain (3647 proteins identified). Being $^1\!/_3$ the estimated fraction of the active proteome in *S. cerevisiae*, [66, 44], these number confirmed the reliability and showed the potentiality of the shotgun MS technique applied to the M28 system to accurately measure proteome differences among different individuals. The hierarchical clustering of protein abundances revealed a high clusteredness of M28 spores forming a disjoint group from BY4743 without a clear separation between filigreed and smooth spores (Fig.

3.9). The pairwise comparison of protein abundances among the four spores revealed a significant variability between meiotic individuals. We fully confirmed the previously described portrait of M28 tetrad 1 [34] reporting the profound effect of the SSY1 mutation in shaping the amino acid metabolism of TFL-resistant spores. Actually, when comparing TFL-resistant with TFL-sensitive spores we found a down regulation of several amino acid permeases (Gnp1p, Dip5p, Bap2p) involved in the uptake of several amino acids (Leu, Ser, Thr, Cys, Met, Asn, Gln, Ala, Gly, Ile and Val) as consequence of Ssy1p frameshift insertion. To compensate the block in the amino acid import system, several proteins related to the amino acid metabolism were up-regulated in the TFL-resistant background creating a highly interconnected protein-protein-interactions (ppi) network (Fig. 3.10). Conversely, when comparing spores carrying the same filamentous morphotype (M281B and M281C) against the two smooth ones (M281A and M281D) we did not identify a strong filamentous-related response, with few differentially abundant proteins not connected by pp interactions (Fig. 3.11). The M28 meiotic segregants showing the highest variability at protein level were the TFL-R spores characterized by an opposite morphotype, M281B (Filigreed/TFL-resistant) and M281D (Smooth/TFL-resistant). The high over-expression of the transcription repressor Xbp1p (>1000-fold) in the M281D spore could explain the pronounced cellular elongation and pseudo-hypal growth characterizing this spore (Fig. 3.3). XBP1 overexpression from a GAL promoter was shown to stimulate pseudohyphal differentiation through the inhibition of CLB2 [137]. Thus, the cellular elongation observed during pseudo-hyphal growth could be due to a delay in the inactivation of Cdc28p/Cln1,2p by the Cdc28p/Clb1,2 mitotic kinases with the consequence of a prolonged period of polarized growth [137]. Additionally, Xbp1Δ homozygous diploid *S. cerevisiae* strain was shown to be inhibited for pseudohyphal growth on low-ammonium or glycerol agar media [137]. Interestingly, in M281D the differentiation from unpolarized cell to pseudohyphal growth occurs only in solid media, as generally described by Gimeno et al. [31], and is not only triggered by nitrogen-deficiency or different stress factors as reported for the reference *S. cerevisiae* strain and Sigma1278b strain [31, 229]. As shown in Fig. 3.3 in fact, M28-spores and particularly M281D can undergo this phenotypic transition in a rich medium (YP) supplemented with 2% glucose. The Bud4p substrate of the Cdc28p/Clb1,2, required for the axial budding pattern, was also up-regulated

3-fold in M281D. Together with XBP1, SSN3 is highly over-expressed in the M281D smooth spore (>200-fold). It has been shown that Ssn3 promotes the degradation of the transcription factor Ste12 by phosphorylation and thereby regulates *S. cerevisiae* filamentous growth [42]. Downregulation of Srb10 due to nitrogen limitation, lead to Ste12 accumulation with the consequent induction of filamentation [148]. Interestingly, Srb10 also phosphorylates Gal4, Msn2 and Gcn4. Loss of Srb10 allows nuclear accumulation of Msn2 as consequence of both Ste12 and Gcn4 stabilization [37]. Both Msn2p and Gcn4 have been associated to an increase of filamentous growth when over-expressed but were not detected in the M281B/M281D comparison. Notably, several genes found down-regulated in the filigreed spore have an ortholog in *Candida albicans* annotated in the "filamentous growth" GO category: SSN3, SNF2, GCN2, CTA1, GZF3, MNS1, ECI1, SUR7, ECM4, CAB1, BUD4 and YGR127W. Additionally, several proteins changing in abundance in this comparison are known to be involved in filamentous growth. Particularly, the serine/threonine protein kinase Ksp1p, is up-regulated more than 60-fold in the filamentous spore M281B thus supporting its involvement in filamentation [21]. SSK1, DFG10, ISW2 and RVS167 genes all have an ortholog in *Candida albicans* annotated in the "filamentous growth" GO category and were up-regulated in the filigreed spores with a fold difference between 2 and 8. Another differentially abundant protein was the product of the FLO11 gene, described as the key player of colony development [71, 215, 208] being the convergence point of two major parallel signal transduction pathways, the MAPK pathway and cAMP-regulated pathway [176]. With its unusually large promoter (approximately 3Kb) FLO11 is regulated in response to environmental changes by the two previously mentioned pathways [176, 107, 27, 71] as well as by a toggle-like bimodal expression regulation involving two ncRNAs (ICR1 and PWR1) [28], and finally by chromatin modifications heritable from mother to daughter cells [77, 150]. Interestingly, when comparing the two spores carrying the same filigreed phenotype we detected a 4.5 fold over-expression of the Flo11p protein in the M281B background. Flo11p was also found more expressed in M281D when compared to M281C (7-fold up-regulation), probably contributing to the enhanced pseudohyphal growth observed in M281D. The different abundance of Flo11p in M281B and M281C, together with phenotypic observations of a different degree of filamentation, invasiveness and pseudohyphal differentiation for the two spores led

us to hypothesize a different regulatory mechanism for the two filigreed spores.

4.4 M28 meiotic products showed specific patterns of histone H3 tri- and bi-methylation and histone H4 acetylation

Looking at the phenotypic variability of the 4 spores (not only at the smooth or filigreed morphotype) obtained from the dissection of the M28 tetrad 1 one could hypothesize that this behavior could be reconducted to the presence of the SSY1 mutation. This can anyway be only partially true. When analyzing protein abundance differences between the 4 spores in fact we drew out a considerable variability among the all spores, also when comparing spores with the same TFL-phenotype. Coherently with phenotypic observations and genome sequencing data, we did not probe a strong response segregating with the morphotype, even in the filamentous - enhancing YPE 2% medium. This puzzling picture with few genetic variations explaining only a part of the expected heritable variability prompted us to explore the chromatin organization across the M28 tetrad 1 spores with the aim to unveil possible hidden sources of M28 physiological variability. Epialleles represent heritable states of sequence-identical genes showing a different chromatin pattern and being stably inherited over many generations whilst showing higher reversion rates compared to genetic alleles [90, 57]. Therefore, we asked if different chromatin states among the spore could be at the root of their variability. Interestingly, cluster of nucleosomes have been proposed to be inherited by the daughter cell [88, 73, 197]. After DNA replication parental nucleosomes are inherited and successively modificated by enzymes that establish the parental modification pattern on the newly deposited nucleosomes [6, 48]. Therefore, we set up an experiment of chromatin immunoprecipitation sequencing (ChIP - Seq) aimed to investigate the histone H3 tri- and bi-methylation at lysine 4 as well as the histone H3 global acetylation. The same experimental conditions (M281A, M281B, M281C and M281D grown in liquid YPE 2% and harvesting of cell in early exponential phase, OD = 0.6) used for the shotgun MS investigation were applied in order to produce a ChIP-seq dataset com-

parable and crosslinkable to the MS data. Following the ChIP-seq guidelines and practices proposed by the ENCODE and modENCODE consortia [109] we produced a high quality datasets composed of 52 libraries. To guarantee the reproducibility of our data we carried out the ChIP investigation in three independent biological replicates for each sample and two independent biological replicates for the input (sample DNAs immuno-precipitated with antibody against histones H3 and H4) libraries. The ChIP libraries were sequenced with Illumina sequencing (2x300 bp paired-end reads) producing fragments with an average insert size of 430 bp. ChIP-enriched regions were identified setting a 200bp window size [228]. This choice reflects our aim of analyzing histone modifications domains rather than single nucleosome modifications. Actually, several works proposed the spreading of a histone modification over neighbor histones [10, 177, 48, 72]. Dodd and collaborators extended this view proposing a theoretical model in which modified nucleosome can stimulate the conversion of non-adjacent nucleosomes, thus hypothesising the possibility of a modification to "jump" over differently modified nucleosomes. Notably, this ChIP-sequencing dataset represents the first investigation of H3 Met3 K4, M3 Met2 K4 and H4 Ac histone modifications patterns in a natural *S. cerevisiae* complete tetrad. Our results are in agreement with previous finding showing both histone H3 tri-methylation at lysine 4 and histone acetylation peaking at the promoter and 5' region of genes [161, 115]. Conversely, histone H3 bi-methylation at lysine 4 appeared to be shifted toward the gene body (Fig. 3.13). These data are coherent with the general view of histone methyl status as an active mark for transcription [179]. To further support these findings we cross referenced the ChIP-sequencing dataset with the shotgun MS dataset. We found that 71% (average for all the four spores) of the proteins identified with MS were also characterised by having an enriched profile for the tri-methylation at the Lys 4 of histone H3 at the 5' region. This percentage was drastically reduced to 44.5% (average for all the four spores) for the H3 K4 bi-methylation and 42% (average for all the four spores) for the histone H4 Ac mark. Since both H3 3Met K4 and H4 Ac showed the same ChIP coverage profile along the genes, we also evaluated the percentage of co-occurence of these histone marks. Among the acetylated ChIP island, the 79.5% (average for all the four spores) also showed the H3 3Met K4 mark. This data was reflected at the protein level since the 83% of proteins being associated to the histone H4 acetylation also displayed

the tri-methylation of histone H3. The finding of enriched 3Met K4 H3 regions not associated to any detected proteins is not surprising considering: i) possible biases in the MS dataset toward specific class of proteins (i.e insoluble proteins of cell wall/membrane or low abundant proteins) ii) the link between variation in histone marks and variation in gene expression has already been reported to be not systematic [147, 1, 169, 94]. Conversely, finding proteins not associated to any of the identified detected histone marks could be the consequence of complex regulatory control of gene expression that can be modulated by both specific histone marks or transcription factors, acting synergistically or antagonistically. In this optic, Filleton and collaborators recently showed a not fully overlap between gene expression regulation and chromatin variations in both natural yeast and reference laboratory strain [56]. The main goal of the ChIP-seq analysis was to investigate whether the spores carrying the same phenotype (TFL or morpho) shared epigenomic patterns. For the TFL-phenotype this could explain the metabolic rearrangements previously shown at the gene expression levels and confirmed by our proteomic investigations. For the morphotype, this analysis could potentially drive to the discovery of one ore multiple epialleles responsible for the filamentous phenotype or, coherently with the proteomic investigation could represent an additional trait of diversity between the two morphotypes, probably deriving from a distinct differentiation process. Indeed, pairwise comparisons of chromatin modifications among the four spores revealed a vast number of loci exhibiting different histone marks between spores. The major variability was observed at the H3 2Met K4 and H4 Ac histone marks. Concerning the TFL-response we found a depletion of the histone H3 3Met K4 mark in genes encoding proteins involved in amino acid uptake. This finding can explain the down-regulation of the relative proteins identified in the MS investigation. Similarly, the enrichment of the histone H4 acetylation mark in several amino acid metabolic genes can be at the basis of the their over-expression in the TFL-resistant background [34] as well as their increase in protein levels. Notably, in both cases we did not identify a co-occurence of histone modifications but rather a specific histone modification governing a specific response: the block of amino acid uptake in the TFL-R spores (regulated by H3 3Met K4) and the activation of amino acid metabolic pathways in the TFL-S spores (regulated by H4 Ac). In addition, we showed how the SSY1 single nucleotide insertion is translated into a massive alteration of cell metabolism

in TFL-R spores by affecting the chromatin modification marks through both the tri-methylation of the lysine 4 at the histone H3 and global acetylation of histone H4. Nonetheless, we could not provide evidence for the exact mechanism connecting the genetic mutation with the epigenome rearrangement. Concerning the filamentous response we did not probe a strong response possibly associated to modifications that could explain the phenotypic changes taking place in the two filigreed spores M281B and M281C. Nevertheless, few filamentous-associated loci (based on the SGD database) showed a differential enrichment at the H3 3Met K4 mark (RGI2, RPL14B, SWD2 and RPL21B). For the H4 Ac mark 3 enriched regions fall in genes reported to be associated with genes involved in filamentation (KSP1, HTZ1, ATG1). Notably, KSP1 resulted enriched in both M281B and M281D. Intriguingly, this finding could explain the 60-fold variation at the protein level of Ks1p in the M281B vs M281D comparison. Concerning the H3 2Met K4 mark, two enriched genes have been associated with filamentation: NOP53, shown to increased filamentous growth in null mutants (SGD database) and VPS53, shown to decrease filamentous growth when over-expressed. The estimation of ChIP relative abundances for each strain as reported in (REF material) allowed us to compare histone modification patterns among the four spores. Surprisingly, we found enriched ChIP islands present only in one spores and absent in all the other three. We called these regions "spore-specific chromatin domains" (SSCDs) and reported their number in Table 3.7. We identified between 32 to 243 SSCDs. The highest number of spore specific domains was observed for the histone H4 acetylation while for the tri- and bi-methylation of histone H3 the spores tend to display less SSCDs. Notably, between the unique histone acetylation patterns of M281B [5] we identified three members of the FLO gene family, including the main player of filamentation, the FLO11 genes. FLO11 was already shown to control colony development through histone acetylation [77]. In addition to the recent work of Filleton and collaborators [56] analysing the epigenome variability among *S. cerevisiae* populations, our ChIP-seq investigation results shed light into the inter-tetrad variation of chromatin structure. Additionally, the added values of this investigation are i) the use of a proteomic dataset, thus adding the possibility to directly investigate the path from histone to protein ii) the use of four closely related individuals differing for few mutations (99.99% genetic similarity) but exhibiting an extensive variability at the phenotypic level. In this regard M28 is a unique system

to study how a natural environment can shape the physiology of yeast by altering the epigenome creating stable heritable chromatin state (epialleles). The biological importance of epigenome differences between four spores lies in the possibility of a natural strain to face hostile environmental conditions generating four meiotic individuals. Meiosis (thus spore formation) was found to be a process adopted in several environmental conditions, even in those considered as not-stressing, to reveal the effects of deleterious mutations. Indeed, Mortimer observed the sporulation of certain wine strains also in sugar-rich media [142]. If the spores produced by an homothallic strains germinate they can produce completely homozygous diploids through the mating type switch followed by auto-diploidization. The generation of new homozygous diploids, termed "genome renewal", was proposed to represent a rapid means of evolution wiping out deleterious heterozygous mutations of the heterozygous parental strains [142] or manifest recessive characters that could confer an advantage in particular environments. For instance, a similar scenario could be the case of the recessive Ssy1 mutation, found to block amino acid uptake, whereas for the filamentation trait we did not find an associated genetic variation that could explain the appearance of this new phenotype in the meiotic products. However, the investigation of chromatin status among the tetrad revealed a high variability in the three analyzed chromatin marks and, surprisingly, part of this variability is spore specific. Thus, we interpret these results as a further layer integrating the "genome renewal" theory proposing chromatin rearrangements as a direct and versatile way to environmental adaptation allowing the acquisition of new traits through heritable modifications of histone marks. Actually, the generation of structured fluffy colonies as well as the generation of pseudo-hyphal structures have been proposed as a community response allowing natural yeasts to survive under unfavourable conditions [105], thus fulfilling a crucial role in wild yeast communities.

4.5 Investigation of protein conformational changes among epigenetically switched spores revealed prion-like protein rearrangements

Saccharomyces cerevisiae has been shown to naturally acquire a filamentous phenotype [175, 32]. Additionally, it can undergo a morphological transition from the typical smooth/unicellular morphotype to a filamentous/multicellular state [71, 215]. This process, defined "dimorphism", represents a powerful adaptive mechanism exploited by both pathogenic and non pathogenic fungi [175]. *Candida albicans*, the major human fungal pathogen, can reversibly switch between several morphological states [185]. This phenotypic plasticity is strictly related to pathogenicity since the filamentous form enables the microorganism to invade and thrive in human tissues [184]. Surprisingly, during the investigation of morphotype stability of the M28 meiotic products in different growth conditions we found the ability of each strain to naturally and reversibly switch from a filamentous to a smooth phenotype and vice-versa with a surprisingly elevated reversion rate, several orders of magnitude higher than the yeast natural mutation rate, estimated to be $1.67 \pm 0.04 \times 10{-}10$ per base per generation for to the single-nucleotide mutation and $5.03 \pm 0.99 \times 10{-}12$ per base per generation for insertions/deletions [227]. Differently, in the M28 tetrad 1 the multicellular-to-unicellular phenotypic switch frequency ranges from $2.5 \times 10{-}3$ to 0.04 in the ethanol growth medium. The observed frequencies as well as the reversibility of this phenotypic switch, together with the results described so far, led us to hypothesize an epigenetic mechanism at the base for the regulation of this process. Since the acquisition of multicellularity in the budding yeast has been recently reported in certain cases to be also epigenetically regulated by protein conformational changes in prion proteins [86], we wondered if such a mechanism could be involved in M28 and how it can be linked to the chromatin rearrangement we identified. Holmes and collaborators showed the involvement of the [MOT3+] prion in regulating the acquisition of facultative multicellularity in *S. cerevisiae* [86]. Prions are a class of proteins containing one or more unstructured domains, generally rich in asparagine and glutamine (Q/N rich regions). These domains allow prions to spontaneously fold in different structural states with at least one of them

capable to trigger the structural conversion of correctly folded proteins in a self-perpetuating process leading to the generation of stable heritable aggregates. To investigate the possible involvement of prion-like proteins in the phenotypic switch we treated strains with a non-denaturing concentration of guanidine hydrochloride (GdHCl), a strong chaotropic agent known to reversibly inhibit prion propagation in yeast [55]. Our results showed a significantly decrease of the multicellular-to-unicellular transition and viceversa (Fig. 3.20). Interestingly, the effect of GdHCl varied considerably among the 4 spores, reducing the phenotypic switch frequency in M281A, M281B and M281C whilst increasing in M281D, the same spore found to separate from the other three at the proteomic and chromatin structure levels. In the light of our previous results showing a separation at both protein and chromatin levels of M281D from M281A-C we found this discrepancy very intriguing. Therefore, we decided to focus our further analyses on M281D (switch from smooth to filigreed) and to investigate the transition from filigreed to smooth we also explored M281B (which shows the same TFL phenotype of M281D). However, first of all, we took advantage of the homothallism of M28-meiotic derivatives (we called this F0) to carry out the analysis of the phenotypic switch frequency of the meiotic products of each diploidized spore for all the four M28 spores. All the dissected spores showed the same phenotype observed in the F0, thus confirming the stable inheritance of this epigenetically determined trait, but with a general significant reduction of the morphotype conversion frequency among spores observing 11-fold reduction in M281A, 2.5-fold reduction in M281B, 30-fold reduction in in M281C and 7-fold increase in M281D. In the view of a possible "dilution effect" of a putative cytosolic determinant through the generations we strengthened the efforts to perform further analyses to assess whether a prion-like effect existed. Since prion-like proteins are enriched in both RNA-binding proteins and transcription factors [3, 130], two class of proteins functionally associated with gene expression pathways, we decided to investigate global gene expression profiles of each selected spore, before and after the phenotypic switch. This analysis was possible since the switched phenotype is stably inherited from generation to generation. The M281B investigation showed a massive variation accompanying the morphological transition during growth in presence of ethanol, with more than 562 genes changing in expression by at least a factor 4 in the M281B strain. The gene ontology enrichment analysis

revealed the protein refolding and unfolding processes to be among the most significantly affected ones together with the oxidative stress response, known to be linked to protein oxidation, protein misfolding and aggregate formation [81]. Notably, FLO11 was highly expressed in the filigreed colonies, confirming its central role in structured complex colony generation [215]. It is worth to note also that 70% of heat-shock proteins (Hsps), but not co-chaperones, was over-expressed in the filigreed background. Oddly, the same gene expression analysis applied to the M281D spores did not highlight any variation at the gene expression level. However, the high variability at the phenotypic and cellular level between the two states (switched and not-switched) led us to interpret this result more as a consequence of the heterogeneity of the M281D community, representing a bottleneck for the analysis of the gene expression due to the higher noise in transcript level detection compared to other techniques, rather than to a real absence of gene expression variations. Encouraged by our previous phenotypic characterizations (the guanidine treatment and gene expression results showing an extensive variation accompanying the dimorphic transition from filigreed to smooth) we decided to follow the hypothesis of an involvement of protein folding in the epigenetic regulation of multicellularity in the M28 strains. To deepen into this possibility we decided to apply the recently developed limited proteolysis mass spectrometry technique (LiP-MS) [54]. This method relies on the fact that proteolysis of proteins that underwent conformational changes results in altered proteolytic patterns compared to normally folded target protein that can be detected by mass spectrometry [54]. Therefore, the LiP-MS technique allows a proteome-wide investigation of structural transitions of aggregation-prone proteins in complex biological backgrounds. The possibility to capture protein conformational changes directly in their biological matrices and on a large scale makes the LiP-SRM the gold standard method for systematic identification of protein structural transitions in yeast. We performed the LiP-SRM experiment in M281B and M281D grown in both ethanol- and glucose- supplemented media, before and after the phenotypic switch. Using two different growth conditions we aimed to shed light on the effect of growth medium on the prion-mediated regulation of this phenotypic transition. This experiment represents the first systematic identification of protein structural changes on a natural *S. cerevisiae* strain able to grow in a multicellular fashion. This will have a significant impact on the study of multicellularity in

yeast, being moreover, to our knowledge, the first large scale analysis of protein structural alterations to investigate aggregation-driven cell morphology. Our results show an extensive proteome rearrangement following the phenotypic transition with approximately 10% of the proteins undergoing a structural transition. Additionally, the comparison between the two cultural conditions revealed a significant impact of the carbon source in shaping proteome rearrangements. We also detected a remarkable difference between the two meiotic derivatives, thus confirming our previous findings of a spore-specific switch frequency. The M281B proteome in fact appears to be more prone to proteomic changes during the ethanol growth compared to M281D which shows, on the contrary, a larger number of protein conformational changes during growth in presence of glucose. Interestingly, the Mot3 transcription factor, did not show a conformational rearrangement in the M281B and M281D strains, suggesting an alternative and more complex scenario in which one or multiple players contribute to the unicellular-to-multicellular transition. To find possible causative changes among this global rearrangement, we integrated transcriptomic, proteomic and genomic data following the hypothesis of an involvement of prion-like transcription factors in the epigenetic regulation of multicellularity. Actually, the structural switch of prion-like proteins functionally associated with gene expression could explain the extensive transcription variation between switched and not-switched spores as well as elucidate the epigenetic nature of this process. Thus, we identified 25 proteins whose structural rearrangements could epigenetically regulate the unicellular-to-multicellular transition by modulating the expression of genes involved in morphogenesis. All the targets we identified are highly connected in a protein-protein interaction network (Fig. 3.23, 3.24). Interestingly, 11/25 targets are RNA-binding proteins. Simultaneously to the LiP investigation a collaborator from the Lindquist lab (Whitehead Institute for Biomedical Research, Cambridge, USA) applied an orthogonal approach (data unpublished) aimed to identify RNA-binding proteins undergoing conformational changes during the phenotypic switch in M281D. Strikingly, this investigation converged in some of our targets with more robust evidence on the Hrp1 RNA-binding proteins. Therefore, we decided to genetically fuse HRP1 with the green fluorescent protein (GFP) as a tag in M281D trying to detect possible intracellular differences between M281D (smooth) and its switched counterpart (filigreed). Notably, the fused Gfp-Hrp1 RNA-binding protein

clearly showed foci localized in the nucleus indicating that aggregation is taking place (Fig. 3.25). Moreover, the number of foci statistically increased in the M281D switched strain when compared to the wild type, confirming data from our collaborators showing an increased rate of aggregation of Hrp1 in the switched spore (data not shown). Further validations will be required to pinpoint the region of Hrp1 undergoing the structural conversion through the Selected Reaction Monitoring (SRM) mass spectrometry technique. Additionally, ongoing experiments aimed to follow the segregation of morphotype in the meiotic products of the M281D per M281Dswitched, M281D x M281D, M281Dswitched per M281Dswitched crosses will shed light on the question whether the protein rearrangement of Hrp1 is causative of the morphological switch, expecting in such a case to observe a 4:0 segregation of filamentation as observed for the major part of prions [35], or rather if it is the consequence of another mechanism, possibly involving chromatin remodelling. In this case we would expect to observe a 2:2 segregation of phenotype due to the inheritance of chromatin marks differently to a prion-like mechanism where the morphotype would be determined by the propagation of the self-feeding conformational change in the progeny.

Chapter 5

Concluding remarks

This work started with the aim to dissect the filamentation response described years ago by Cavalieri et al. [33], showed to segregate 2:2 in the progeny of a natural *Saccharomyces cerevisiae* strain (M28) isolated from damaged grapes in Tuscany (Italy). After an initial detailed characterization of the morphotype it became more and more clear that M28 as a system was ruled by complicated and fine tuned regulatory mechanisms possibly evolved to allow the microorganism to adapt to a complex and fluctuating environment as the fermentation wine. We adopted a multidisciplinary approach ranging from gene expression, genomic structure and proteomics to acquire the necessary overview on the entire system. This investigation confirmed the strong dependance of the morphotype from environmental conditions and revealed, to our surprise, an extensive physiological and phenotypic variability among the four meiotic products of M28 exhibiting different degree of filamentation, pseudohyphal and invasive growth. Although all these features were already observed in previous works, the new fascinating aspect here is that they segregate in the progeny of a low heterozygous diploid strain lacking a single genetic variation associable to those traits. We found the source of M28 spore variability to mainly lie in chromatin rearrangement domains. Actually, we proposed phenotypic plasticity being the result of a synergistic effect between specific, stable, inheritable distributions on the chromatin marks. Such epialleles could represent a rapid adaptive mechanism, allowing the stable appearance of new and potentially advantageous traits in the progeny of a diploid strain. Epigenetics plays here an important role and this study in M28

highlighted the profound differences that can characterize individual epigenomes like those of closely related meiotic products as well as the differences that can take place during the life of a cell leading to the change in its physiology and morphology like that observed in the reversible phenotypic smooth/filigreed switch. A further layer of complexity in the M28 system is given by the structural switch of a subset of proteins associated with the unicellular-to-multicellular epigenetic transition. If protein conformational transitions are causative for the phenotypic switch or rather the results of an epigenetic change at specific epialleles still remains elusive. Nonetheless, our results lead us to hypothesize that differential histone mark distributions could directly affect phenotypic switches through the regulation of genes that consequently affects protein folding. In conclusion, the interplay between genetic and epigenetic signals represents a sophisticate system that allow M28 to sense and respond to different external stimuli conferring, thanks to the variability among the spores, the capability to rapidly adapt to fluctuation of the natural environment but still maintaining the competence to switch back to the original phenotype thus conferring an exceptional plasticity to this wonderful organism.

Bibliography

[1] Abraham AL, Nagarajan M, Veyrieras JB, Bottin H, Steinmetz LM, Yvert G, Genetic modifiers of chromatin acetylation antagonize the reprogram- ming of epi-polymorphisms, PLoS Genet, 2012;8:e1002958.

[2] An W, Histone acetylation and methylation: combinatorial players for transcriptional regulation, Subcell Biochem, 2007;41:351-69.

[3] Alberti S, Halfmann R, King O, Kapila A, Lindquist S, A systematic survey identifies prions and illuminates sequence features of prionogenic proteins, Cell, 2009 Apr 3;137(1):146-58. doi: 10.1016/j.cell.2009.02.044.

[4] Alspaugh JA, Davidson RC, Heitman J, Morphogenesis of *Cryptococcus neoformans*, Contrib Microbiol, 2000; 5:217-38.

[5] Amoah-Buahin E, Bone N, Armstrong J, Hyphal Growth in the Fission Yeast *Schizosaccharomyces pombe*, Eukaryot Cell, 2005 Jul;4(7):1287-97.

[6] Annunziato AT, Split decision: what happens to nucleosomes during DNA replication?, J Biol Chem, 2005 Apr 1;280(13):12065-8. Epub 2005 Jan 21.

[7] Aparicio O1, Geisberg JV, Struhl K, Curr, Chromatin immunoprecipitation for determining the association of proteins with specific genomic sequences in vivo, Protoc Cell Biol. 2004 Sep;Chapter 17:Unit 17.7. Doi: 10.1002/0471143030.cb1707s23.

[8] Bakalinsky, A. T., and R. Snow, The chromosomal constitution of wine strains of *Saccharomyces cerevisiae*, Yeast, 1990, 6:367–382.

[9] Bannister AJ, Kouzarides T, Regulation of chromatin by histone modifications, Cell Res, 2011 Mar;21(3):381-95. doi: 10.1038/cr.2011.22. Epub 2011 Feb 15.

[10] Bannister, A.J., Zegerman, P., Partridge, J.F., Miska, E.A., Thomas, J.O., Allshire, R.C., and Kouzarides T, Selective recognition of methylated lysine 9 on histone H3 by the HP1 chromo domain, Nature, 2001, 410, 120–124.

[11] Barrales RR, Korber P, Jimenez J, Ibeas JI, Chromatin modulation at the FLO11 promoter of *Saccharomyces cerevisiae* by HDAC and Swi/Snf complexes, Genetics, 2012 Jul;191(3):791-803. doi: 10.1534/genetics.112.140301. Epub 2012 Apr 27.

[12] Bannister AJ, Schneider R, Kouzarides T, Histone methyla- tion: dynamic or static?, Cell, 2002; 109:801-806

[13] Banuett F, Identification of genes governing filamentous growth and tumor induction by the plant pathogen *Ustilago maydis*, Proc Natl Acad Sci U S A, 1991 May 1;88(9):3922-6.

[14] Baudin A, et al., A simple and efficient method for direct gene deletion in *Saccharomyces cerevisiae*, Nucleic Acids Res, 1993, 21(14):3329-30

[15] Ben-Ami, R., R. E. Lewis, and D. P. Kontoyiannis, Immuno- compromised hosts: immunopharmacology of modern antifungals, Clin. Infect. Dis, 2008, 47: 226–235.

[16] Benjamini Yoav, Hochberg Yosef, Controlling the false discovery rate: a practical and powerful approach to multiple testing, Journal of the Royal Statistical Society, 1995, (PDF)., Series B 57 (1): 289–300. MR 1325392

[17] Berger SL, Histone modifications in transcriptional regulation, Curr Opin Genet Dev, 2002 Apr;12(2):142-8.

[18] Berman, J., Morphogenesis and cell cycle progression in *Candida albicans*, Curr. Opin. Microbiol, 2006, 9: 595–601.

[19] Bernstein, B. E. et al., Methylation of histone H3 Lys 4 in coding regions of active genes, Proc. Natl Acad Sci. USA, 2002, 99, 8695–8697

[20] Bernstein, B.E., Kamal, M., Lindblad-Toh, K., Bekiranov, S., Bai- ley, D.K., Huebert, D.J., McMahon, S., Karlsson, E.K., Kul- bokas III, E.J., Gingeras, T.R., Genomic maps and comparative analysis of histone modifications in human and mouse, Cell, 2005, 120: 169–181.

[21] Bharucha N, Ma J, Dobry CJ, Lawson SK, Yang Z, Kumar A, Analysis of the yeast kinome reveals a network of regulated protein localization during filamentous growth, Mol Biol Cell. 2008 Jul;19(7):2708-17. doi: 10.1091/mbc.E07-11-1199. Epub 2008 Apr 16.

[22] Bolger AM, Lohse M, Usadel B, Trimmomatic: a flexible trimmer for Illumina sequence data, Bioinformatics, 2014 Aug, 1;30(15):2114-20. doi: 10.1093/bioinformatics/btu170. Epub 2014 Apr 1.

[23] Brachmann CB, Davies A, Cost GJ, Caputo E, Li J, Hieter P and Boeke JD Designer deletion strains derived from Saccharomyces cerevisiae S288C: a useful set of strains and plasmids for PCR-mediated gene disruption and other applications, Yeast, 1998, 14:115-32

[24] Byvoet P, In vivo turnover and distribution of radio-N-methyl in arginine-rich histones from rat tissues, Arch Biochem Biophys, 1972, 152:887-888.

[25] Byvoet P, Shepherd GR, Hardin JM, Noland BJ, The distribution and turnover of labeled methyl groups in histone fractions of cultured mammalian cells, Arch Biochem Biophys, 1972, 148:558-567.

[26] Brown KM, Landry CR, Hartl DL, Cavalieri D,Cascading transcriptional effects of a naturally occurring frameshift mutation in *Saccharomyces cerevisiae*, Mol Ecol. 2008 Jun;17(12):2985-97. doi: 10.1111/j.1365-294X.2008.03765.x. Epub 2008 Apr 18.

[27] Bruckner S., and Mosch H.U., Choosing the right lifestyle: adhesion and development in *Saccharomyces cerevisiae*, FEMS Microbiol Rev, 2011, 36: 25–58.

[28] Bumgarner, S. L., R. D. Dowell, P. Grisafi, D. K. Gifford, and G. R. Fink, Toggle involving cis-interfering noncoding RNAs controls variegated gene expression in yeast, Proc. Natl. Acad. Sci. USA, 2009 106: 18321–18326

[29] Bumgarner, S. L., G. Neuert, B. F. Voight, A. Symbor-Nagrabska, P. Grisafi et al., Single-cell analysis reveals that noncoding RNAs contribute to clonal heterogeneity by modulating tran- scription factor recruitment, Mol. Cell, 2012 45: 470–482.

[30] Cairns BR, Kim YJ, Sayre MH, Laurent BC, Kornberg RD, A multisubunit complex containing the SWI1/ADR6, SWI2/SNF2, SWI3, SNF5, and SNF6 gene products isolated from yeast, Proc Natl Acad Sci U S A, 1994;91:1950–4. [PubMed: 8127913]

[31] Carlos J. Gimeno, Per 0. Ljungdahl, Cora A. Styles,and Gerald R. Fink, Unipolar Cell Divisions in the Yeast *S. cerevisiae* Lead to Filamentous Growth:Regulation by Starvation and RAS, Cell. 1992 Mar 20;68(6):1077-90

[32] Casalone E, Barberio C, Cappellini L, Polsinelli M., Res Microbiol. Characterization of *Saccharomyces cerevisiae* natural populations for pseudohyphal growth and colony morphology, Research in Microbiology, 2005 Mar; 156(2):191-200. doi:10.1016/j.resmic.2004.09.008

[33] Cavalieri D, Barberio C, Casalone E, Pinzauti F, Sebastiani F, Mortimer R K, Polsinelli M, Genetic and molecular diversity in *S. Cerevisiae* natural populations, Food Technol Biotechnol, (1998), 36:45–50.TIT

[34] Cavalieri D, Townsend JP, Hartl DL.,Manifold anomalies in gene expression in a vineyard isolate of *Saccharomyces cerevisiae* revealed by DNA microarray analysis, Proc Natl Acad Sci U S A. 2000 Oct 24;97(22):12369-74.

[35] Chernoff YO, Uptain SM, Lindquist SL, Analysis of prion factors in yeast, Methods Enzymol, 2002;351:499-538.

[36] Chernoff Y. O., Lindquist S. L., Ono B., Inge-Vechtomov S. G., and Liebman S. W., Role of the chaperone protein Hsp104 in propagation of the yeast prion-like factor [psi?], Science, 1995, 268, 880–884

[37] Chi Y, Huddleston MJ, Zhang X, Young RA, Annan RS, Carr SA, Deshaies RJ, Negative regulation of Gcn4 and Msn2 transcription factors by Srb10 cyclin-dependent kinase, Genes Dev, 2001 May 1;15(9):1078-92.

[38] Cosma MP. Ordered recruitment: gene-specific mechanism of transcription activation, Mol Cell, 2002;10:227–36. [PubMed: 12191469]

[39] Cullen PJ, Sprague GF Jr, The regulation of filamentous growth in yeast, Genetics, 2012 Jan;190(1):23-49. doi: 10.1534/genetics.111.127456.

[40] Cummings, J. and Fogel, S, Genetic homology of wine yeasts with *Saccharomyces cerevisiae*, J. Inst. Brew, 1978, 84, 267–270

[41] Cutler NS, Pan X, Heitman J, Cardenas ME, The TOR signal transduction cascade controls cellular differentiation in response to nutrients, Mol Biol Cell, 2001 Dec;12(12):4103-13.

[42] De Boer M, Bebelman JP, Gonçalves PM, Maat J, Van Heerikhuizen H, Planta RJ, Regulation of expression of the amino acid transporter gene BAP3 in *Saccharomyces cerevisiae*, Mol Microbiol. 1998 Nov;30(3):603-13.

[43] de Boer M, Nielsen PS, Bebelman JP, Heerikhuizen H, Andersen HA, Planta RJ, Stp1p, Stp2p and Abf1p are involved in regulation of expression of the amino acid transporter gene BAP3 of *Saccharomyces cerevisiae*, Nucleic Acids Res. 2000 Feb 15;28(4):974-81.

[44] De Godoy LM, Olsen JV, Cox J, Nielsen ML, Hubner NC, Fröhlich F, Walther TC, Mann M, Comprehensive mass-spectrometry-based proteome quantification of haploid versus diploid yeast, Nature. 2008 Oct 30;455(7217):1251-4. doi: 10.1038/nature07341. Epub 2008 Sep 28. PMID:18820680

[45] De La Torre MJ, Millan MC, Perez-Juan P, Morales J, Ortega JM, Indigenous yeasts associated with two Vitis vinifera grape varieties cultured in southern Spain, Microbios, 1999, 100:27–40.

[46] DePace AH, Santoso A, Hillner P, Weissman JS, A critical role for amino-terminal glutamine/asparagine repeats in the formation and propagation of a yeast prion, Cell, 1998 Jun 26;93(7):1241-52.

[47] DePristo M, Banks E, Poplin R, Garimella K, Maguire J, Hartl C, Philippakis A, del Angel G, Rivas MA, Hanna M, McKenna A, Fennell T, Kernytsky A, Sivachenko A, Cibulskis K, Gabriel S, Altshuler D, Daly M, A framework for variation discovery and genotyping using next-generation DNA sequencing data, NATURE GENETICS, 2011 43:491-498

[48] Dodd IB, Micheelsen MA, Sneppen K, Thon G, Theoretical analysis of epigenetic cell memory by nucleosome modification, Cell, 2007 May 18;129(4):813-22.

[49] Doronina VA, Staniforth GL, Speldewinde SH, Tuite MF, Grant CM, Oxidative stress conditions increase the frequency of de novo formation of the yeast [PSI+] prion, Mol Microbiol, 2015 Apr, 96(1):163-74. doi: 10.1111/mmi.12930. Epub 2015 Feb 11.

[50] Z. Du, K.W. Park, H. Yu, Q. Fan, L. Li, Newly identified prion linked to the chromatin-remodeling factor Swi1 in *Saccharomyces cerevisiae*, Nat. Genet., 2008, pp. 460–465

[51] Dühring S, Germerodt S, Skerka C, Zipfel PF, Dandekar T, Schuster S, Host-pathogen interactions between the human innate immune system and *Candida albicans*-understanding and modeling defense and evasion strategies, Front Microbiol, 2015 Jun 30;6:625. doi: 10.3389/fmicb.2015.00625. eCollection 2015.

[52] Simon S. Eaglestone, Lloyd W. Ruddock, Brian S. Cox, and Mick F. Tuite, Guanidine hydrochloride blocks a critical step in the propagation of the prion-like determinant [PSI+] of *Saccharomyces cerevisiae*, Proc Natl Acad Sci U S A., 2000 Jan, 4; 97(1): 240–244.

[53] Felsenfeld G, Groudine M, Controlling the double helix, Nature, 2003 Jan 23;421(6921):448-53.

[54] Y. Feng, G. De Franceschi, A. Kahraman, M. Soste, A. Melnik, P.J. Boersema, P.P. de Laureto, Y. Nikolaev, A.P. Oliveira, P. Picotti, Global analysis of protein structural changes in complex proteomes, Nat. Biotechnol, 2014, 32(10):1036-44.

[55] Ferreira PC, Ness F, Edwards SR, Cox BS, Tuite MF, The elimination of the yeast [PSI+] prion by guanidine hydrochloride is the result of Hsp104 inactivation, Mol Microbiol, 2001 Jun, 40(6):1357-69.

[56] Filleton F, Chuffart F, Nagarajan M, Bottin-Duplus H, Yvert G., The complex pattern of epigenomic variation between natural yeast strains at single-nucleosome resolution, Epigenetics Chromatin, 2015 Jul, 31;8:26. doi: 10.1186/s13072-015-0019-3. eCollection 2015.

[57] Finnegan EJ, Epialleles - a source of random variation in times of stress, Curr Opin Plant Biol, 2002 Apr;5(2):101-6.

[58] Fleming AB, Beggs S, Church M, Tsukihashi Y, Pennings S, The yeast Cyc8-Tup1 complex cooperates with Hda1p and Rpd3p histone deacetylases to robustly repress transcription of the subtelomeric FLO1 gene, Biochim Biophys Acta, 2014 Nov;1839(11):1242-55. doi: 10.1016/j.bbagrm.2014.07.022. Epub 2014 Aug 7.

[59] Fontana A, de Laureto PP, Spolaore B, Frare E, Picotti P, Zambonin M, Probing protein structure by limited proteolysis, Acta Biochim Pol, 2004, 51(2):299-321. Review.

[60] Hanna Forsberg,C. Fredrik Gilstring,Arezou Zargari,Paula Martínez, Per O. Ljungdahl, The role of the yeast plasma membrane SPS nutrient sensor in the metabolic response to extracellular amino acids, Mol Microbiol. 2001 Oct;42(1):215-28

[61] Hanna Forsberg and Per O. Ljungdahl*, Genetic and Biochemical Analysis of the Yeast Plasma Membrane Ssy1p-Ptr3p-Ssy5p Sensor of Extracellular Amino Acids, Mol Cell Biol. 2001 Feb; 21(3): 814–826.doi: 10.1128/MCB.21.3.814-826.2001 - PMCID: PMC86673

[62] Gagiano M, Bauer FF, Pretorius IS, The sensing of nutritional status and the relationship to filamentous growth in *Saccharomyces cerevisiae*, FEMS Yeast Res. 2002 Dec;2(4):433-70.

[63] Gagiano, M., Van Dyk, D., Bauer, F.F., Lambrechts, M.G. and Pretorius, Divergent regulation of the evolutionarily closely related promoters of the *Saccharomyces cerevisiae* STA2 and MUC1 genes, J. Bacteriol, (1999) 181, 6497–6508.

[64] Gancedo JM, Control of pseudohyphae formation in *Saccharomyces cerevisiae*, FEMS Microbiol Rev, 2001 Jan;25(1):107-23.

[65] Garza S, Teixidó JA, Sanchis V, Viñas I, Condón S, Heat resistance of *Saccharomyces cerevisiae* strains isolated from spoiled peach puree, Int J Food Microbiol, 1994, 23:209–213.

[66] Ghaemmaghami S, Huh WK, Bower K, Howson RW, Belle A, Dephoure N, O'Shea EK, Global analysis of protein expression in yeast, Weissman JS. Nature, 2003 Oct 16;425(6959):737-41. PMID:14562106

[67] R. Daniel Gietz, Robin A, Transformation of yeast by lithium acetate/single-stranded carrier DNA/polyethylene glycol method, Woods. Methods in Enzymology, 2002, Volume 350 Pages 87–96

[68] Glatter T, Ludwig C, Ahrné E, Aebersold R, Heck AJ, Schmidt A, Large-scale quantitative assessment of different in-solution protein digestion protocols reveals superior cleavage efficiency of tandem Lys-C/trypsin proteolysis over trypsin digestion, J Proteome Res, 2012 Nov 2;11(11):5145-56. doi: 10.1021/pr300273g. Epub 2012 Oct 16.

[69] Godfrey K, Invasive fungal infection occurring in low birthweight infants, Nurs Times, 2003 Dec, 2-8;99(48):51.

[70] Goldstein A.L., and McCusker J.H., Three new dominant drug resistance cassettes for gene disruption in *Saccharomyces cerevisiae*, Yeast, 1999, 15: 1541–1553.

[71] Granek JA, Magwene PM, Environmental and genetic determinants of colony morphology in yeast, PLoS Genet, 2010 Jan 22;6(1):e1000823. doi: 10.1371/journal.pgen.1000823.

[72] Grewal S.I. and Elgin S.C., Heterochromatin: new possibilities for the inheritance of structure, Curr. Opin. Genet. Dev, 2002, 12, 178–187

[73] Gruss C, Gutierrez C, Burhans WC, DePamphilis ML, Koller T, Sogo JM, Nucleosome assembly in mammalian cell extracts before and after DNA replication, EMBO J, 1990 Sep;9(9):2911-22.

[74] Guijo, S., J. C. Mauricio, J. M. Salmon, and J. M. Ortega, Determi- nation of the relative ploidy in different *Saccharomyces cerevisiae* strains used for fermentation and flor film ageing of dry sherry-type wines, Yeast, 1997, 13:101–117.

[75] Guo B., Styles C.A., Feng Q. and Fink G.R, A Saccharo- myces gene family involved in invasive growth, cell-cell adhesion, and mating, Proc. Natl. Acad. Sci. USA, 2000, 97, 12158–12163.

[76] R. Halfmann, S. Alberti, S. Lindquist, Prions, protein homeostasis, and phenotypic diversity, Trends Cell Biol., 2010, pp. 125–133

[77] Halme A, Bumgarner S, Styles C, Fink GR, Genetic and epigenetic regulation of the FLO gene family generates cell-surface variation in yeast, Cell, 2004 Feb 6;116(3):405-15.

[78] Hampsey M1, Reinberg D, Tails of intrigue: phosphorylation of RNA polymerase II mediates histone methylation, Cell, 2003 May 16;113(4):429-32.

[79] Hartmann H.A., Kahmann R., Bölker M, The pheromone response factor coordinates filamentous growth and pathogenic development in *Ustilago maydis*, EMBO J, 1996, 15, 1632–1641.

[80] Henselová M, Hudecová D, Differences in the microflora of scarified and unscarified seeds of Karwinskia humboldtiana (Rhamnaceae), Folia Microbiol (Praha), 2001, 46:543–548.

[81] Herczenik E, Gebbink MF, Molecular and cellular aspects of protein misfolding and disease, FASEB J, 2008 Jul, 22(7):2115-33. doi: 10.1096/fj.07-099671.

[82] Herskowitz I., Rine J. and Strathern J., Mating-type determination and mating-type interconversion in *Saccharomyces cerevisiae*. In Jones,E.W., Pringle,J.R. and Broach,J.R. (eds), The Molecular and Cellular Biology of the Yeast Saccharomyces. Cold Spring Harbor Press, Plainview, NY, 1992, pp. 583–656.

[83] Ira Herskowitz, Life Cycle of the Budding Yeast *Saccharomyces cerevisiae*, Microbiological Reviews, Dec. 1988, p. 536-553-Copyright C 1988, American Society for Microbiology

[84] Hogan DJ, Riordan DP, Gerber AP, Herschlag D, Brown PO, Diverse RNA-binding proteins interact with functionally related sets of RNAs, suggesting an extensive regulatory system, PLoS Biol, 2008 Oct, 28;6(10):e255. doi: 10.1371/journal.pbio.0060255.

[85] K. E. van Holde, Chromatin, New York: Springer-Verlag, (1989) GIUSTO??

[86] Holmes DL, Lancaster AK, Lindquist S, Halfmann R, Heritable remodeling of yeast multicellularity by an environmentally responsive prion, Cell, Mar 28 2013, 153(1):153-65. doi: 10.1016/j.cell.2013.02.026.

[87] Ismaïl Iraqui, Stephan Vissers, Florent Bernard, Johan-Owen de Craene, Eckhard Boles, Antonio Urrestarazu, and Bruno André, Amino Acid Signaling in *Saccharomyces cerevisiae*: a Permease-Like Sensor of External Amino Acids and F-Box Protein Grr1p Are Required for Transcriptional Induction of the AGP1 Gene, Which Encodes a Broad-Specificity Amino Acid Permease, Mol Cell Biol. 1999 Feb; 19(2): 989–1001.

[88] Jackson V, Chalkley R, Histone segregation on replicating chromatin, Biochemistry, 1985 Nov, 19;24(24):6930-8.

[89] Janke C, Magiera MM, Rathfelder N, Taxis C, Reber S, Maekawa H, Moreno-Borchart A, Doenges G, Schwob E, Schiebel E, Knop M, A versatile toolbox for PCR-based tagging of yeast genes: new fluorescent proteins, more markers and promoter substitution cassettes, Yeast, 2004 Aug;21(11):947-62.

[90] Johannes F, Colomé-Tatché M, Quantitative epigenetics through epigenomic perturbation of isogenic lines, Genetics, 2011 May;188(1):215-27. doi: 10.1534/genetics.111.127118. Epub 2011 Mar 8.

[91] Jiang YW, Kang CM, Induction of *S. cerevisiae* filamentous differentiation by slowed DNA synthesis involves Mec1, Rad53 and Swe1 checkpoint proteins, Mol Biol Cell , (2003) 14: 5116–5124.

[92] Jones SK Jr, Bennett RJ, Fungal mating pheromones: choreographing the dating game, Fungal Genet Biol, 2011 Jul;48(7):668-76. doi: 10.1016/j.fgb.2011.04.001. Epub 2011 Apr 8.

[93] Kadosh D, Struhl K, Repression by Ume6 involves recruitment of a complex containing Sin3 corepressor and Rpd3 histone deacetylase to target promoters, Cell, 1997 May 2;89(3):365-71.

[94] Kasowski M, Kyriazopoulou-Panagiotopoulou S, Grubert F, Zaugg JB, Kundaje A, Liu Y, et al., Extensive variation in chromatin states across humans, Science, 2013;342:750–2.

[95] Kim TS, Kim HY, Yoon JH, Kang HS, Recruitment of the Swi/Snf complex by Ste12-Tec1 promotes Flo8-Mss11-mediated activation of STA1 expression, Mol Cell Biol, 2004 Nov;24(21):9542-56.

[96] Hanna Klasson, Gerald R. Fink, and Per O. Ljungdahl, Ssy1p and Ptr3p Are Plasma Membrane Components of a Yeast System That Senses Extracellular Amino Acids, Mol Cell Biol. 1999 Aug; 19(8): 5405–5416.

[97] King OD, Gitler AD, Shorter J, The tip of the iceberg: RNA-binding proteins with prion-like domains in neurodegenerative disease, Brain Res, 2012 Jun, 26;1462:61-80. doi: 10.1016/j.brainres.2012.01.016. Epub 2012 Jan 21.

[98] Kornberg RD, Lorch Y, Twenty-five years of the nucleosome, fundamental particle of the eukaryote chromosome, Cell, 1999 Aug 6;98(3):285-94.

[99] Kovacs GG, Budka H, Prion diseases: from protein to cell pathology, Am J Pathol, 2008 Mar;172(3):555-65. doi: 10.2353/ajpath.2008.070442. Epub 2008 Feb 2.

[100] Kristiansson E, Thorsen M, Tamás MJ, Nerman O, Evolutionary forces act on promoter length: identification of enriched cis-regulatory elements, Mol Biol Evol, 2009 Jun;26(6):1299-307. doi: 10.1093/molbev/msp040. Epub 2009 Mar 3.

[101] Kron SJ, Filamentous growth in budding yeast, Trends Microbiol, 1997 Nov;5(11):450-4.

[102] Kulkarni AA, Abul-Hamd AT, Rai R, El Berry H, Cooper TG, Gln3p nuclear localization and interaction with Ure2p in *Saccharomyces cerevisiae*, J Biol Chem, 2001 Aug 24; 276(34):32136-44. Epub 2001 Jun 14

[103] Kunkee, R. E., and L. F. Bisson. 1993. Wine-making yeasts, p. 69–126. In A. H. Rose and J. S. Harrison (ed.), The yeasts: yeast technology. Academic Press, London, England

[104] Kupiec M, Byers B, Esposito RE, Meiosis and sporulation in *Saccharomyces cerevisiae*. In The molecular and cell biology of the yeast Sac- charomyces, Pringle JR, Broach JR, Jones EW eds, 1997, pp 889–1036. Cold Spring Harbor Laboratory Press, Cold Spring Harbor, N.Y.

[105] Kuthan M, Devaux F, Janderová B, Slaninová I, Jacq C, Palková Z, Domestication of wild *Saccharomyces cerevisiae* is accompanied by changes in gene expression and colony morphology, Mol Microbiol. 2003 Feb;47(3):745-54.

[106] Kwon-Chung KJ, A new genus, filobasidiella, the perfect state of *Cryptococcus neoformans*, Mycologia, 1975 Nov-Dec; 67(6):1197-200

[107] Lambrechts M.G., Bauer F.F., Marmur J., and Pretorius I.S., Muc1, a mucin-like protein that is regulated by Mss10, is critical for pseudohyphal differentiation in yeast, Proc Natl Acad Sci USA 93, 1996: 8419–8424.

[108] A.K. Lancaster, J.P. Bardill, H.L. True, J. Masel, The spontaneous appearance rate of the yeast prion [PSI +] and its implications for the evolution of the evolvability properties of the [PSI +] system, Genetics, 2010, pp. 393–400

[109] Landt SG, Marinov GK, Kundaje A, Kheradpour P, Pauli F, Batzoglou S, Bernstein BE, Bickel P, Brown JB, Cayting P, Chen Y, DeSalvo G, Epstein C, Fisher-Aylor KI, Euskirchen G, Gerstein M, Gertz J, Hartemink AJ, Hoffman MM, Iyer VR, Jung YL, Karmakar S, Kellis M, Kharchenko PV, Li Q, Liu T, Liu XS, Ma L, Milosavljevic A, Myers RM, Park PJ, Pazin MJ, Perry MD, Raha D, Reddy TE, Rozowsky J, Shoresh N, Sidow A, Slattery M, Stamatoyannopoulos JA, Tolstorukov MY, White KP, Xi S, Farnham PJ, Lieb JD, Wold BJ, Snyder M, ChIP-seq guidelines and practices of the ENCODE and modENCODE consortia, Genome Res, 2012 Sep;22(9):1813-31. doi: 10.1101/gr.136184.111.

[110] Langmead B, Salzberg S., Fast gapped-read alignment with Bowtie 2. Nature Methods. 2012, 9:357-359.

[111] Las Heras-Vazquez FJ, Mingorance-Cazorla L, Clemente-Jimenez JM, Rodriguez-Vico F, Identification of yeast species from orange fruit and juice by RFLP and sequence analysis of the 5.8S rRNA gene and the two internal transcribed spacers, FEMS Yeast Res, 2003, 3:3–9

[112] Lasserre JP, Dautant A, Aiyar RS, Kucharczyk R, Glatigny A, Tribouillard-Tanvier D, Rytka J, Blondel M, Skoczen N, Reynier P, Pitayu L, Rötig A, Delahodde A, Steinmetz LM10, Dujardin G, Procaccio V, di Rago JP, Yeast as a system for modeling mitochondrial disease mechanisms and discovering therapies, Dis Model Mech, 2015 Jun;8(6):509-26. doi: 10.1242/dmm.020438.

[113] Levine M, Tjian R, Transcription regulation and animal diversity, Nature, 2003;424:147–51. [PubMed: 12853946

[114] Li B, Carey M, Workman JL, The role of chromatin during transcription, Cell, 2007 Feb, 23;128(4):707-19.

[115] Liu CL, Kaplan T, Kim M, Buratowski S, Schreiber SL, Friedman N, et al., Single-nucleosome mapping of histone modifications in *S. cerevisiae*, PLoS Biol, 2005;3:e328

[116] Liu H, Köhler J, Fink GR, Suppression of hyphal formation in *Candida albicans* by mutation of a STE12 homolog, Science, 1994 Dec 9; 266(5191):1723-6. Erratum in: Science 1995 Jan 6;267(5194):17.

[117] Liu H, Styles CA, Fink GR, Elements of the yeast pheromone response pathway required for filamentous growth of diploids, Science, 1993 Dec 10;262(5140):1741-4.

[118] Lo, H. J., J. R. Kohler, B. Di Domenico, D. Loebenberg, A. Cacciapuoti et al., Nonfilamentous C. albicans mutants are avirulent, Cell, 1997, 90: 939–949.

[119] Lobo Z and Maitra PK, Physiological role of glucose-phosphorylating enzymes in *Saccharomyces cerevisiae*, Arch Biochem Biophys, 1977, 182(2):639-45 PMID: 332086

[120] Lopandic K, Gangl H, Wallner E, Tscheik G, Leitner G, Querol A, Borthe N, Breitenbach M, Prillinger H, Tiefenbrunner W, Genetically different wine yeasts isolated from Austrian vine- growing regions influence wine aroma differently and contain putative hybrids between *Saccharomyces cerevisiae* and Saccha- romyces kudriavzevii, FEMS Yeast, 2007, Res 7:953–965

[121] Michael C. Lorenz, N. Shane Cutler, and Joseph Heitman, Characterization of Alcohol-induced Filamentous Growth in *Saccharomyces cerevisiae*, Mol Biol Cell, 2000 Jan; 11(1): 183–199.

[122] Lorenz MC, Pan X, Harashima T, Cardenas ME, Xue Y, Hirsch JP, Heitman J, The G protein-coupled receptor gpr1 is a nutrient sensor that regulates pseudohyphal differentiation in *Saccharomyces cerevisiae*, Genetics, 2000 Feb;154(2):609-22.

[123] Lorenz MC, Heitman J, Yeast pseudohyphal growth is regulated by GPA2, a G protein alpha homolog, EMBO J, 1997 Dec 1;16(23):7008-18.

[124] Lorenz MC, Heitman J, Regulators of pseudohyphal differentiation in *Saccharomyces cerevisiae* identified through multicopy suppressor analysis in ammonium permease mutant strains, Genetics. 1998 Dec;150(4):1443-57.

[125] Lorenz MC, Heitman J, The MEP2 ammonium permease regulates pseudohyphal differentiation in *Saccharomyces cerevisiae*, EMBO J, 1998 Aug 10;17(5):1236-47.

[126] Luger K, Richmond TJ, DNA binding within the nucleosome core, Curr Opin Struct Biol, 1998 Feb;8(1):33-40.

[127] McGovern PE, Zhang J, Tang J, Zhang Z, Hall GR, et al., Fermented beverages of pre- and proto-historic China, Proc Natl Acad Sci U S A, 2004, 101: 17593–17598.

[128] Maddelein ML, Wickner RB, Two prion-inducing regions of Ure2p are nonoverlapping, Mol Cell Biol, 1999 Jun;19(6):4516-24.

[129] Madhani HD, Fink GR, The control of filamentous differentiation and virulence in fungi, Trends Cell Biol. 1998 Sep;8(9):348-53.

[130] Malinovska, L., Kroschwald, S., & Alberti, S, Protein disorder, prion propensities, and self- organizing macromolecular collectives, Biochimica et Biophysica Acta (BBA)-Proteins and Proteomics, 2013, 1834(5), 918-931.

[131] Mao X, Cao F, Nie X, Liu H, Chen J, The Swi/Snf chromatin remodeling complex is essential for hyphal development in *Candida albicans*, FEBS Lett, 2006 May 15;580(11):2615-22. Epub 2006 Apr 21.

[132] J. Masel, A. Bergman, The evolution of the evolvability properties of the yeast prion [PSI +], Evolution, 2003, pp. 1498–1512

[133] J. Masel, C.K. Griswold. The strength of selection against the yeast prion [PSI +], Genetics, 2009, pp. 1057–1063

[134] Masneuf I, Hansen J, Groth C, Piskur J, Dubourdieu D, New hybrids between Saccharomyces sensu stricto yeast species found among wine and cider production strains, Appl Environ Microbiol, 1998, 64:3887–

[135] McKenna A, Hanna M, Banks E, Sivachenko A, Cibulskis K, Kernytsky A, Garimella K, Altshuler D, Gabriel S, Daly M, DePristo MA, The Genome

Analysis Toolkit: a MapReduce framework for analyzing next-generation DNA sequencing data, GENOME RESEARCH, 2010 20:1297-303

[136] Medoff G, Maresca B, Lambowitz AM, Kobayashi G, Painter A, Sacco M, Carratu L, Correlation between pathogenicity and temperature sensitivity in different strains of Histoplasma capsulatum, J Clin Invest, 1986 Dec;78(6):1638-47.

[137] Miled C, Mann C, Faye G, Xbp1-mediated repression of CLB gene expression contributes to the modifications of yeast cell morphology and cell cycle seen during nitrogen-limited growth, Mol Cell Biol. 2001 Jun;21(11):3714-24

[138] Mirabella AC, Foster BM1, Bartke T, Chromatin deregulation in disease, Chromosoma, 2016 Mar;125(1):75-93. doi: 10.1007/s00412-015-0530-0. Epub 2015 Jul 19.

[139] Mitchell SF, Jain S, She M, Parker R, Global analysis of yeast mRNPs, Nat Struct Mol Biol, 2013, Jan;20(1):127-33. doi: 10.1038/nsmb.2468. Epub 2012 Dec 9.

[140] Morrissey WF, Davenport B, Querol A, Dobson AD, The role of indigenous yeasts in traditional Irish cider fermentations, J Appl Microbiol, 2004, 97:647–655.

[141] Mortimer R. K. & Hawthorne D. C., Yeast genetics, In The Yeasts, 1969, pp. 386–453. Edited by A. H. Rose & J. S. Harrison. London:Academic Press

[142] Mortimer R. K., Romano P., Suzzi G. and Polsinelli M, Genome renewal: a new phenomenon revealed from a genetic study of 43 strains of *Saccharomyces cerevisiae* derived from natural fermentation of grape musts, Yeast, 1994, 10, 1543–1552.

[143] Mortimer R K, Evolution and variation of the yeast (Saccharomyces), Genome Res, (2000) 10:891.

[144] Mukhopadhyay, S., Krishnan, R., Lemke, E.A., Lindquist, S., and Deniz, A.A. A natively unfolded yeast prion monomer adopts an ensemble of collapsed

and rapidly fluctuating structures, Proc. Natl. Acad. Sci. USA, 2007, 104, 2649–2654

[145] Murphy HA, Kuehne HA, Francis CA, Sniegowski PD, Mate choice assays and mating propensity differences in natural yeast populations, Biol Lett, 2006, 2:553–556. Abstract/FREE Full Text

[146] Naumov GI, Naumova ES, Sniegowski PD, Saccharomyces paradoxus and *Saccharomyces cerevisiae* are associated with exudates of North American oaks, Can J Microbiol, 1998, 44:1045–1050.

[147] Nagarajan M, Veyrieras JB, de Dieuleveult M, Bottin H, Fehrmann S, Abraham AL, et al., Natural single-nucleosome epi-polymorphisms in yeast, PLoS Genet, 2010;6:e1000913

[148] Nelson C, Goto S, Lund K, Hung W, Sadowski I, Srb10/Cdk8 regulates yeast filamentous growth by phosphorylating the transcription factor Ste12, Nature, 2003 Jan 9;421(6919):187-90.

[149] Nyanga LK, et al., Yeasts and lactic acid bacteria microbiota from masau (Ziziphus mauritiana) fruits and their fermented fruit pulp in Zimbabwe, Int J Food Microbiol, 2007, 120:159–166.

[150] Octavio L.M., Gedeon K., and Maheshri N., Epige- netic and conventional regulation is distributed among acti- vators of FLO11 allowing tuning of population-level heterogeneity in its expression, PLoS Genet, 2009, 5: e1000673.

[151] Oppikofer M1, Kueng S, Gasser SM, SIR-nucleosome interactions: structure-function relationships in yeast silent chromatin, Gene, 2013 Sep 15;527(1):10-25. doi: 10.1016/j.gene.2013.05.088. Epub 2013 Jun 18.

[152] Ostling J, Ronne H, Negative control of the Mig1p repressor by Snf1p-dependent phosphorylation in the absence of glucose, Eur J Biochem, 1998 Feb 15;252(1):162-8.

[153] Owen-Hughes T. Colworth memorial lecture. Pathways for remodelling chromatin, Biochem Soc Trans, 2003;31:893–905. [PubMed: 14505445]

[154] Owsianowski E, Walter D, Fahrenkrog B, Negative regulation of apoptosis in yeast, Biochim Biophys Acta, 2008 Jul; 1783(7):1303-10.

[155] Owuama CI, Saunders JR, Physiological variants of *Saccharomyces cerevisiae* and Kloeckera apiculata from palm wine and cashew juice, J Appl Bacteriol, 1990, 68:491–494

[156] Palková Z, Váchová L, Yeast cell differentiation: Lessons from pathogenic and non-pathogenic yeasts, Semin Cell Dev Biol, 2016 Apr, 12. pii: S1084-9521(16)30101-X. doi: 10.1016/j.semcdb.2016.04.006. [Epub ahead of print]

[157] Palková Z, Multicellular microorganisms: laboratory versus nature, EMBO Rep, 2004 May;5(5):470-6.

[158] Pasteur L, Études sur le vin. Paris (France): Imprimeurs Imperials, 1866, 266 p.

[159] Patel BK, Gavin-Smyth J, Liebman SW, The yeast global transcriptional co-repressor protein Cyc8 can propagate as a prion, Nat Cell Biol, 2009 Mar;11(3):344-9. doi: 10.1038/ncb1843. Epub 2009 Feb 15.

[160] Peterson CL, Laniel MA, Histones and histone modifications, Curr Biol, 2004 Jul 27;14(14):R546-51.

[161] Pokholok DK, Harbison CT, Levine S, Cole M, Hannett NM, Lee TI, et al., Genome-wide map of nucleosome acetylation and methylation in yeast, Cell, 2005;122:517–27.

[162] Polsinelli M, Romano P, Suzzi G, Mortimer R, Multiple strains of *Saccharomyces cerevisiae* on a single grape vine, Lett Appl Microbiol, 1996, 23:110–114.

[163] Prusiner SB, Cell biology. A unifying role for prions in neurodegenerative diseases, Science, 2012 Jun, 22;336(6088):1511-3. doi: 10.1126/science.1222951.

[164] Puig S, Querol A, Barrio E, Pérez-Ortín JE, Mitotic recombination and genetic changes in *Saccharomyces cerevisiae* during wine fermentation, Appl Environ Microbiol, 2000 May;66(5):2057-61.

[165] Puig S, Lau M, Thiele DJ, Cti6 is an Rpd3-Sin3 histone deacetylase-associated protein required for growth under iron-limiting conditions in *Saccharomyces cerevisiae*, J Biol Chem, 2004;279:30298–30306.

[166] Ramón R. Barrales, Juan Jimenez, and José I. Ibeas, Identification of Novel Activation Mechanisms for FLO11 Regulation in *Saccharomyces cerevisiae*, Genetics, 2008 Jan; 178(1): 145–156.doi: 10.1534/genetics.107.081315.

[167] Reed B. Wickner, Herman K. Edskes, Frank Shewmaker, Toru Nakayashiki, Prions of Fungi: Inherited Structures and Biological Roles, Nat Rev Microbiol, 2008 May 12.

[168] Rhoads A, Au KF, PacBio Sequencing and Its Applications, Genomics Proteomics Bioinformatics, 2015 Oct;13(5):278-89. doi: 10.1016/j.gpb.2015.08.002. Epub 2015 Nov 2.

[169] Rintisch C, Heinig M, Bauerfeind A, Schafer S, Mieth C, Patone G, et al., Natural variation of histone modification and its impact on gene expres- sion in the rat genome, Genome Res, 2014;24:942–53.

[170] Rice JC, Allis CD, Histone methylation versus histone acetylation: new insights into epigenetic regulation, Curr Opin Cell Biol, 2001 Jun;13(3):263-73.

[171] Ritchie ME, Phipson B, Wu D, Hu Y, Law CW, Shi W and Smyth GK, limma powers differential expression analyses for RNA-sequencing and microarray studies, Nucleic Acids Research, 2015,43(7), e47.

[172] Rizzetto L, Cavalieri D, A systems biology approach to the mutual interaction between yeast and the immune system, Immunobiology, 2010 Sep-Oct;215(9-10):762-9. doi: 10.1016/j.imbio.2010.05.009. Epub 2010 Jun 9.

[173] Robbins N, Leach MD, Cowen LE, Lysine deacetylases Hda1 and Rpd3 regulate Hsp90 function thereby governing fungal drug resistance, Cell Rep, 2012 Oct, 25;2(4):878-88. doi: 10.1016/j.celrep.2012.08.035. Epub 2012 Oct 4.

[174] Rodriguez A, et al., The hexokinase 2 protein regulates the expression of the GLK1, HXK1 and HXK2 genes of *Saccharomyces cerevisiae*, Biochem, 2001, J 355(Pt 3):625-31 PMID: 11311123

[175] Ryan O, Shapiro RS, Kurat CF, Mayhew D, Baryshnikova A, Chin B, Lin ZY, Cox MJ, Vizeacoumar F, Cheung D, Bahr S, Tsui K, Tebbji F, Sellam A, Istel F, Schwarzmüller T, Reynolds TB, Kuchler K, Gifford DK, Whiteway M, Giaever G, Nislow C, Costanzo M, Gingras AC, Mitra RD, Andrews B, Fink GR, Cowen LE, Boone C, Global gene deletion analysis exploring yeast filamentous growth, Science, 2012 Sep 14; 337(6100):1353-6. doi: 10.1126/science.1224339.

[176] S Rupp, E Summers, H J Lo, H Madhani, and G Fink, MAP kinase and cAMP filamentation signaling pathways converge on the unusually large promoter of the yeast FLO11 gene, MBO J, 1999 Mar 1; 18(5): 1257–1269.doi: 10.1093/emboj/18.5.1257.

[177] Rusche´ L.N., and Rine J., Conversion of a gene-specific repressor to a regional silencer, Genes Dev, 2001, 15, 955–967

[178] Russo VEA, Martienssen RA, Riggs AD, Epigenetic Mechanisms of Gene Regulation, New York Cold Spring Harbor Press, 1996.

[179] Santos-Rosa H, Schneider R, Bannister AJ, Sherriff J, Bernstein BE, Emre NC, Schreiber SL, Mellor J, Kouzarides T, Active genes are tri-methylated at K4 of histone H3, Nature, 2002 Sep 26;419(6905):407-11. Epub 2002 Sep 11.

[180] Schneider, R., Bannister, A.J., Myers, F.A., Thorne, A.W., Crane- Robinson, C., and Kouzarides T., Histone H3 lysine 4 methylation patterns in higher eukaryotic genes., Nat. Cell Biol, 2004 6: 73–77.

[181] Serio TR, Lindquist SL, [PSI+]: an epigenetic modulator of translation termination efficiency, Annu Rev Cell Dev Biol, 1999;15:661-703.

[182] Serio TR, Cashikar AG, Kowal AS, Sawicki GJ, Moslehi JJ, Serpell L, Arnsdorf MF, Lindquist SL, Nucleated conformational conversion and the replication of conformational information by a prion determinant, Science, 2000 Aug, 25;289(5483):1317-21.

[183] Shannon M. Doyle, Olivier Genest & Sue Wickner, Protein rescue from aggregates by powerful molecular chaperone machines, Nature Reviews Molecular Cell Biology, 2013, 14, 617–629 doi:10.1038/nrm3660

[184] Shapiro RS, Robbins N, Cowen LE, Regulatory circuitry governing fungal development, drug resistance, and disease, Microbiol Mol Biol Rev, 2011 Jun;; 75(2):213-67. doi: 10.1128/MMBR.00045-10.

[185] Si H, Hernday AD, Hirakawa MP, Johnson AD, Bennett RJ, *Candida albicans* white and opaque cells undergo distinct programs of filamentous growth, PLoS Pathog, 2013 Mar; 9(3):e1003210. doi: 10.1371/journal.ppat.1003210.

[186] Simon MN, De Virgilio C, Souza B, Pringle JR, Abo A, Reed SI, Role for the Rho-family GTPase Cdc42 in yeast mating-pheromone signal pathway, Nature, 1995 Aug 24;376(6542):702-5.

[187] Matthias Sipiczki, Diversity, variability and fast adaptive evolution of the wine yeast (*Saccharomyces cerevisiae*) genome—a review, Annals of Microbiology, March 2011, Volume 61, Issue 1, pp 85–93.

[188] Slutsky B, Staebell M, Anderson J, Risen L, Pfaller M, Soll DR, "White-opaque transition": a second high-frequency switching system in *Candida albicans*, J Bacteriol, 1987 Jan;169(1):189-97.

[189] Sossou SK, Ameyapoh Y, Karou SD, de Souza C, Study of pineapple peelings processing into vinegar by biotechnology, Pak J Biol Sci, 2009, 12:859–865.

[190] Spellman P. T., Sherlock G., Zhang M. Q., Iyer V. R., Anders K., et al. , Comprehensive identification of cell cycle-regulated genes of the yeast *Saccharomyces cerevisiae* by microarray hybridization, Mol. Biol. Cell, 1998, 9: 3273–3297

[191] Srikantha T, Tsai L, Daniels K, Klar AJ, Soll DR, The histone deacetylase genes HDA1 and RPD3 play distinct roles in regulation of high-frequency phenotypic switching in *Candida albicans*, J Bacteriol, 2001 Aug;183(15):4614-25.

[192] St'ovíček V, Váchová L, Kuthan M, Palková Z, General factors important for the formation of structured biofilm-like yeast colonies, Fungal Genet Biol, 2010 Dec;47(12):1012-22. doi: 10.1016/j.fgb.2010.08.005. Epub 2010 Aug 20.

[193] K.A. Steinkraus, M. Kaeberlein and B.K. Kennedy, Replicative Aging in Yeast The Means to the End, Annu Rev Cell Dev Biol, 2008;24:29-54. doi: 10.1146/annurev.cellbio.23.090506.123509

[194] Strahl BD, Allis CD, The language of covalent histone modifications, Nature, 2000 Jan 6;403(6765):41-5.

[195] Stuart GR, Copeland WC, Strand MK, Construction and application of a protein and genetic interaction network (yeast interactome), Nucleic Acids Res, 2009 Apr;37(7):e54. doi: 10.1093/nar/gkp140. Epub 2009 Mar 9.

[196] Sudarsanam P, Winston F. The Swi/Snf family nucleosome-remodeling complexes and transcriptional control, Trends Genet, 2000;16:345–51. [PubMed: 10904263] Sugasawa K, Ishimi Y, Eki T, Hurwitz J, Kikuchi A, Hanaoka F, Nonconservative segregation of parental nucleosomes during simian virus 40 chromosome replication in vitro, Proc Natl Acad Sci U S A., 1992 Feb, 1;89(3):1055-9.

[197] Sugasawa K, Ishimi Y, Eki T, Hurwitz J, Kikuchi A, Hanaoka F, Nonconservative segregation of parental nucleosomes during simian virus 40 chromosome replication in vitro, Proc Natl Acad Sci U S A, 1992 Feb, 1;89(3):1055-9.

[198] Tang L, Nogales E, Ciferri C, Structure and function of SWI/SNF chromatin remodeling complexes and mechanistic implications for transcription, Prog Biophys Mol Bio, 2010 Jun-Jul;102(2-3):122-8. doi: 10.1016/j.pbiomolbio.2010.05.001. Epub 2010 May 20.

[199] Thomas G, Lange HW, Hempel K, Relative stability of lysine-bound methyl groups in arginie-rich histones and their subfrations in Ehrlich ascites tumor cells in vitro, Hoppe Seylers Z Physiol Chem, 1972, 353:1423-1428.

[200] Thornton, R. J. (1986). Genetic characterisation of New Zealand and Australian wine yeasts. Ant. van Leeuw. 52, 97–103.Tubb,

[201] Tjeertes JV, Miller KM, Jackson SP, Screen for DNA-dam- age-responsive histone modifications identifies H3K9Ac and H3K56Ac in human cells, EMBO J, 2009; 28:1878-1889. M A Treitel and M Carlson, Repression by SSN6-TUP1 is directed by MIG1, a repressor/activator protein, Proc Natl Acad Sci U S A, 1995 Apr 11; 92(8): 3132–3136.

[202] Stephen Tonna, Assam El-Osta, Mark E. Cooper & Chris Tikellis, Metabolic memory and diabetic nephropathy: potential role for epigenetic mechanisms, Nature Reviews Nephrology, 2010 June , 6, 332-341 doi:10.1038/nrneph.2010.55

[203] M A Treitel and M Carlson, Repression by SSN6-TUP1 is directed by MIG1, a repressor/activator protein, Proc Natl Acad Sci U S A, 1995 Apr 11; 92(8): 3132–3136.

[204] True H. L., The battle of the fold: chaperones take on prions, Trends Genet, 2006, 22, 110–117

[205] Türkel S. Hyperosmotic stress represses the transcription of HXT2 and HXT4 genes in *Saccharomyces cerevisiae*, Folia Microbiol, 1999, Praha. 44(4):372-6

[206] Tsvetanova NG, Klass DM, Salzman J, Brown PO, Proteome-wide search reveals unexpected RNA-binding proteins in *Saccharomyces cerevisiae*, PLoS One, 2010 Sep 10;5(9). pii: e12671. doi: 10.1371/journal.pone.0012671.

[207] M.F. Tuite, T.R. Serio, The prion hypothesis: from biological anomaly to basic regulatory mechanism, Nat. Rev. Mol. Cell Biol., 2010, pp. 823–833

[208] Vachova, L., Stovicek, V., Hlavacek, O., Chernyavskiy, O., Stepanek, L., Kubinova, L., and Palkova, Z, Flo11p, drug efflux pumps, and the extracellular matrix cooperate to form biofilm yeast colonies, J Cell Biol, 2011, 194: 679–687.

[209] L. G. Vallier and M. Carlson, Synergistic Release from Glucose Repression by Mig1 and Ssn Mutations in *Saccharomyces Cerevisiae*, Genetics, 1994 May; 137(1): 49–54.

[210] Van Zyl WH, Lodolo EJ, Gericke M, Conversion of homothallic yeast to heterothallism through HO gene disruption, Curr Genet, 1993;23(4):290-4.

[211] Verstrepen KJ, Klis FM, Flocculation, adhesion and biofilm formation in yeasts, Mol Microbiol, 2006 Apr;60(1):5-15.

[212] Vidal M, Gaber RF, RPD3 encodes a second factor required to achieve maximum positive and negative transcriptional states in *Saccharomyces cerevisiae*, Mol Cell Biol, 1991 Dec;11(12):6317-27.

[213] Vignali M, Hassan AH, Neely KE, Workman JL, ATP-dependent chromatin-remodeling complexes, Mol Cell Biol, 2000 Mar;20(6):1899-910.

[214] Vinod PK, Sengupta N, Bhat PJ, Venkatesh KV, Integration of global signaling pathways, cAMP-PKA, MAPK and TOR in the regulation of FLO11. - PLoS ONE, 2008

[215] Voordeckers K, De Maeyer D, van der Zande E, Vinces MD, Meert W, Cloots L, Ryan O, Marchal K, Verstrepen KJ, Identification of a complex genetic network underlying *Saccharomyces cerevisiae* colony morphology, Mol Microbiol, 2012 Oct, 86(1):225-39. doi: 10.1111/j.1365-2958.2012.08192

[216] Vopálenská I, Hůlková M, Janderová B, Palková Z, The morphology of *Saccharomyces cerevisiae* colonies is affected by cell adhesion and the budding pattern, Res Microbiol. 2005 Nov;156(9):921-31. Epub 2005 Jul 14.

[217] Vyas VK, Kuchin S, Carlson M., Interaction of the repressors Nrg1 and Nrg2 with the Snf1 protein kinase in *Saccharomyces cerevisiae*, Genetics, 2001 Jun;158(2):563-72. Wagner EJ, Carpenter PB, Understanding the language of Lys36 methylation at histone H, Nat Rev Mol Cell Biol, 2012 Jan 23;13(2):115-26. doi: 10.1038/nrm3274.

[218] Wagner EJ, Carpenter PB, Understanding the language of Lys36 methylation at histone H, Nat Rev Mol Cell Biol, 2012 Jan 23;13(2):115-26. doi: 10.1038/nrm3274.

[219] Wan-Sheng Lo and Anne M, The Cell Surface Flocculin Flo11 Is Required for Pseudohyphae Formation and Invasion by *Saccharomyces cerevisiae*, Dranginis, Mol Biol Cell, 1998 Jan; 9(1): 161–171.

[220] Wang, X., Vitalis, A., Wyczalkowski, M.A., and Pappu, R.V, Character- izing the conformational ensemble of monomeric polyglutamine, Proteins, 2006, 63, 297–311.

[221] Wang Z, Zang C, Rosenfeld JA, Schones DE, Barski A, Cuddapah S, Cui K, Roh TY, Peng W, Zhang MQ, Zhao K, Combinatorial patterns of histone acetylations and methylations in the human genome, Nat Genet, 2008 Jul;40(7):897-903. doi: 10.1038/ng.154. Epub 2008 Jun 15.

[222] Joris Winderickxa, Charlotte Delay, Ann De Vos, Harald Klinger, Klaartje Pellens, Thomas Vanhelmont, Fred Van Leuven, Piotr Zabrocki, Protein folding diseases and neurodegeneration: Lessons learned from yeast, Biochim Biophys Acta. 2008 Jul;1783(7):1381-95. doi: 10.1016/j.bbamcr.2008.01.020. Epub 2008 Feb 11

[223] Wolf SS, The protein arginine methyltransferase family: an update about function, new perspectives and the physiologi- cal role in humans, Cell Mol Life Sci, 2009; 66:2109-2121.

[224] Workman JL, Kingston RE. Alteration of nucleosome structure as a mechanism of transcriptional regulation, Annu Rev Biochem, 1998;67:545–79. [PubMed: 9759497]

[225] Yanagida, F., Shinohara, T. and Goto, S, Thallism, ploidy, and killer property of wine yeasts, J. Gen. Appl. Microbiol, 1993, 39, 101–106

[226] Yang XJ, Seto E, HATs and HDACs: from structure, function and regulation to novel strategies for therapy and prevention, Oncogene, 2007; 26:5310-5318.

[227] Yuan O. Zhu, Mark L. Siegal, David W. Hall, Dmitri A. Petrov. Precise estimates of mutation rate and spectrum in yeast, Proc Natl Acad Sci U S A, 2014 Jun 3,. 111(22): E2310–E2318.

[228] Zang C, Schones DE, Zeng C, Cui K, Zhao K, Peng W, A clustering approach for identification of enriched domains from histone modification ChIP-Seq data, Bioinformatics, 2009 Aug 1;25(15):1952-8. doi: 10.1093/bioinformatics/btp340. Epub 2009 Jun 8.

[229] Oscar Zaragoza & Juana M. Gancedo∗, Pseudohyphal growth is induced in *Saccharomyces cerevisiae* by a combination of stress and cAMP signalling, Antonie Van Leeuwenhoek. 2000 Aug;78(2):187-94

[230] Zeng L, Zhou MM, Bromodomain: an acetyl-lysine binding domain, FEBS Lett, 2002 Feb 20;513(1):124-8.

[231] Zhao ZS, Leung T, Manser E, Lim L, Pheromone signalling in *Saccharomyces cerevisiae* requires the small GTP-binding protein Cdc42p and its activator CDC24, Mol Cell Biol, 1995 Oct;15(10):5246-57.

Appendix A - *Chromosomes distribution of spore-specific chromatin domains (SSCDs)*

Fig. A.1: Chromosome I - (H3 3Met K4)

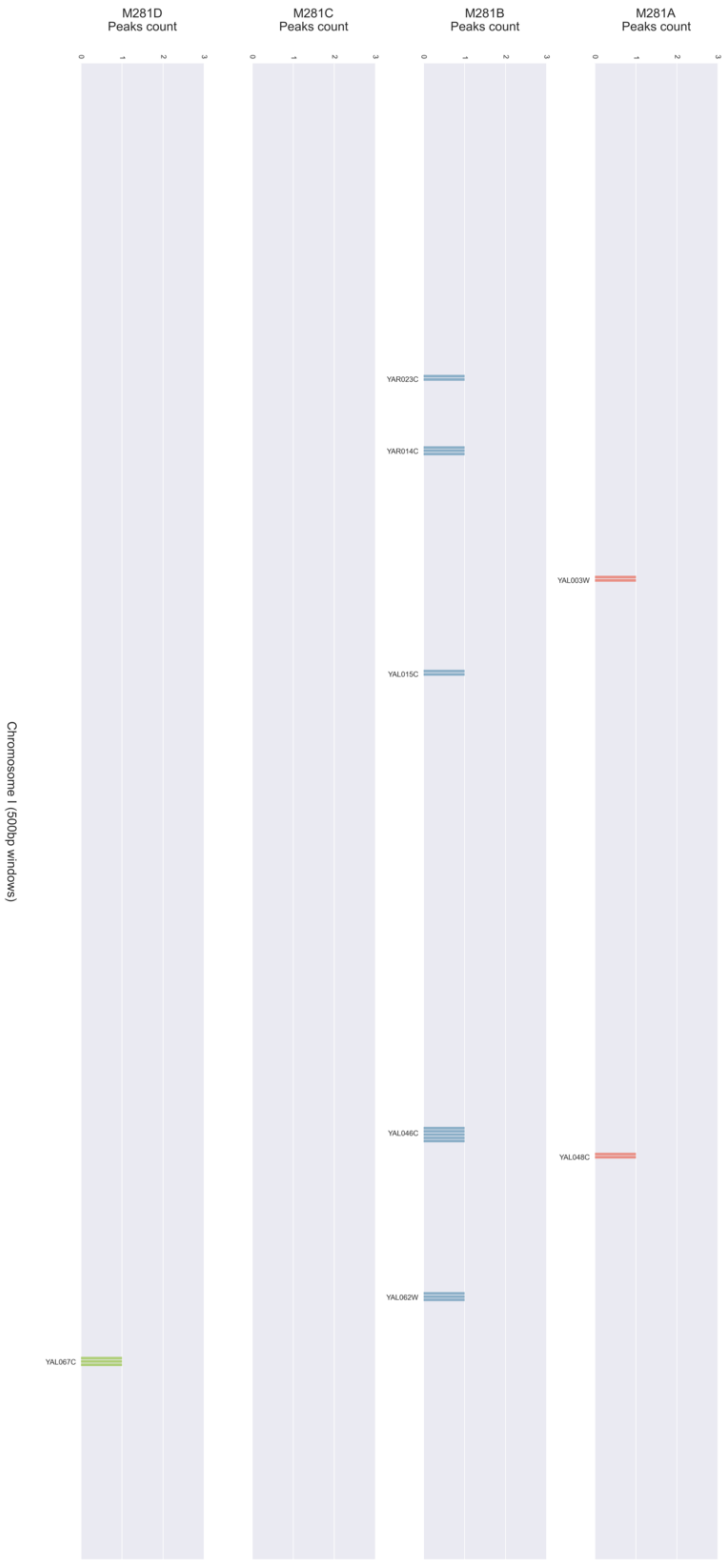

Fig. A.2: Chromosome I - (H3 2Met K4)

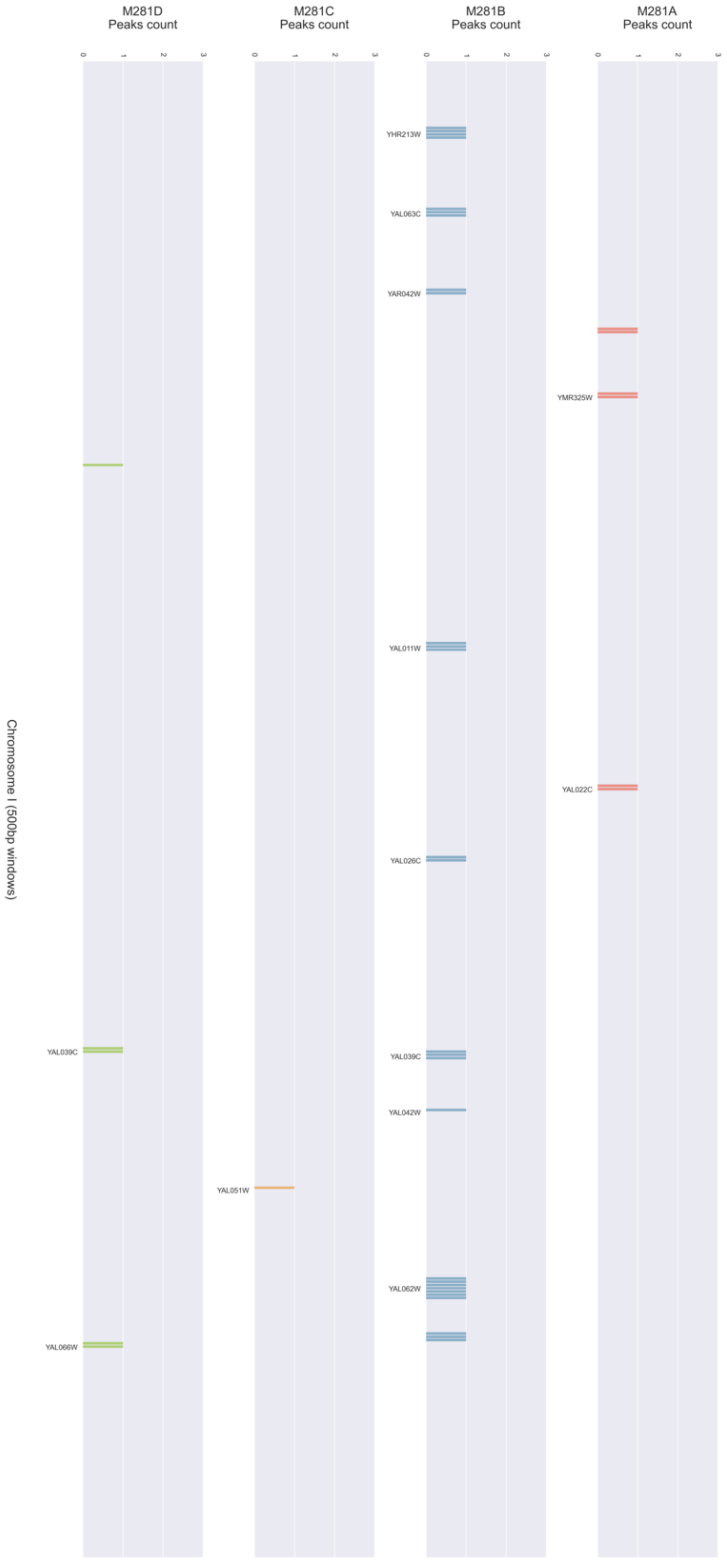

Fig. A.3: Chromosome I - (H4 Ac)

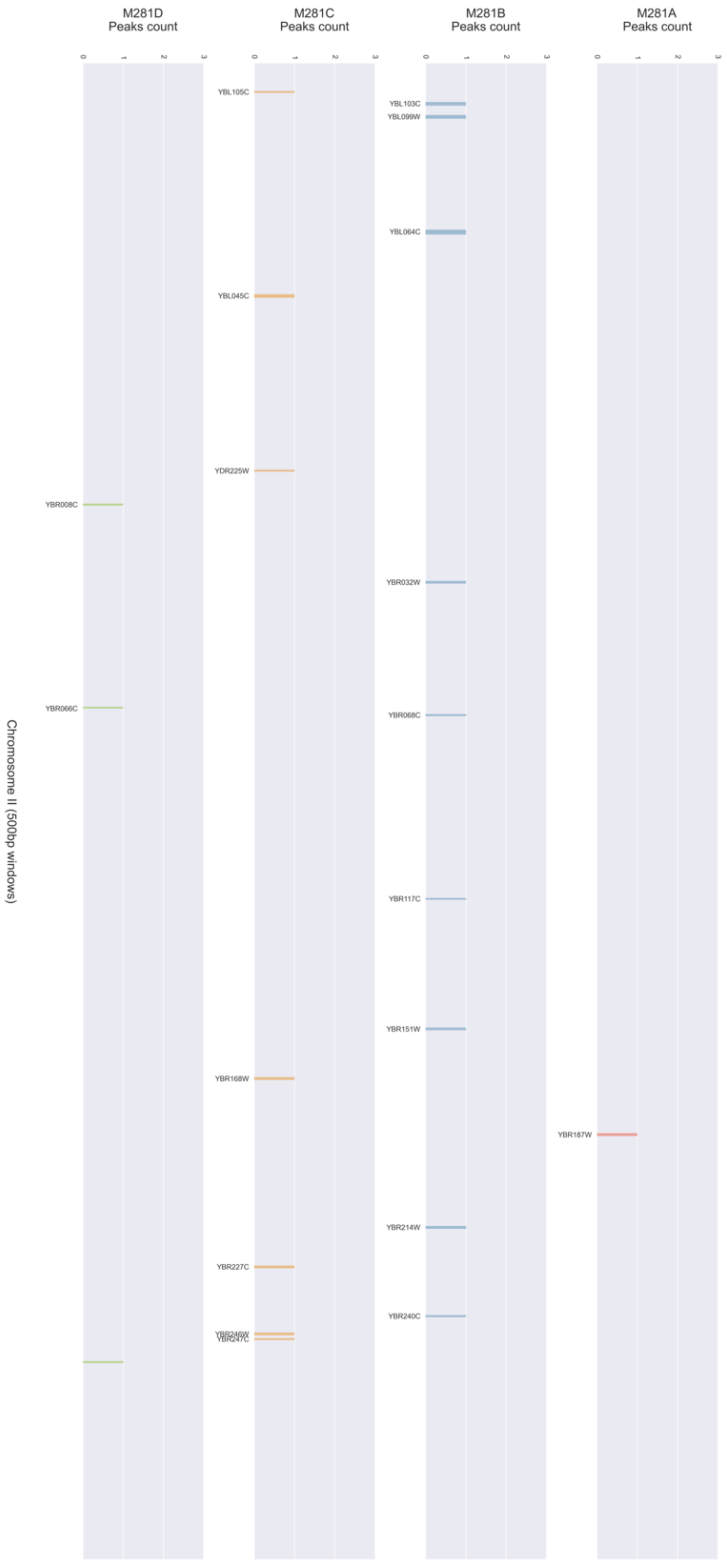

Fig. A.4: Chromosome II - (H3 3Met K4)

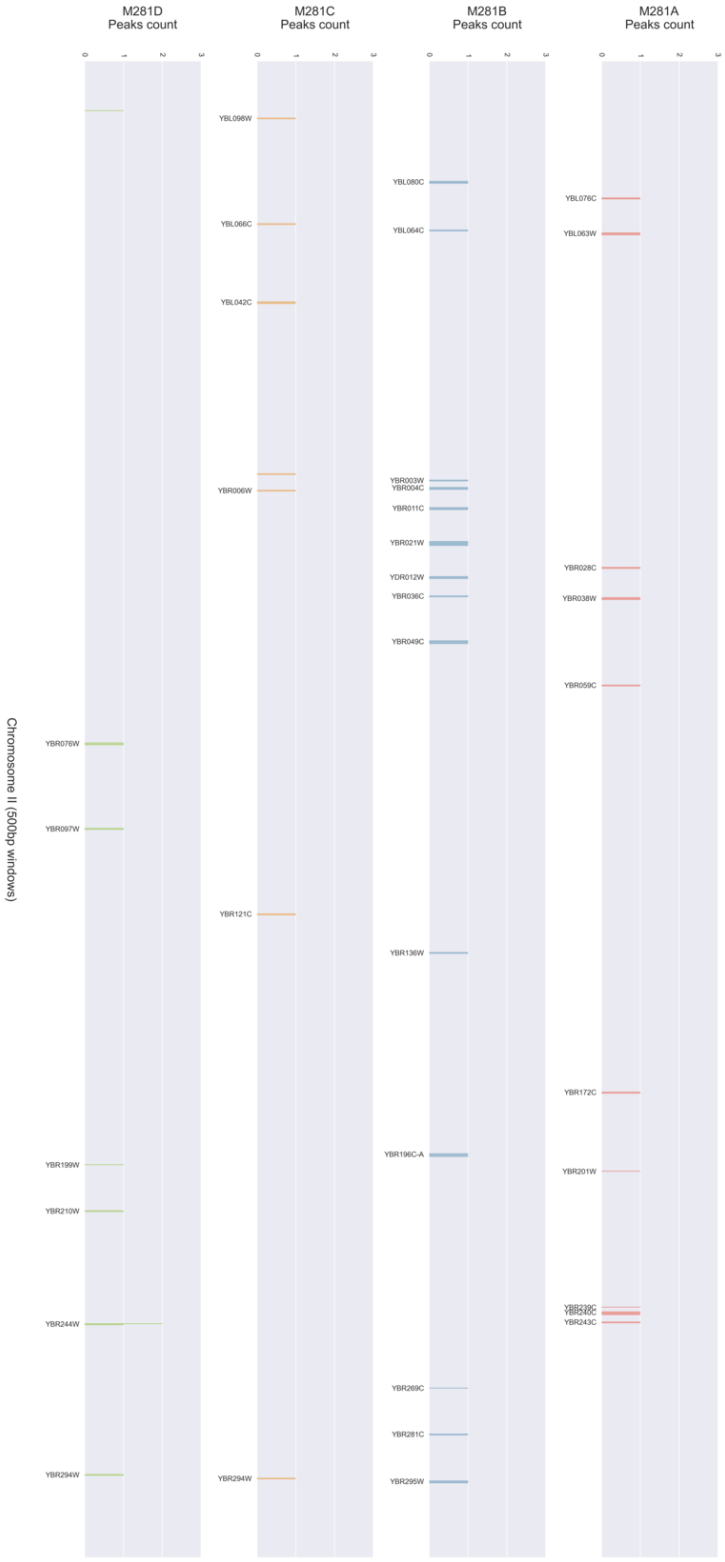

Fig. A.5: Chromosome II - (H3 2Met K4)

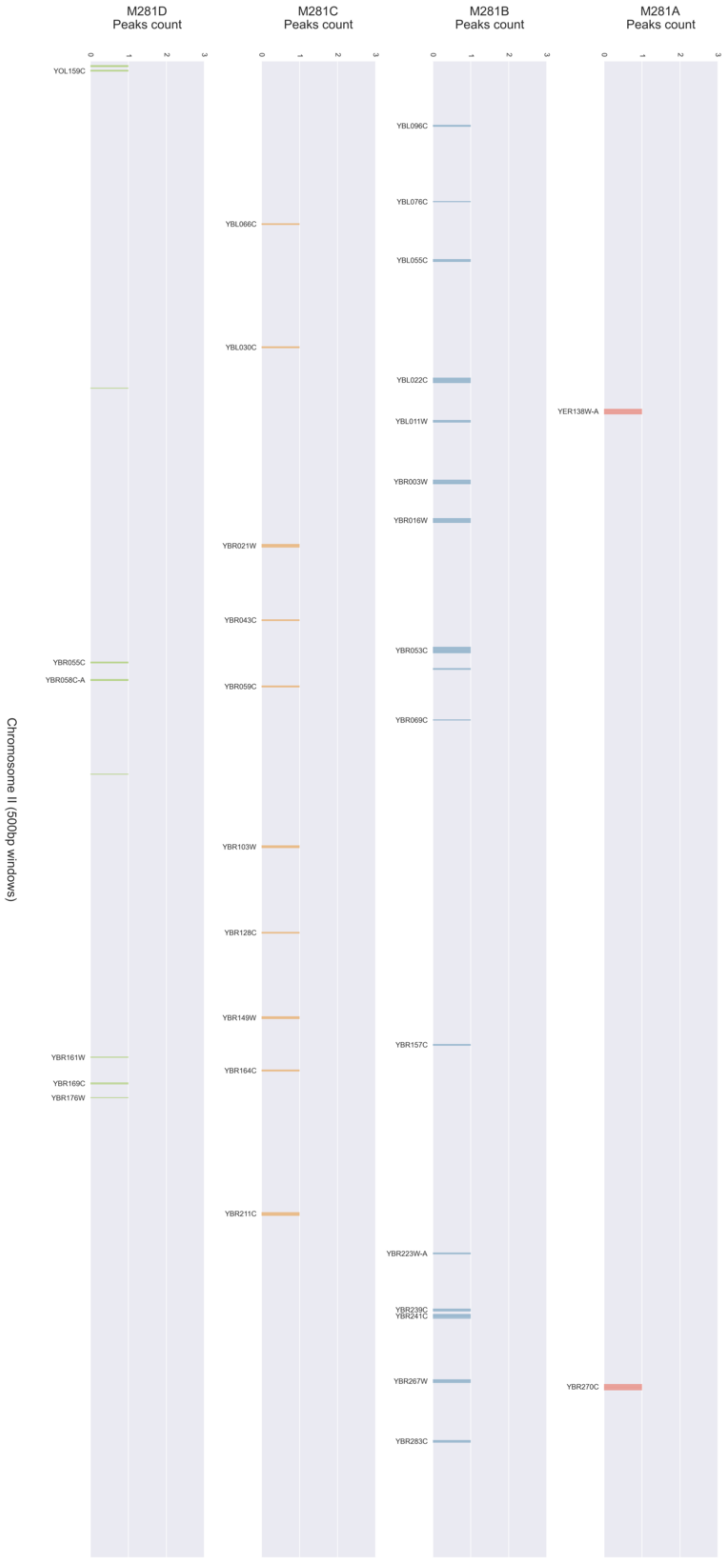

Fig. A.6: Chromosome II - (H4 Ac)

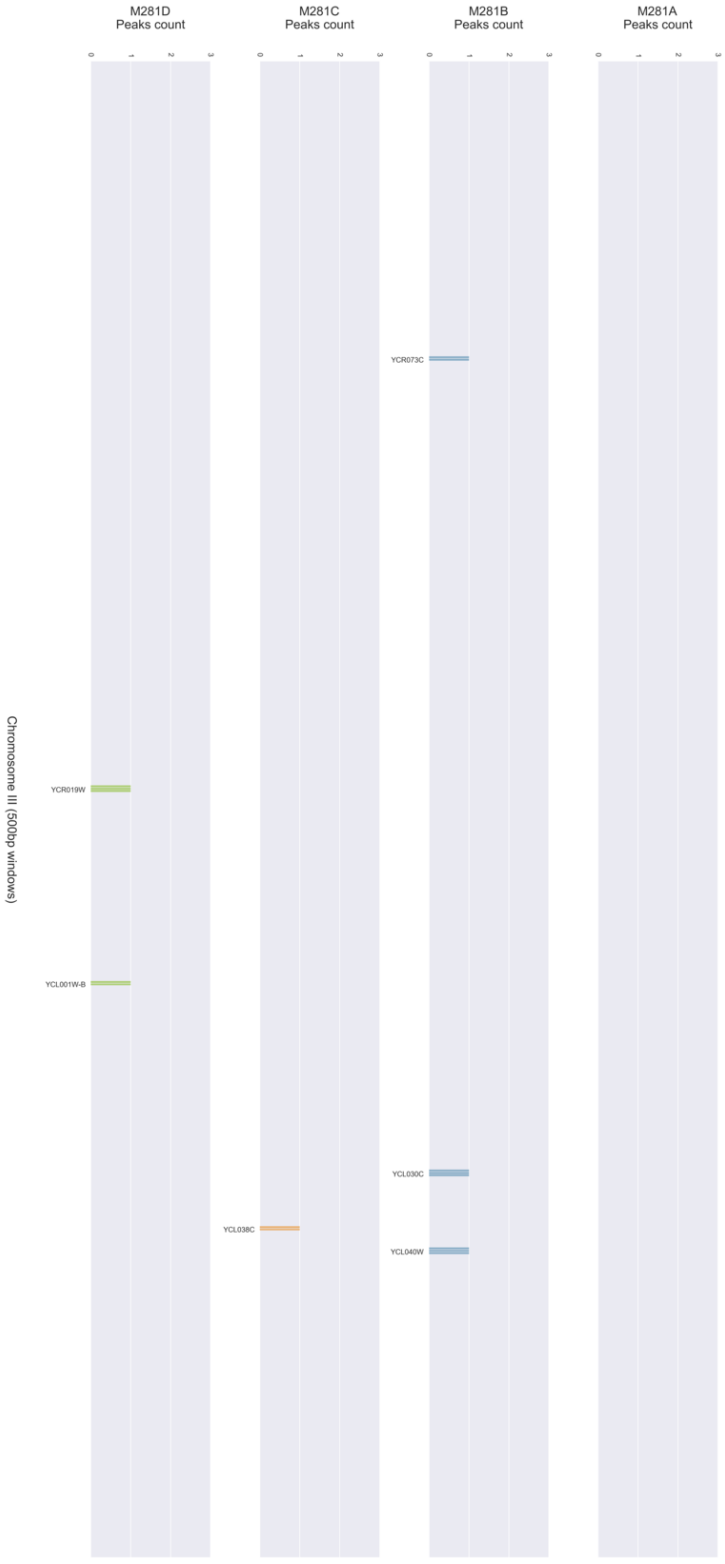

Fig. A.7: Chromosome III - (H3 3Met K4)

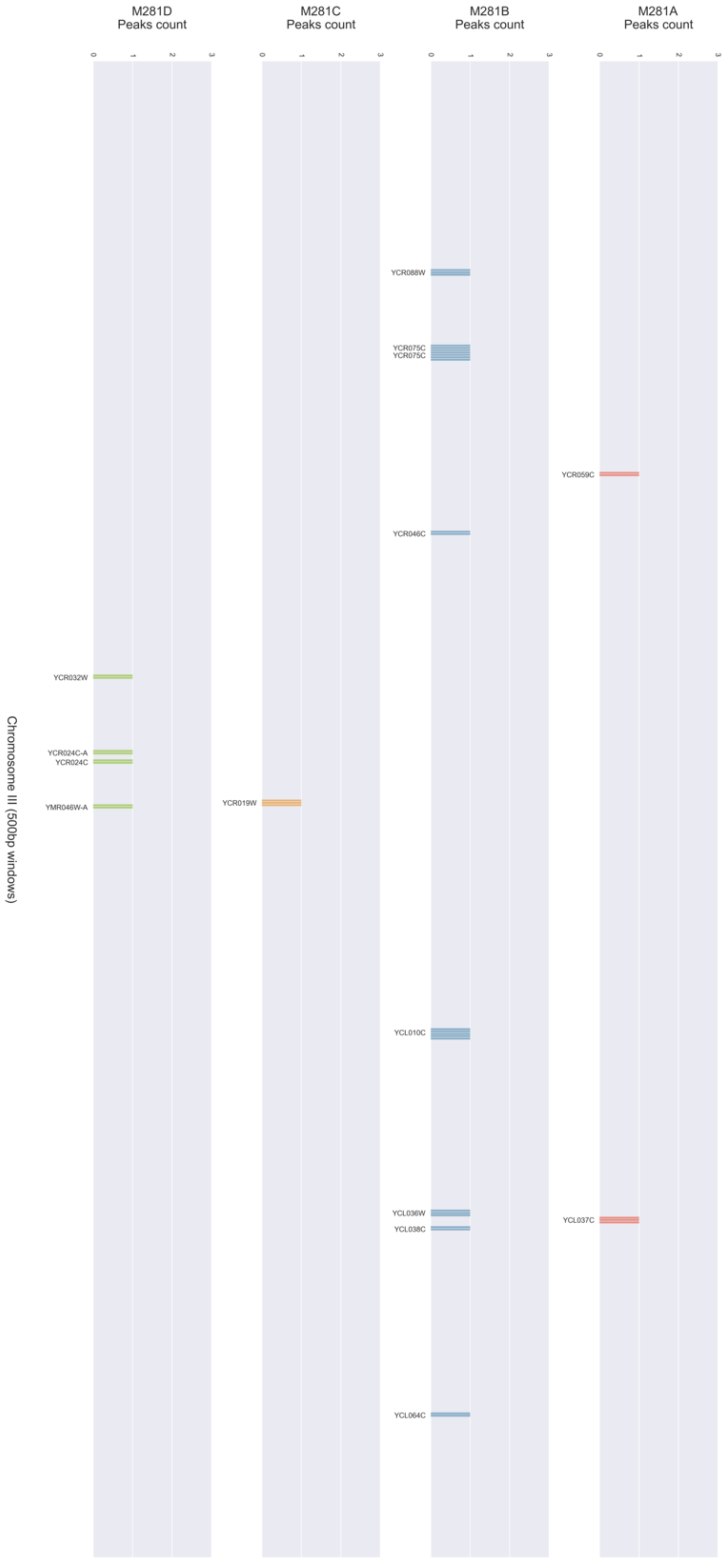

Fig. A.8: Chromosome III - (H3 2Met K4)

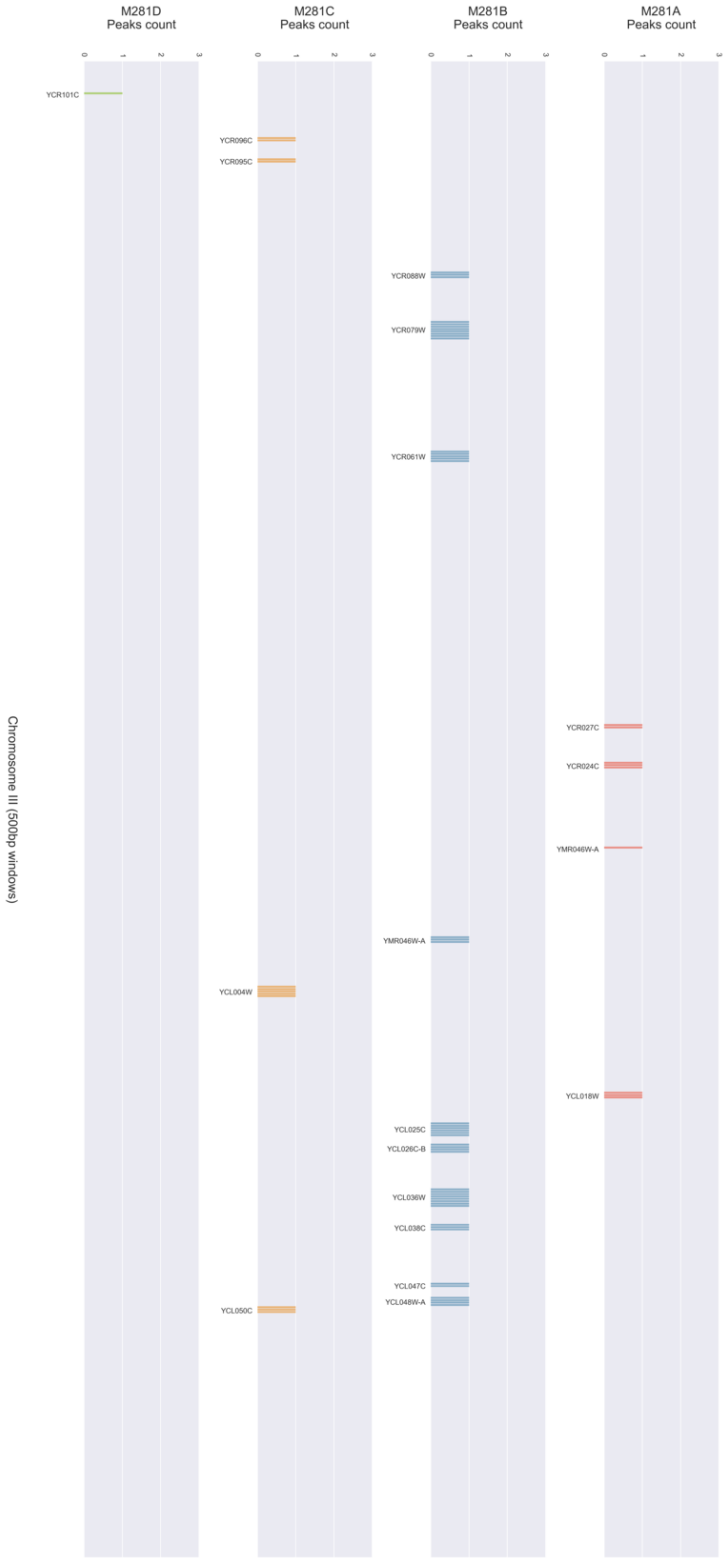

Fig. A.9: Chromosome III - (H4 Ac)

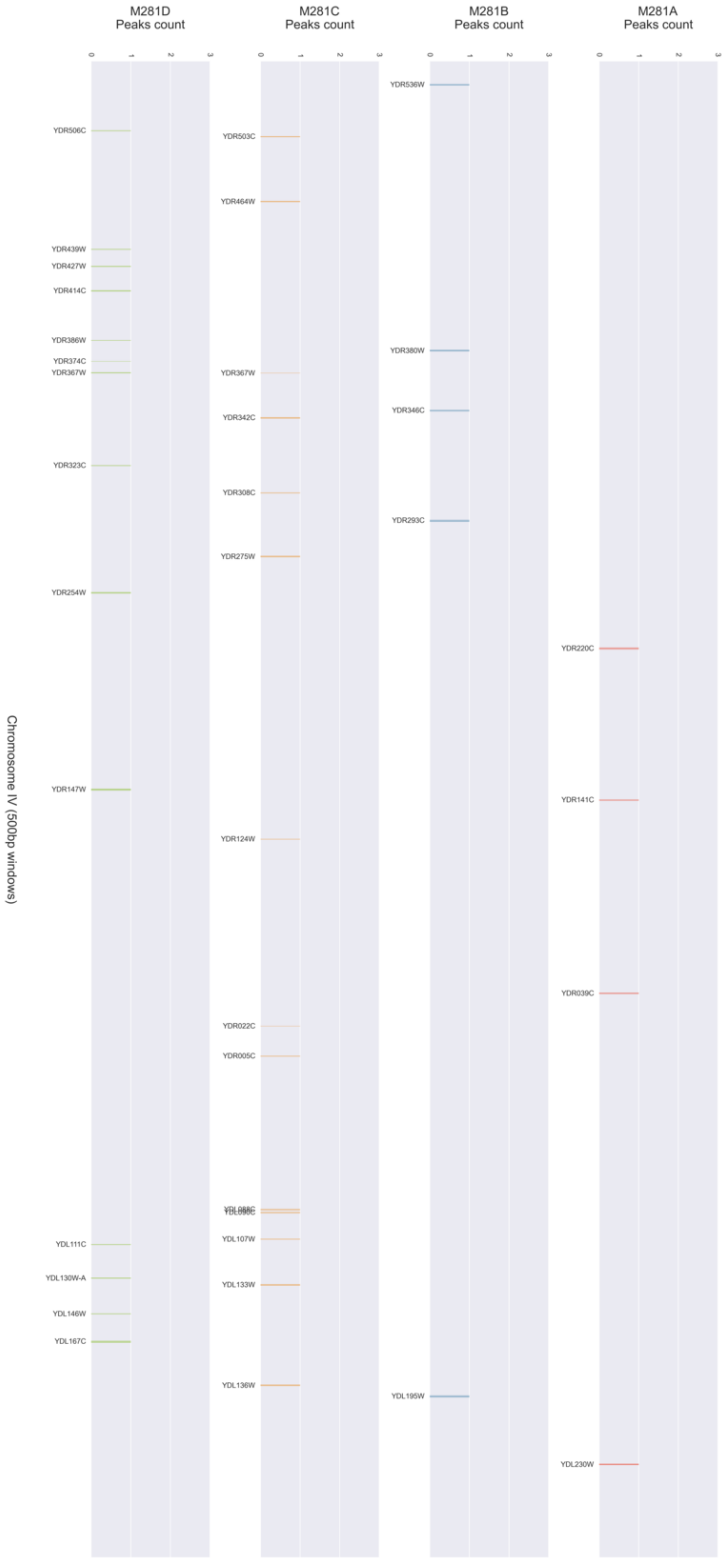

Fig. A.10: Chromosome IV - (H3 3Met K4)

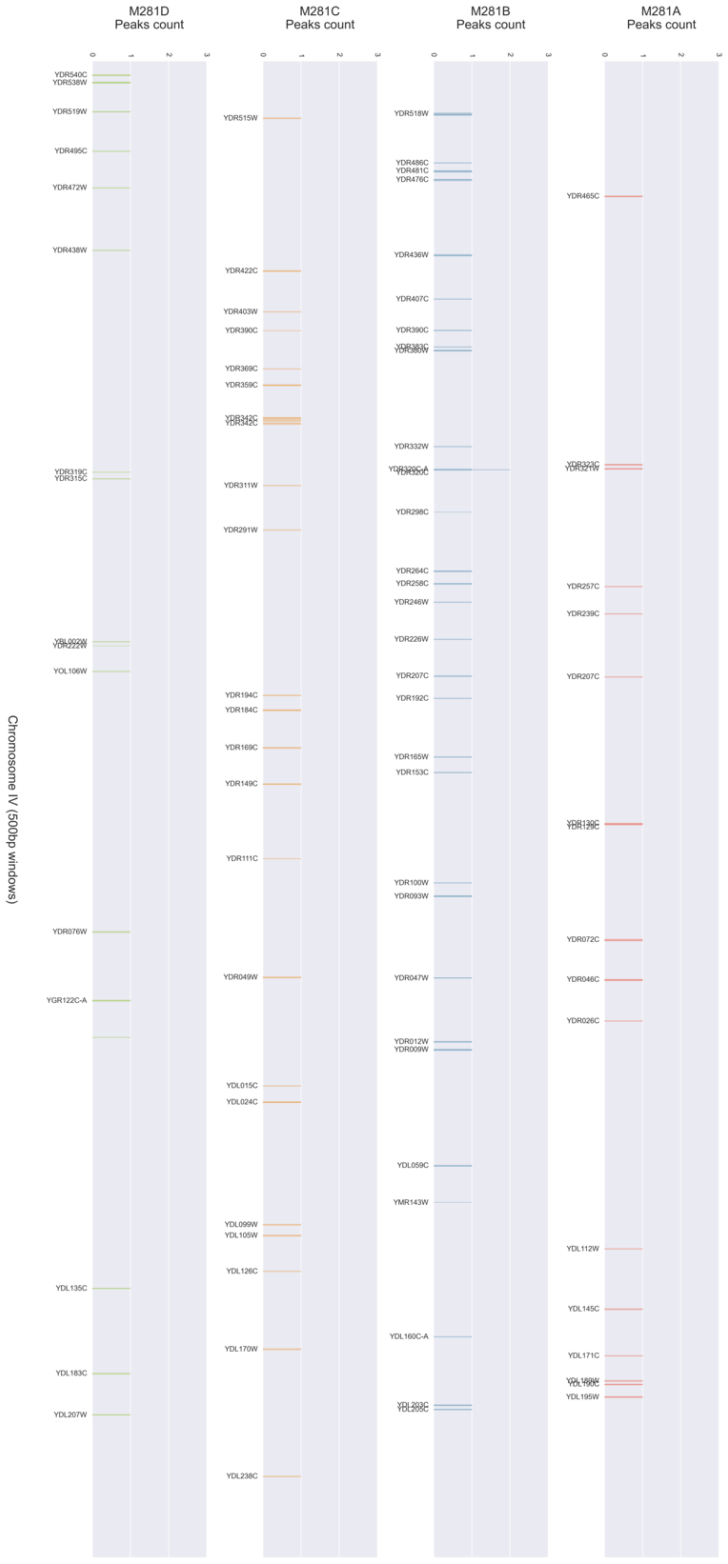

Fig. A.11: Chromosome IV - (H3 2Met K4)

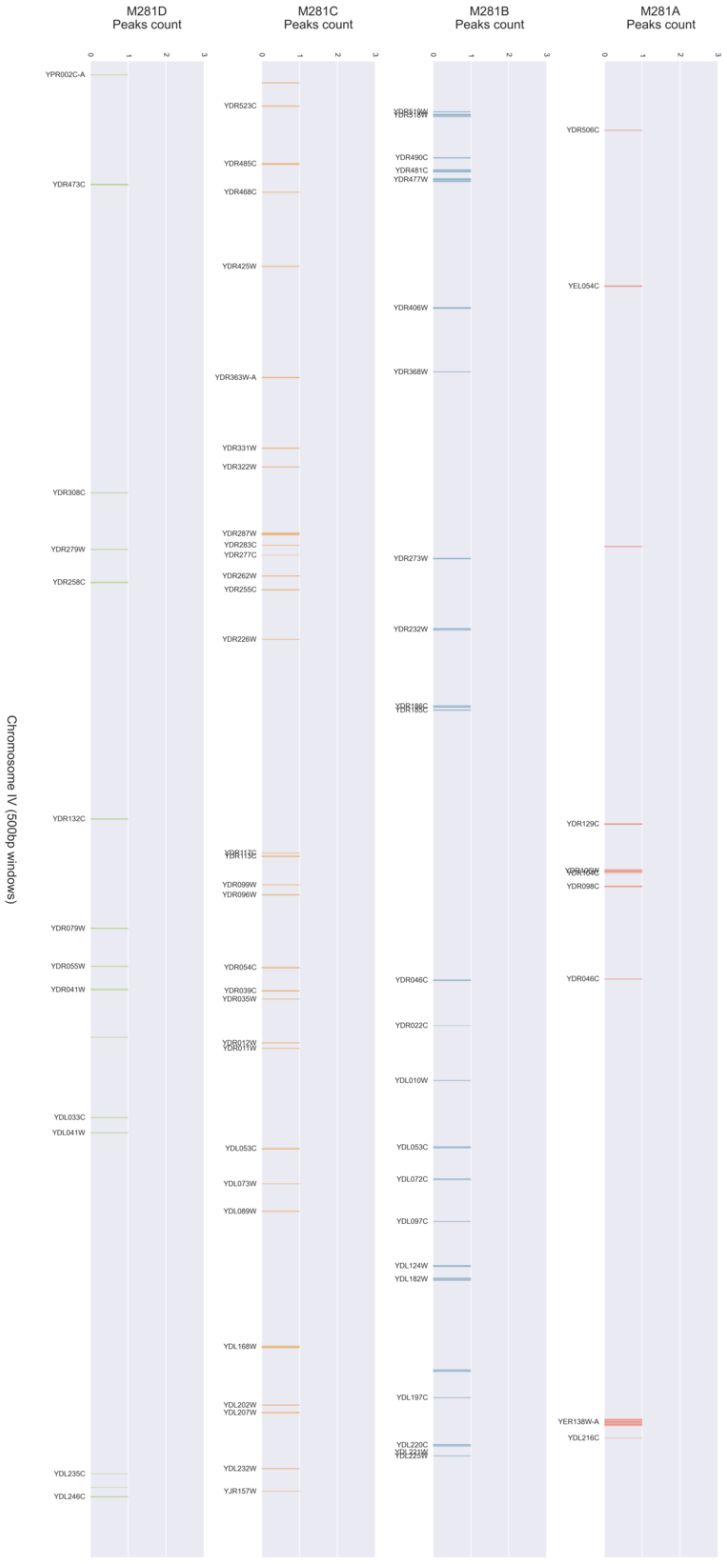

Fig. A.12: Chromosome IV - (H4 Ac)

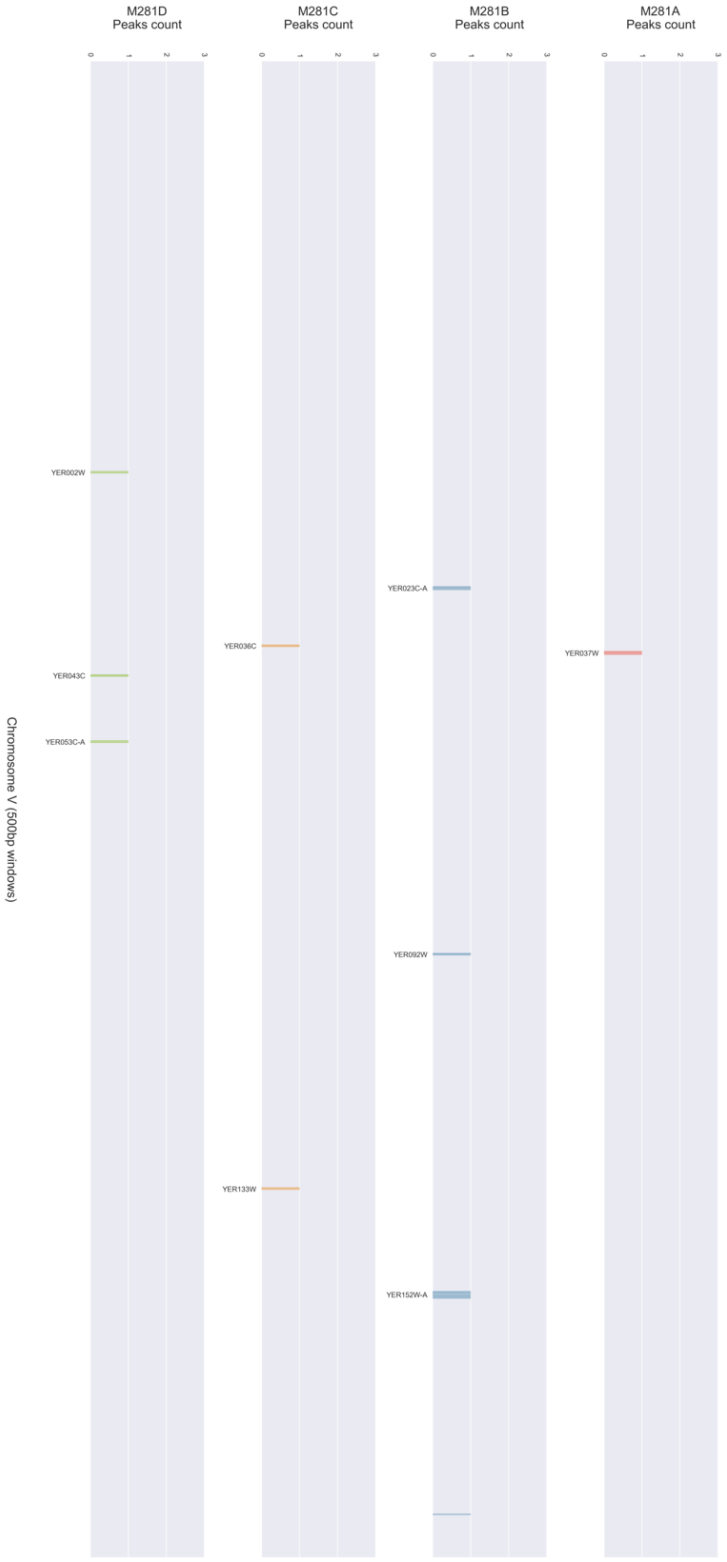

Fig. A.13: Chromosome V - (H3 3Met K4)

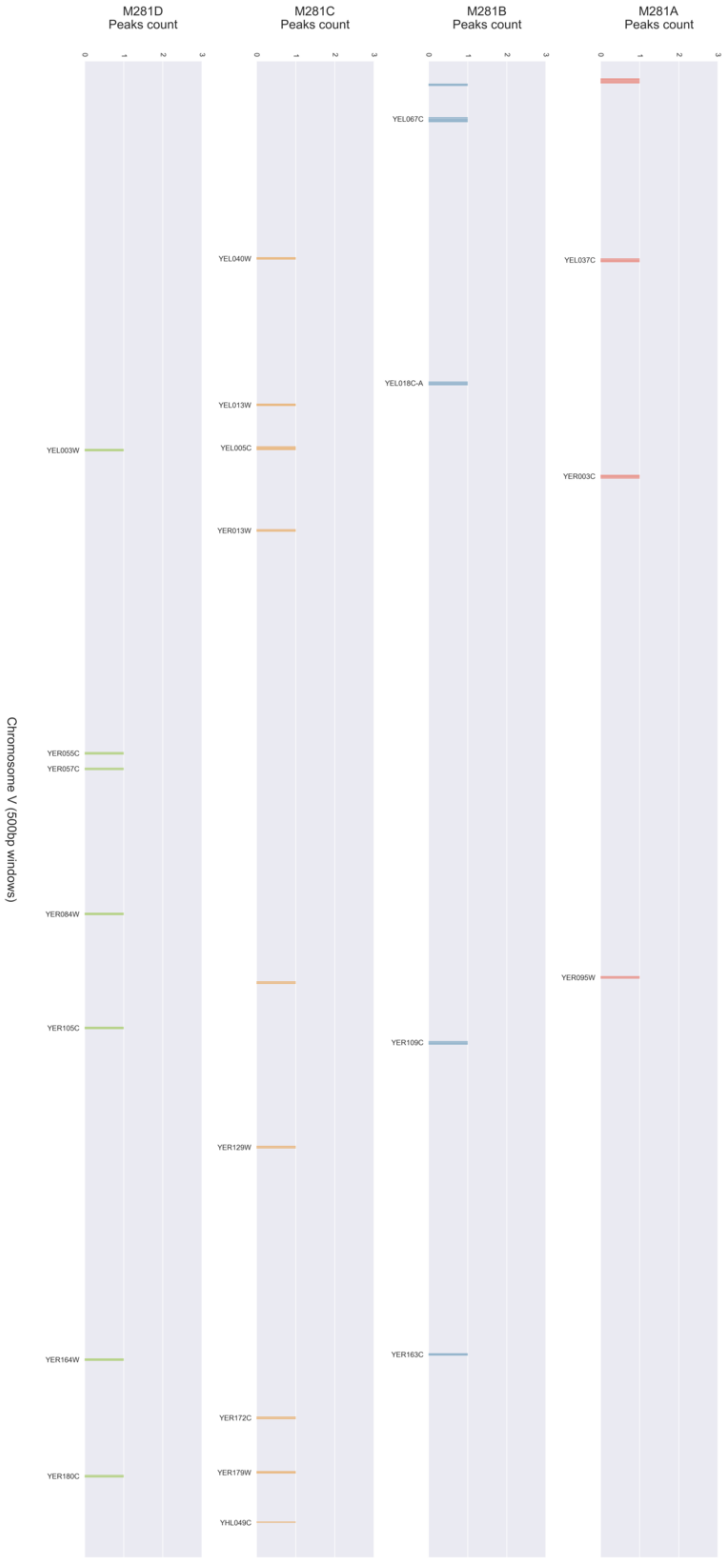

Fig. A.14: Chromosome V - (H3 2Met K4)

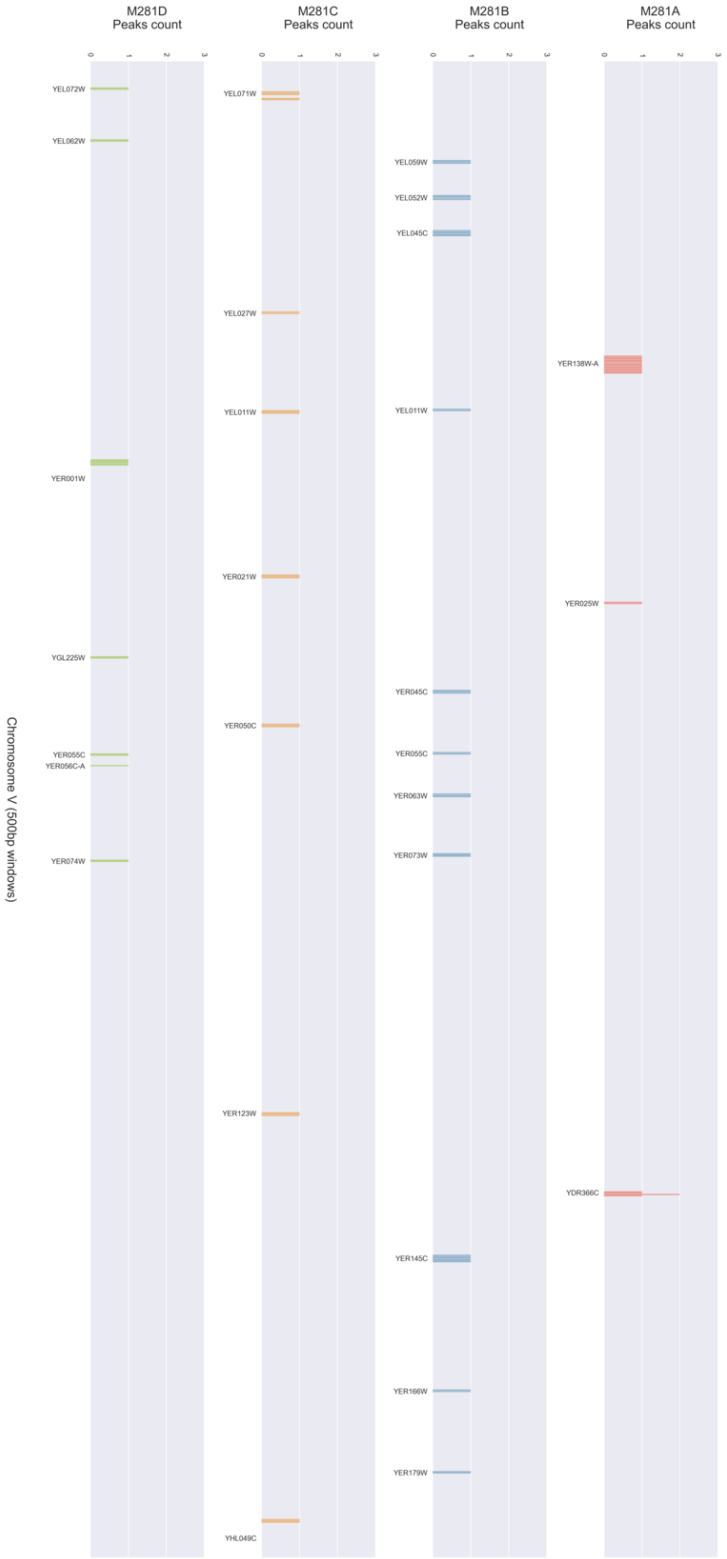

Fig. A.15: Chromosome V - (H4 Ac)

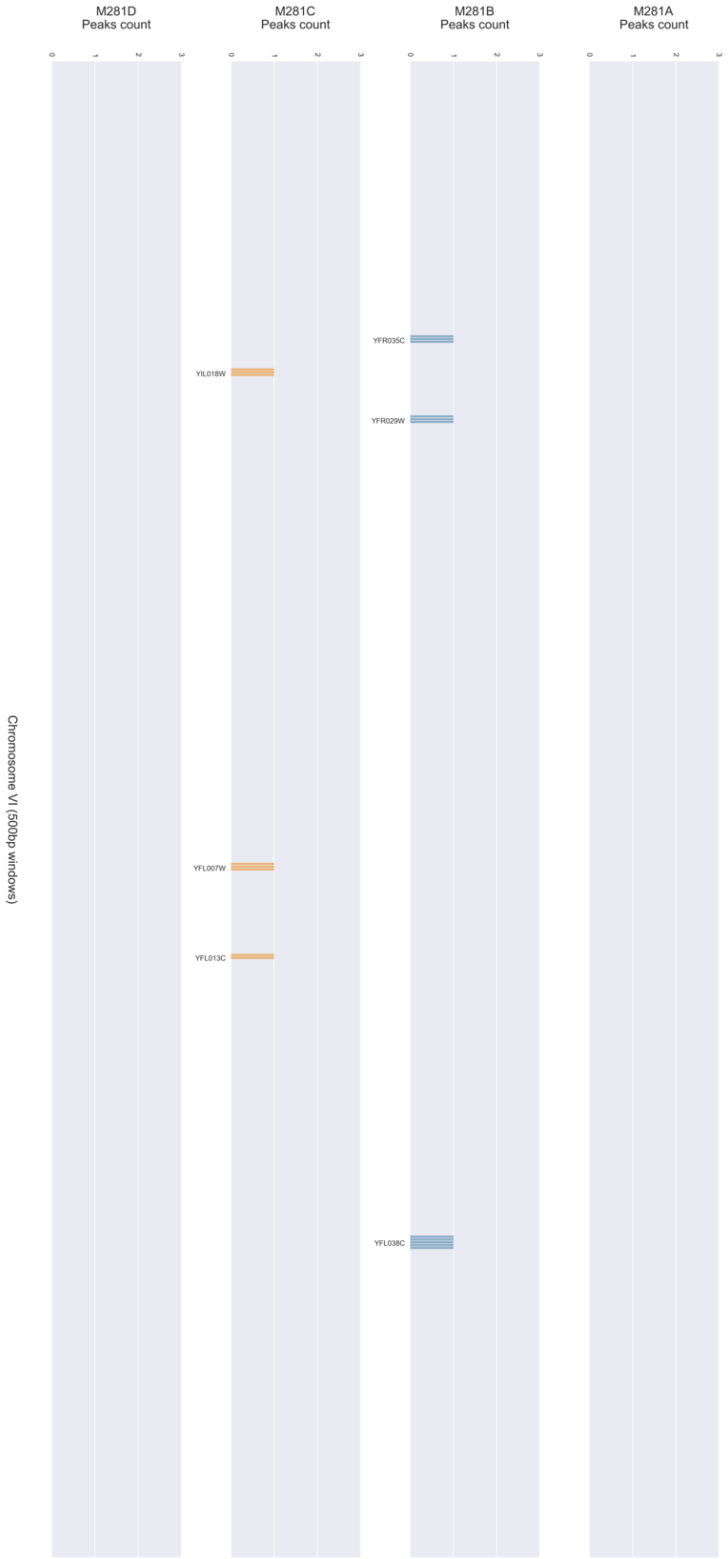

Fig. A.16: Chromosome VI - (H3 3Met K4)

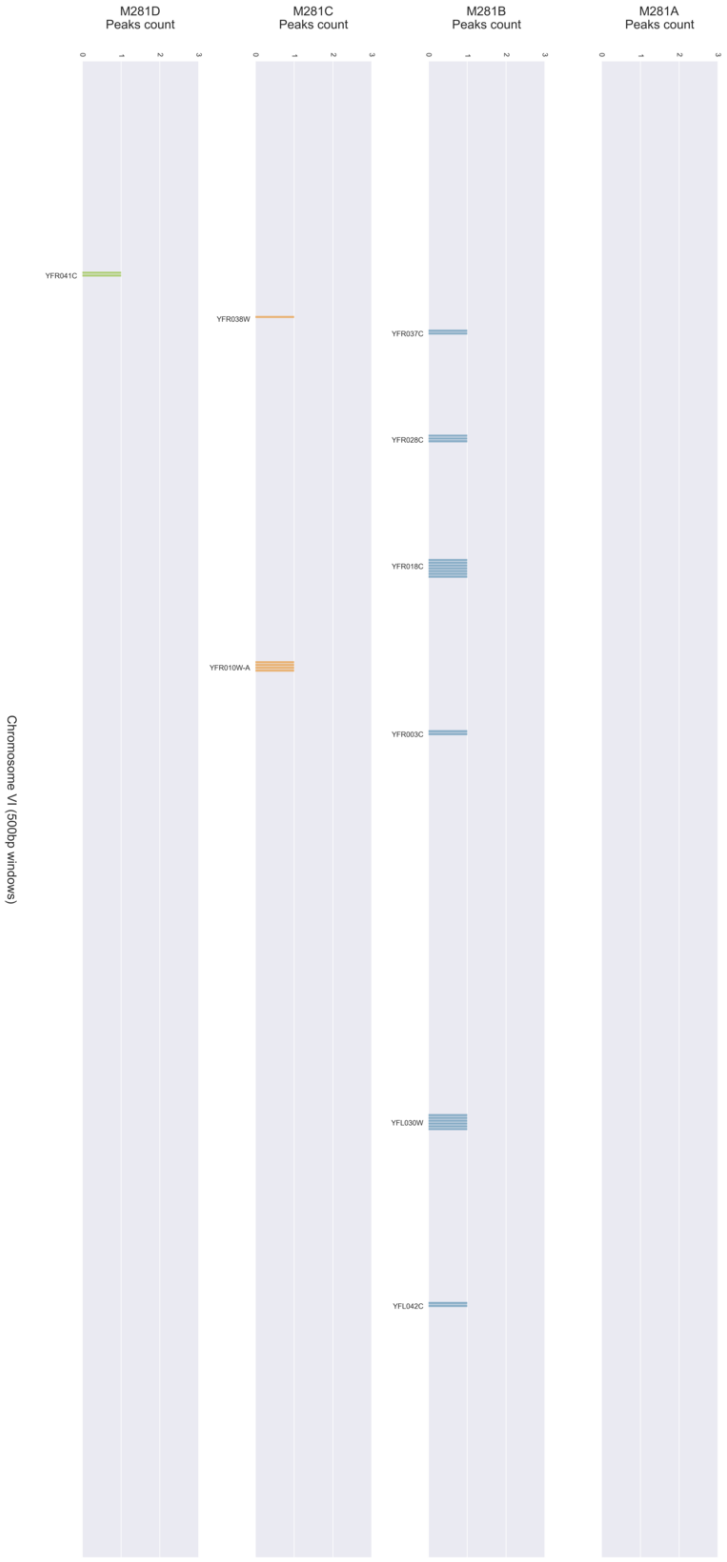

Fig. A.17: Chromosome VI - (H3 2Met K4)

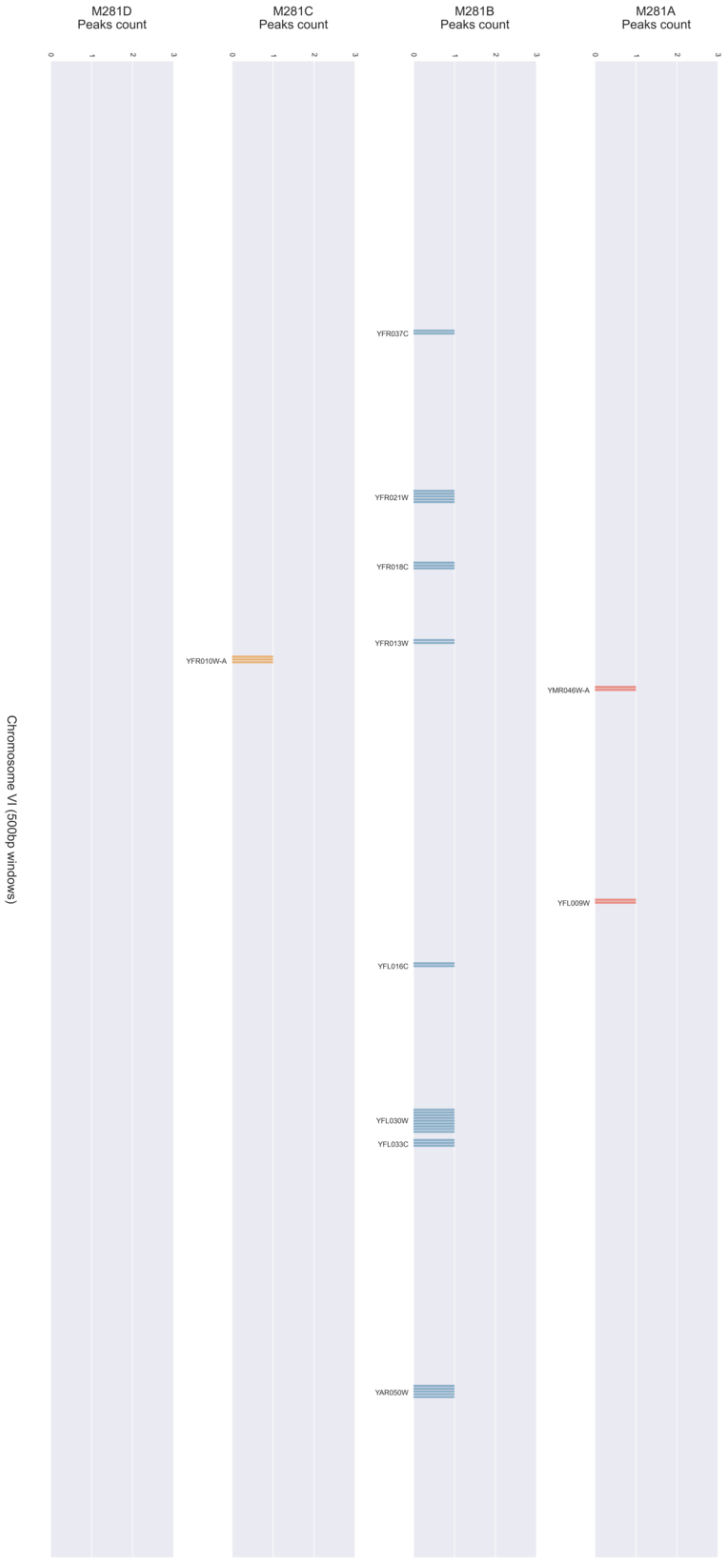

Fig. A.18: Chromosome VI - (H4 Ac)

Fig. A.19: Chromosome VII - (H3 3Met K4)

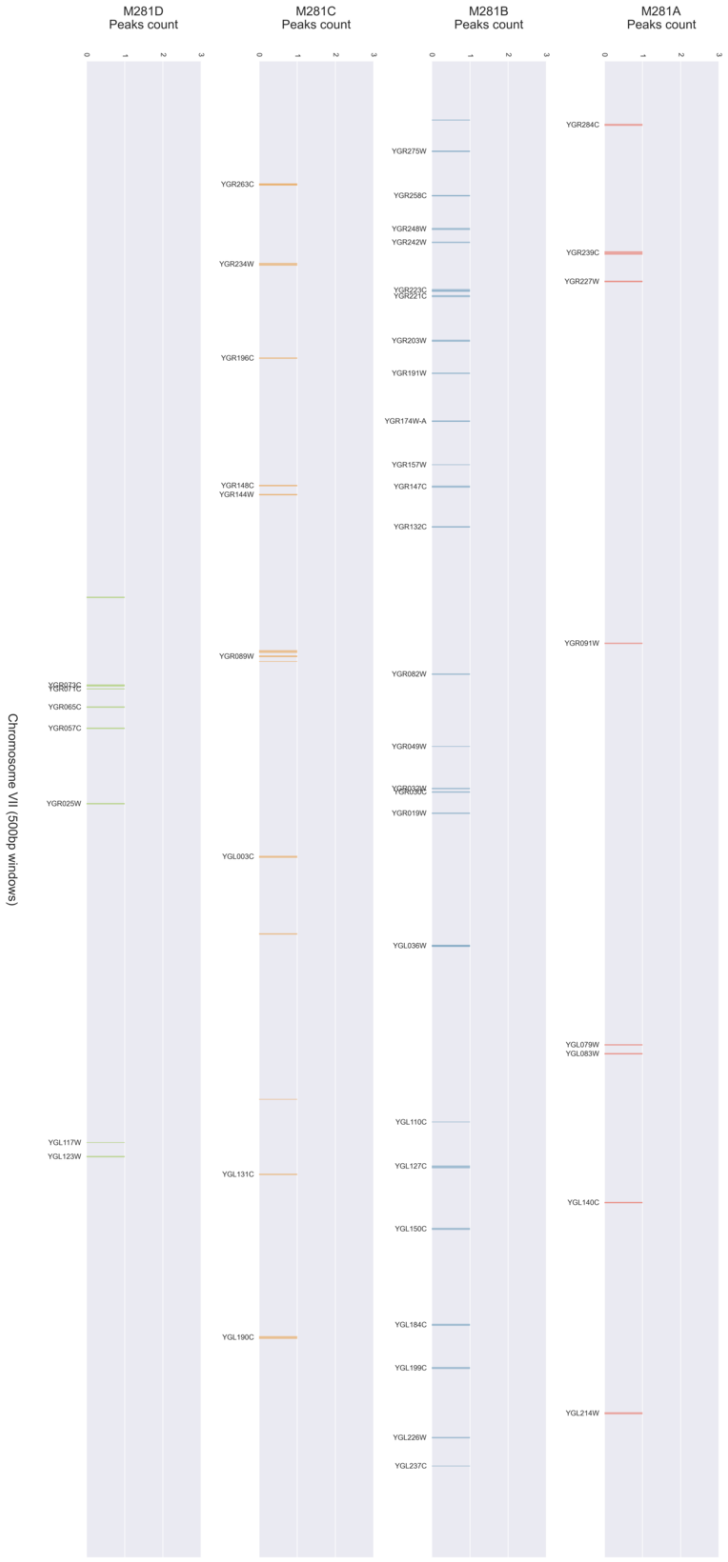

Fig. A.20: Chromosome VII - (H3 2Met K4)

Fig. A.21: Chromosome VII - (H4 Ac)

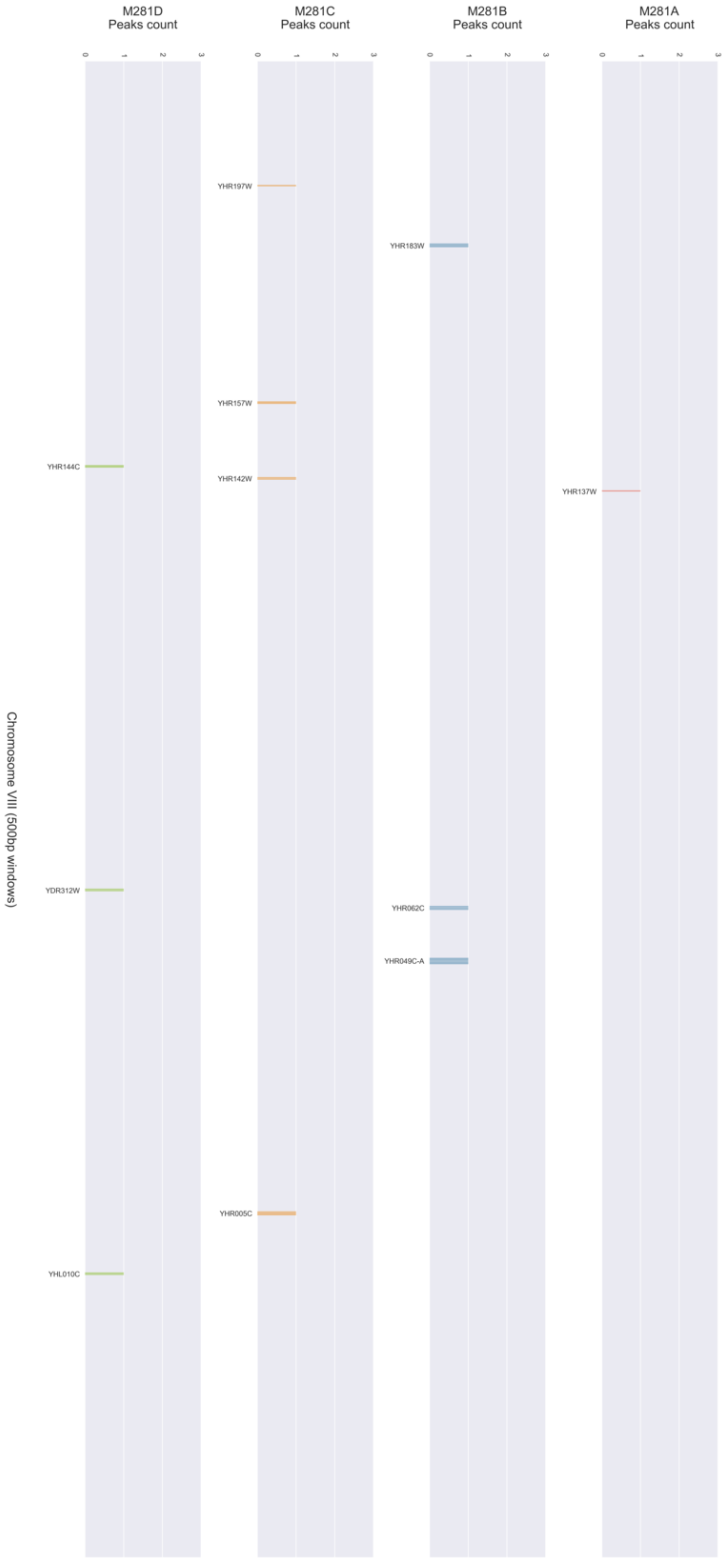

Fig. A.22: Chromosome VIII - (H3 3Met K4)

Fig. A.23: Chromosome VIII - (H3 2Met K4)

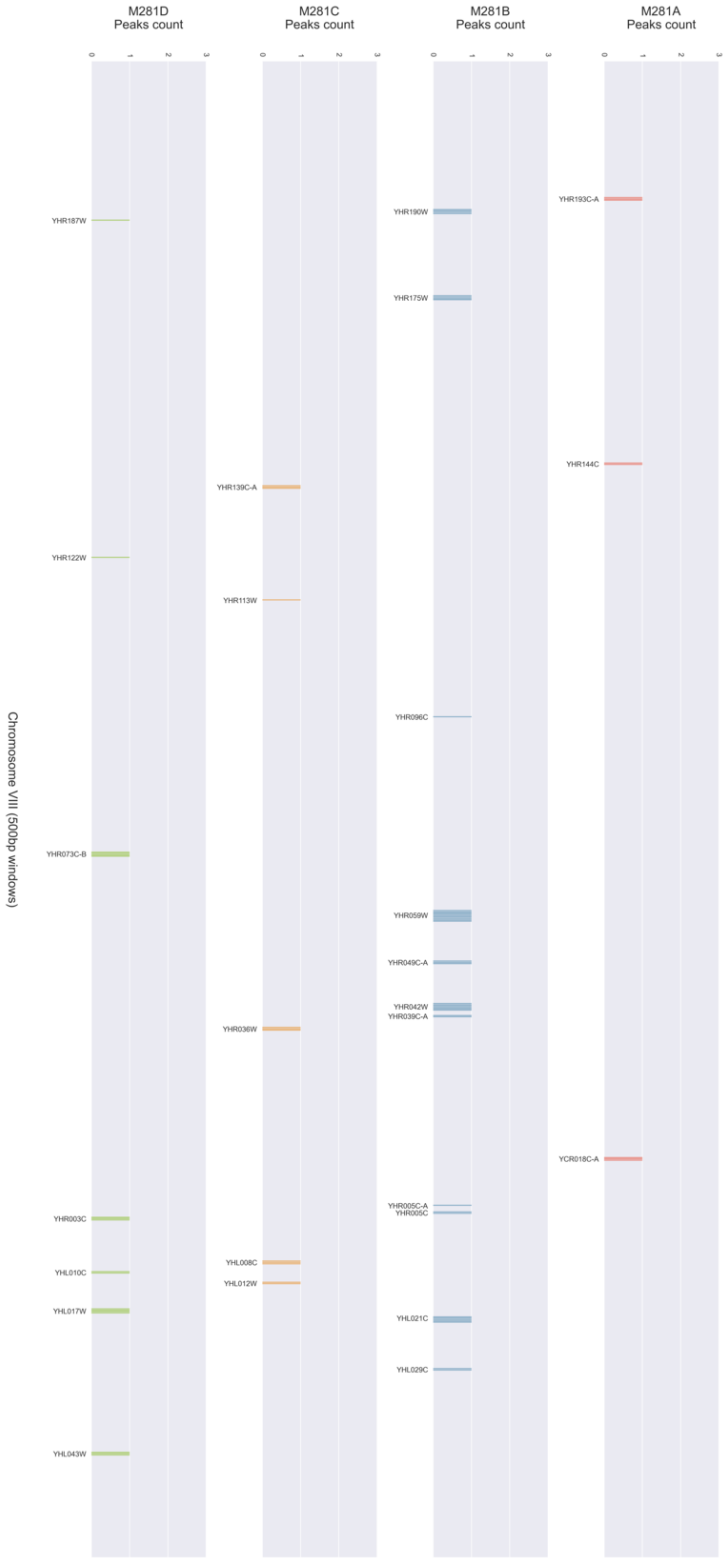

Fig. A.24: Chromosome VIII - (H4 Ac)

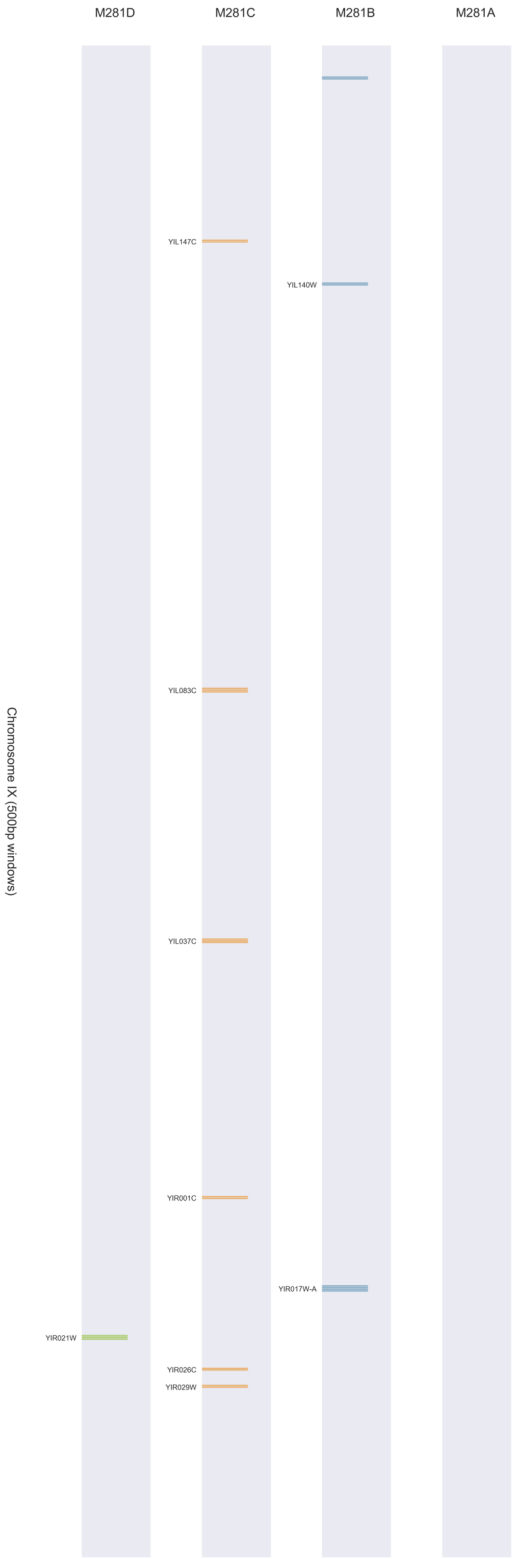

Fig. A.25: Chromosome IX - (H3 3Met K4)

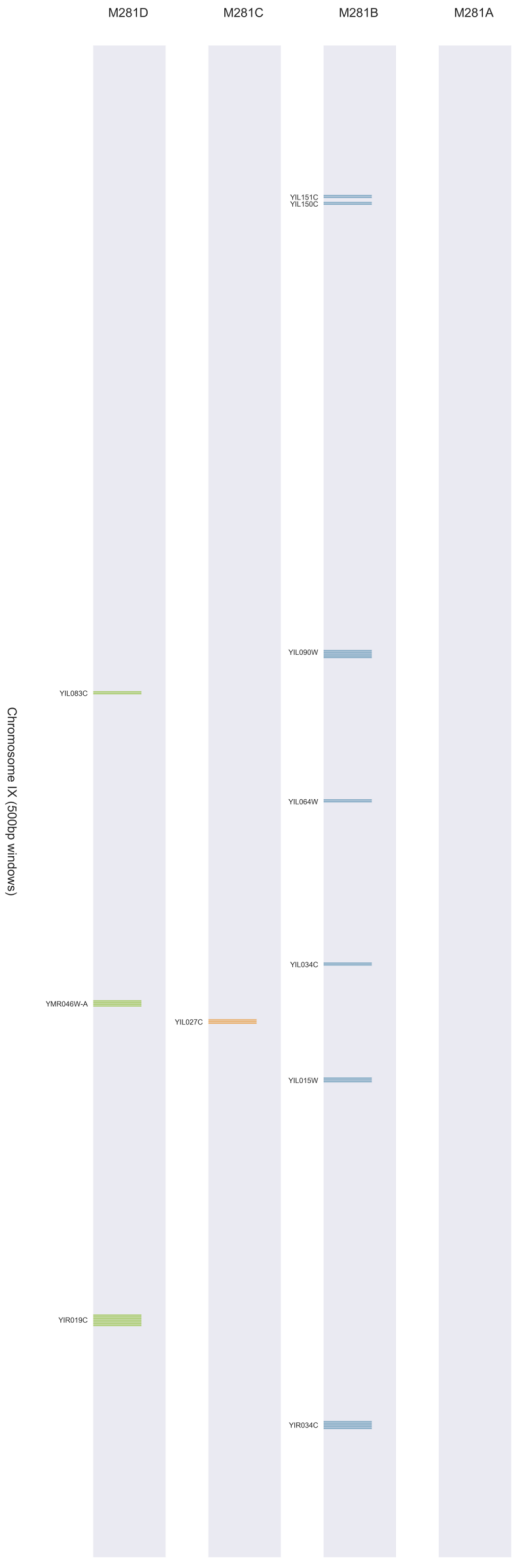

Fig. A.26: Chromosome IX - (H3 2Met K4)

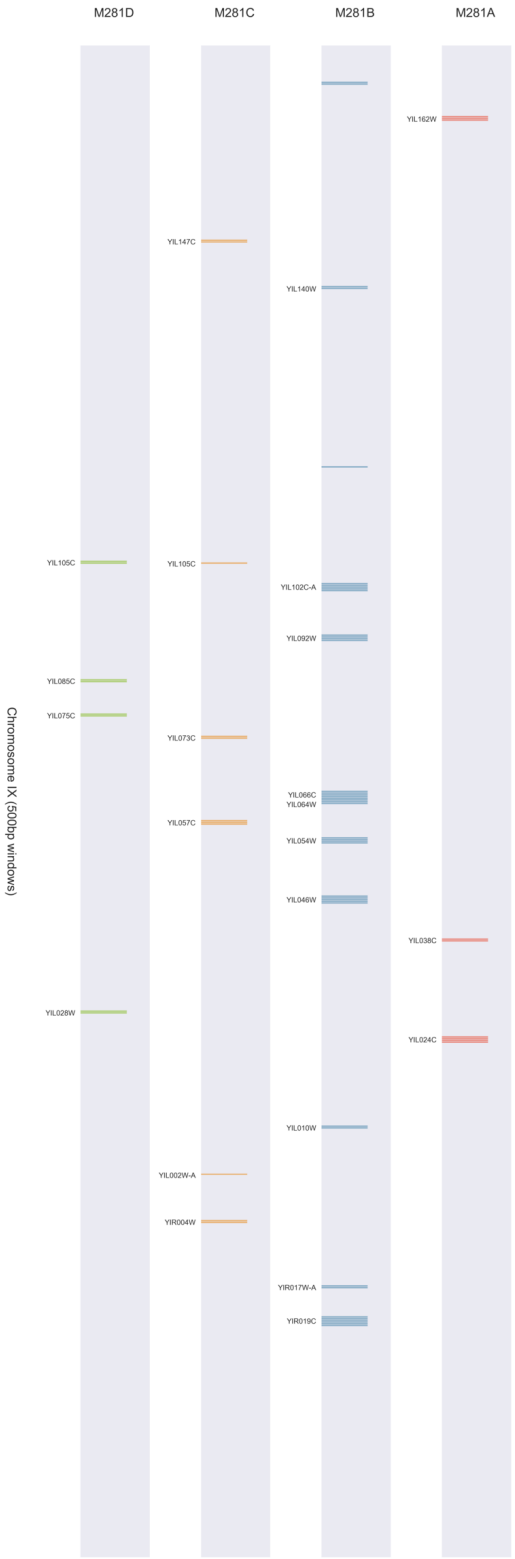

Fig. A.27: Chromosome IX - (H4 Ac)

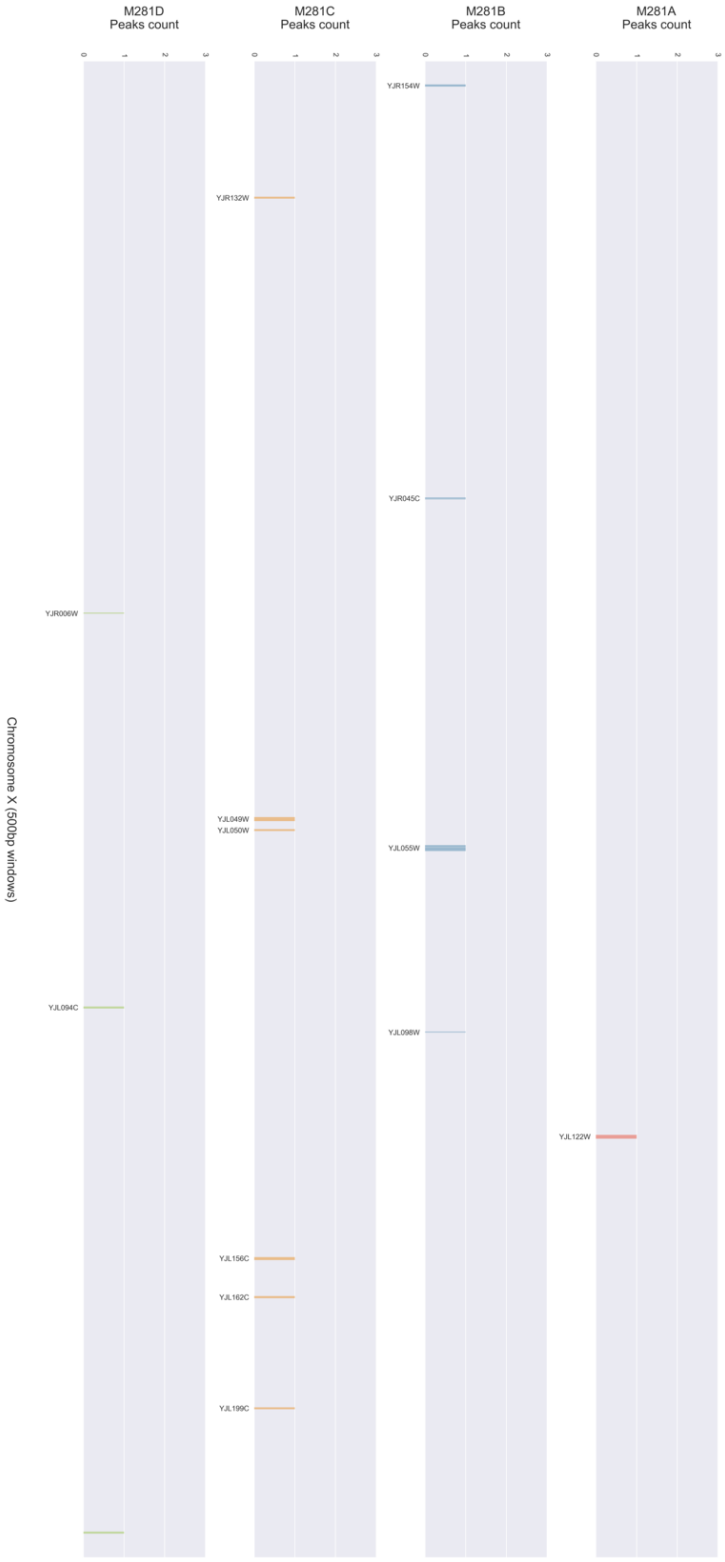

Fig. A.28: Chromosome X - (H3 3Met K4)

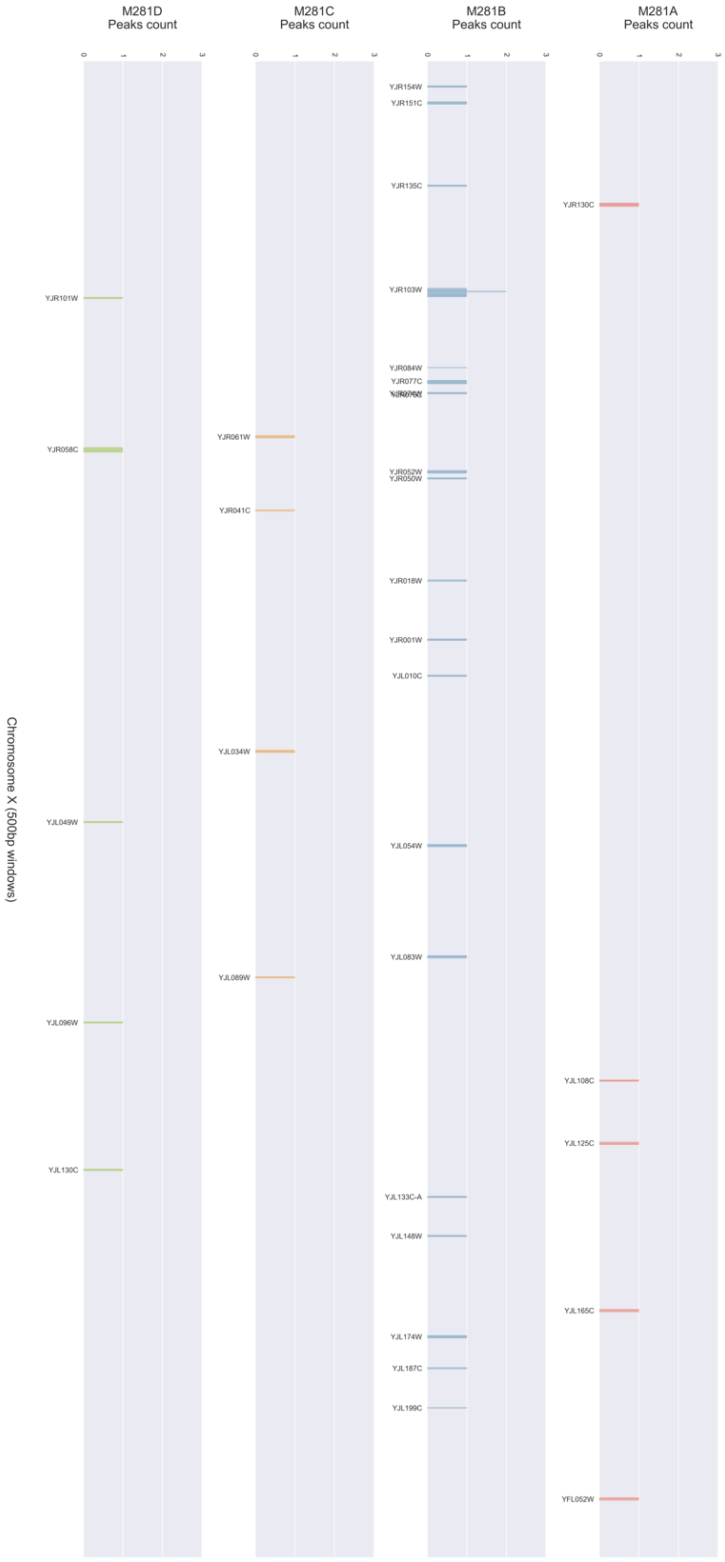

Fig. A.29: Chromosome X - (H3 2Met K4)

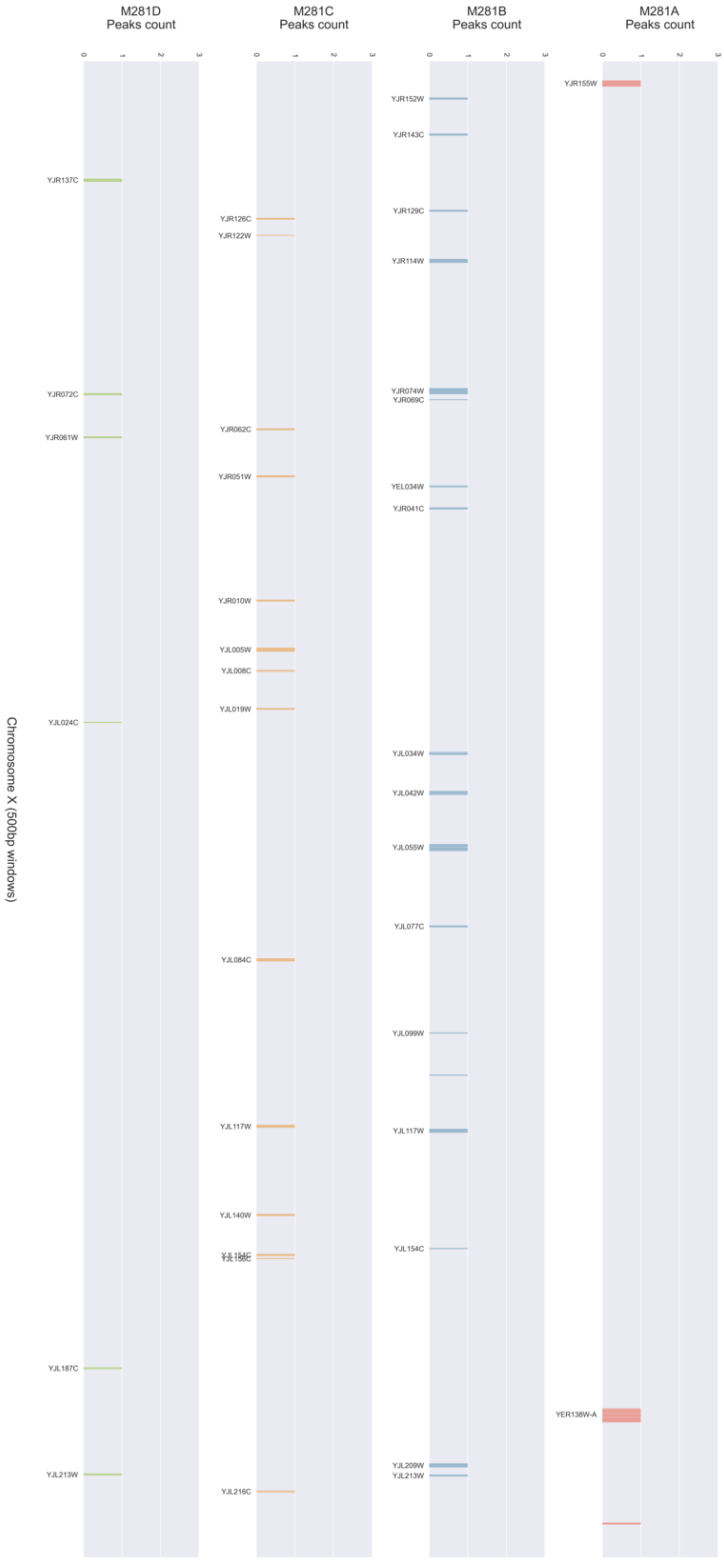

Fig. A.30: Chromosome X - (H4 Ac)

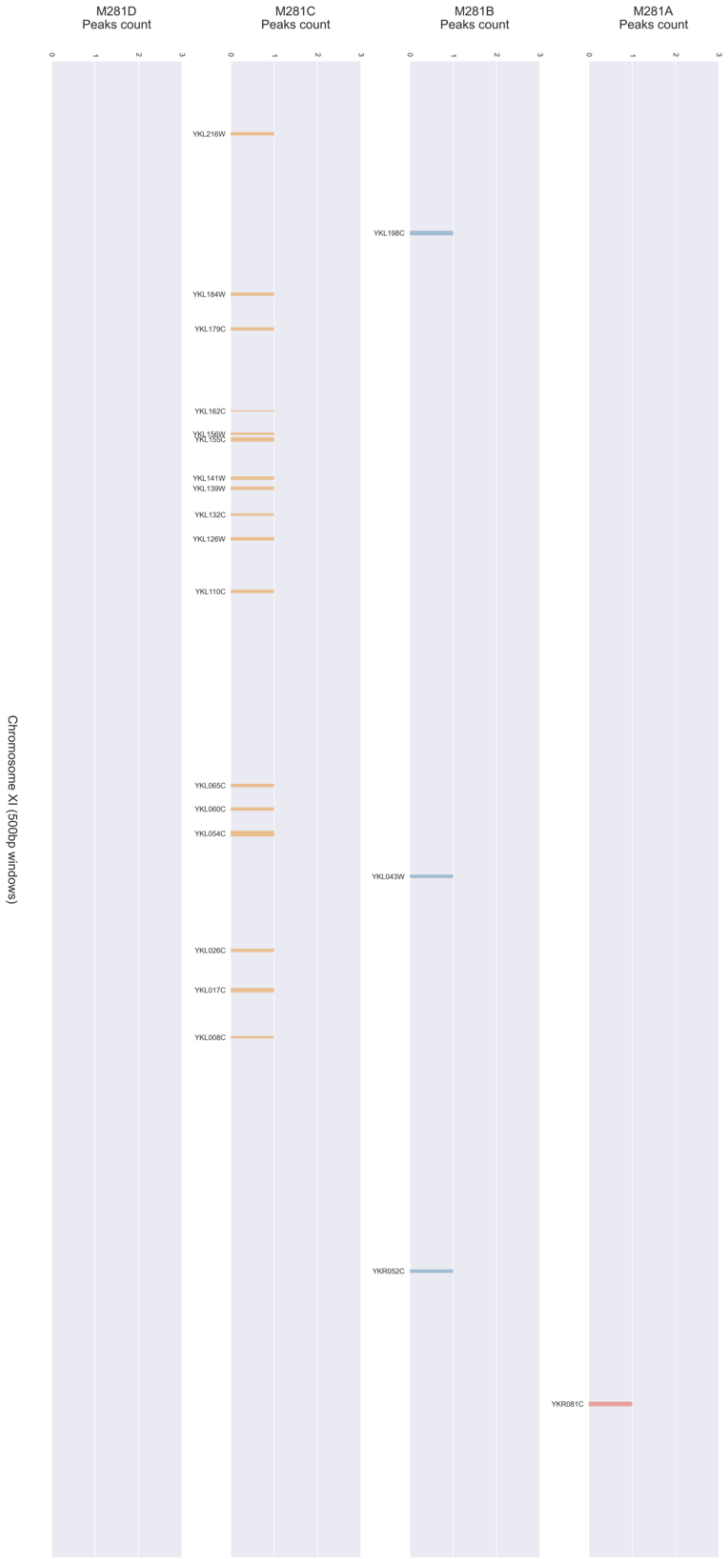

Fig. A.31: Chromosome XI - (H3 3Met K4)

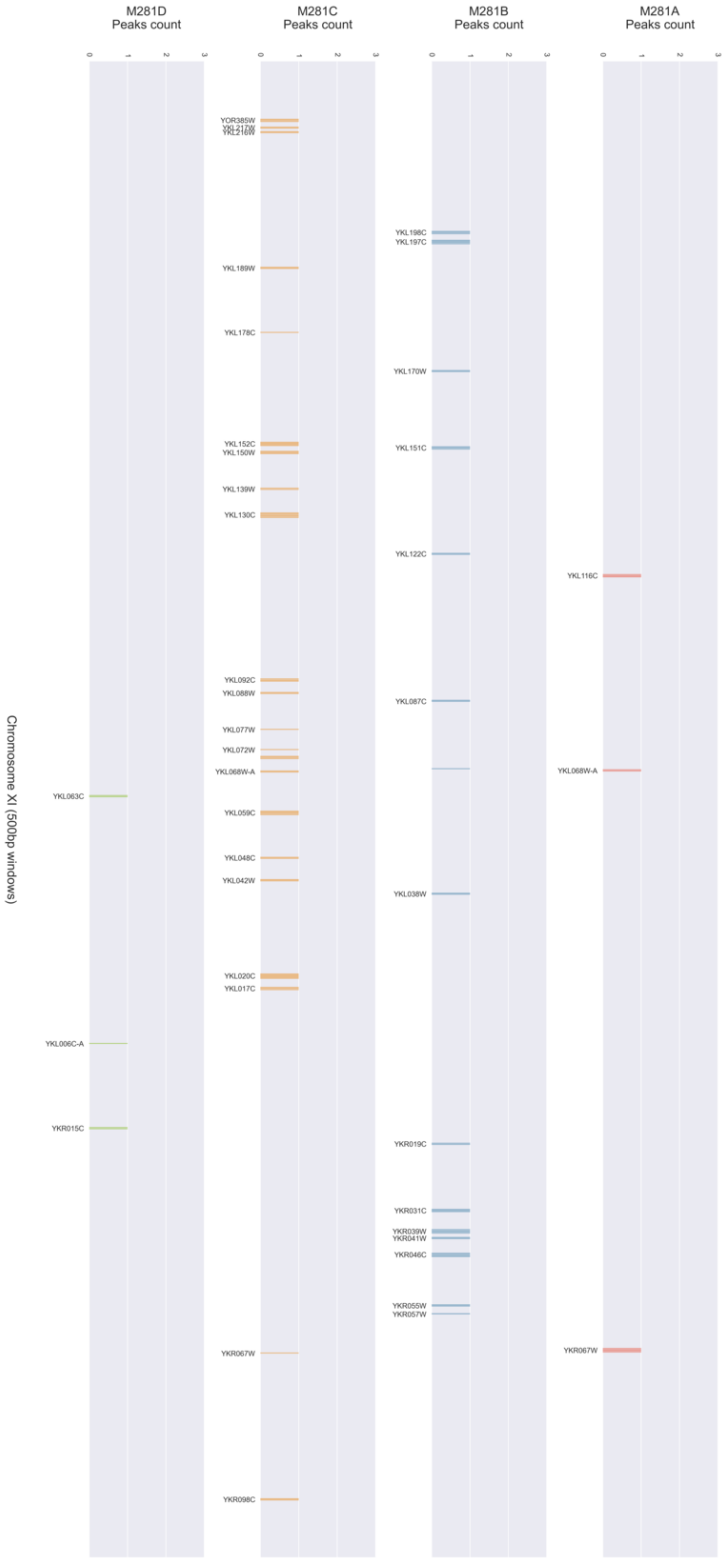

Fig. A.32: Chromosome XI - (H3 2Met K4)

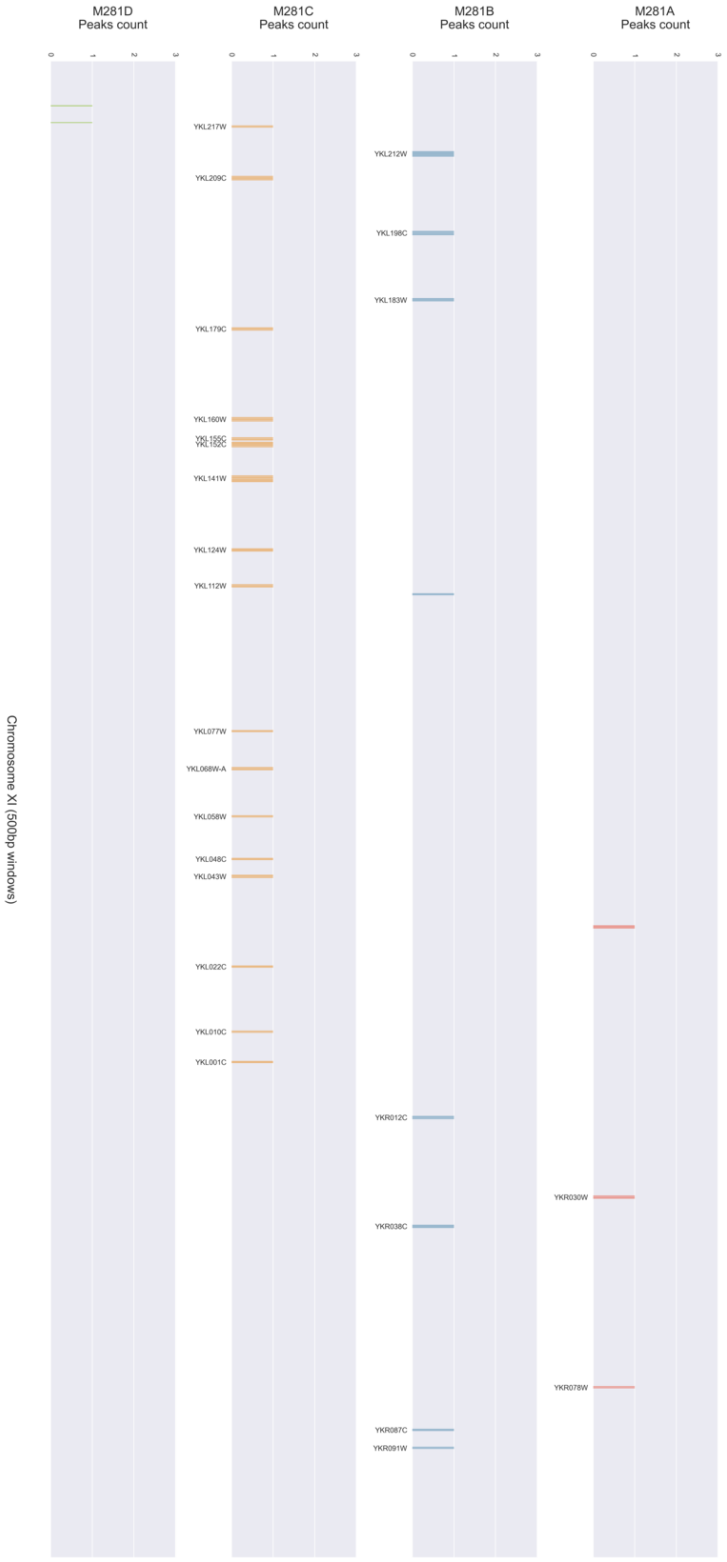

Fig. A.33: Chromosome XI - (H4 Ac)

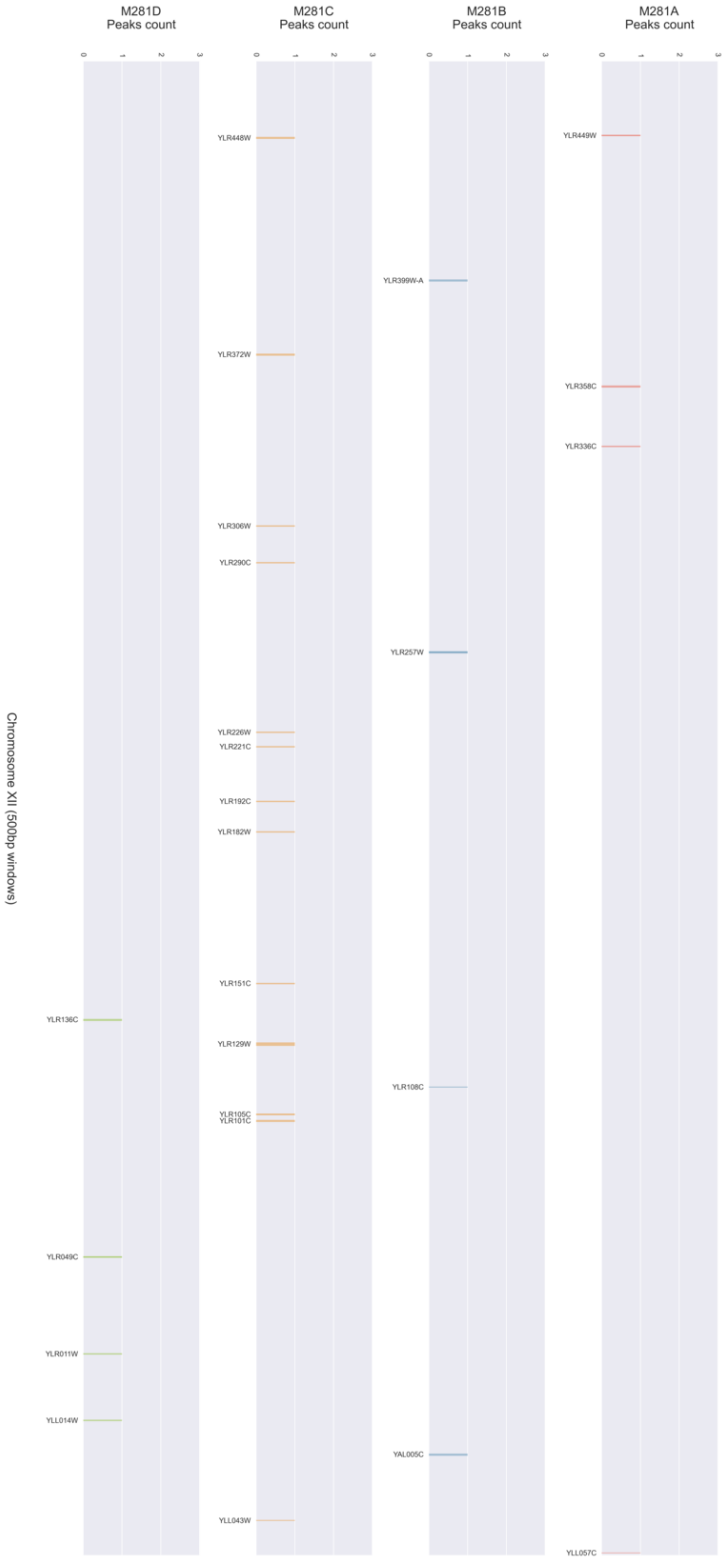

Fig. A.34: Chromosome XII - (H3 3Met K4)

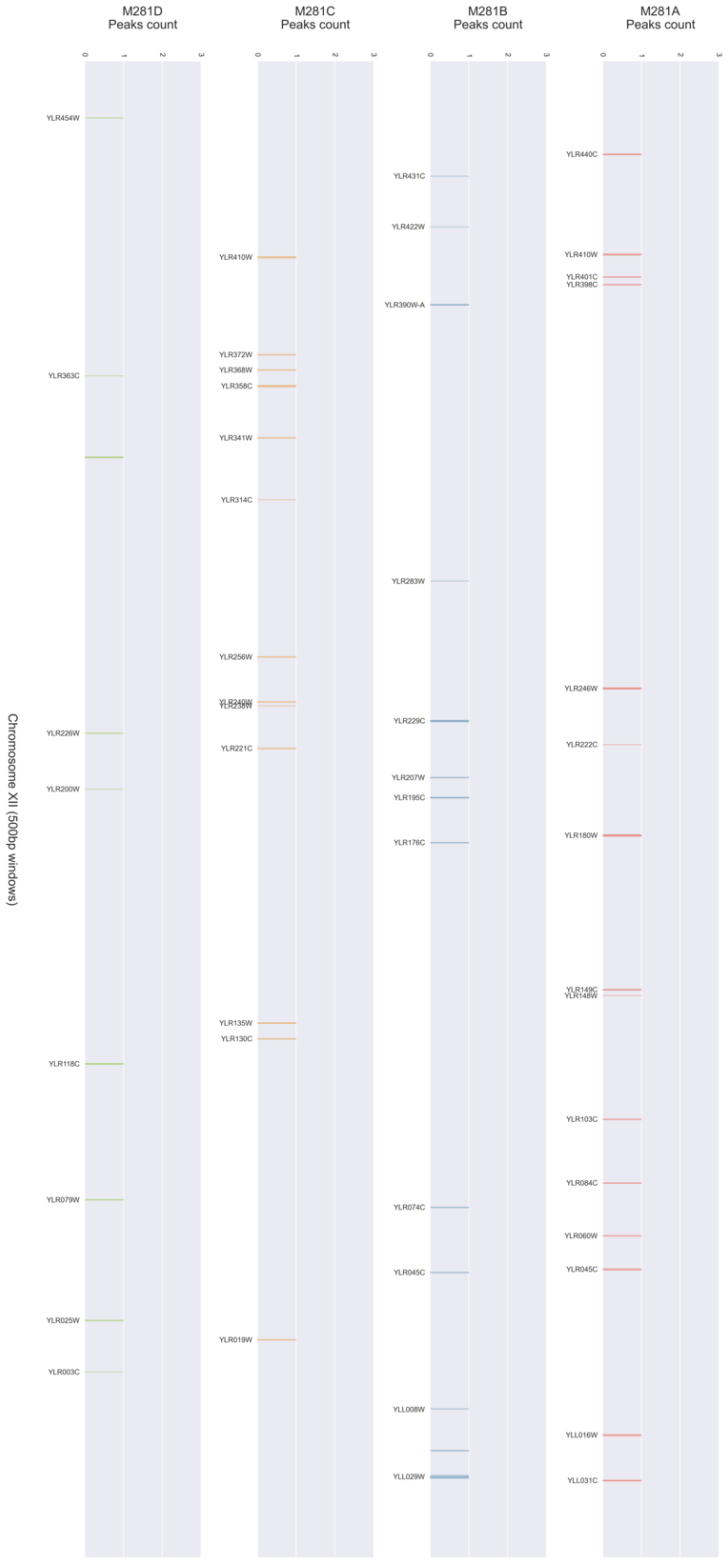

Fig. A.35: Chromosome XII - (H3 2Met K4)

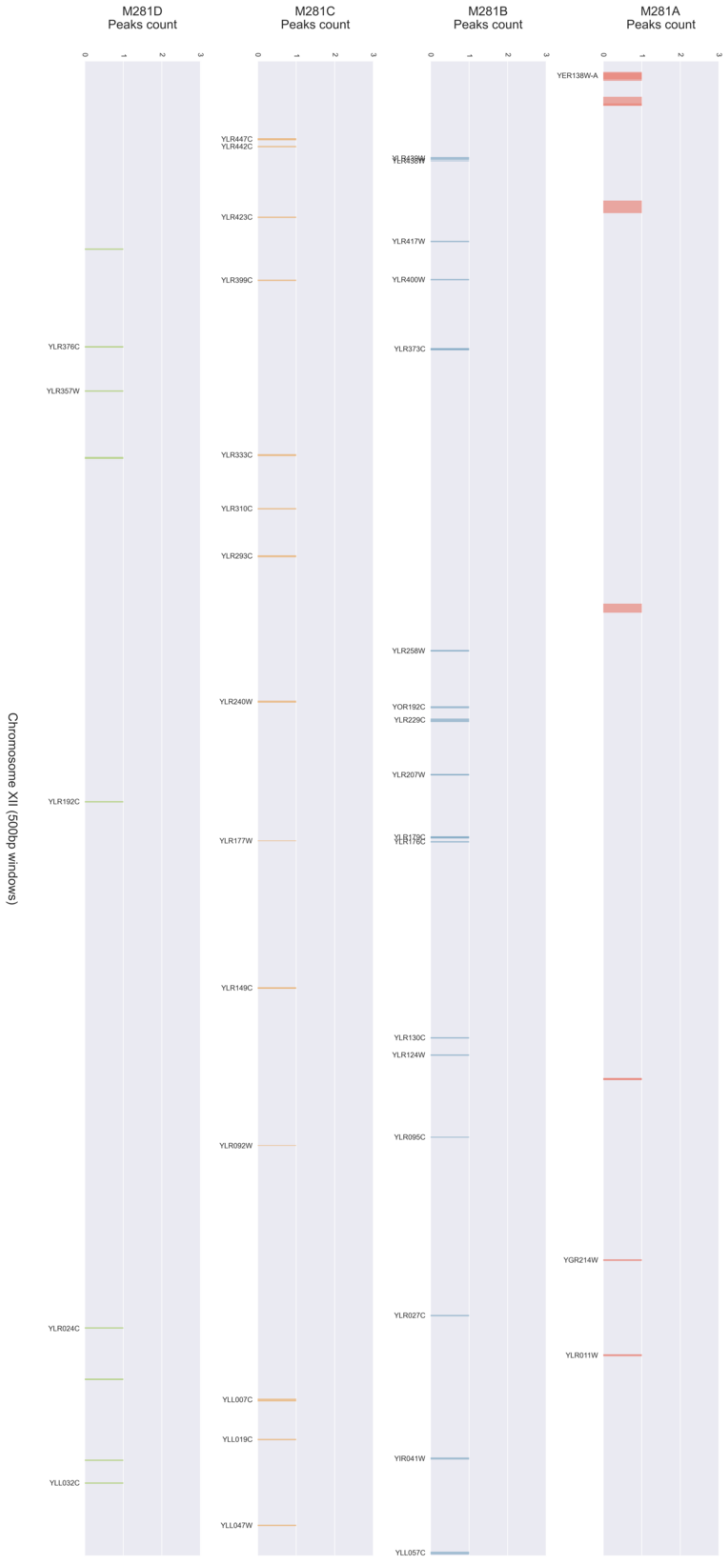

Fig. A.36: Chromosome XII - (H4 Ac)

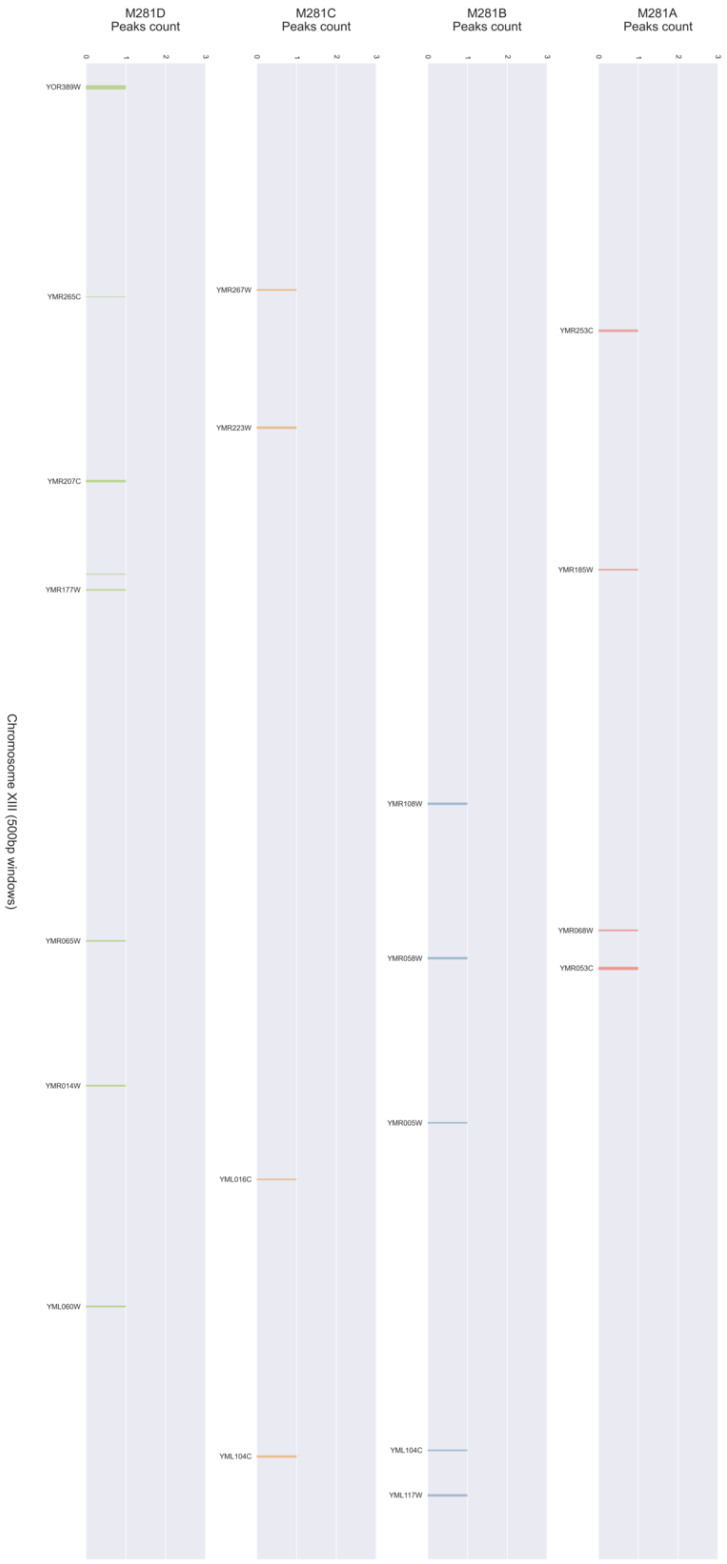

Fig. A.37: Chromosome XIII - (H3 3Met K4)

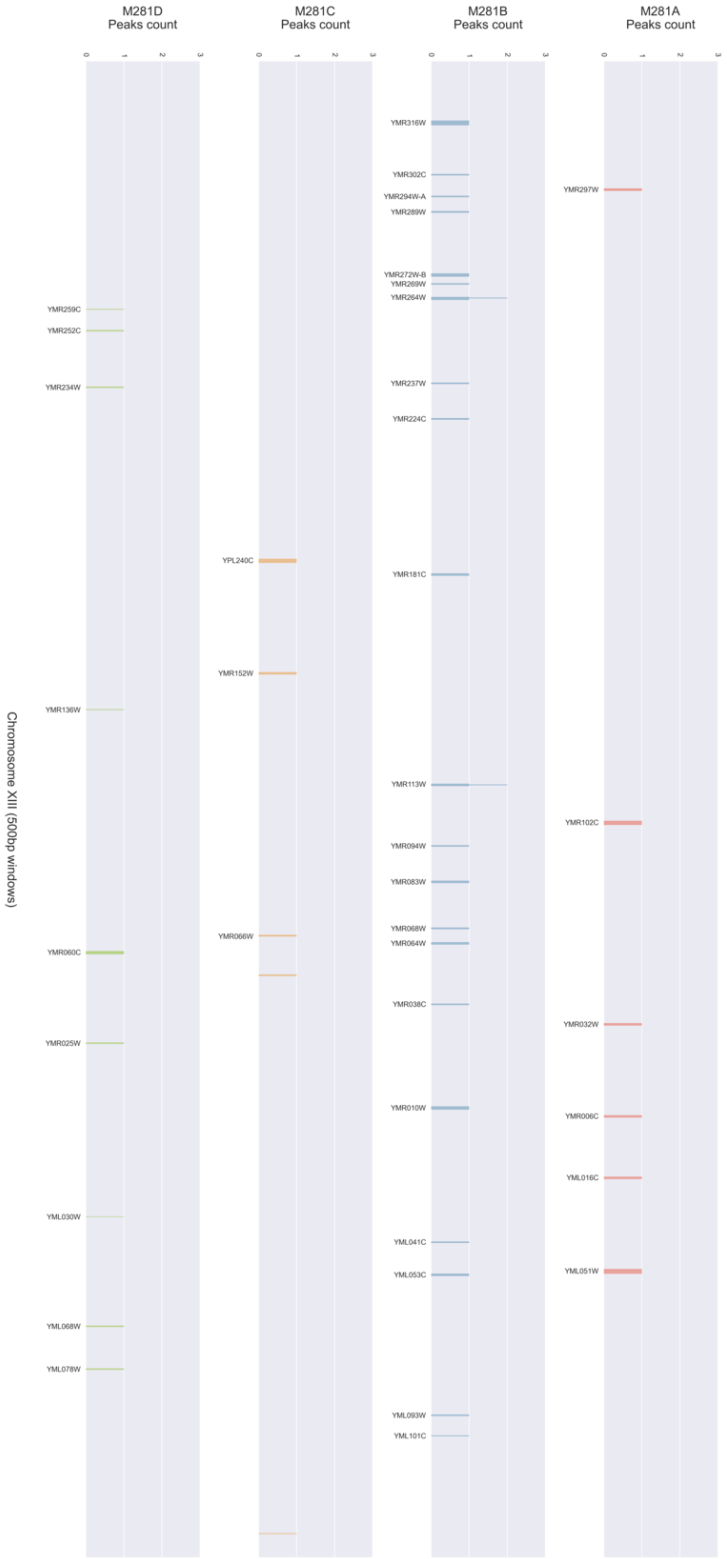

Fig. A.38: Chromosome XIII - (H3 2Met K4)

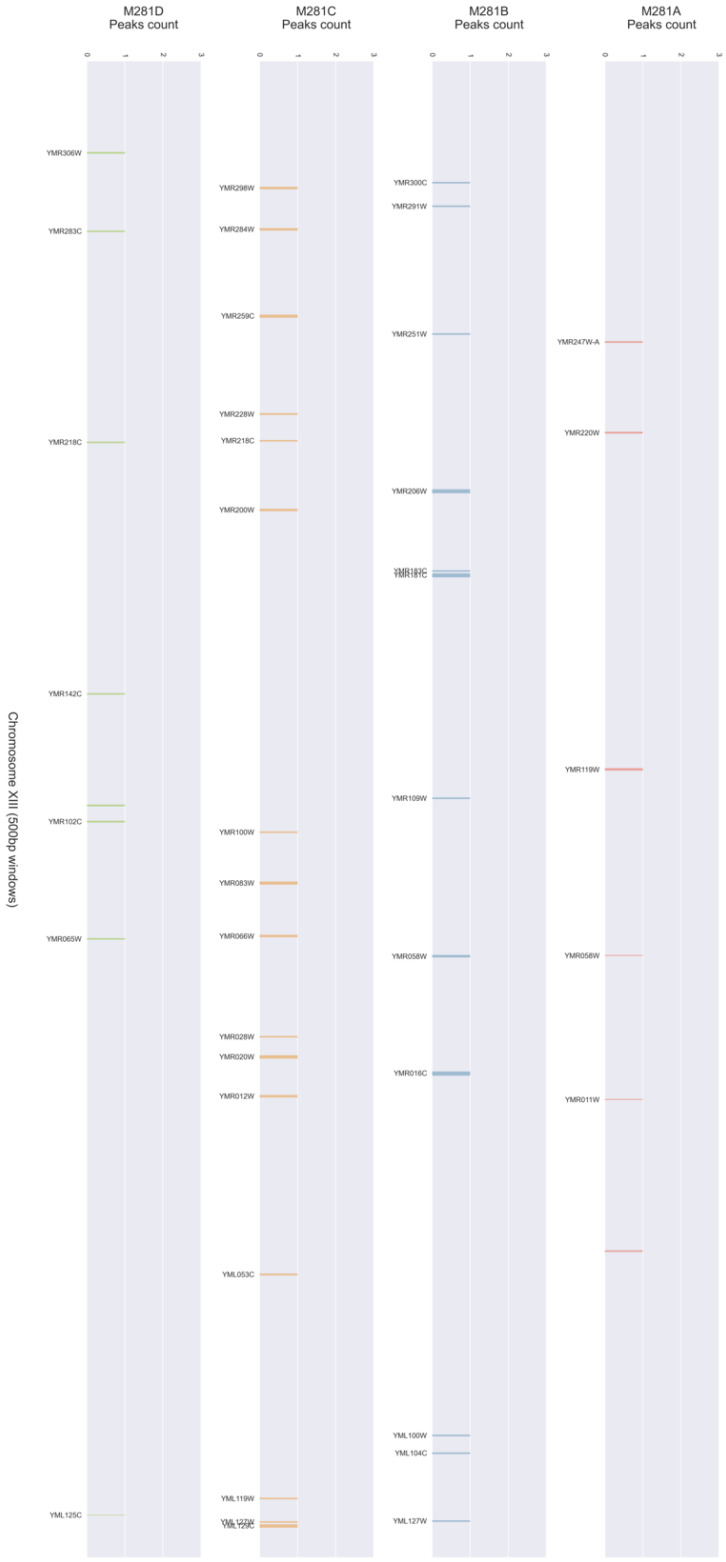

Fig. A.39: Chromosome XIII - (H4 Ac)

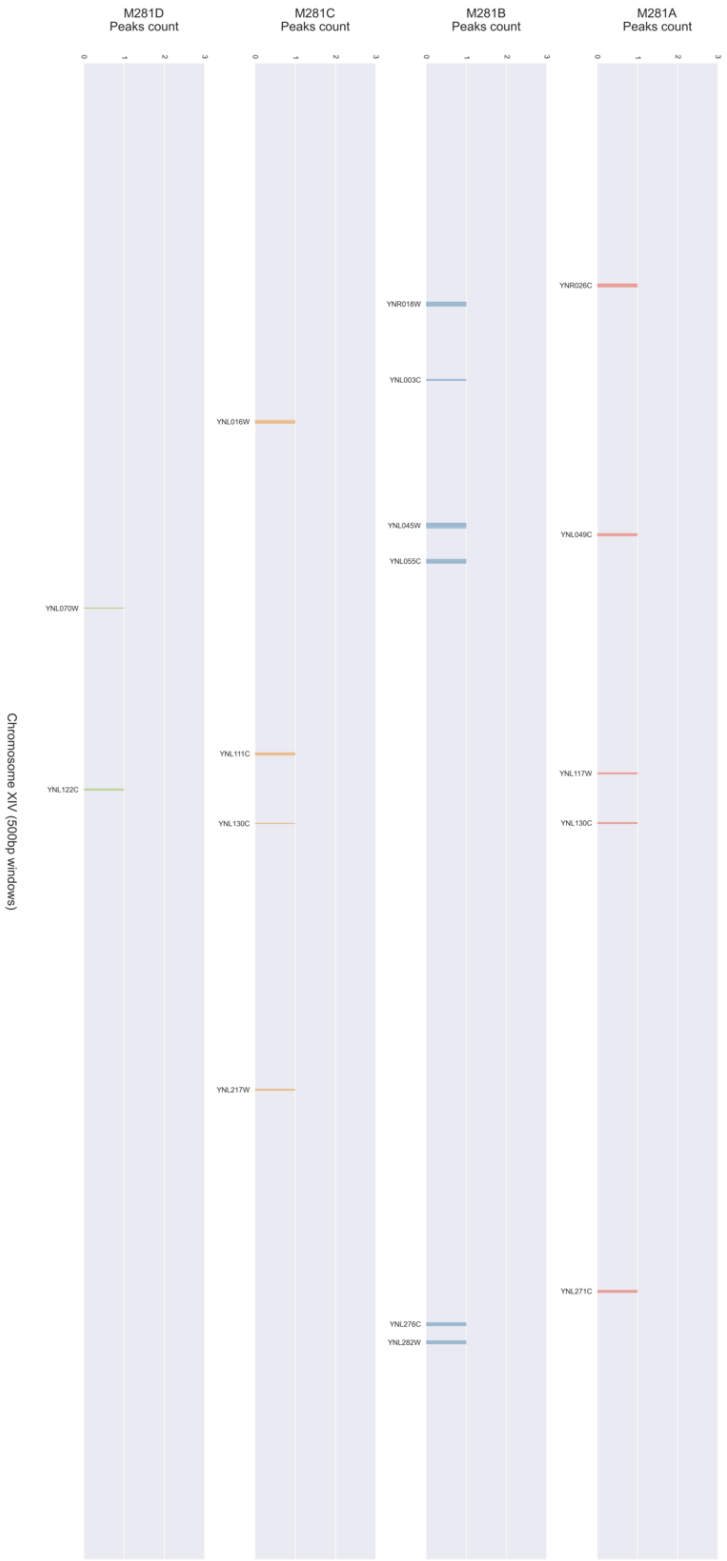

Fig. A.40: Chromosome XIV - (H3 3Met K4)

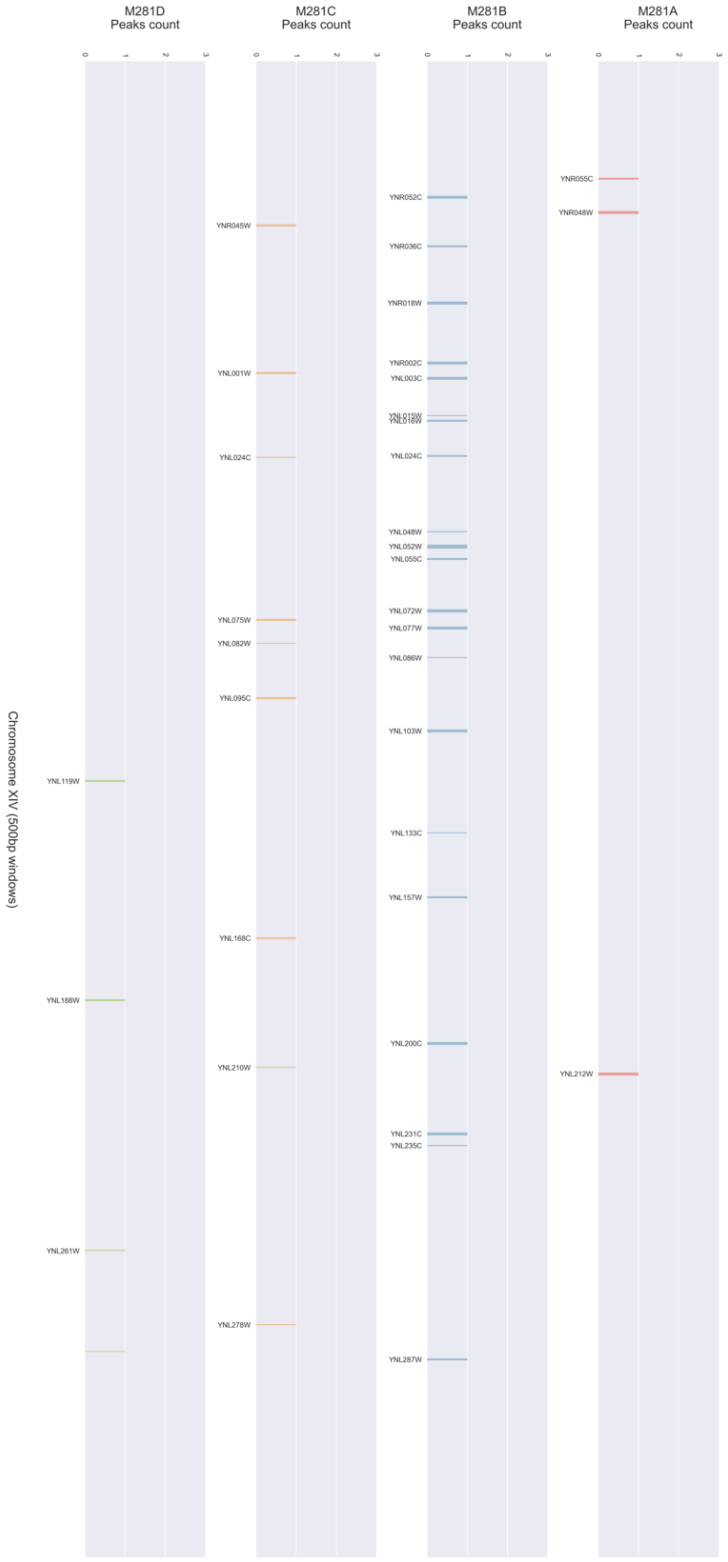

Fig. A.41: Chromosome XIV - (H3 2Met K4)

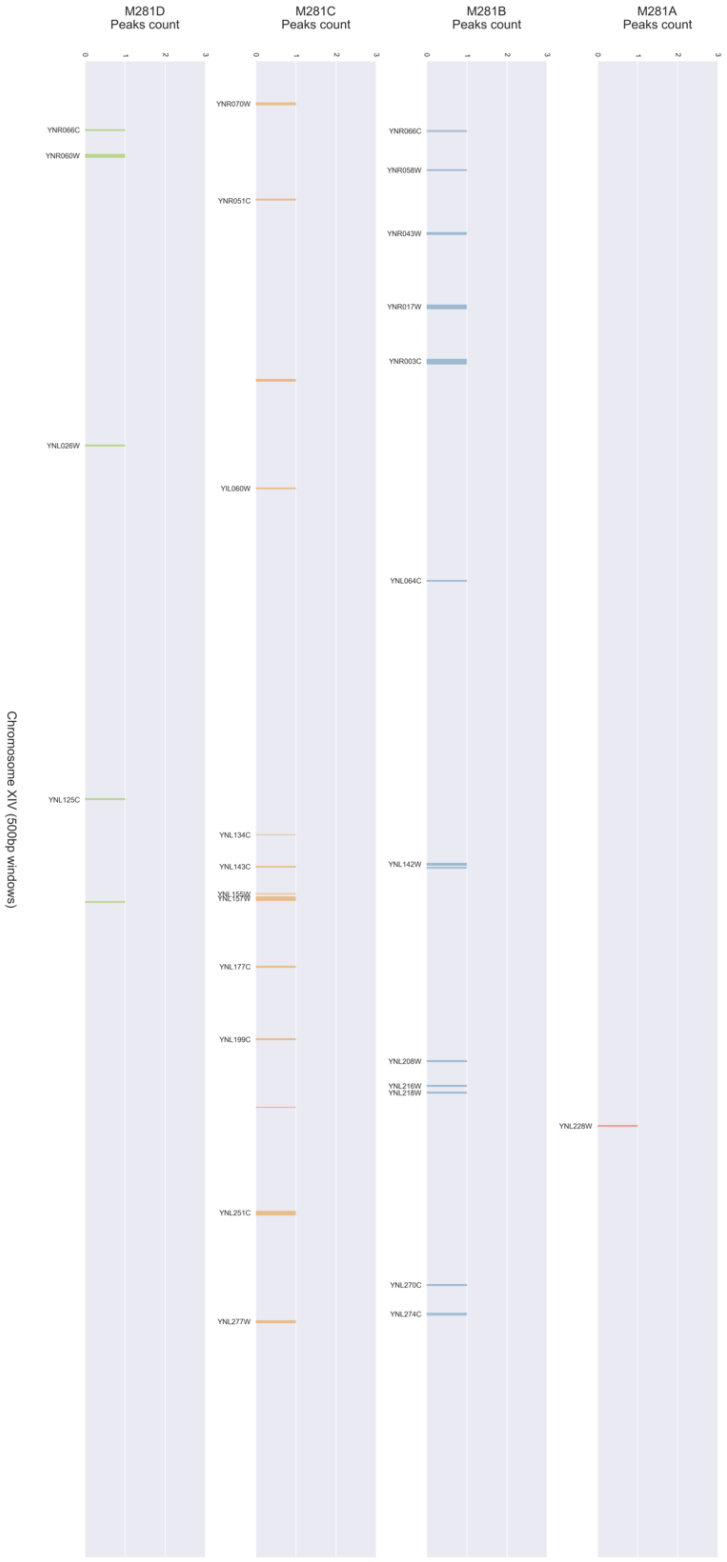

Fig. A.42: Chromosome XIV - (H4 Ac)

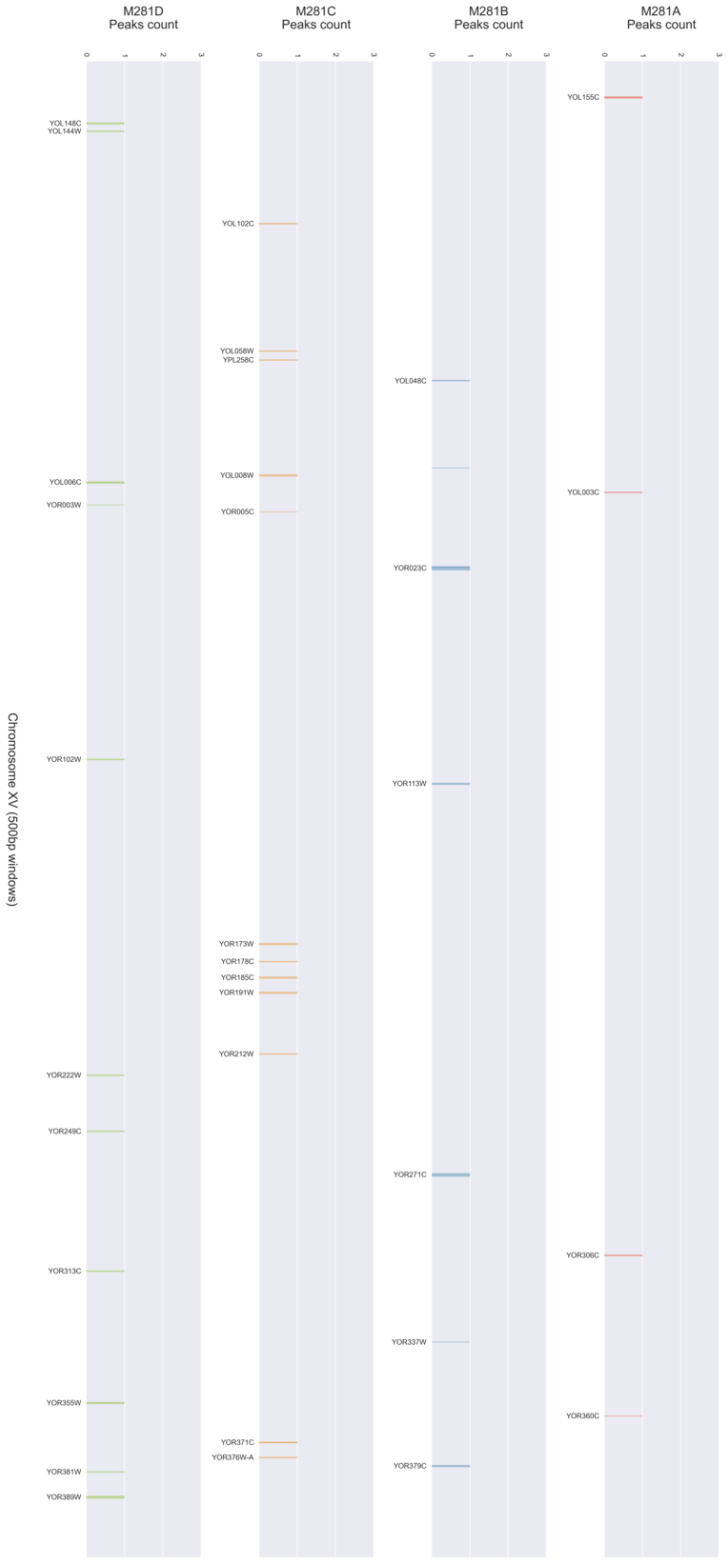

Fig. A.43: Chromosome XV - (H3 3Met K4)

Fig. A.44: Chromosome XV - (H3 2Met K4)

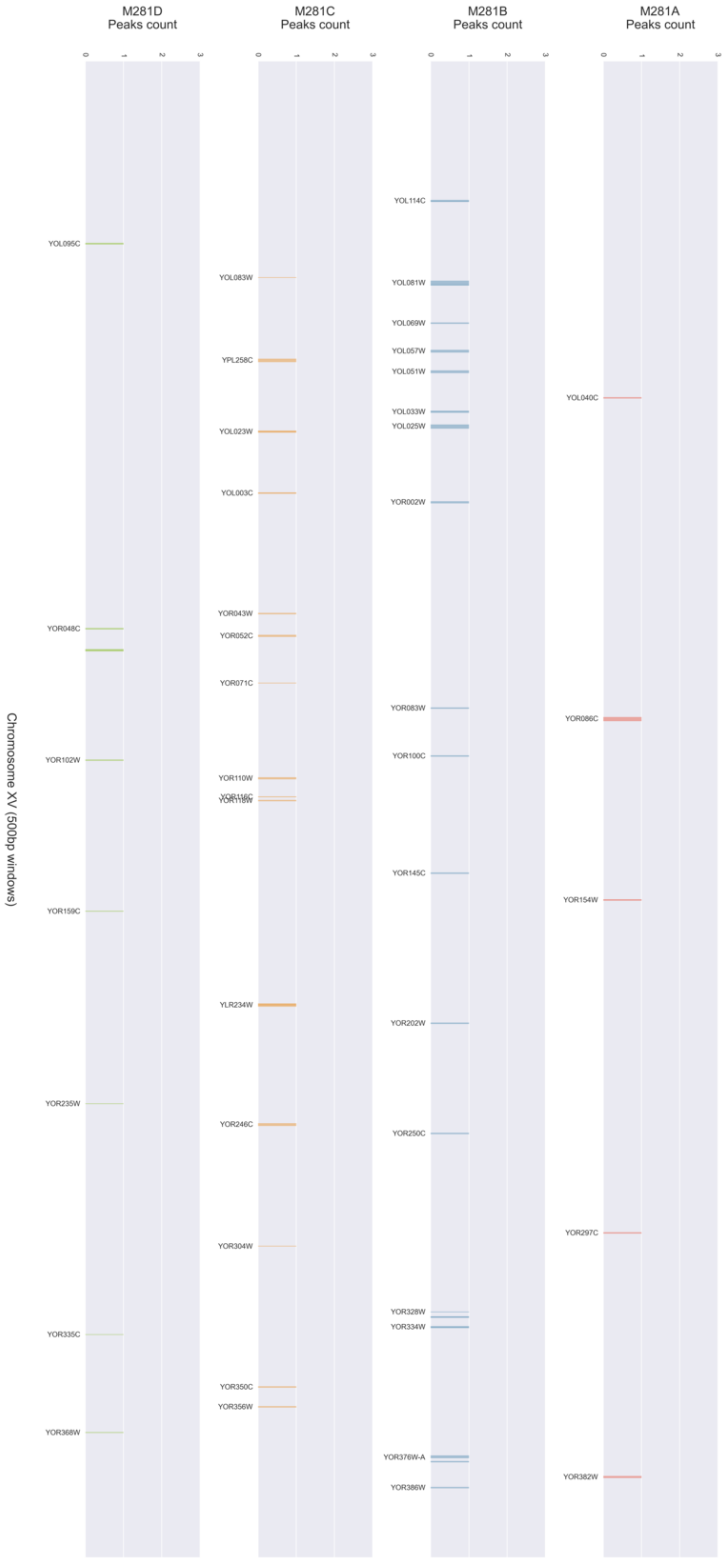

Fig. A.45: Chromosome XV - (H4 Ac)

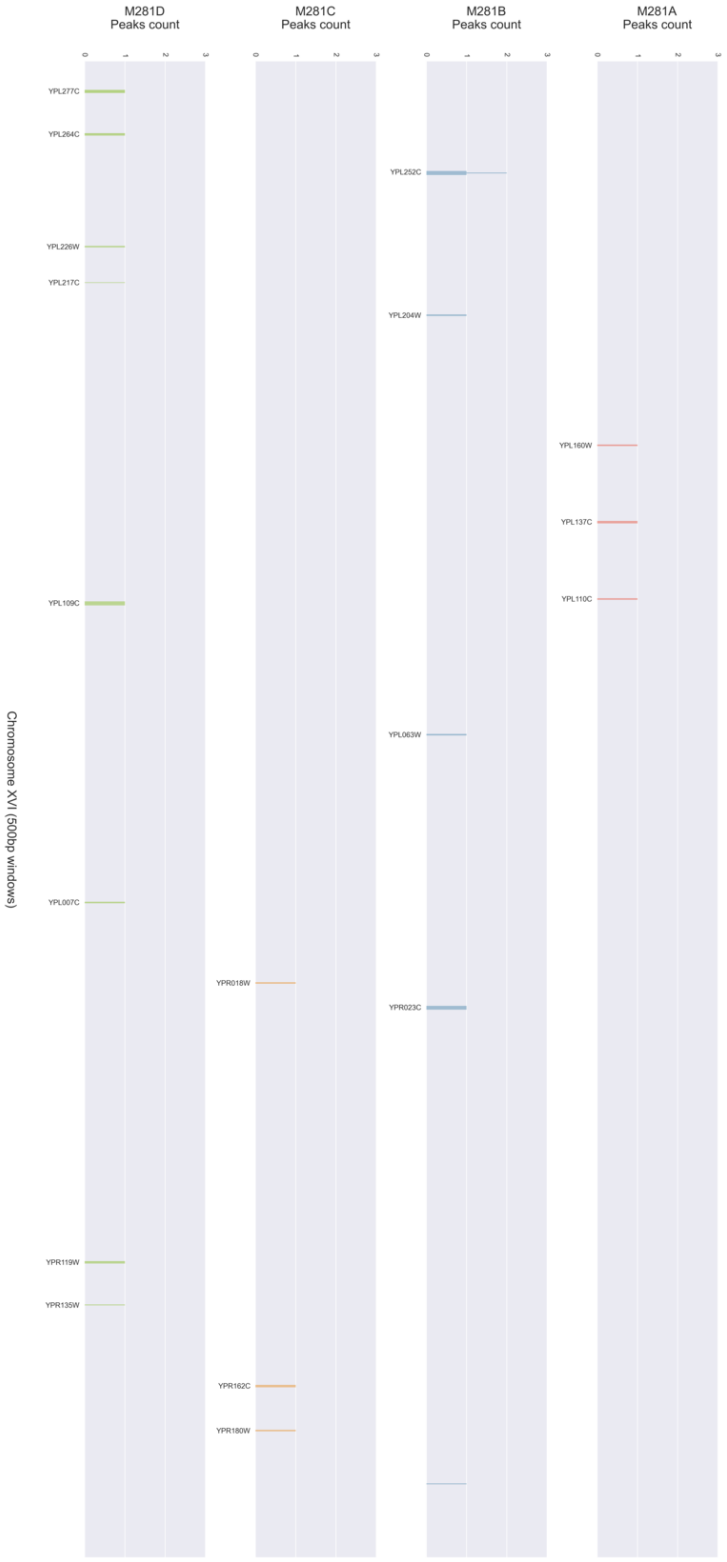

Fig. A.46: Chromosome XVI - (H3 3Met K4)

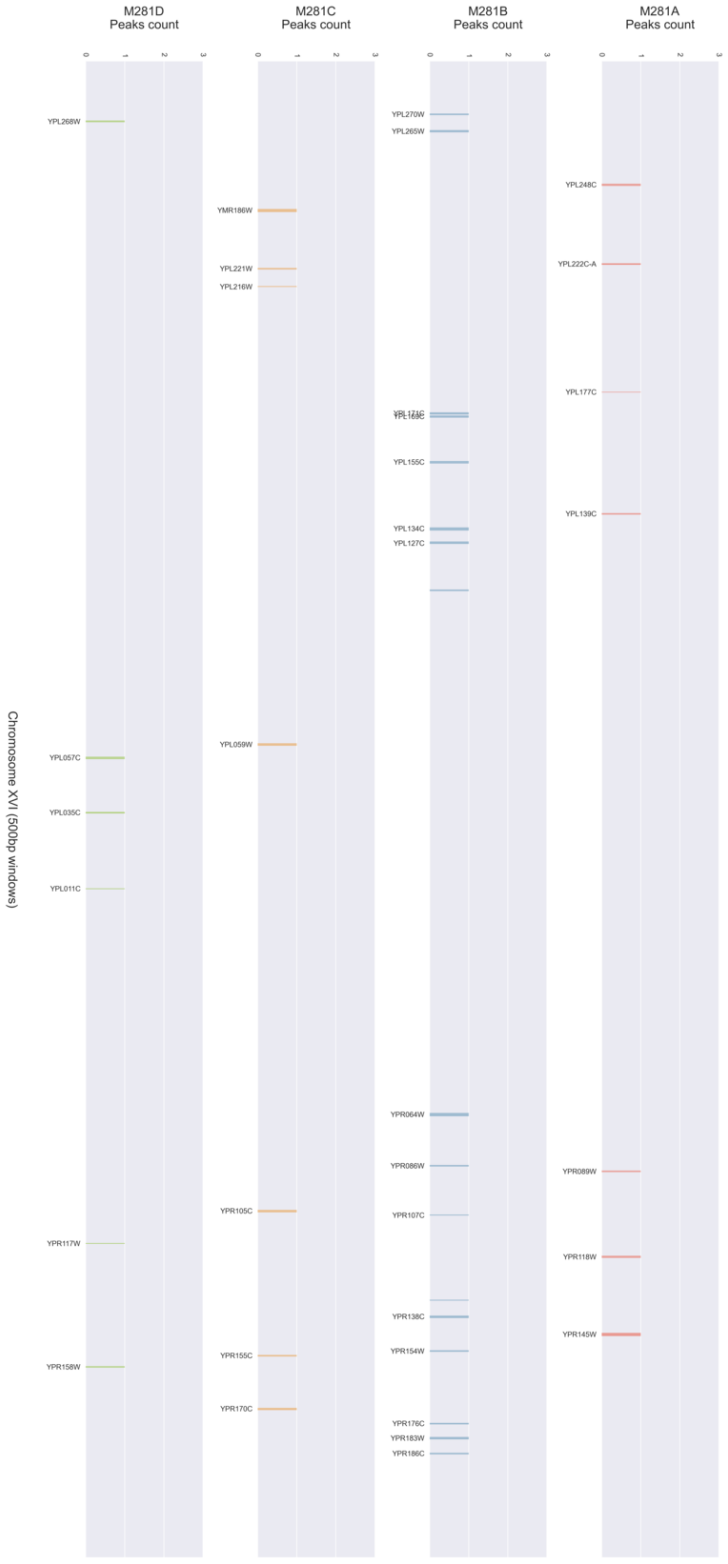

Fig. A.47: Chromosome XVI - (H3 2Met K4)

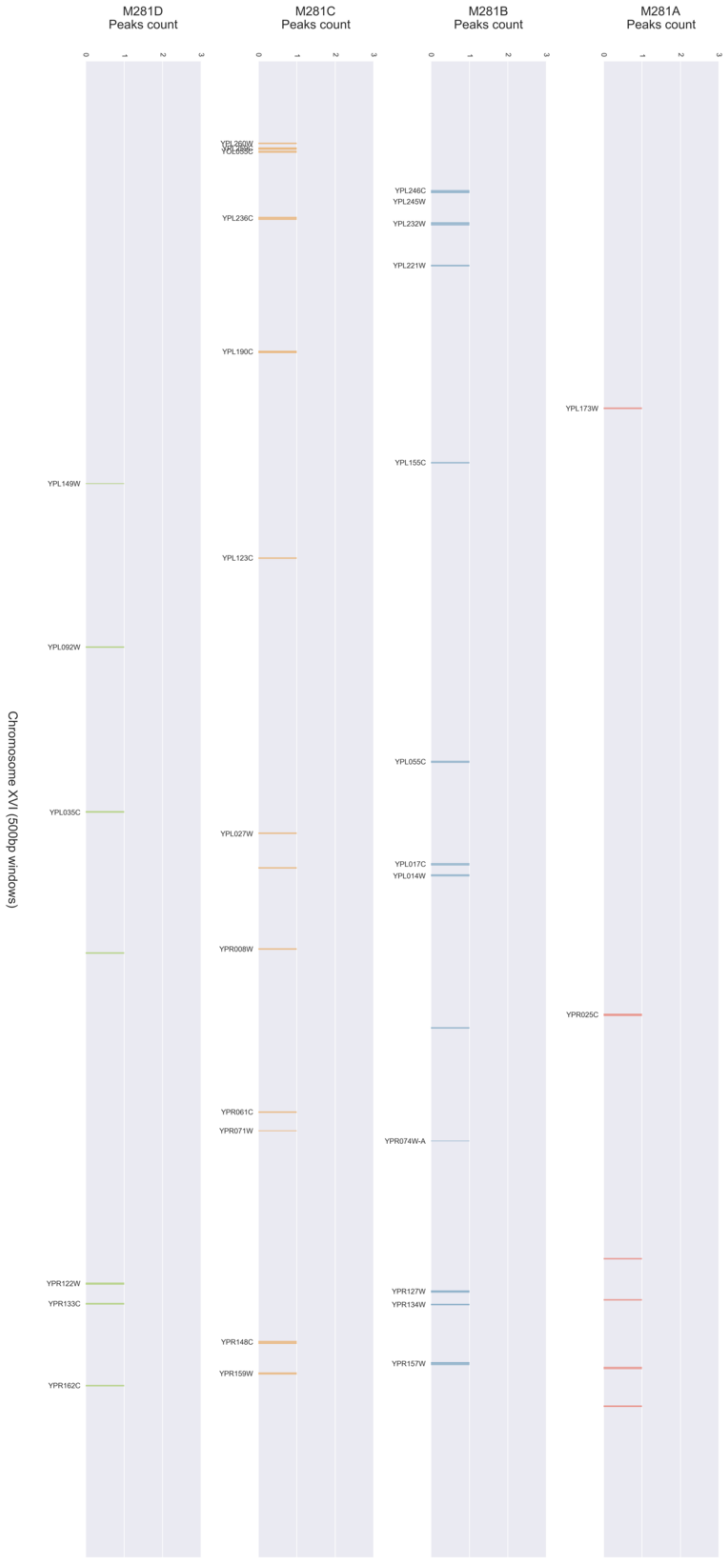

Fig. A.48: Chromosome XVI - (H4 Ac)

Appendix B - *Distribution of enriched regions of H3 bi- and tri- methylation and H4 acetylation across the genes*

Unitig/chromosomes conversion table:

S288c chromosome	M281B PacBio assembly unitig
chr I	unitig_19
chr II	unitig_8
chr III	unitig_15
chr IV	unitig_0
chr V	unitig_11
chr VI	unitig_16
chr VII	unitig_4
chr VIII	unitig_12
chr IX	unitig_13
chr X	unitig_10
chr XI	unitig_7
chr XII	unitig_3
chr XIII	unitig_5
chr XIV	unitig_9
chr XV	unitig_1
chr XVI	unitig_6

Global H3 3Met K4, H3 2Met K4 and H4 Ac genes enriched profiles in M281A

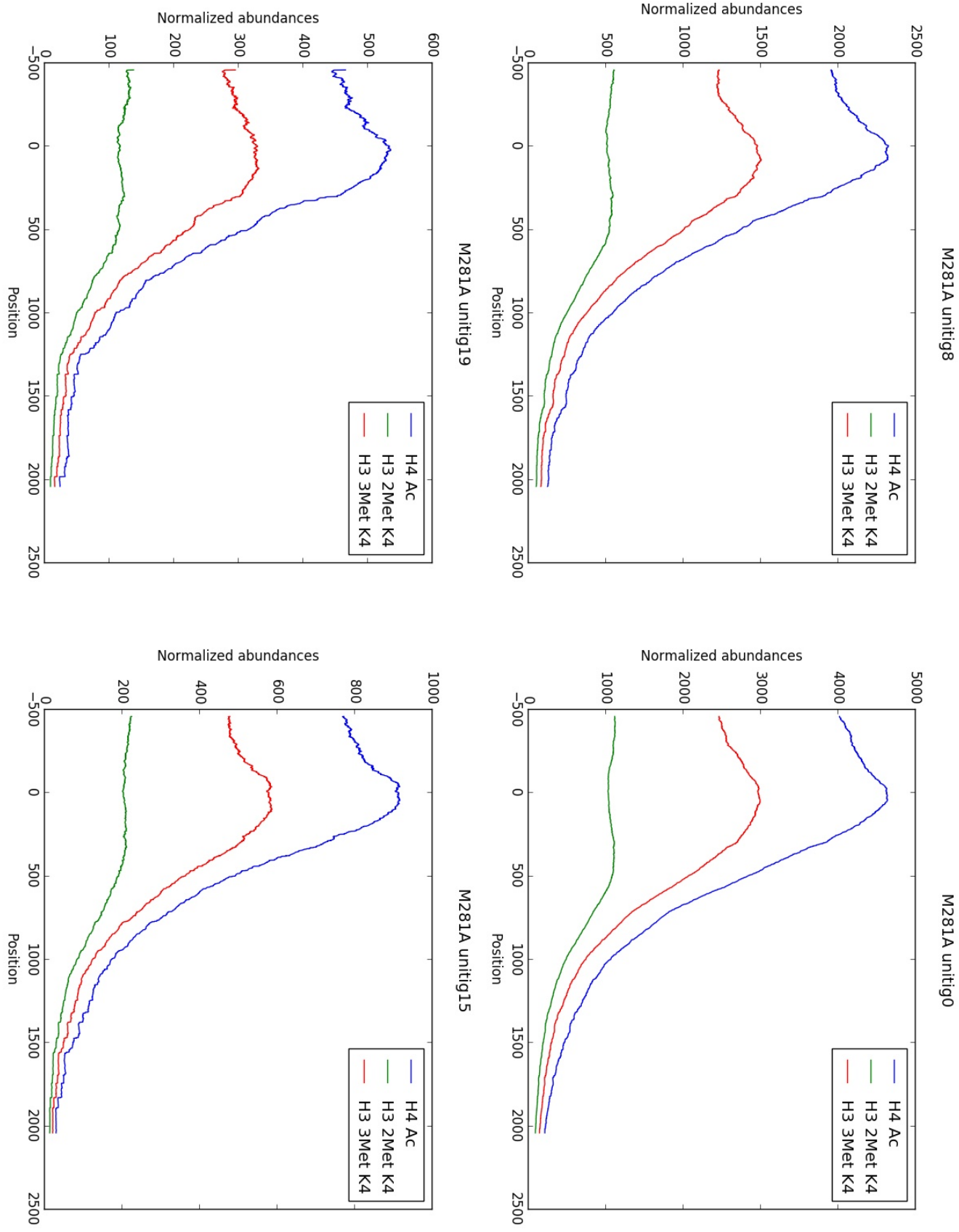

Fig. B.1: Read-count distribution over the genes: chromosomes I-IV

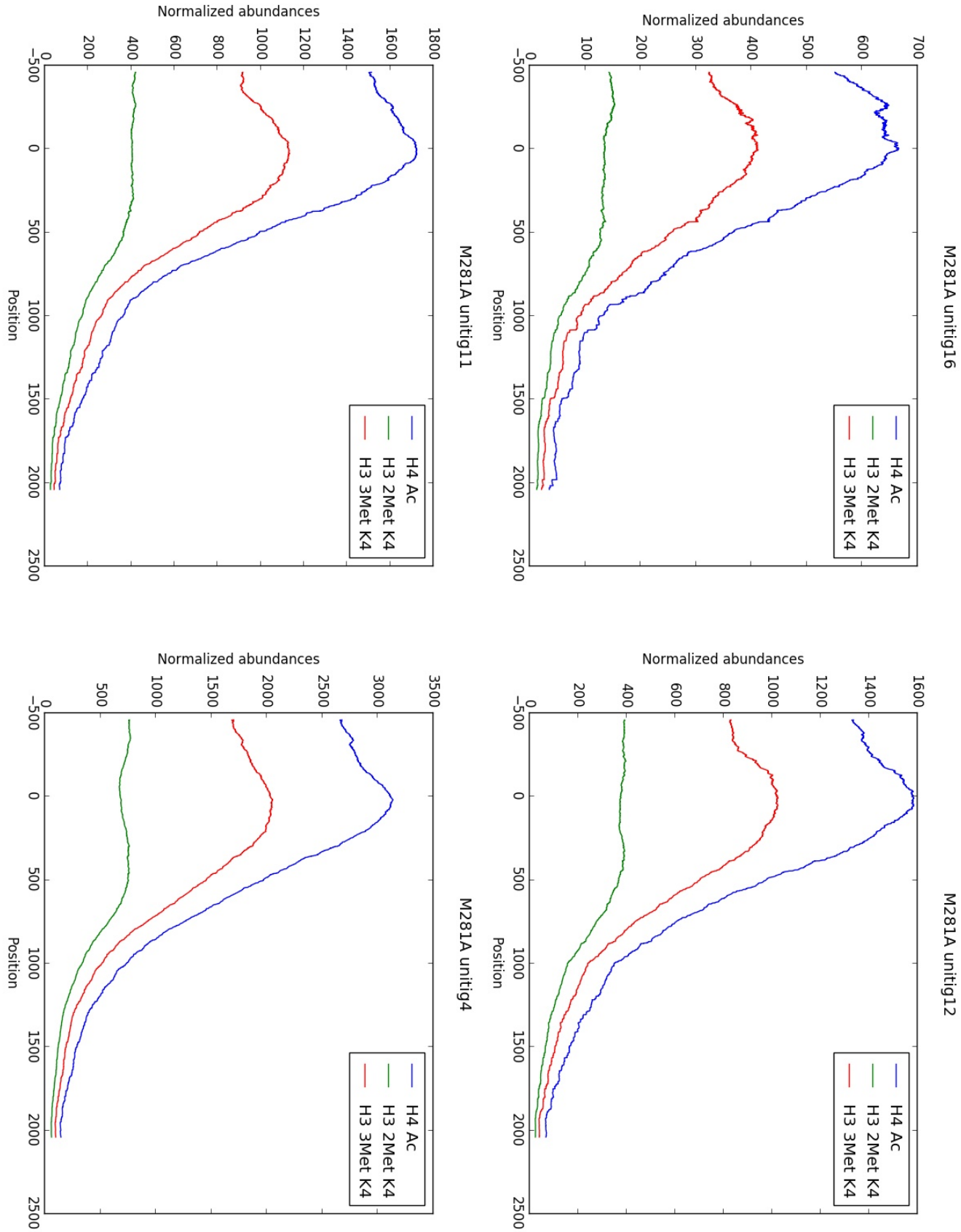

Fig. B.2: Read-count distribution over the genes: chromosomes V-VIII

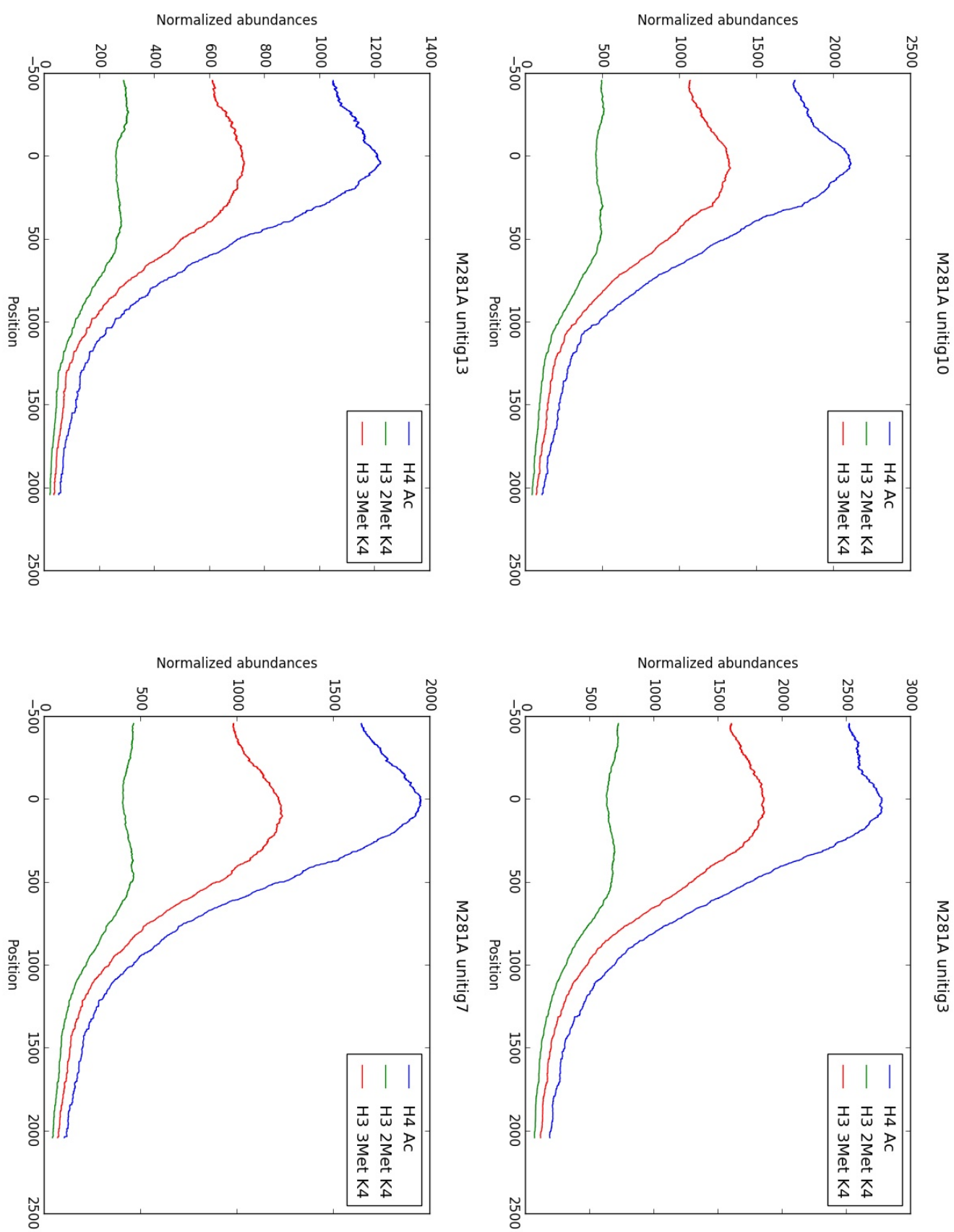

Fig. B.3: Read-count distribution over the genes: chromosomes IX-XII

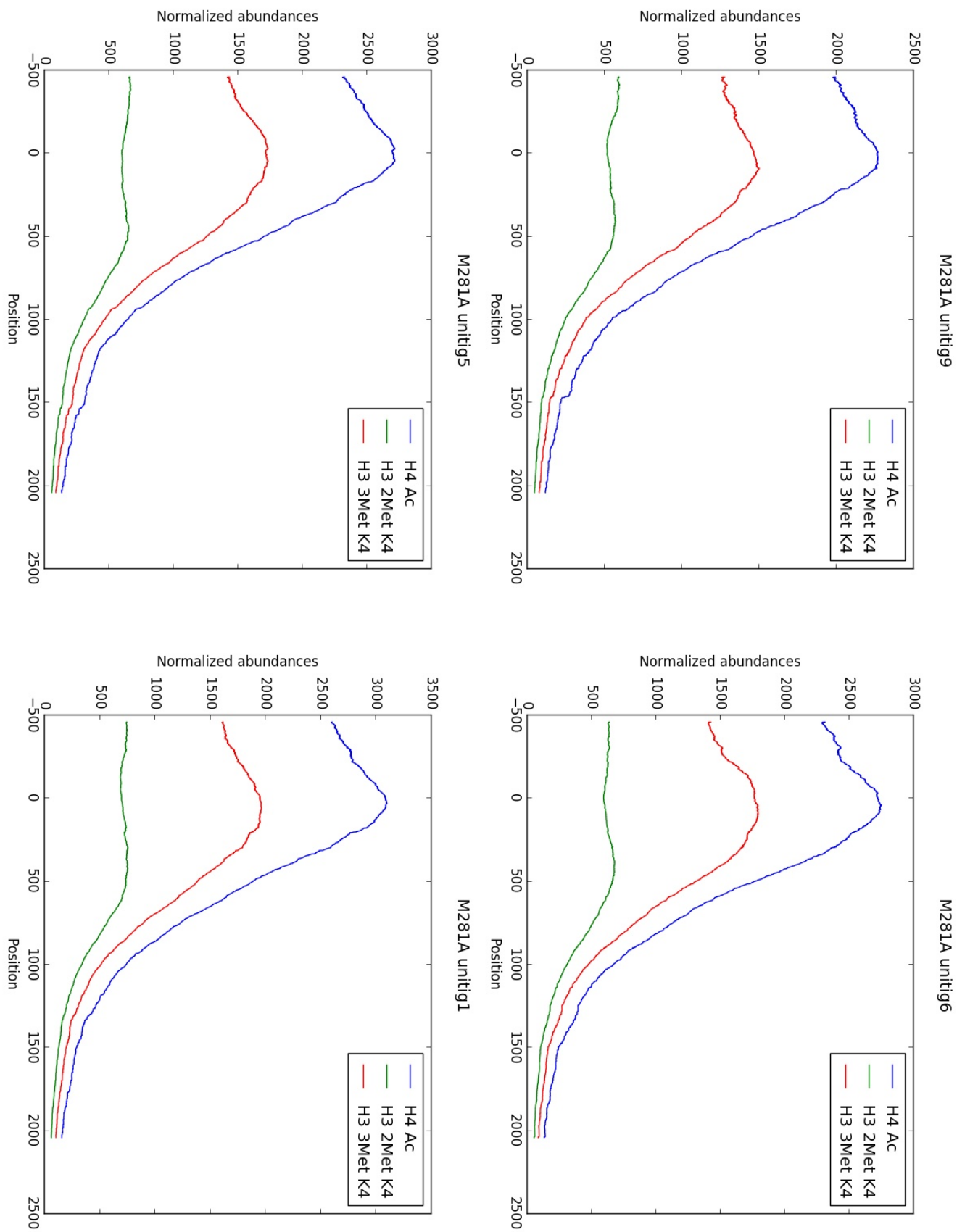

Fig. B.4: Read-count distribution over the genes: chromosomes XIII-XVI

Global H3 3Met K4, H3 2Met K4 and H4 Ac genes enriched profiles in M281B

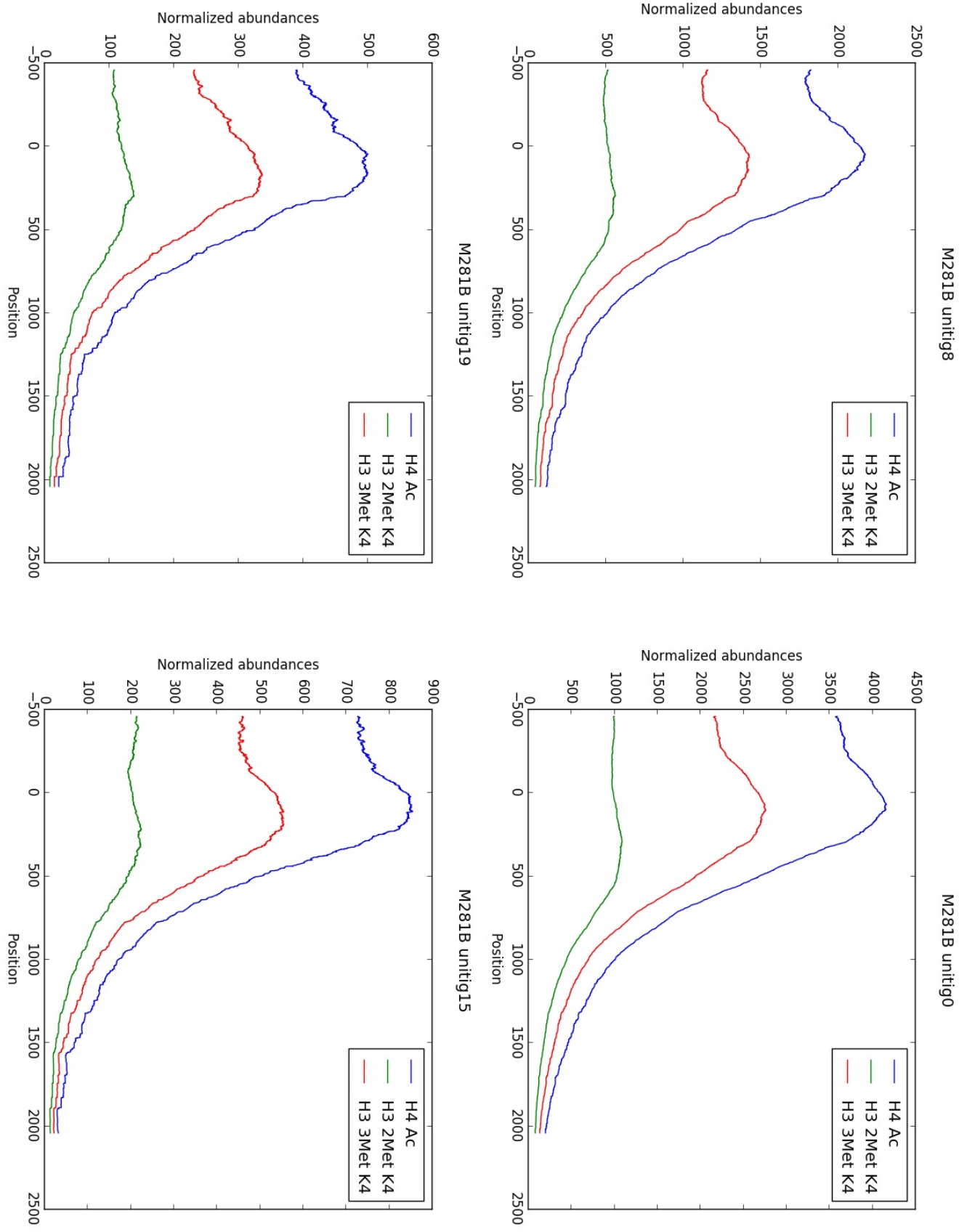

Fig. B.5: Read-count distribution over the genes: chromosomes I-IV

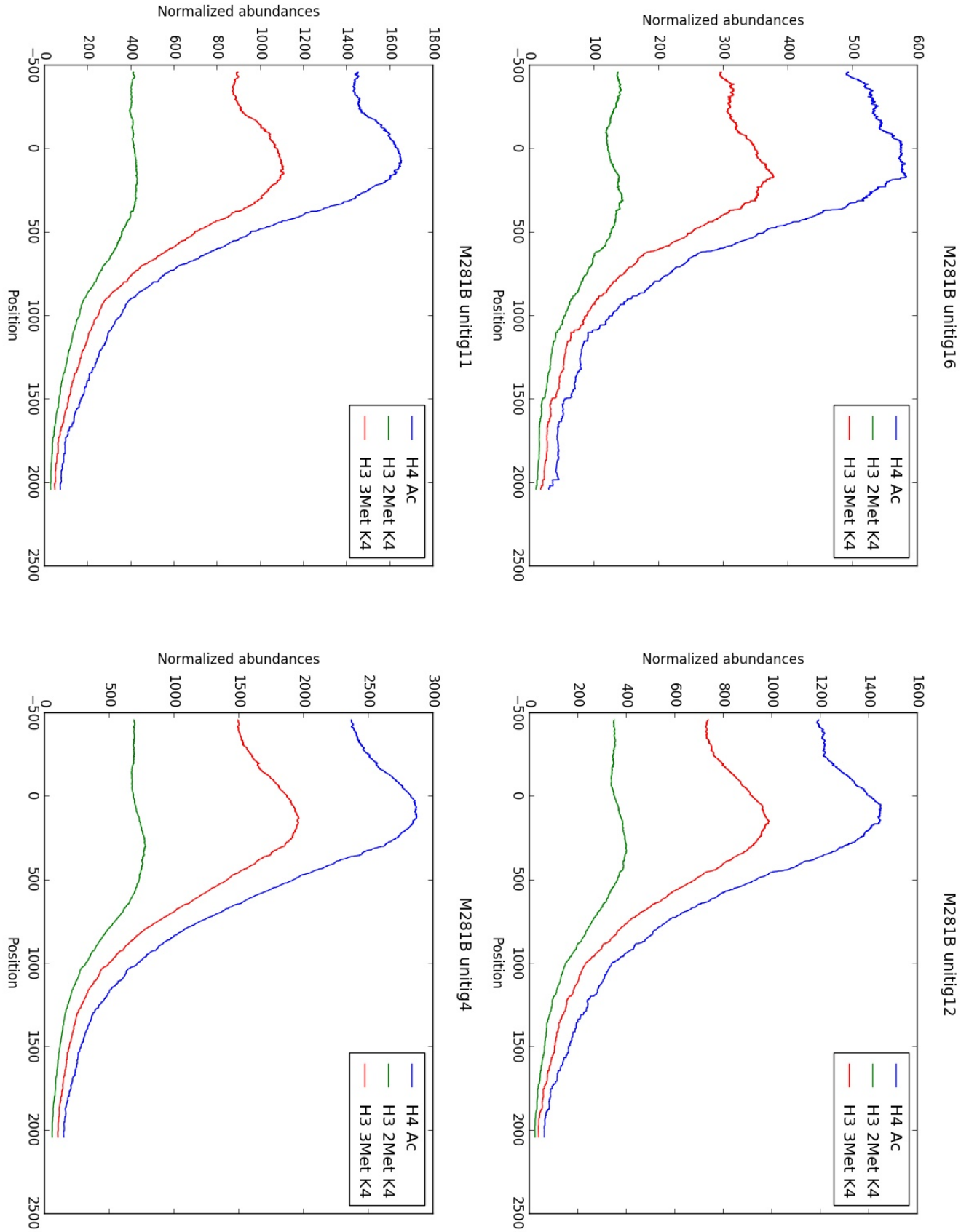

Fig. B.6: Read-count distribution over the genes: chromosomes V-VIII

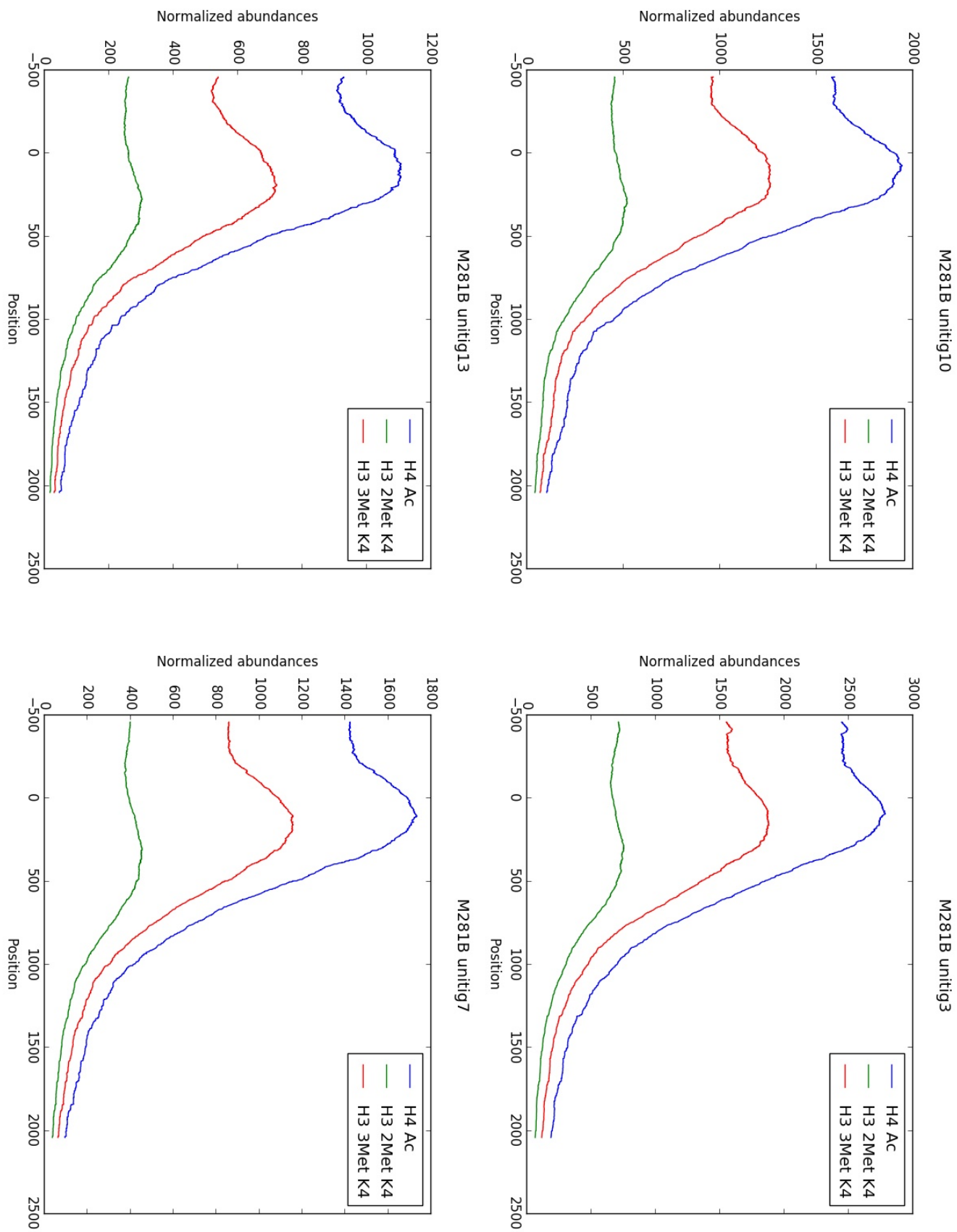

Fig. B.7: Read-count distribution over the genes: chromosomes IX-XII

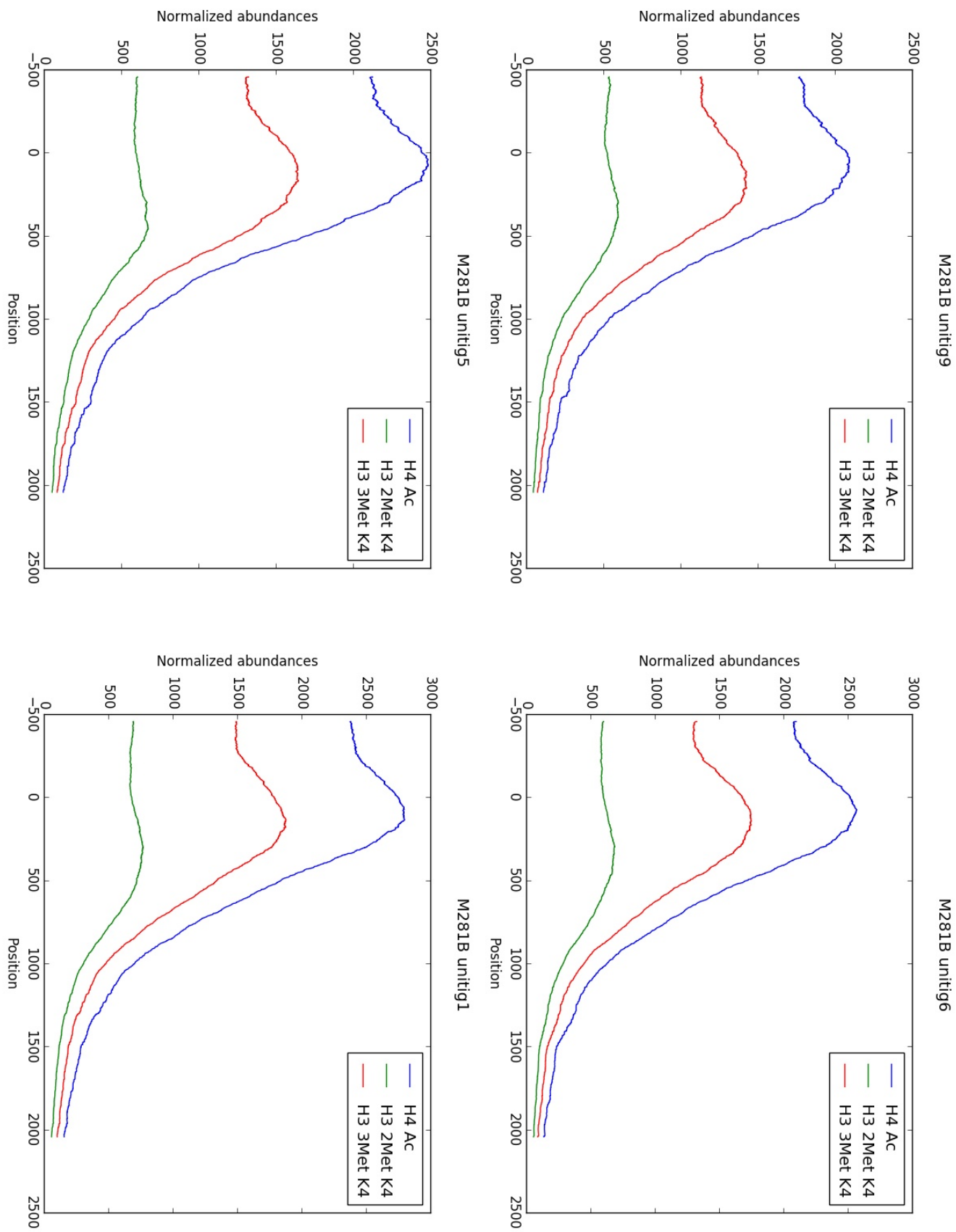

Fig. B.8: Read-count distribution over the genes: chromosomes XIII-XVI

Global H3 3Met K4, H3 2Met K4 and H4 Ac genes enriched profiles in M281C

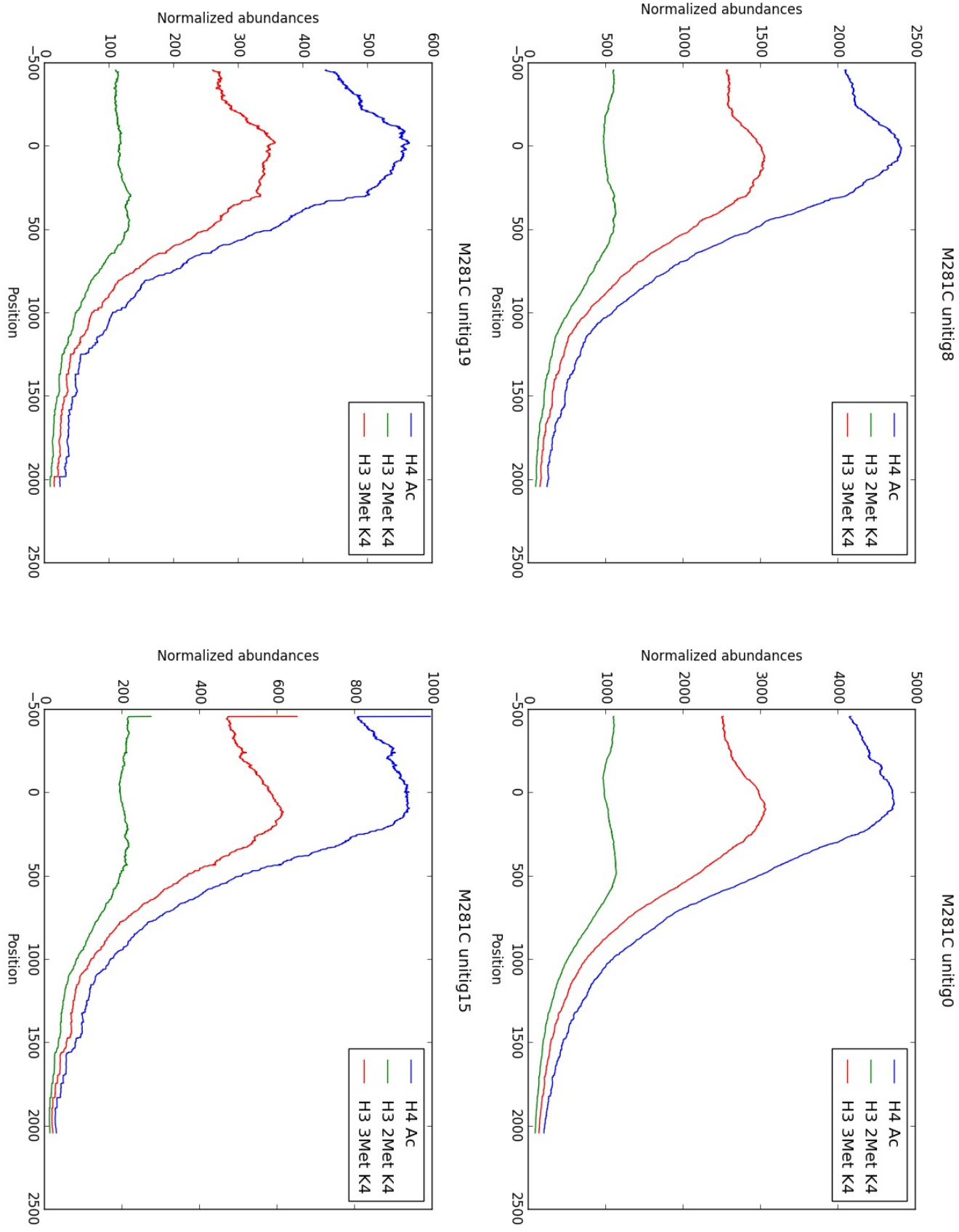

Fig. B.9: Read-count distribution over the genes: chromosomes I-IV

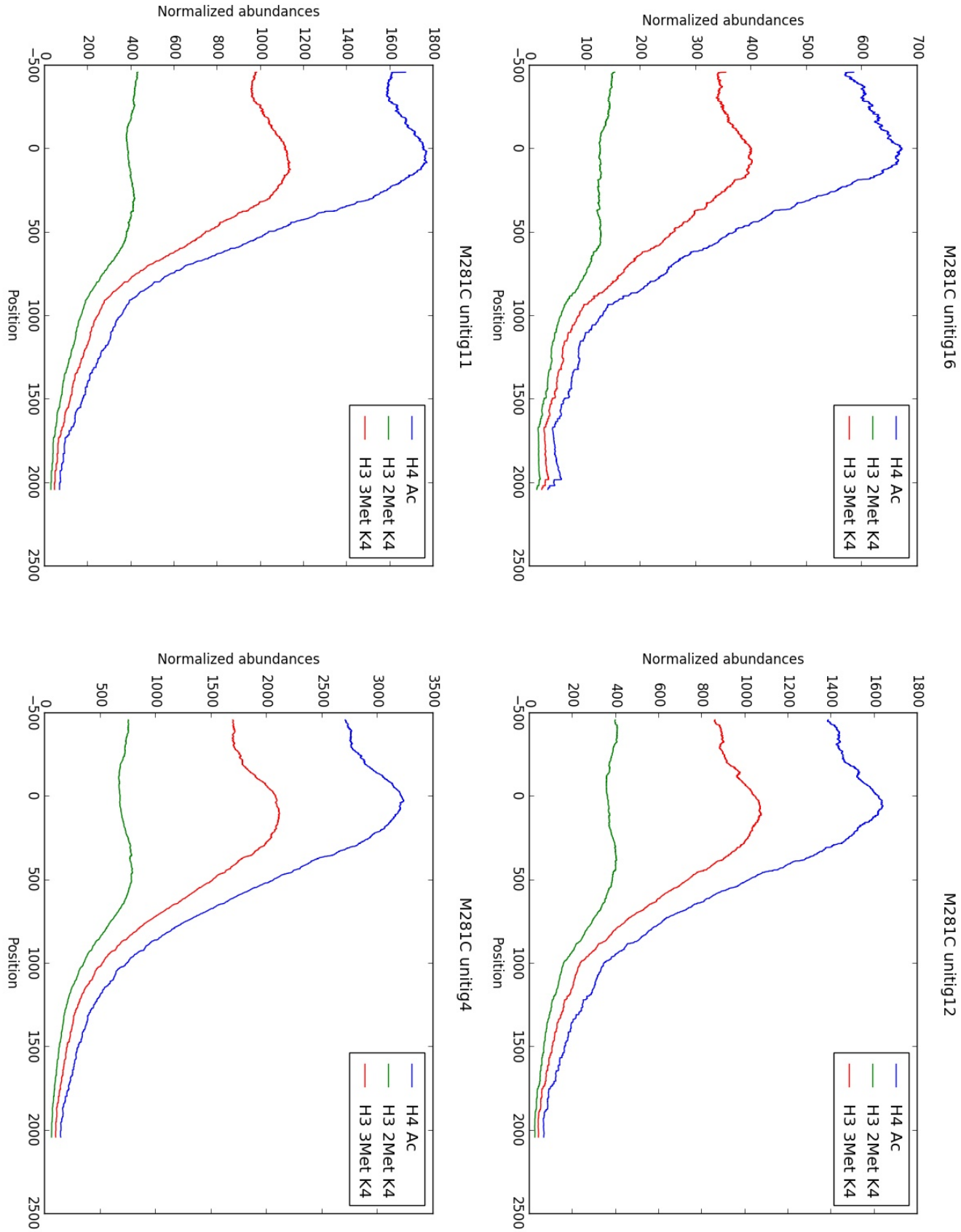

Fig. B.10: Read-count distribution over the genes: chromosomes V-VIII

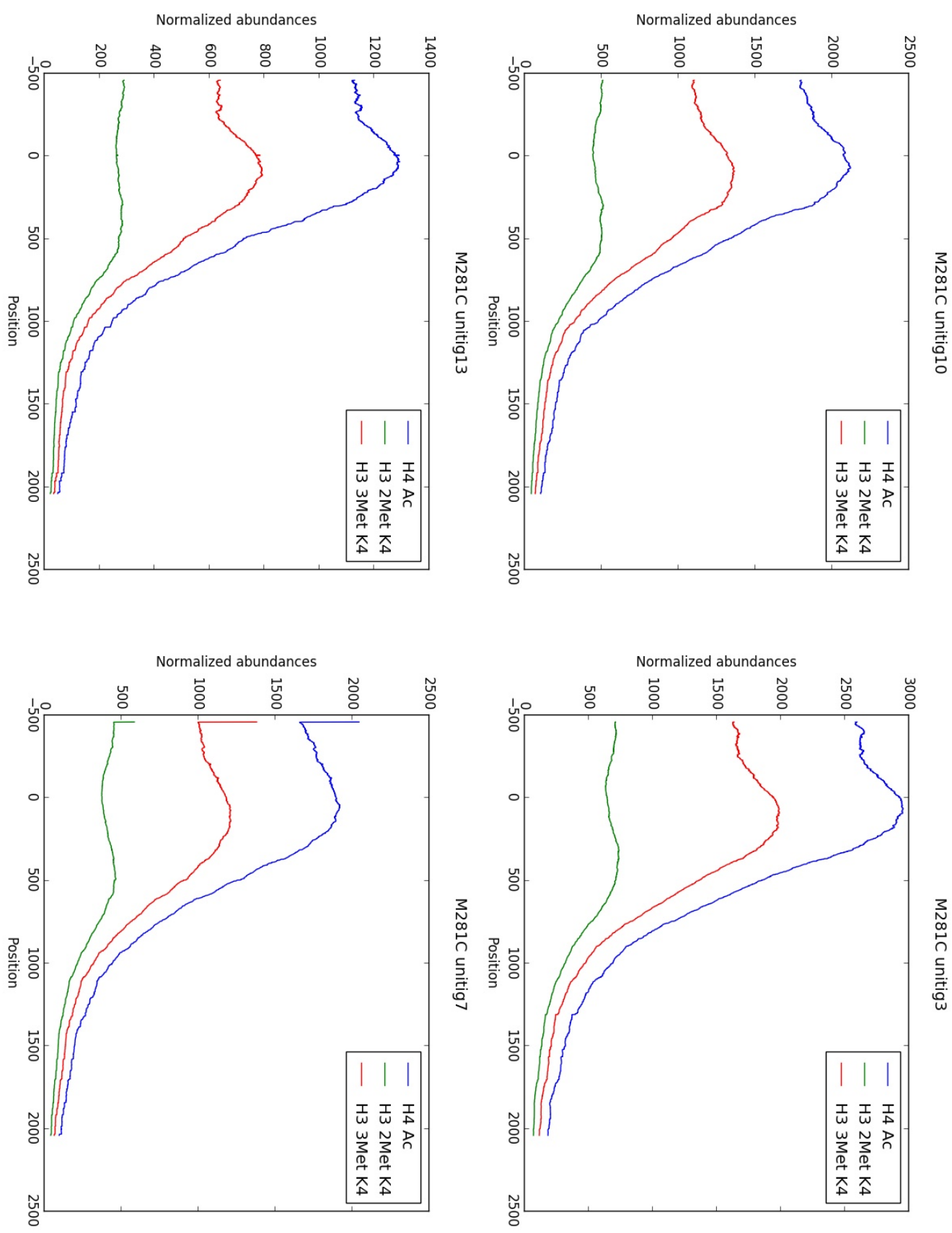

Fig. B.11: Read-count distribution over the genes: chromosomes IX-XII

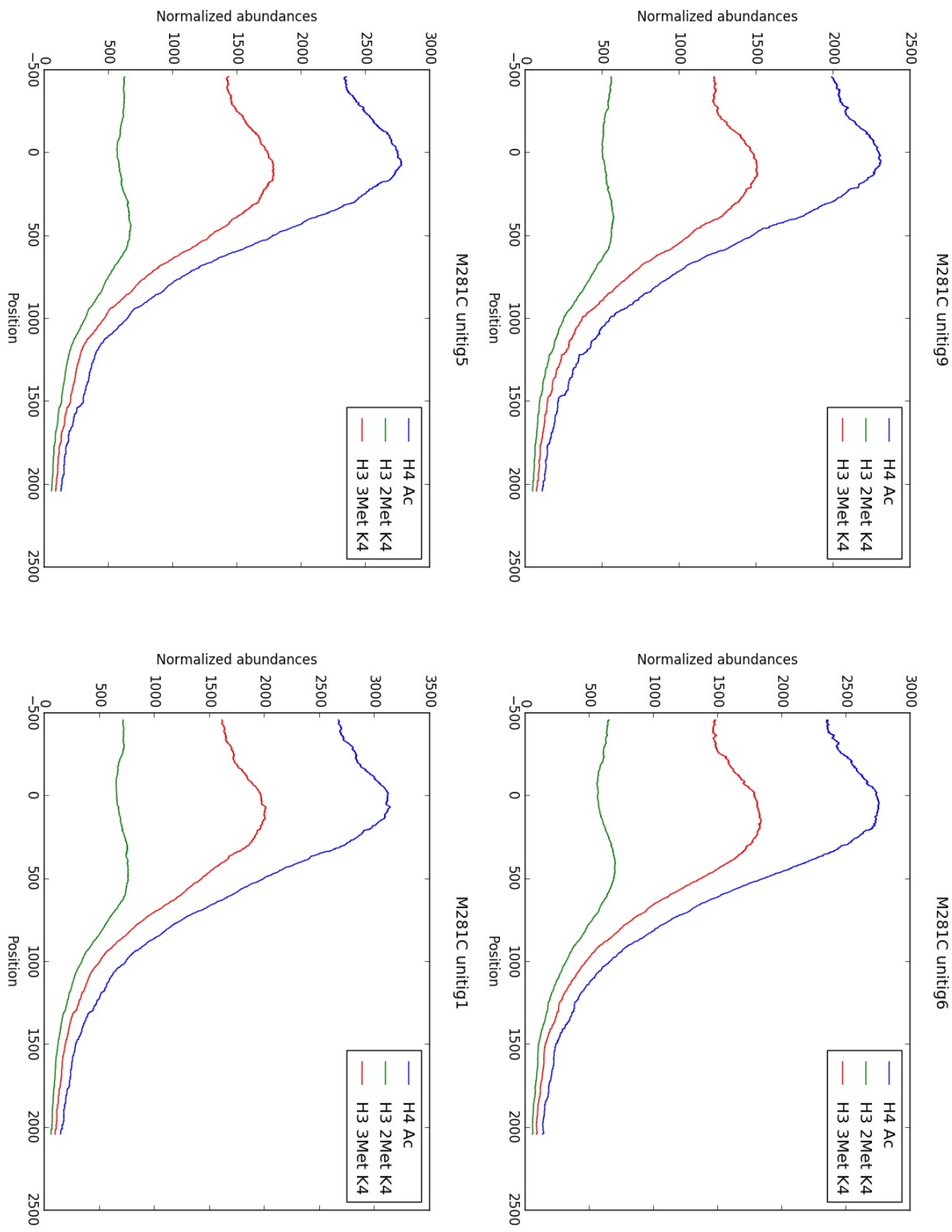

Fig. B.12: Read-count distribution over the genes: chromosomes XIII-XVI

Global H3 3Met K4, H3 2Met K4 and H4 Ac genes enriched profiles in M281D

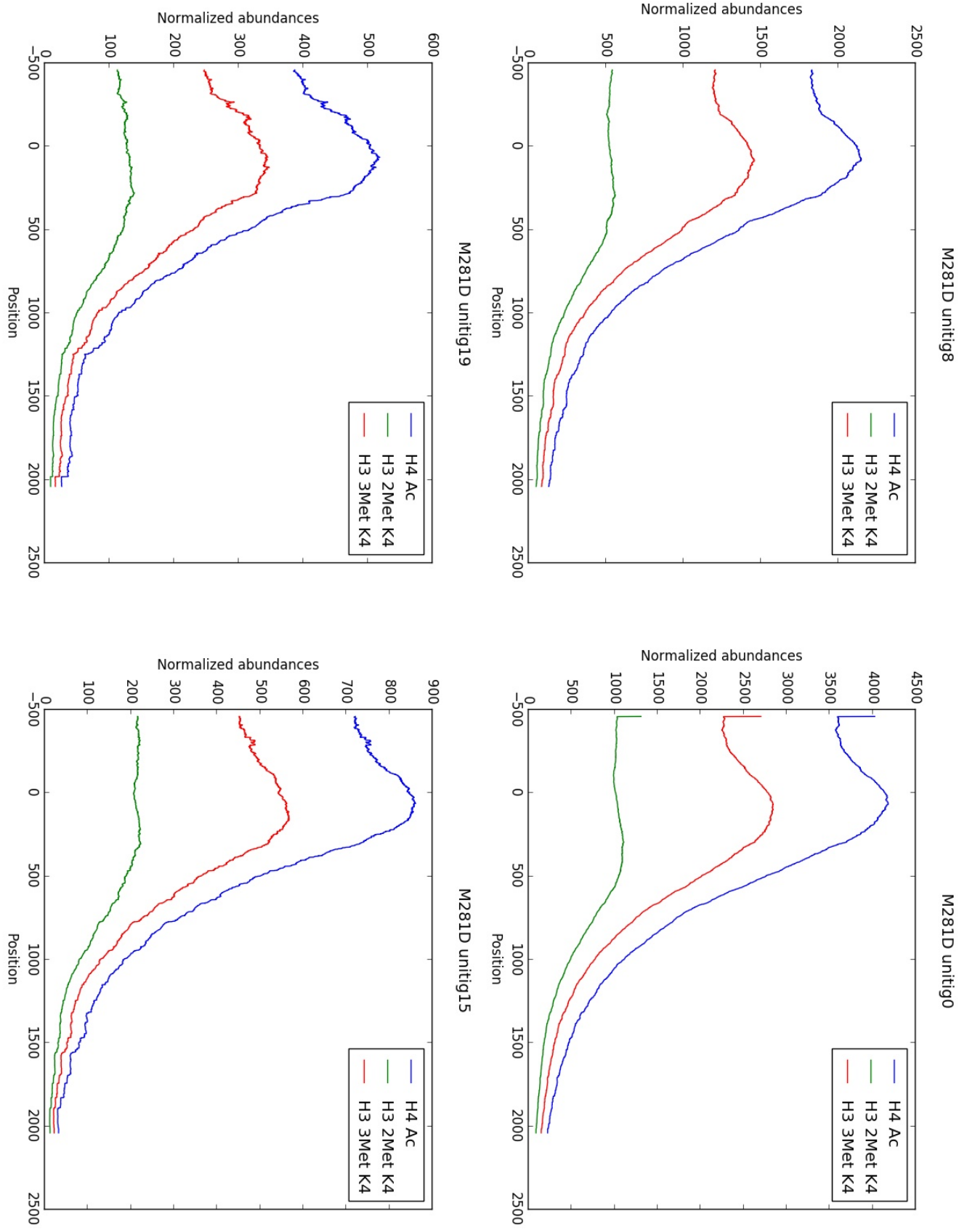

Fig. B.13: Read-count distribution over the genes: chromosomes I-IV

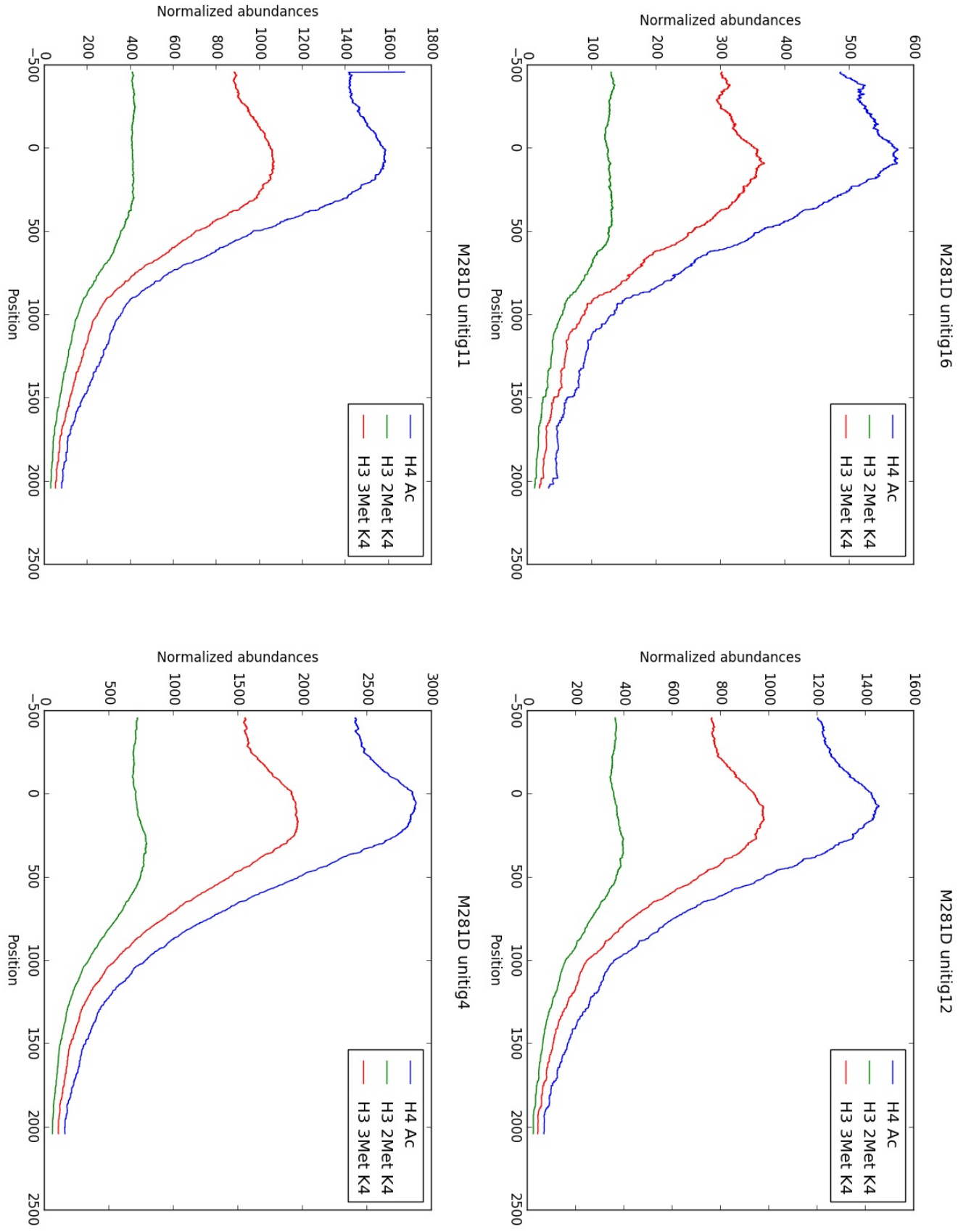

Fig. B.14: Read-count distribution over the genes: chromosomes V-VIII

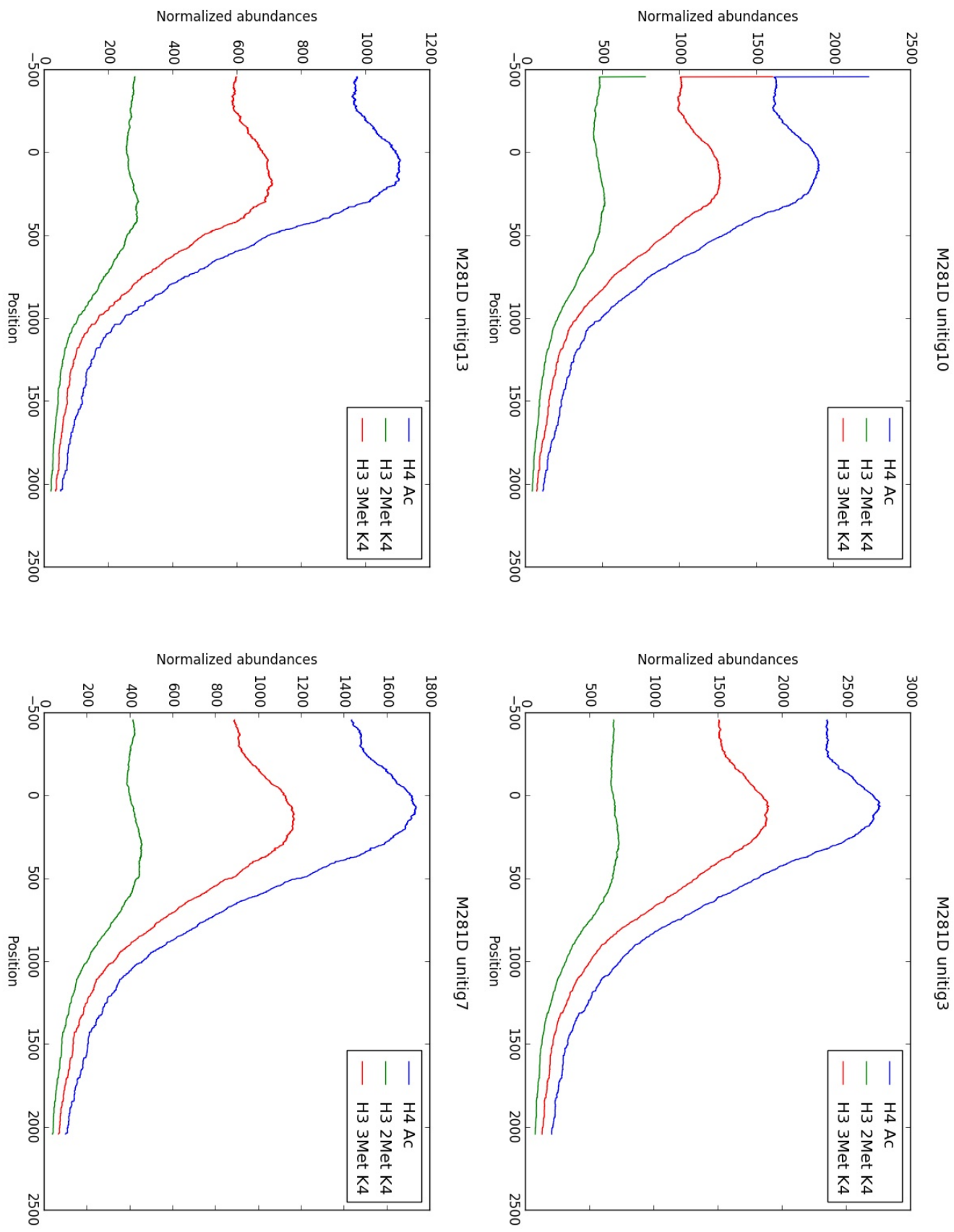

Fig. B.15: Read-count distribution over the genes: chromosomes IX-XII

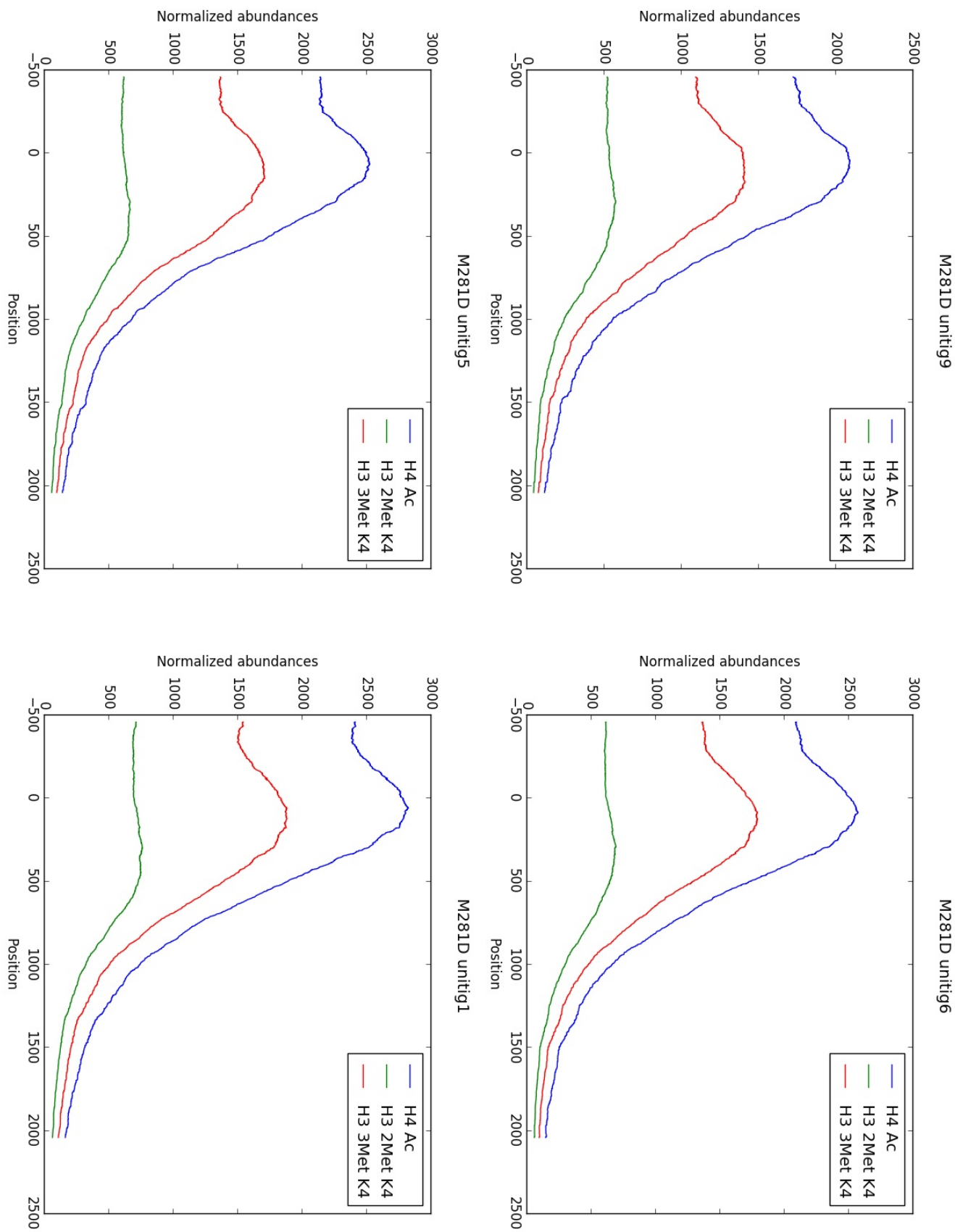

Fig. B.16: Read-count distribution over the genes: chromosomes XIII-XVI

Appendix C - *Hierarchical clustering of relative abundances of spore-specific chromatin domains (SSCDs)*

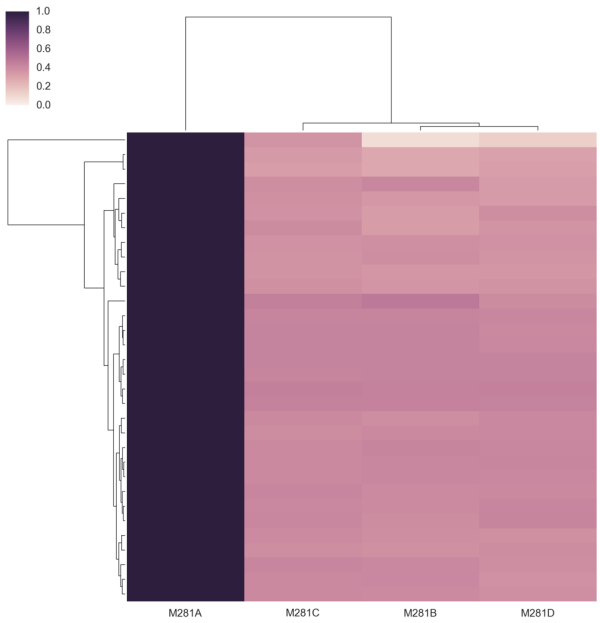

Fig.C.1: Total number of H3 3Met K4 M281A SSCDs = 32

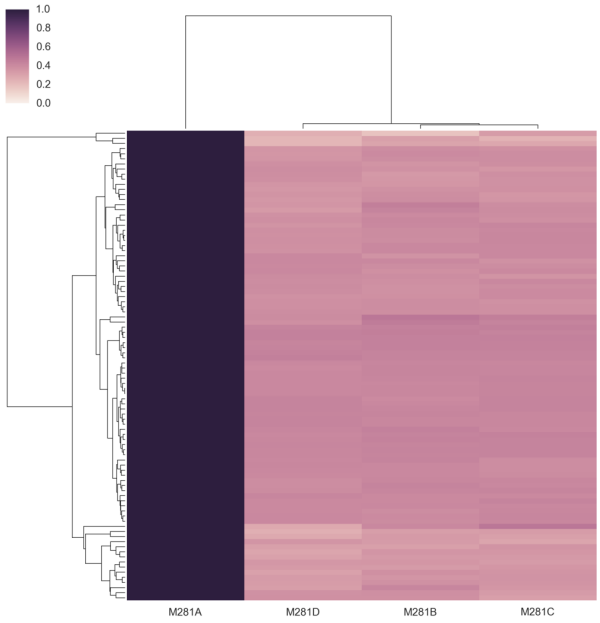

Fig.C.2: Total number of H3 2Met K4 M281A SSCDs 92

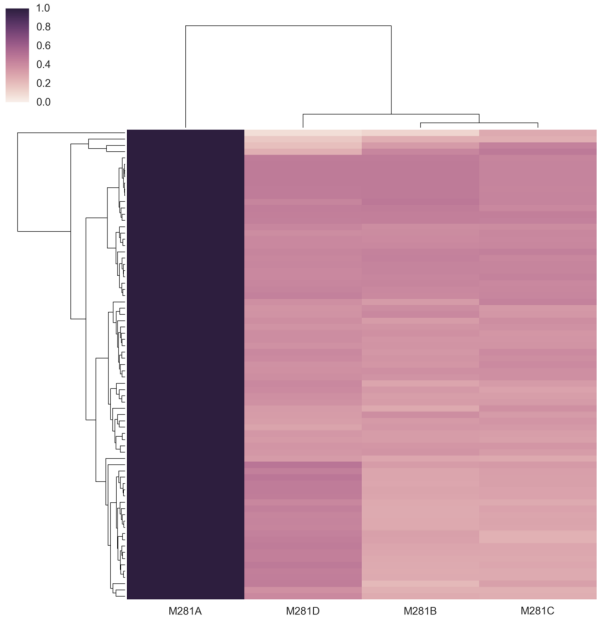

Fig.C.3: Total number of H4 Ac M281A SSCDs 75

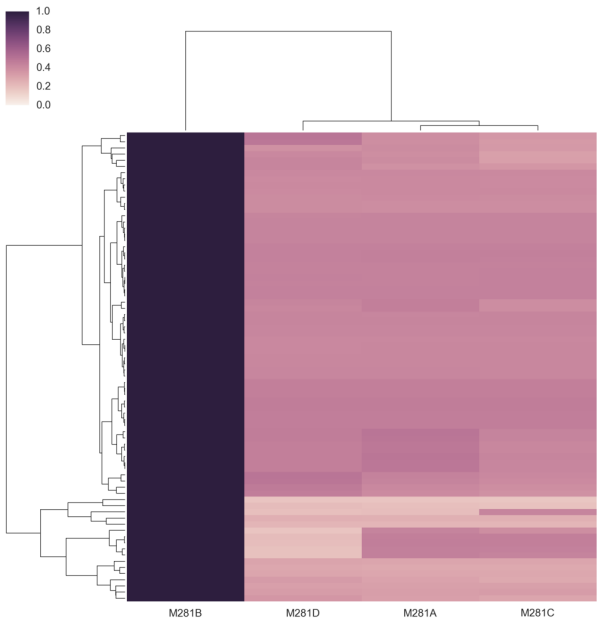

Fig.C.4: Total number of H3 3Met K4 M281B SSCDs 76

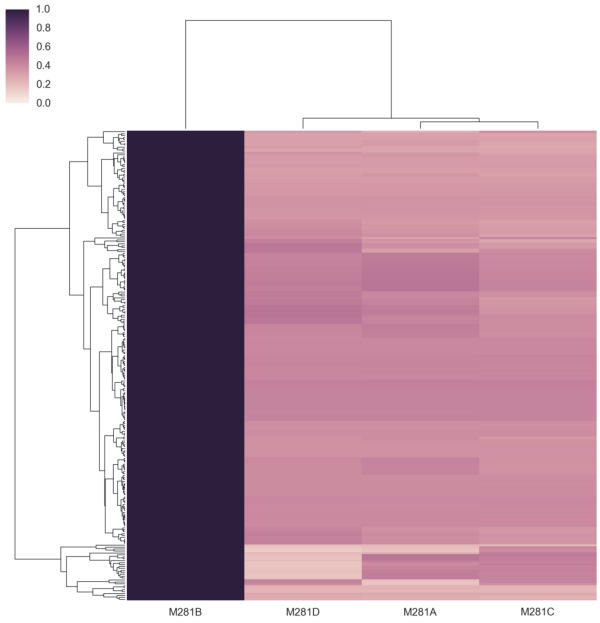

Fig.C.5: Total number of H3 2Met K4 M281B SSCDs 243

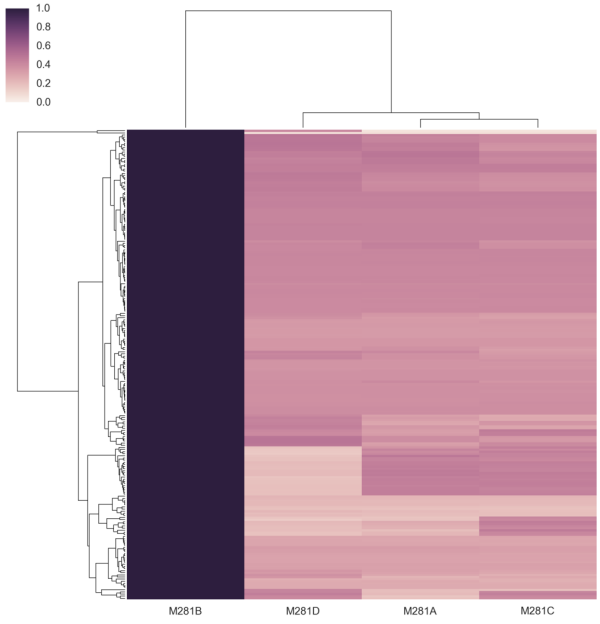

Fig.C.6: Total number of H4 Ac M281B SSCDs 221

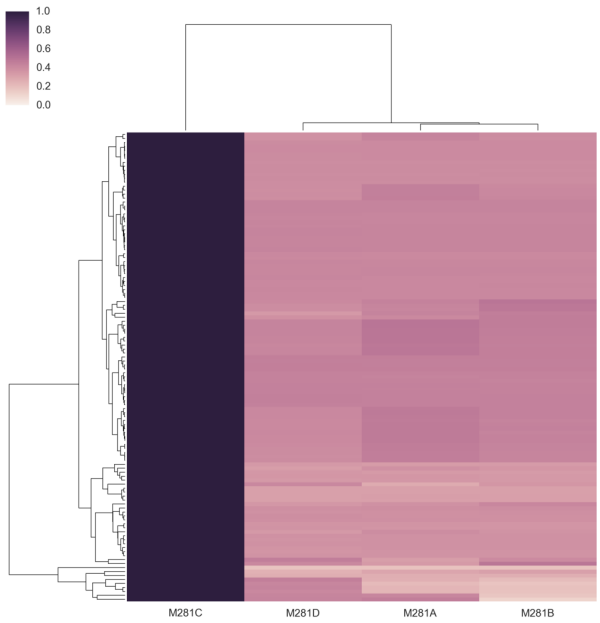

Fig.C.7: Total number of H3 3Met K4 M281C SSCDs 118

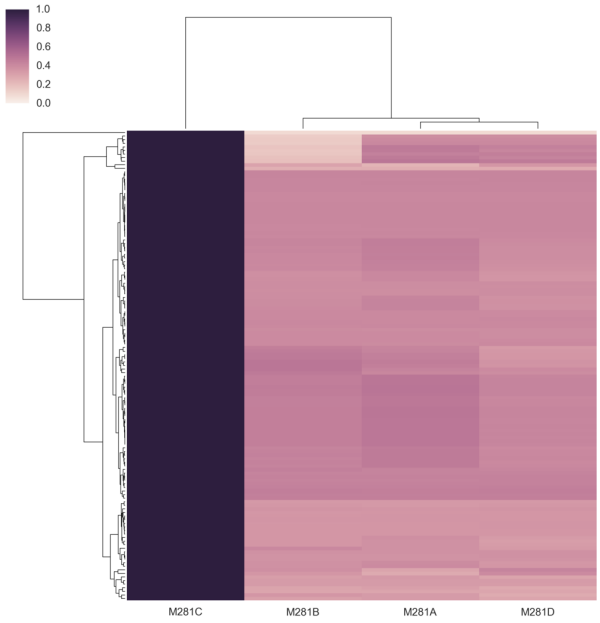

Fig.C.8: Total number of H3 2Met K4 M281C SSCDs 131

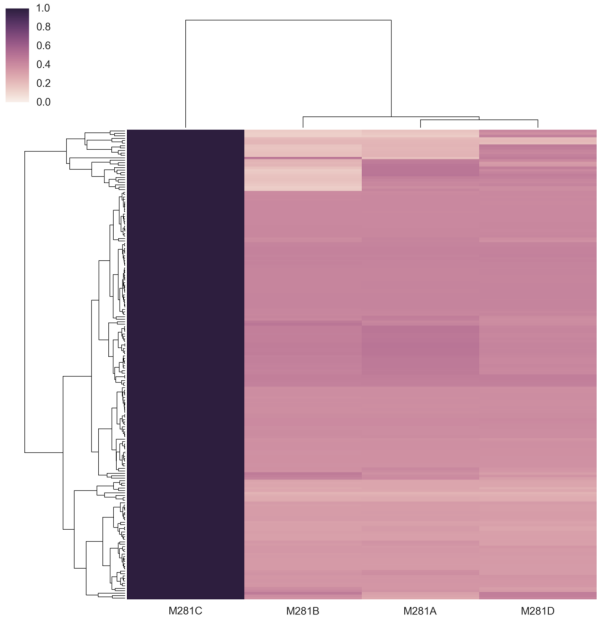

Fig.C.9: Total number of H4 Ac M281C SSCDs 192

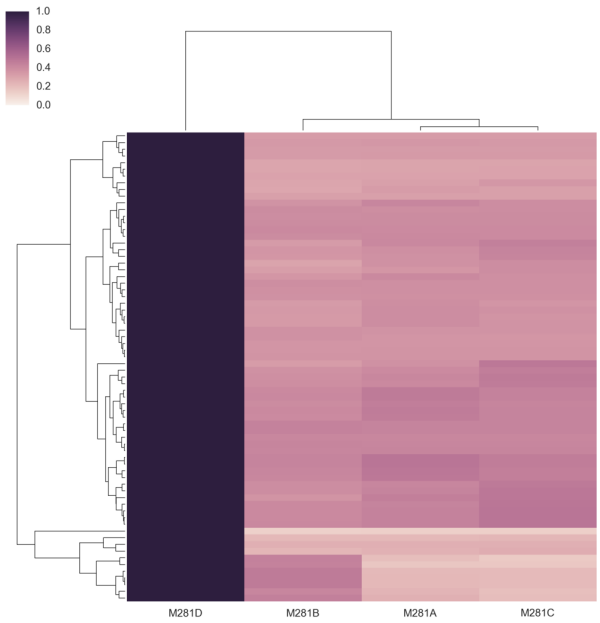

Fig.C.10: Total number of H3 3Met K4 M281D SSCDs 70

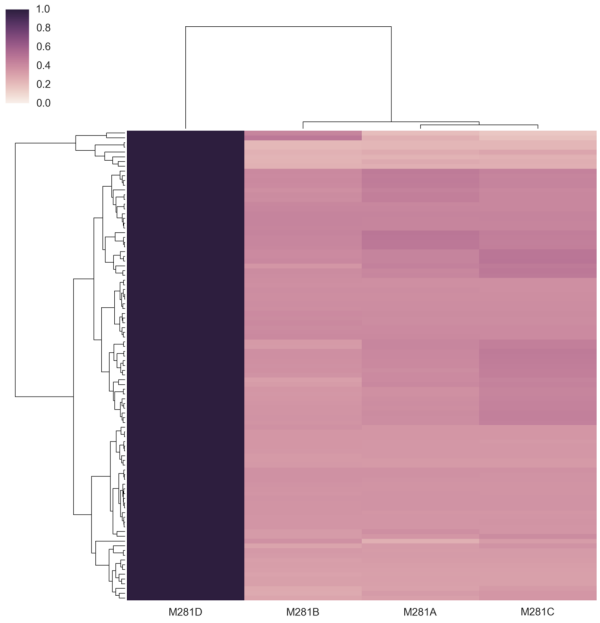

Fig.C.11: Total number of H3 2Met K4 M281D SSCDs 99

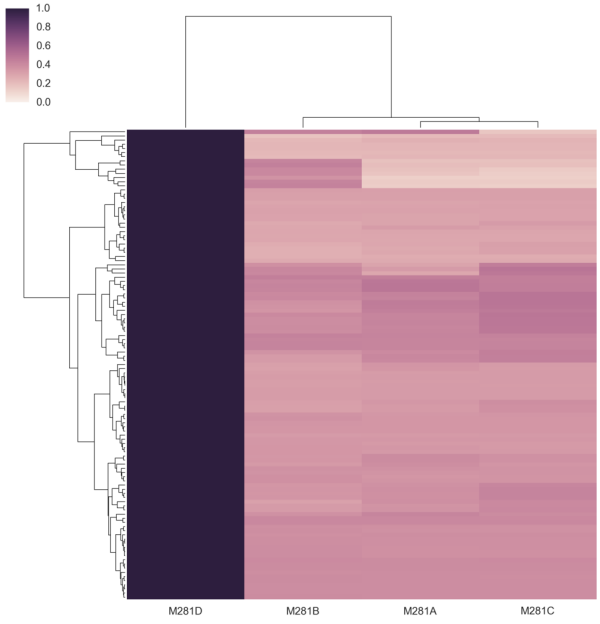

Fig.C.12: Total number of H4 Ac M281D SSCDs 113

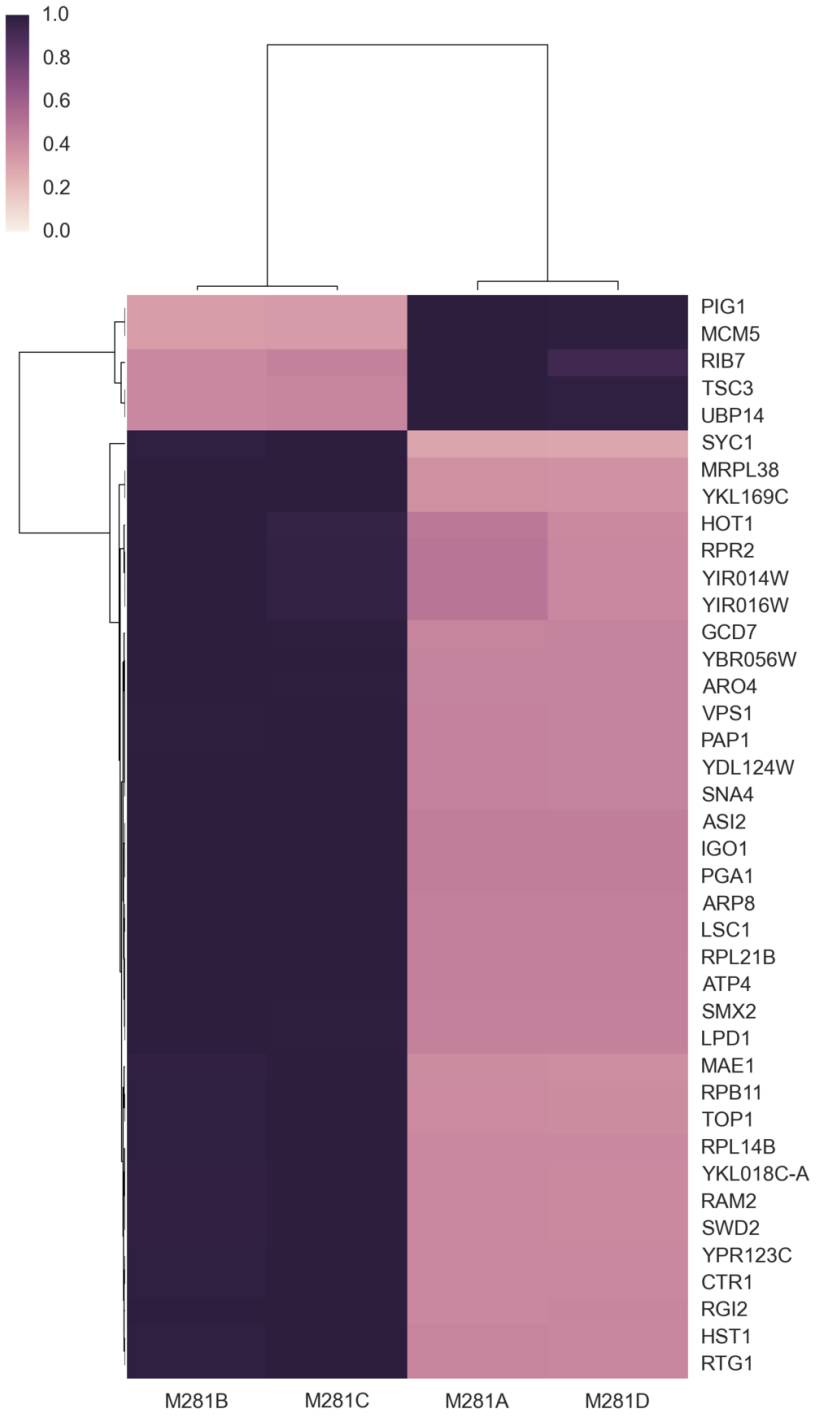

Fig.C.13: Total number of H3 3Met K4 SSCDs morphotype-associated = 40

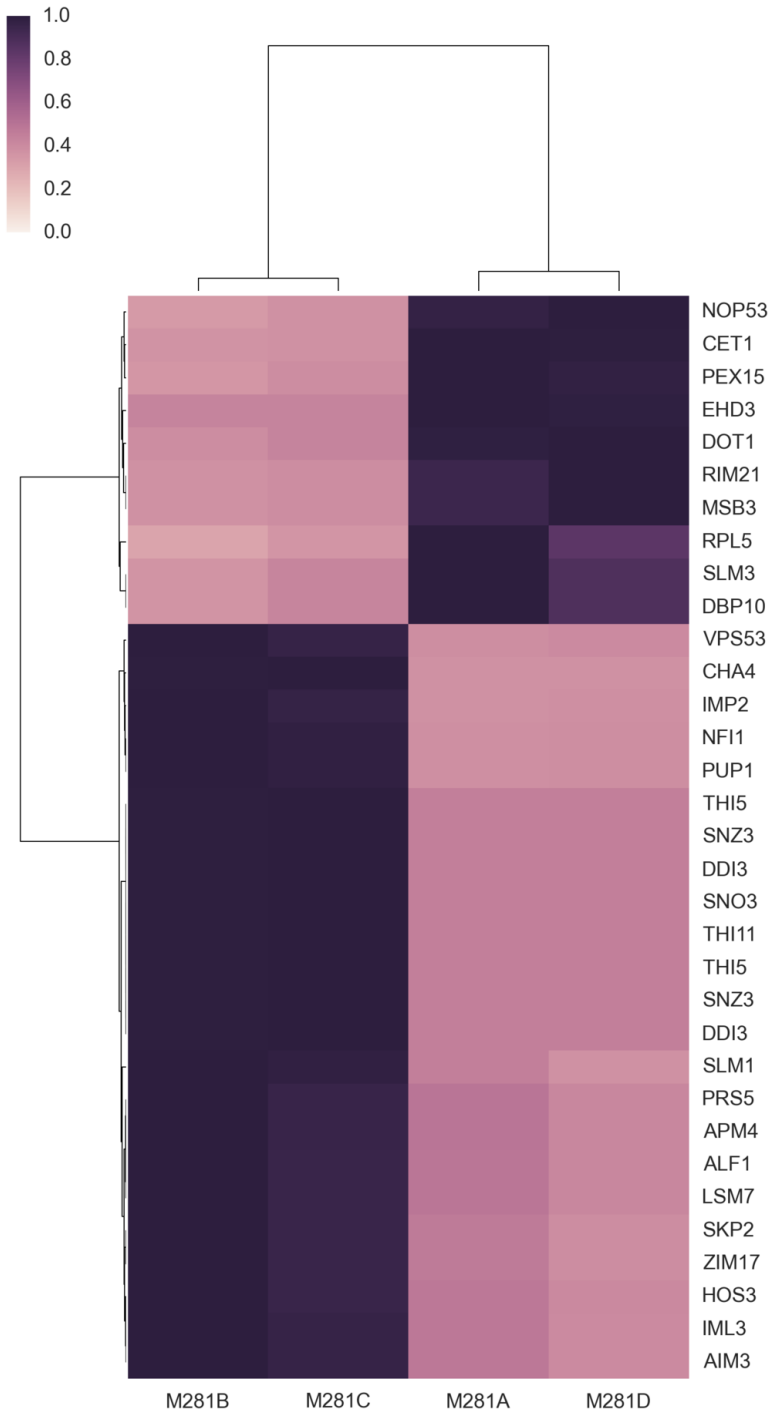

Fig.C.14: Total number of H3 2Met K4 SSCDs morphotype-associated = 33

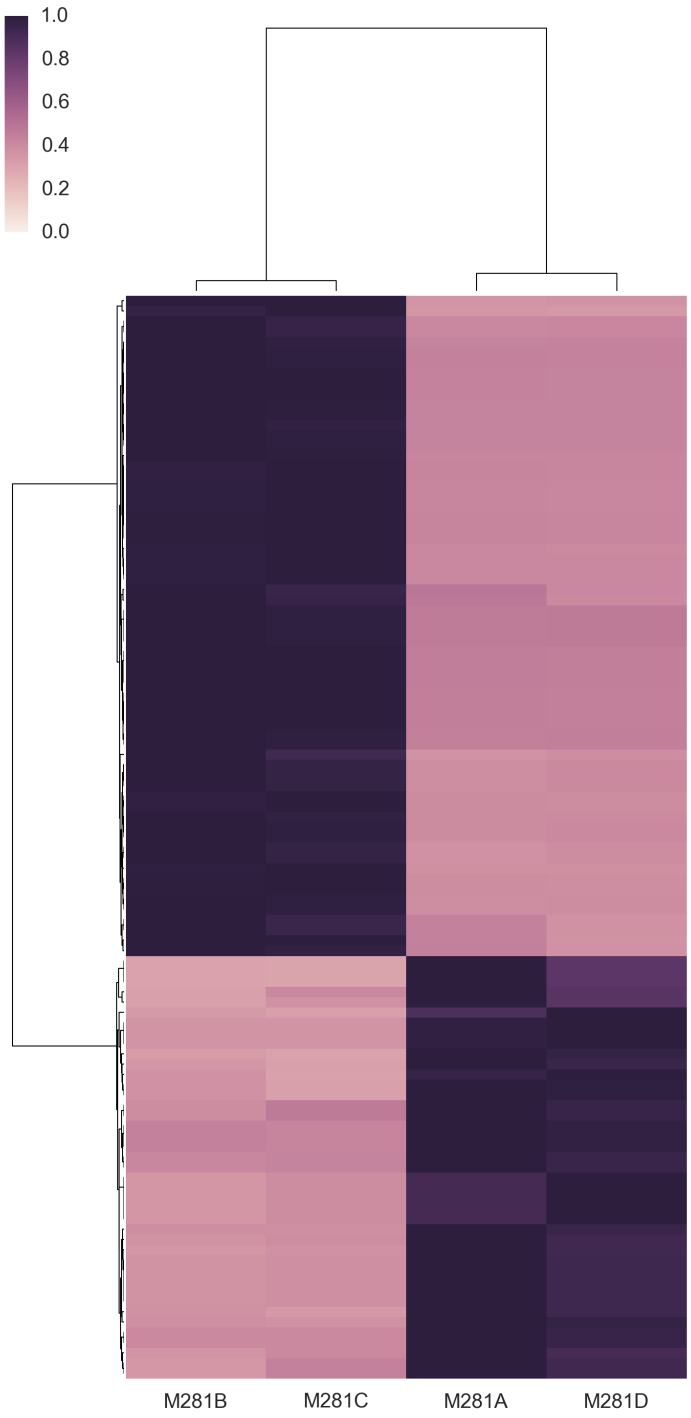

Fig.C.15: Total number of H4 Ac SSCDs morphotype-associated = 64

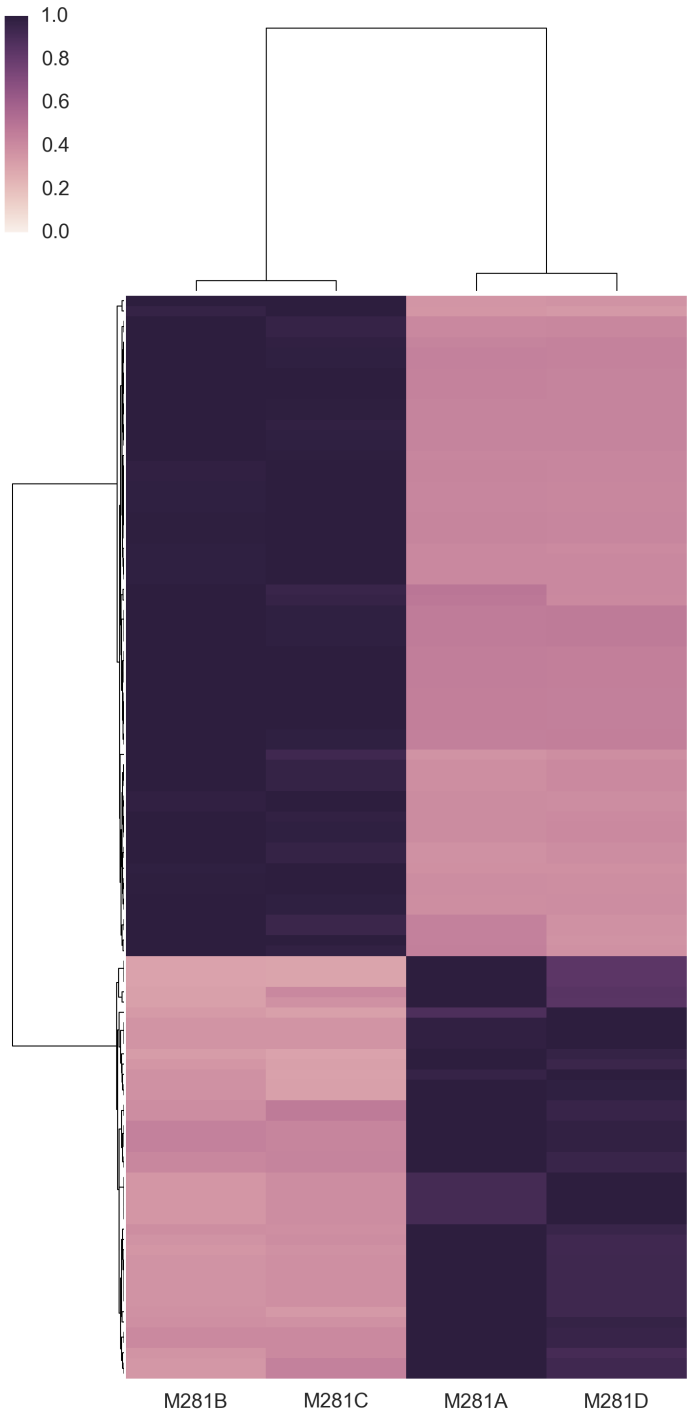

Fig.C.15: Total number of H4 Ac SSCDs morphotype-associated = 64

Fig.C.17: Total number of H3 2Met K4 SSCDs TFL-associated = 270

Fig.C.18: Total number of H4 Ac SSCDs TFL-associated = 600

Appendix D - *Chromosomal distribution of ChIP enriched islands across the M28 spores*

Fig.D.1: Circos plot of significantly enriched H3 3Met K4, H3 2Met K4 and H4 Ac islands in M281A (1-16 external tracks = chromosome number)

Fig.D.2: Circos plot of significantly enriched H3 3Met K4, H3 2Met K4 and H4 Ac islands in M281B (1-16 external tracks = chromosome number)

Fig.D.3: Circos plot of significantly enriched H3 3Met K4, H3 2Met K4 and H4 Ac islands in M281C (1-16 external tracks = chromosome number)

Fig.D.4: Circos plot of significantly enriched H3 3Met K4, H3 2Met K4 and H4 Ac islands in M281D (1-16 external tracks = chromosome number)

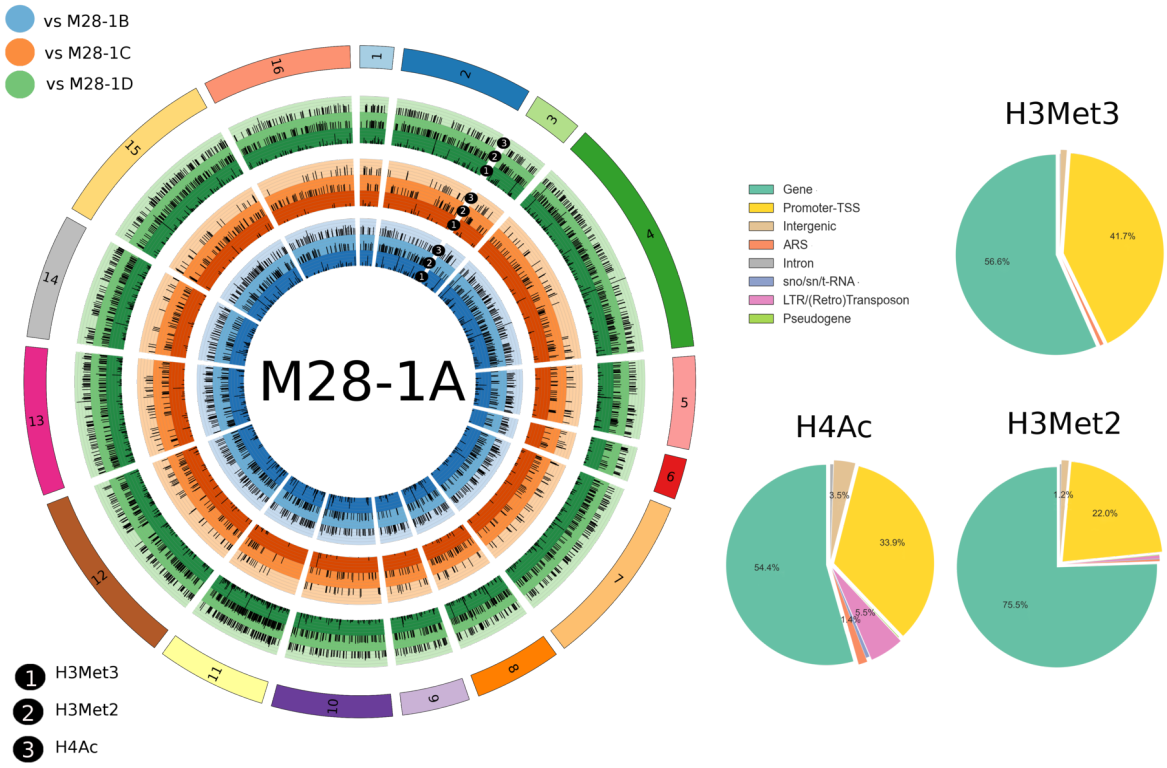

Fig.D.5: Circos plot of significant enriched H3 3Met K4, H3 2Met K4 and H4 Ac islands of M281A compared to M281B, M281C and M281D

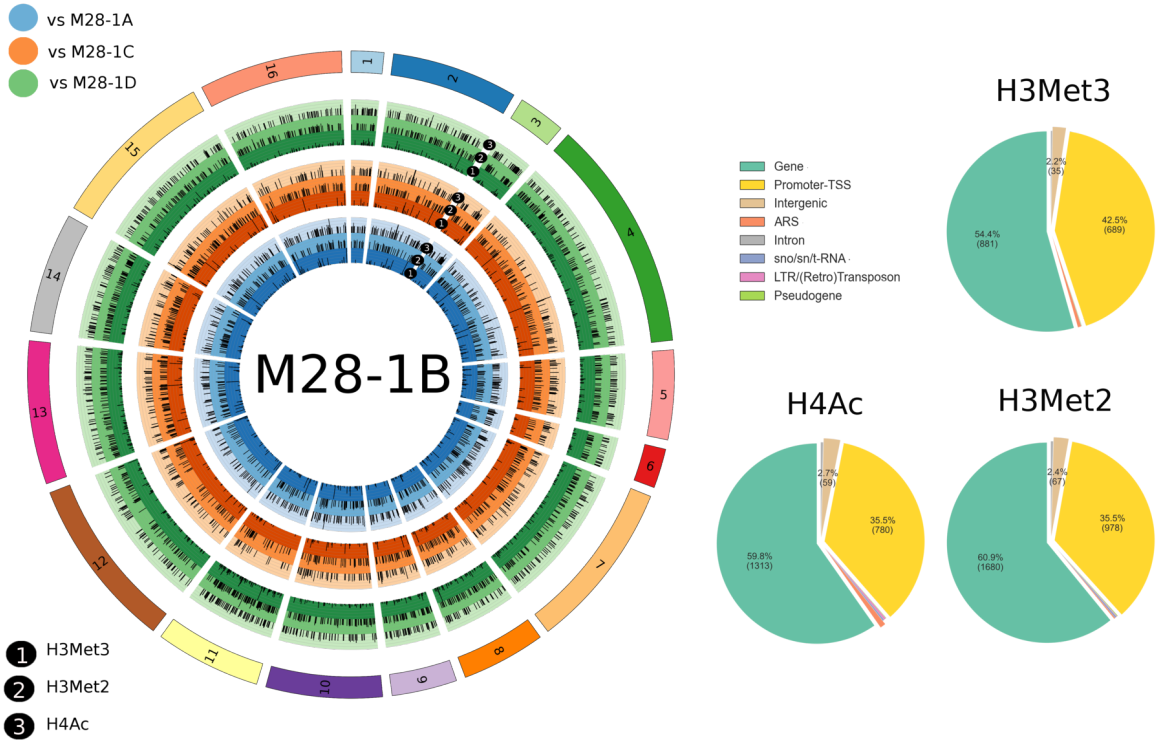

Fig.D.5: Circos plot of significant enriched H3 3Met K4, H3 2Met K4 and H4 Ac islands of M281B compared to M281A, M281C and M281D

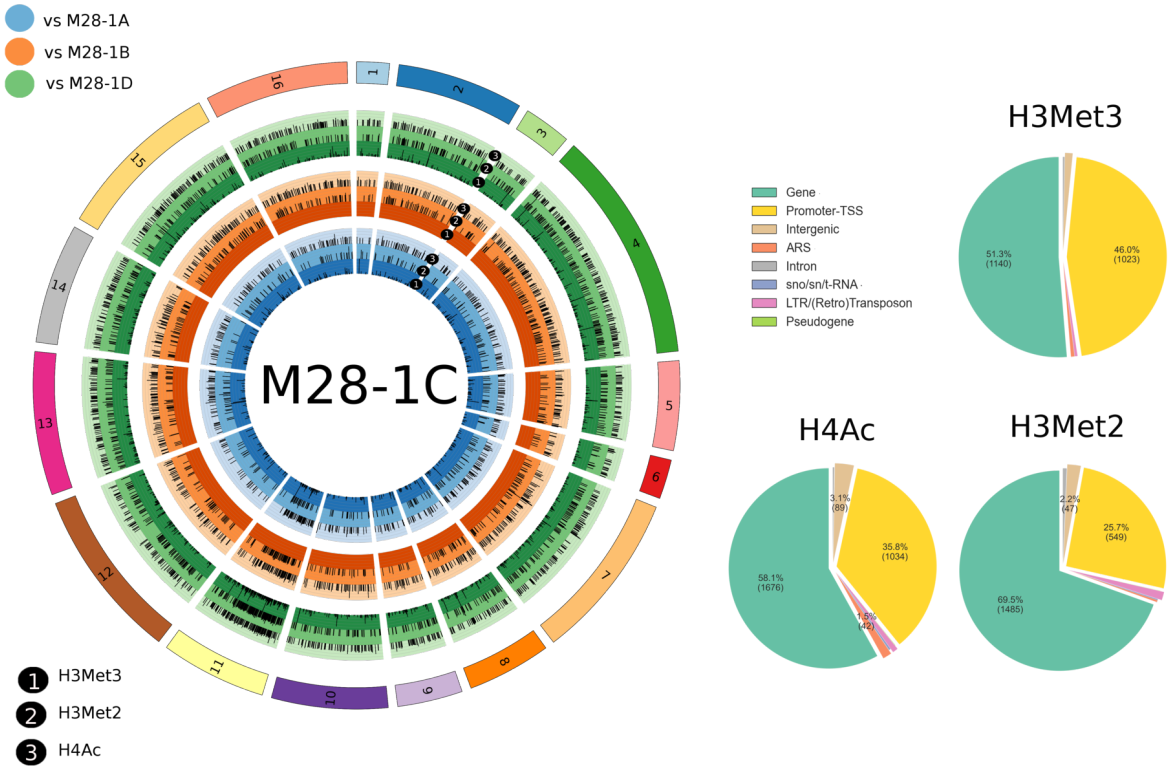

Fig.D.5: Circos plot of significant enriched H3 3Met K4, H3 2Met K4 and H4 Ac islands of M281C compared to M281A, M281B and M281D

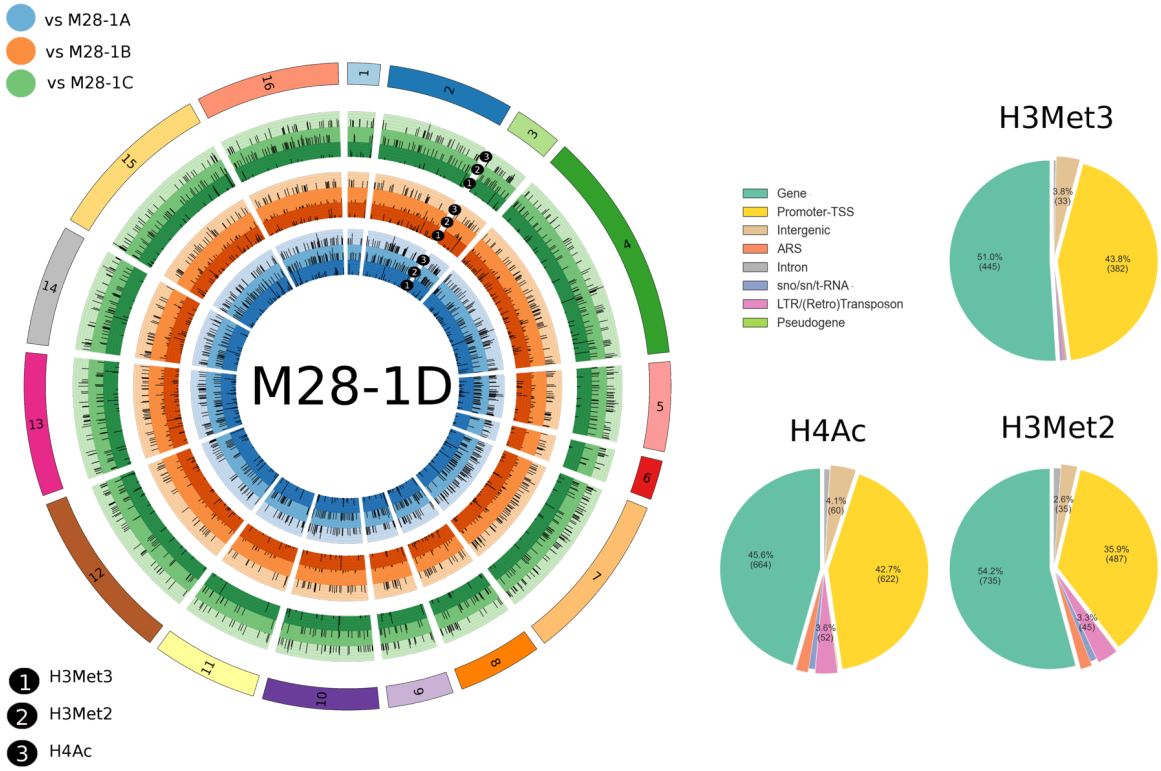

Fig.D.5: Circos plot of significant enriched H3 3Met K4, H3 2Met K4 and H4 Ac islands of M281D compared to M281A, M281B and M281C

Appendix E - *M281B PacBio assembly*

Collinearity plots

Whole genome sequence alignments were obtained using "mummer software" (http://mummer.sourcefor
PMID: 14759262). In general M28 assembly contigs and S288C reference genome show a complete and strict collinearty. As expected gaps are present at the telomeric and centromeric regions but the overall size of chromosomes seems to be conserved. Same conclusions can be draw for chromosomes rearrangements; only two events seems to be occurred between the two strains. A small translocation with inversion in chr I and an inversion on chr XIV. Before to make any hypothesis these hypothetical rearrangements need to be further verified in order to exclude any potential assembly artifacts.

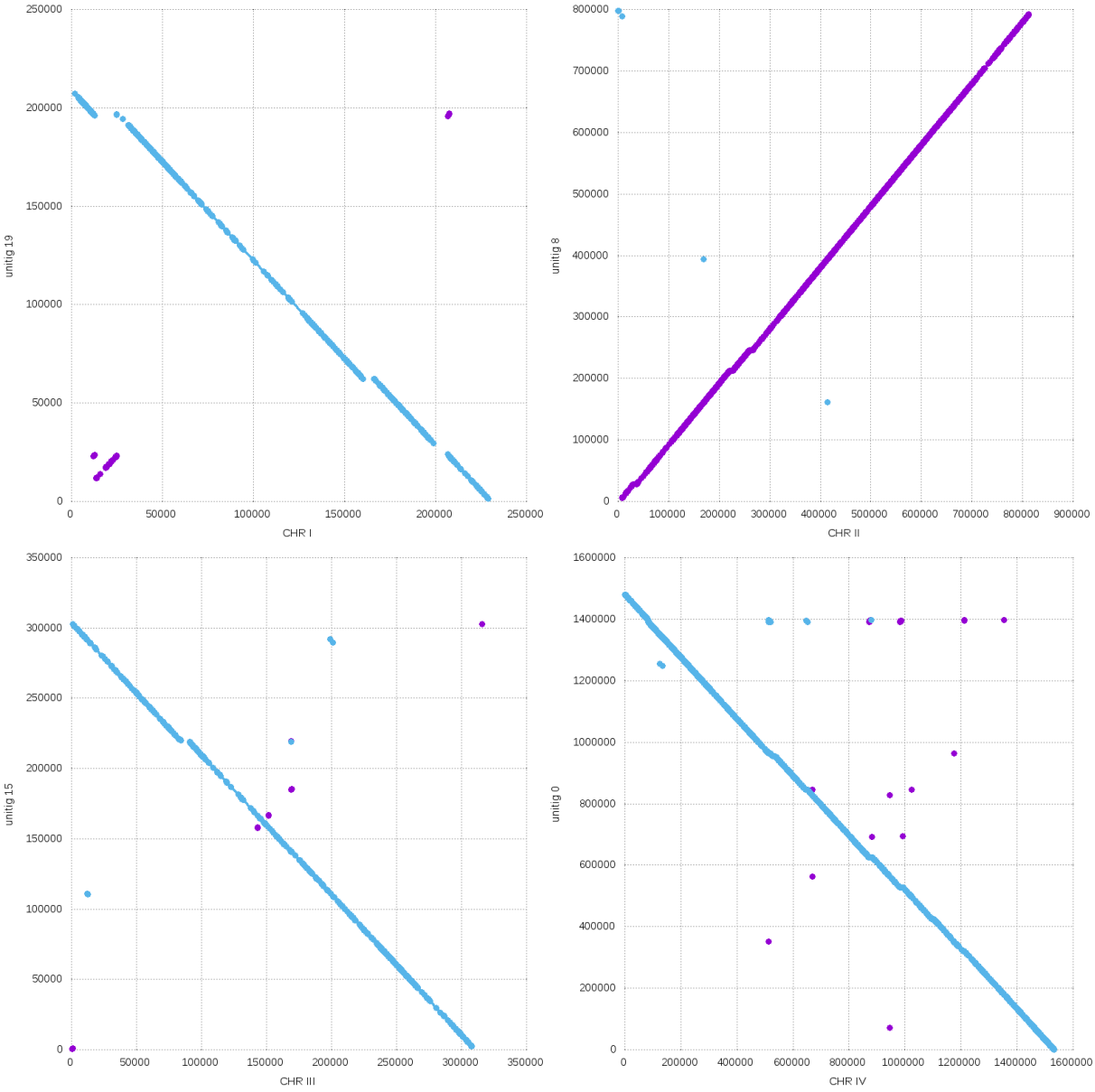

Fig. E.1 Collinearity between *Saccharomyces cerivisiae* S288c reference genome with M281B genome

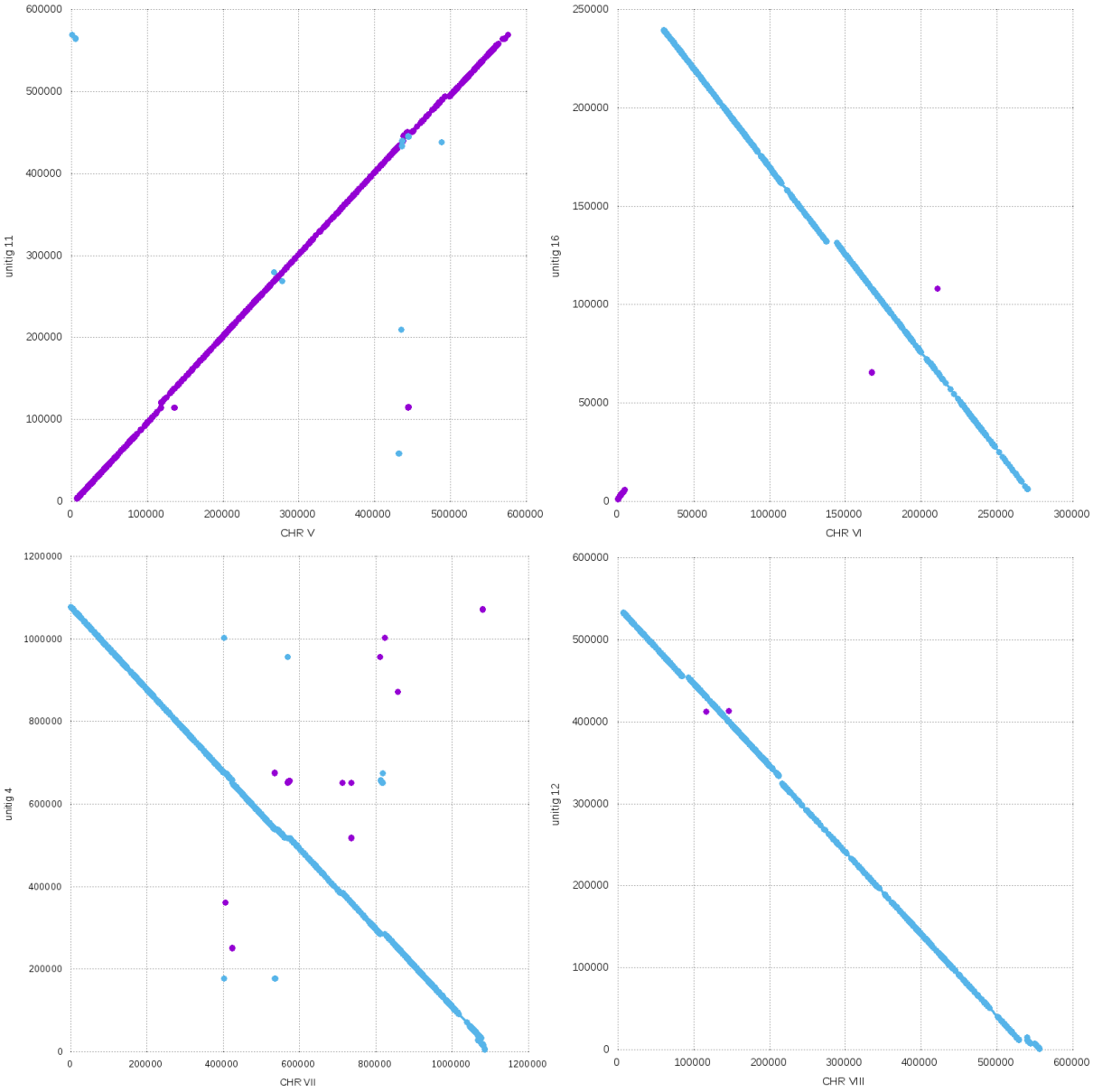

Fig. E.2 Collinearity between *Saccharomyces cerivisiae* S288c reference genome with M281B genome

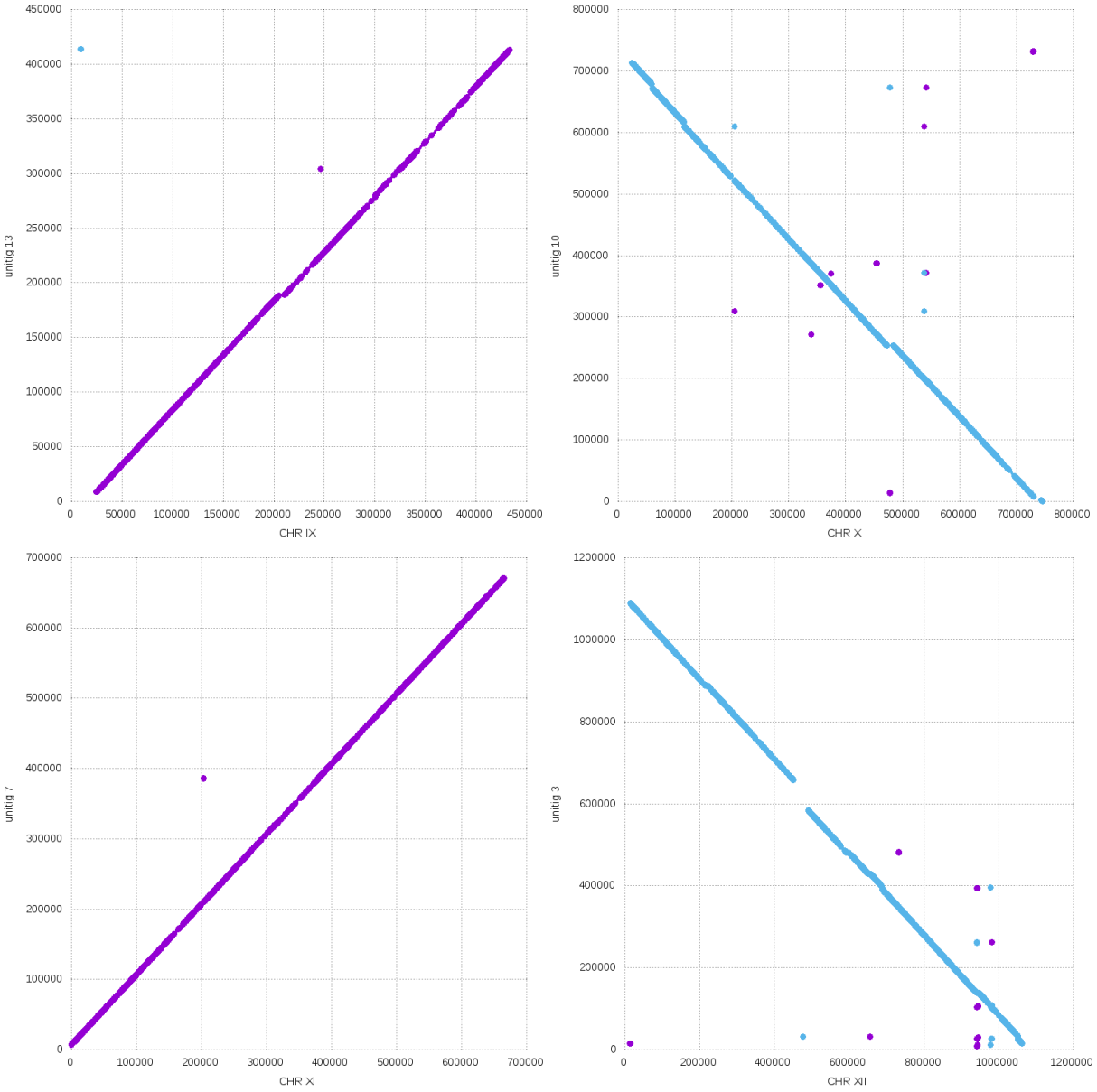

Fig. E.3 Collinearity between *Saccharomyces cerivisiae* S288c reference genome with M281B genome

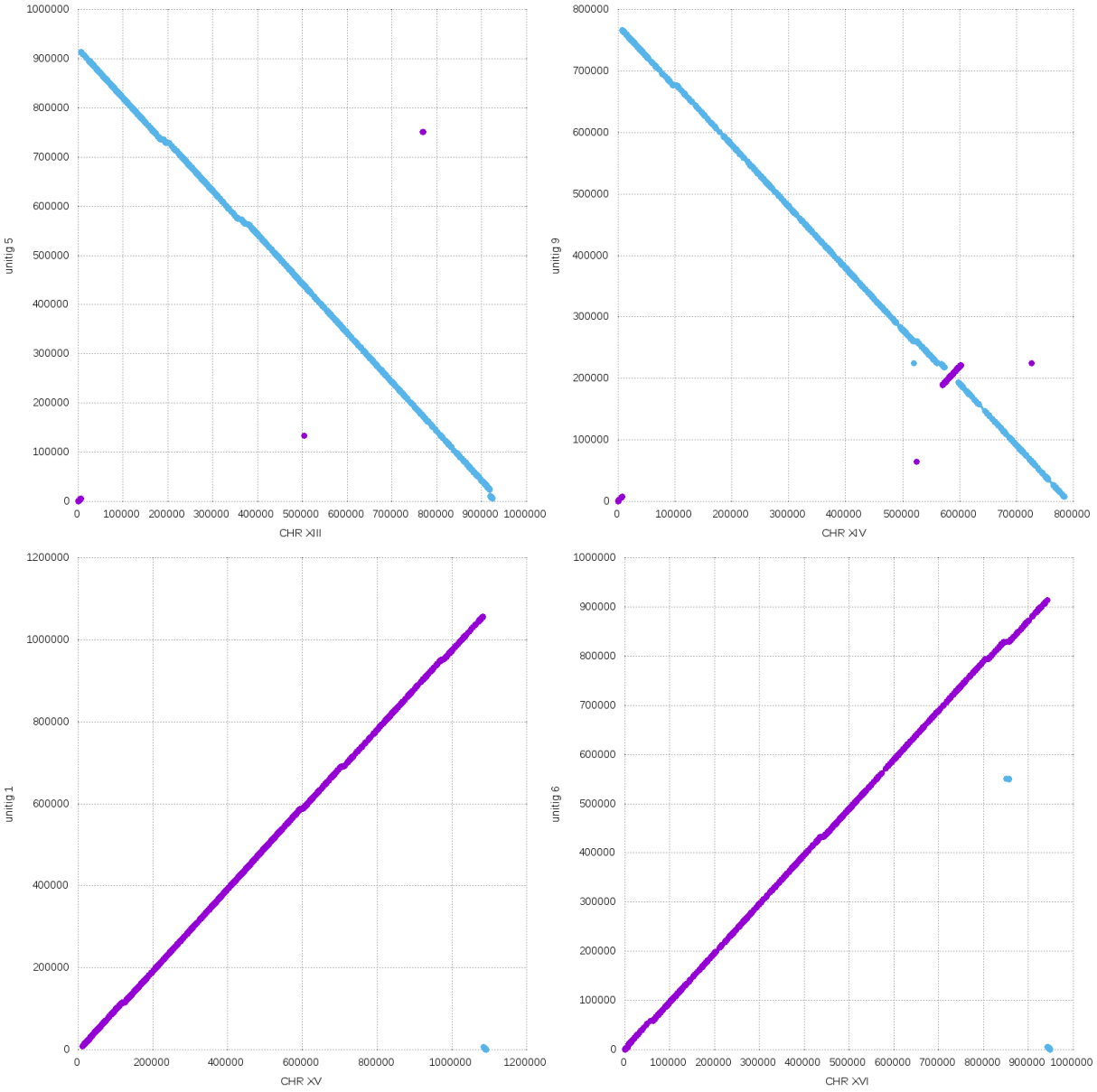

Fig. E.4 Collinearity between *Saccharomyces cerivisiae* S288c reference genome with M281B genome

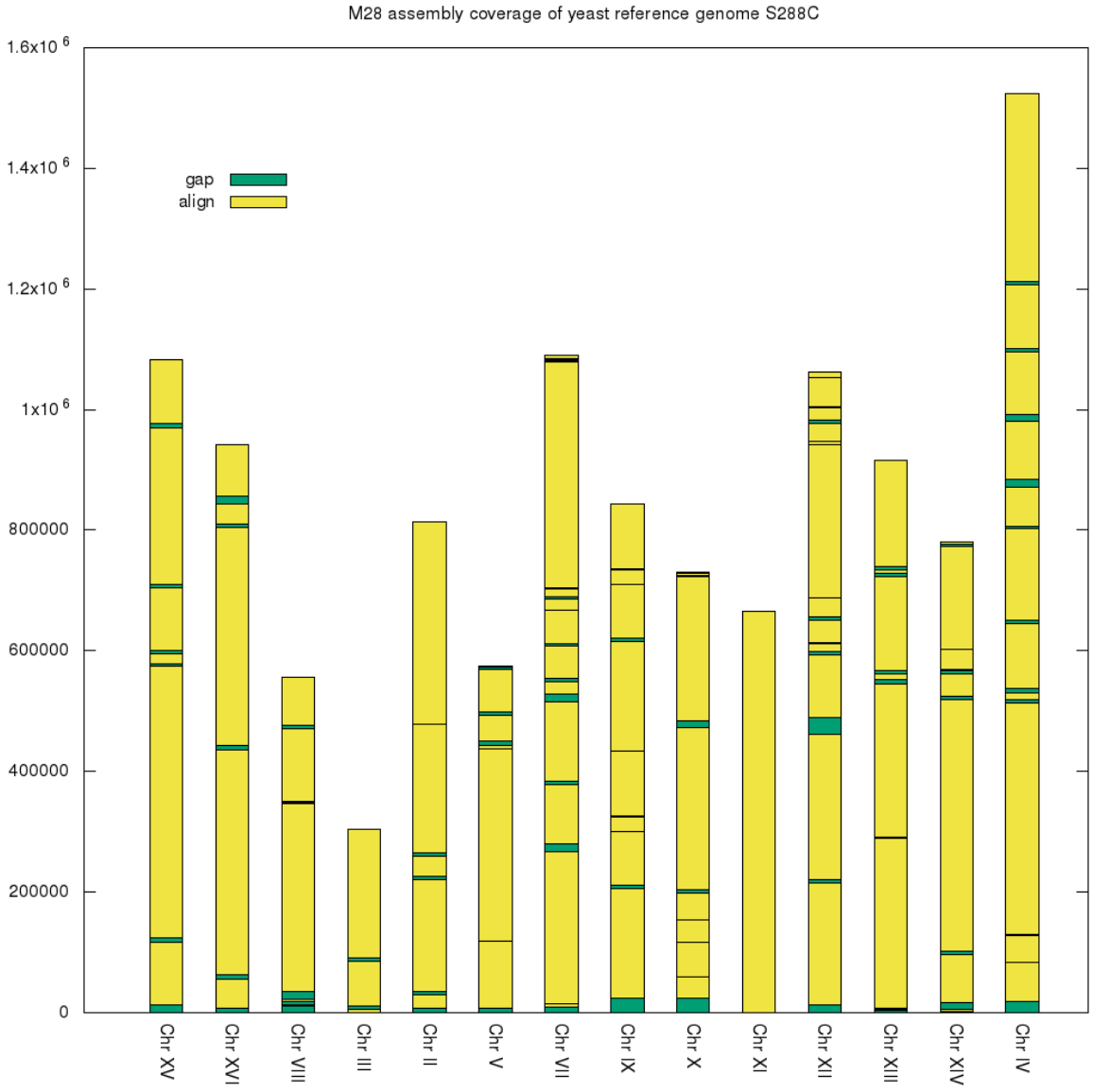

Fig. E.5 M28 assembly coverage of yeast reference genome S288C

Appendix F - *Growth curves of M28 meiotic derivatives in different media*

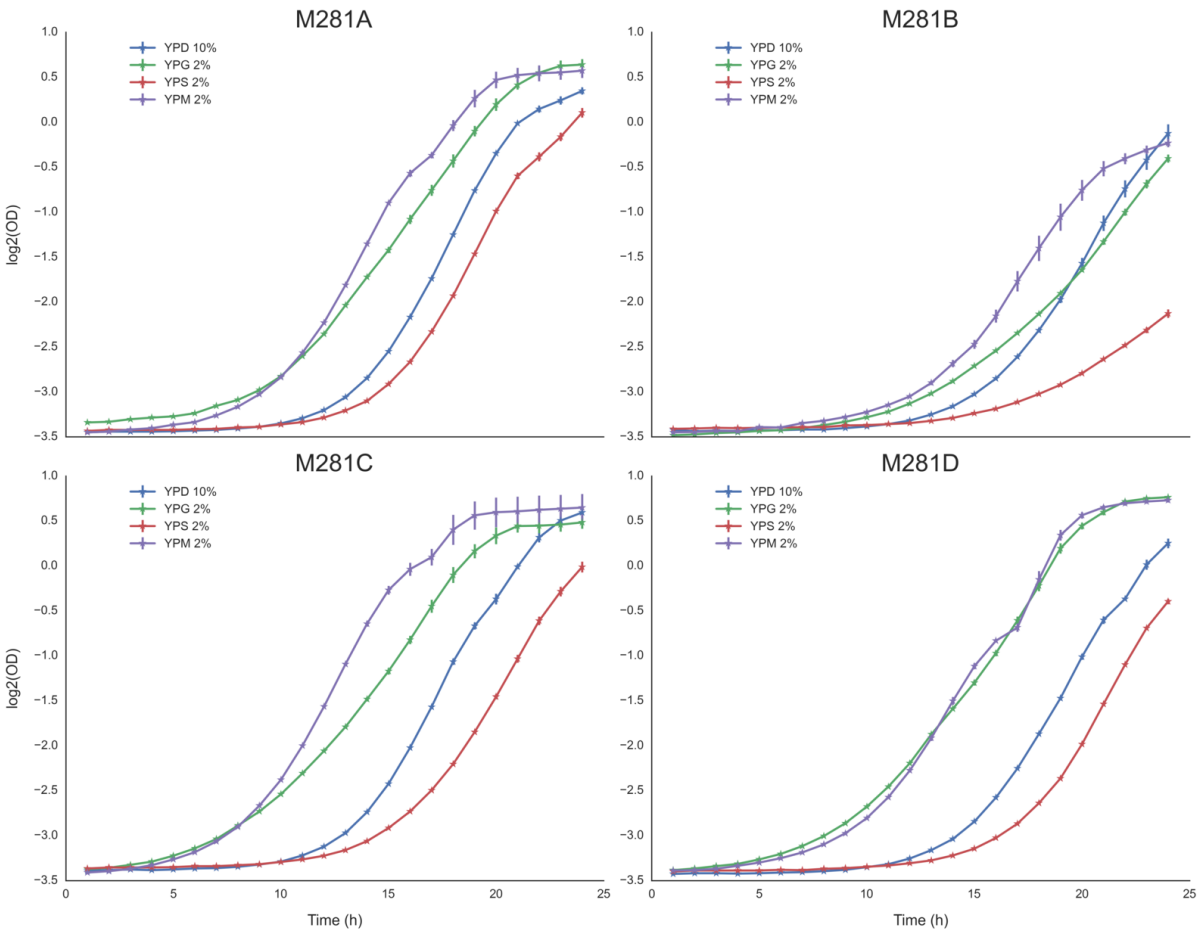

Fig. F.1 Growth curves of M281A-D grown in YP supplemented with: 2% galactose (YPG 2%), 2% mannose (YPM 2%), 2% galactose (YPG 2%) and 10% glucose (YPD 10%)

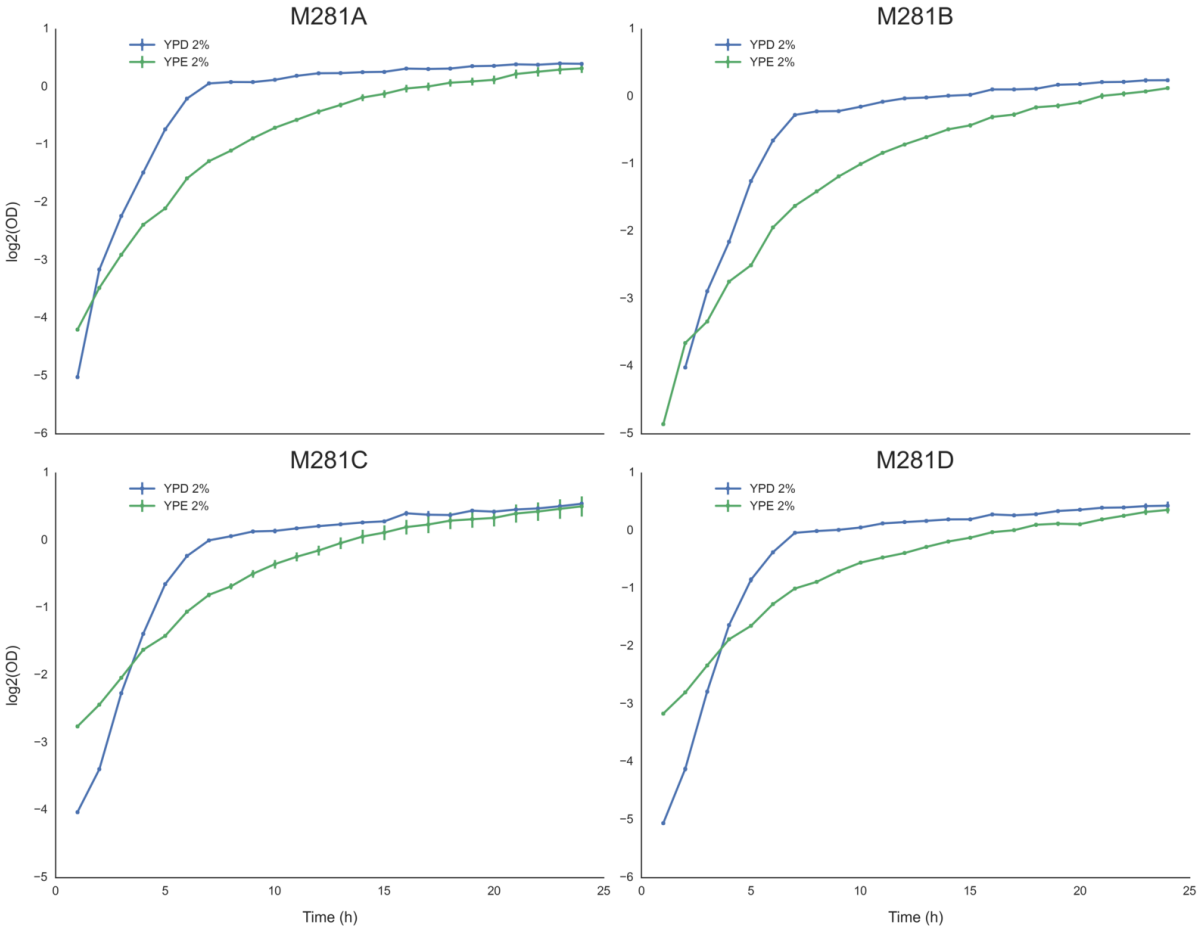

Fig. F.2 Growth curves of M281A-D grown in YP supplemented with: 2% ethanol (YPE 2%) and 2% glucose (YPD 2%)

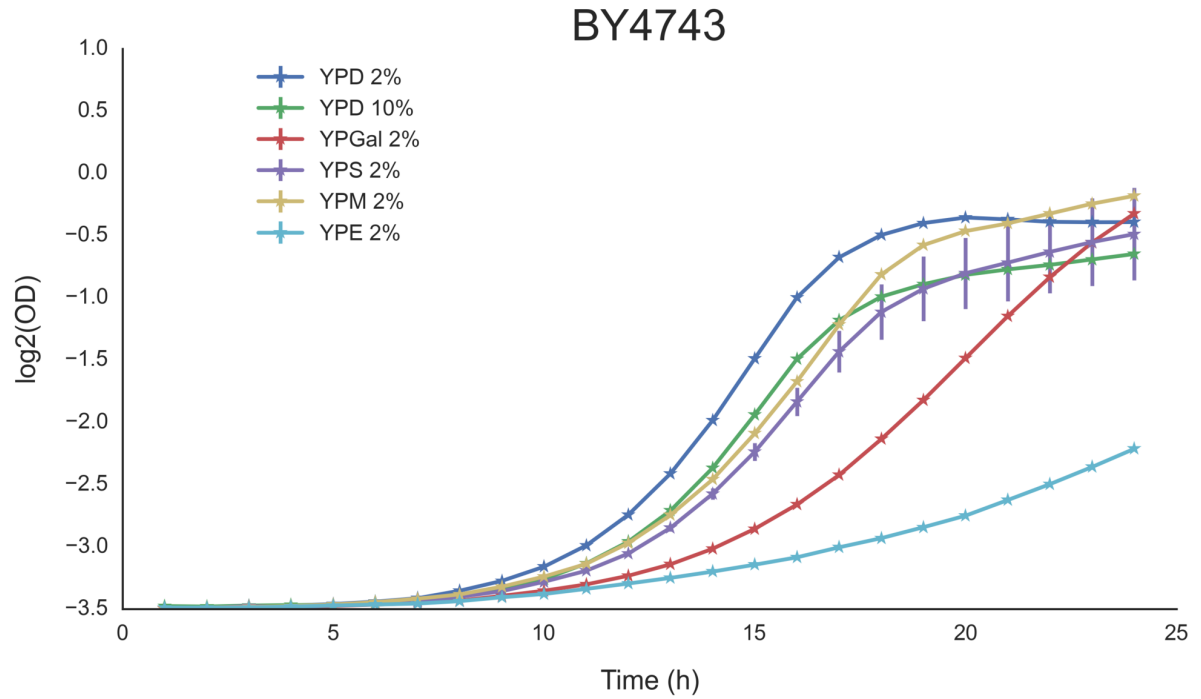

Fig. F.3 Growth curves of diploid referene strain BY4743 grown in YP supplemented with: 2% galactose (YPG 2%), 2% mannose (YPM 2%), 2% galactose (YPG 2%), 10% glucose (YPD 10%), 2% glucose (YPD 2%) and 2% ethanol (YPE 2%)

Appendix G - *Limited proteolysis mass spectrometry results*

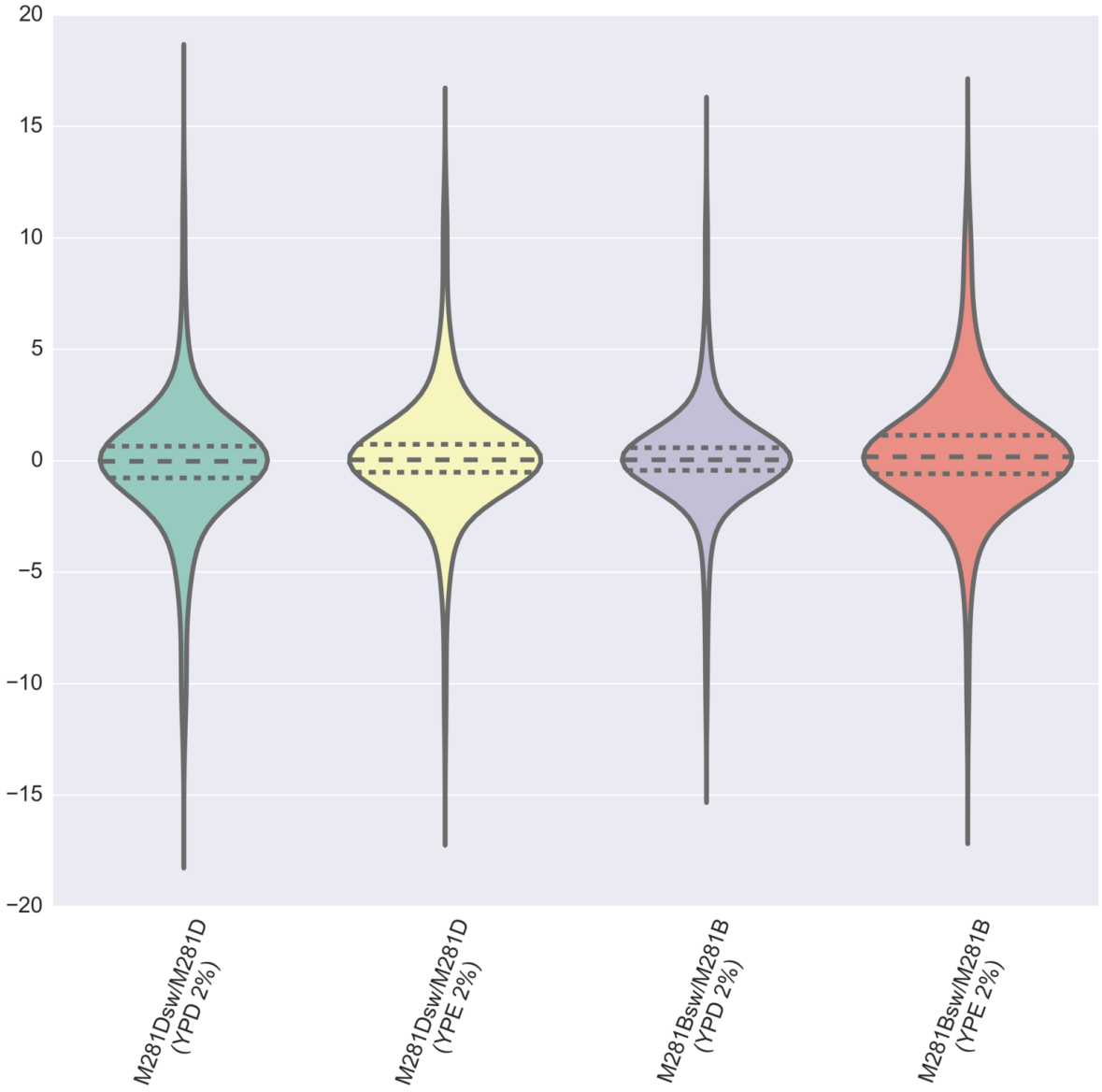

Fig. G.1: Violin plot showing the distribution of peptide quantifications in both M281B and M281D before and after phenotypic switch in YPD 2% and YPE 2%. Peptide abundances are reported as base log2

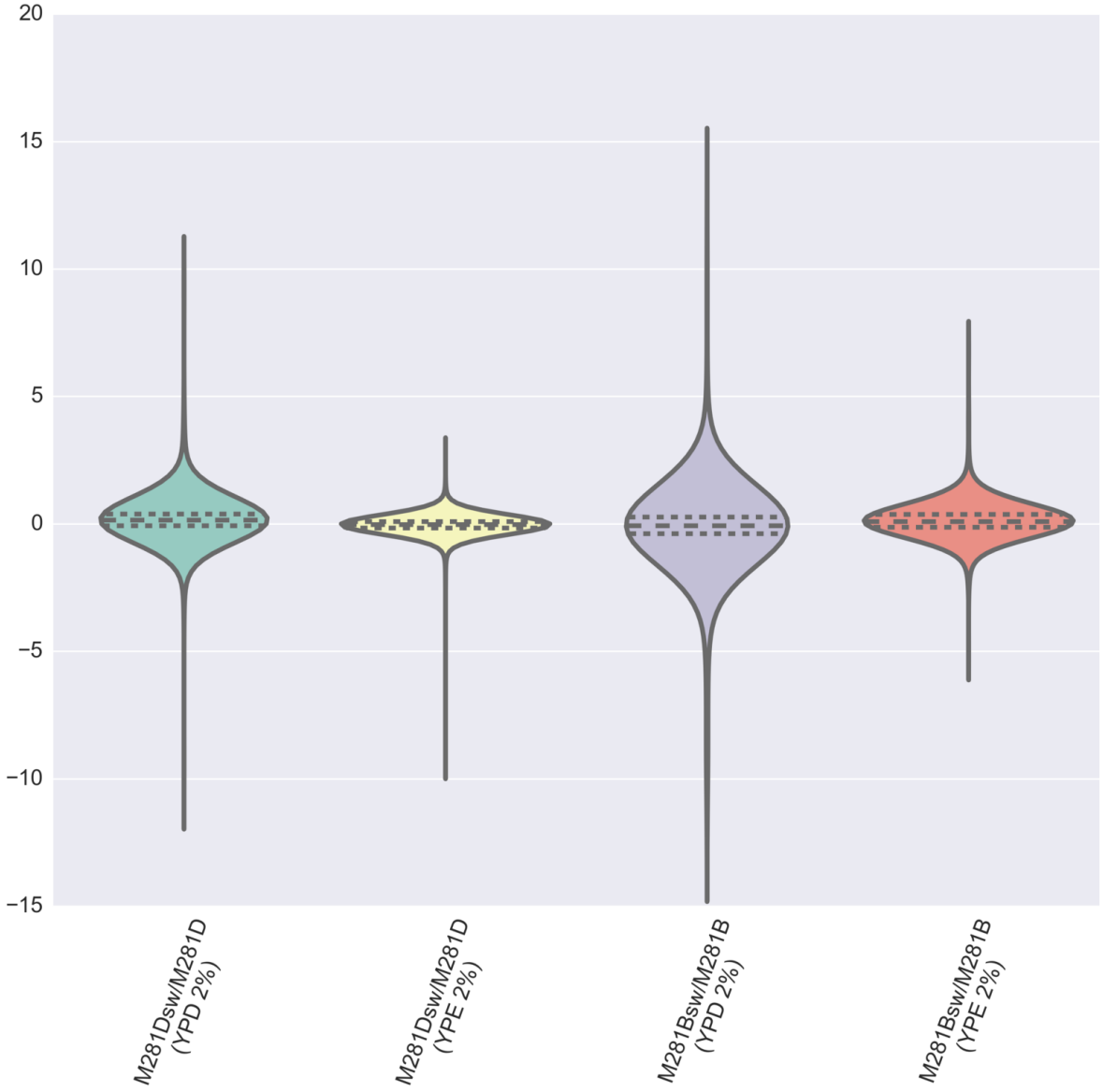

Fig. G.2: Violin plot showing the distribution of protein quantifications in both M281B and M281D before and after phenotypic switch in YPD 2% and YPE 2 %. Protein abundaces are reported as base log2

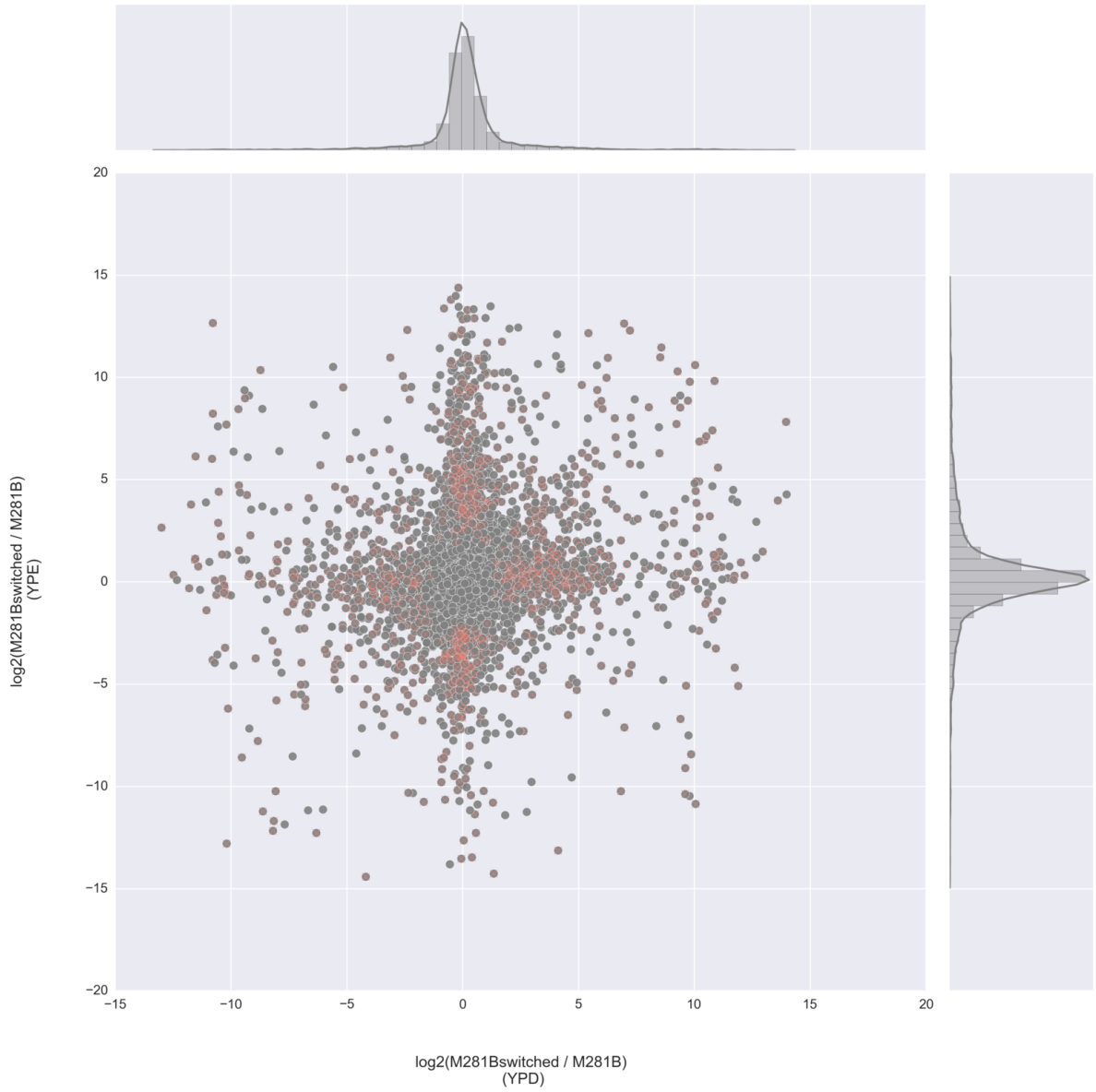

Fig. G.3: Scatterplot comparing peptides conformational changes detected in M281Bswitched / M281B in YPD 2% and M281Bswitched / M281B in YPE 2%. For each dataset a kernel density estimation was drawn. Peptides colored in salmon passed the absolute fold change cutoff of 2 and FDR-adjusted P-value < 0.05

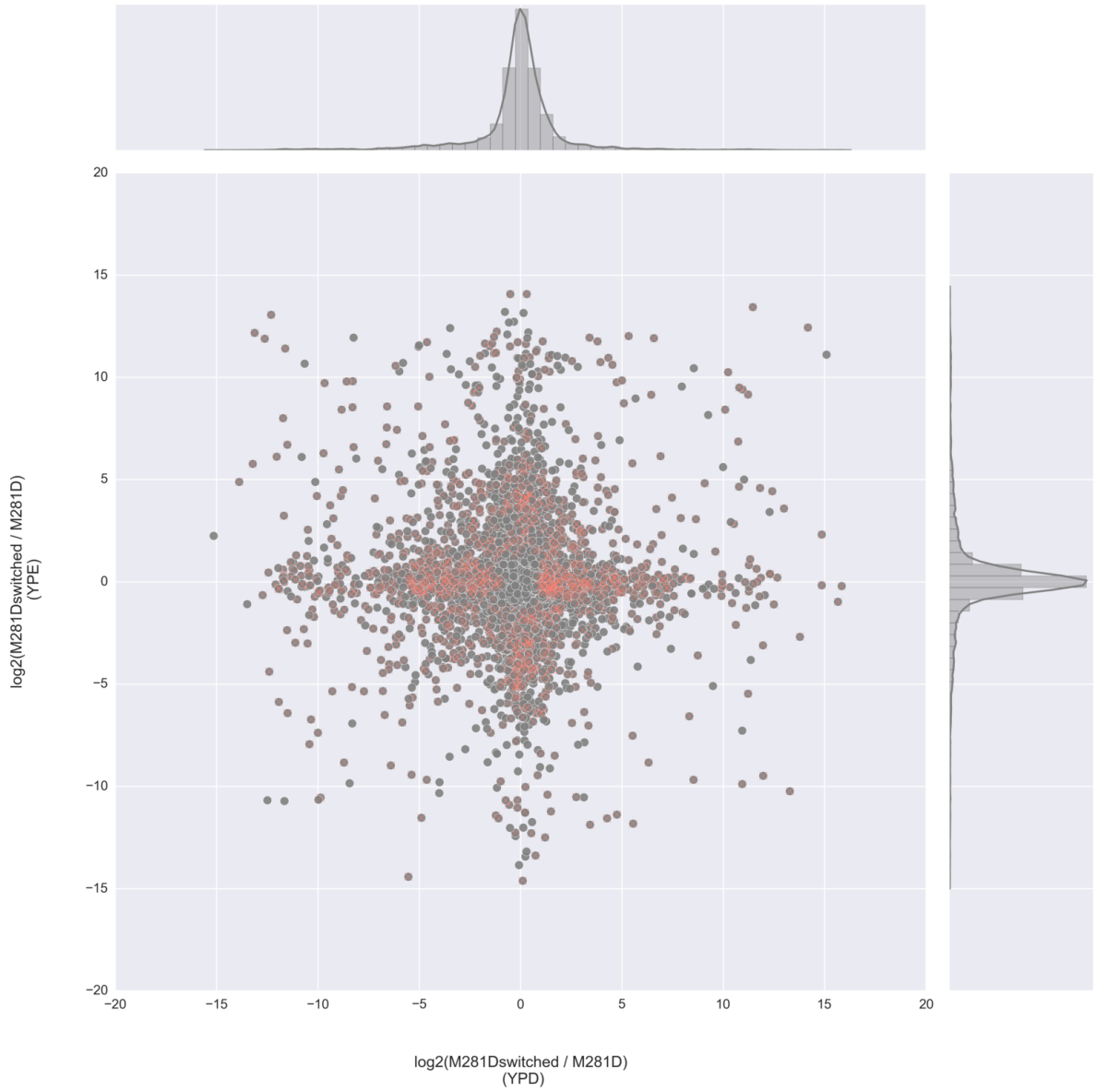

Fig. G.4: Scatterplot comparing peptides conformational changes detected in M281Dswitched / M281D in YPD 2% and M281Dswitched / M281D in YPE 2%. For each dataset a kernel density estimation was drawn. Peptides colored in salmon passed the absolute fold change cutoff of 2 and FDR-adjusted P-value < 0.05

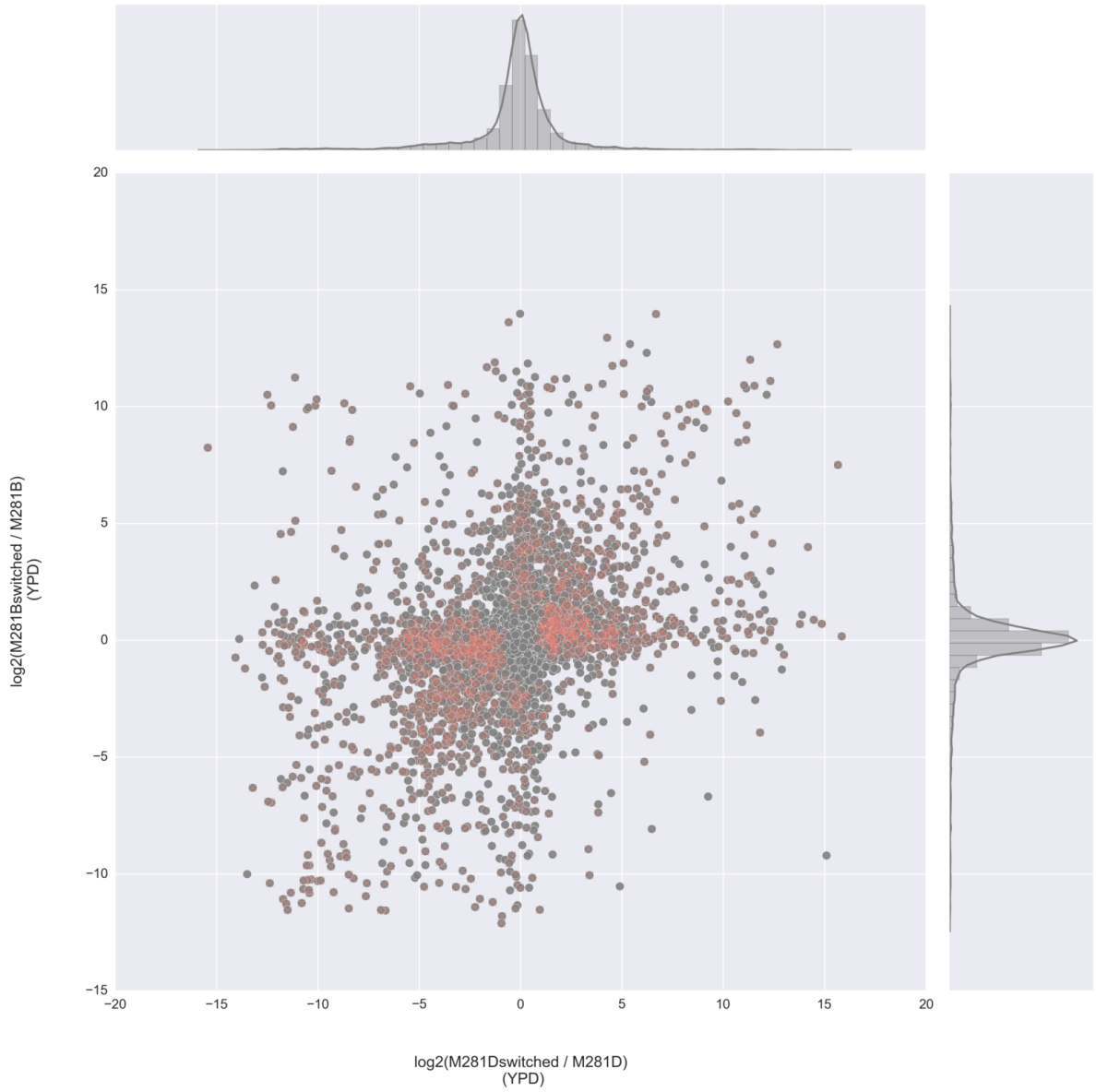

Fig. G.5: Scatterplot comparing peptides conformational changes detected in M281Dswitched / M281D in YPD 2% and M281Bswitched / M281B in YPD 2%. For each dataset a kernel density estimation was drawn. Peptides colored in salmon passed the absolute fold change cutoff of 2 and FDR-adjusted P-value < 0.05

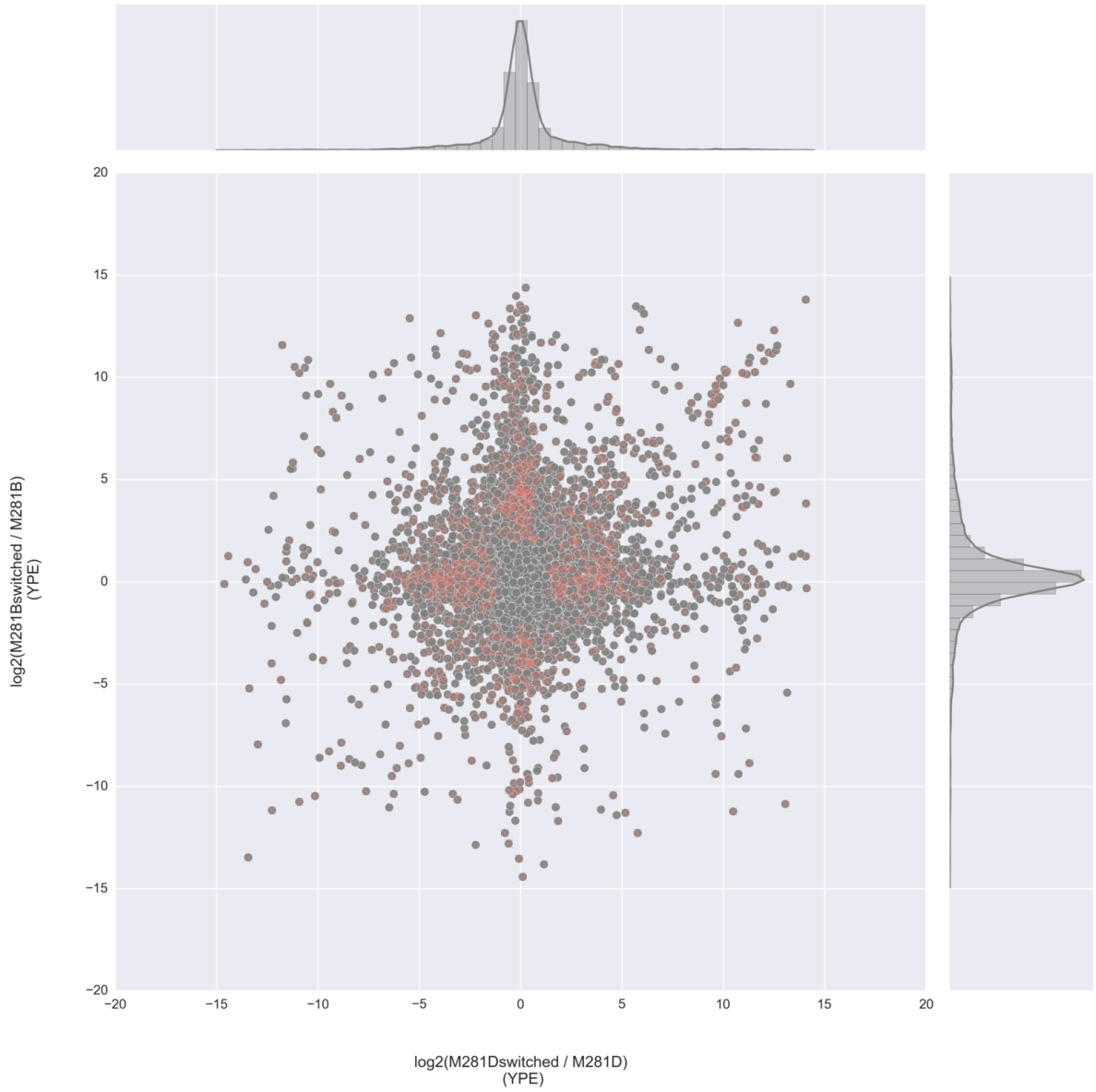

Fig. G.6: Scatterplot comparing peptides conformational changes detected in M281Dswitched / M281D in YPE 2% and M281Bswitched / M281B in YPE 2%. For each dataset a kernel density estimation was drawn. Peptides colored in salmon passed the absolute fold change cutoff of 2 and FDR-adjusted P-value < 0.05